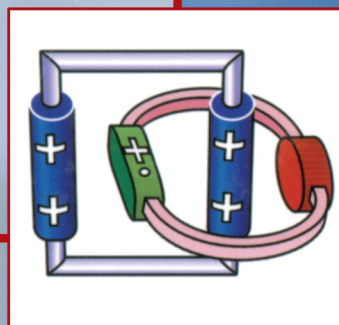
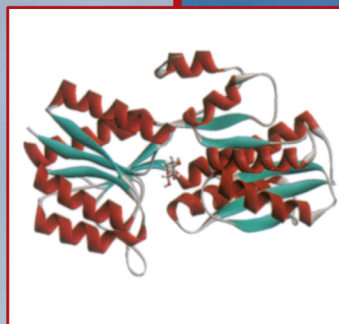
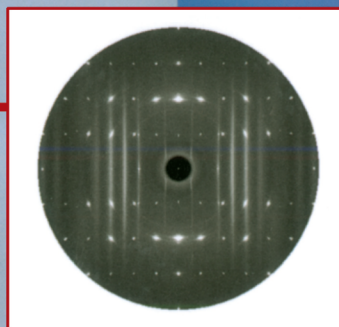
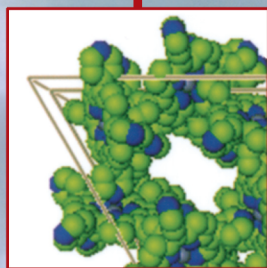


1  
Volume One



# ENCYCLOPEDIA OF SUPRAMOLECULAR CHEMISTRY

EDITED BY  
JERRY L. ATWOOD  
JONATHAN W. STEED

# **Encyclopedia of Supramolecular Chemistry**





# Encyclopedia of Supramolecular Chemistry

Volume 1

A–Min

Pages 1–872

edited by

**Jerry L. Atwood**

*University of Missouri, Columbia, Missouri, U.S.A.*

**Jonathan W. Steed**

*University of Durham, Durham, United Kingdom*



**Taylor & Francis**

Taylor & Francis Group  
Boca Raton London New York

---

CRC is an imprint of the Taylor & Francis Group,  
an informa business



Published in 2004 by  
CRC Press  
Taylor & Francis Group  
6000 Broken Sound Parkway NW, Suite 300  
Boca Raton, FL 33487-2742

© 2004 by Taylor & Francis Group, LLC (except as noted on the opening page of each article)  
CRC Press is an imprint of Taylor & Francis Group

No claim to original U.S. Government works  
Printed in the United States of America on acid-free paper  
10 9 8 7 6 5 4 3 2

International Standard Book Number-10: 0-8247-5056-X (Hardcover)  
International Standard Book Number-13: 978-0-8247-5056-5 (Hardcover)  
**ISBN Volume 1:** 0-8247-4723-2  
**ISBN Volume 2:** 0-8247-4724-0  
**ISBN Online:** 0-8247-4725-9  
**ISBN Print/Online Combo:** 0-8247-4720-8

**Volume 1:**

Front cover, top left and back cover detail: Courtesy of I. Goldberg, author of "Porphyrin-Based Clathrates."  
Front cover, lower left: Courtesy of I. Goldberg, author of "Porphyrin-Based Clathrates."  
Front cover, top right: Courtesy of T. Richard Welberry, author of "Disorder and Diffuse Scattering."  
Front cover, middle right: Courtesy of Dr. Arne Lützen, author of "Carbohydrates, Recognition of."  
Front cover, lower right and back cover detail: Courtesy of Dr. Alberto Credi, author of "Molecular-Level Machines."

**Volume 2:**

Front cover, top left and back cover detail: Courtesy of Dr. Alberto Credi, author of "Molecular-Level Machines."  
Front cover, lower left and back cover detail: Courtesy of Irina S. Terekhova and the estate of Yuri A. Dyadin, authors of "Classical Descriptions of Inclusion Compounds."  
Front cover, top right: Courtesy of Martin Schröder and Neil Champness, authors of "Supramolecular Isomerism."  
Front cover middle right: Courtesy of Dr. Alberto Credi, author of "Molecular-Level Machines."  
Front cover lower right: Courtesy of Dr. Dmitry M. Rudkevich, author of "Self-Assembling Capsules."

This book contains information obtained from authentic and highly regarded sources. Reprinted material is quoted with permission, and sources are indicated. A wide variety of references are listed. Reasonable efforts have been made to publish reliable data and information, but the author and the publisher cannot assume responsibility for the validity of all materials or for the consequences of their use.

No part of this book may be reprinted, reproduced, transmitted, or utilized in any form by any electronic, mechanical, or other means, now known or hereafter invented, including photocopying, microfilming, and recording, or in any information storage or retrieval system, without written permission from the publishers.

**Trademark Notice:** Product or corporate names may be trademarks or registered trademarks, and are used only for identification and explanation without intent to infringe.

---

**Library of Congress Cataloging-in-Publication Data**

---

Catalog record is available from the Library of Congress

---

**informa**

Taylor & Francis Group is the Academic Division of Informa plc.

Visit the Taylor & Francis Web site at  
<http://www.taylorandfrancis.com>

and the CRC Press Web site at  
<http://www.crcpress.com>

**Jerry L. Atwood**  
*University of Missouri, Columbia, Missouri, U.S.A.*  
**Jonathan W. Steed**  
*University of Durham, Durham, United Kingdom*

### ***Editorial Advisory Board***

**Yasuhiro Aoyama**  
*The Institute for Fundamental Research of Organic Chemistry, Division of Supramolecular Chemistry, Kyushu University, Fukuoka-shi, Japan*

**Vincenzo Balzani**  
*Department of Chemistry, University of Bologna, Bologna, Italy*

**Gautam R. Desiraju**  
*School of Chemistry, University of Hyderabad, Hyderabad, India*

**Philip A. Gale**  
*Department of Chemistry, University of Southampton, Southampton, United Kingdom*

**George W. Gokel**  
*Department of Molecular Biology and Pharmacology, Washington University School of Medicine, St. Louis, Missouri, U.S.A.*

**Kenneth D. M. Harris**  
*School of Chemical Sciences, The University of Birmingham, Birmingham, United Kingdom*

**M. Wais Hosseini**  
*Laboratoire de Chimie de Coordination Organique, Université Louis Pasteur, Strasbourg, France*

**Janusz Lipkowski**  
*Institute of Physical Chemistry, Polish Academy of Sciences, Warsaw, Poland*

**Luigi R. Nassimbeni**  
*Department of Chemistry, University of Cape Town, Cape Town, South Africa*

**Colin L. Raston**  
*Department of Chemistry, The University of Western Australia, Perth, Australia*

**Julius Rebek, Jr.**  
*The Skaggs Institute for Chemical Biology, Scripps Institute, La Jolla, California, U.S.A.*

**David N. Reinhoudt**  
*Laboratory of Supramolecular Chemistry and Technology, University of Twente, Enschede, The Netherlands*

**John A. Ripmeester**  
*Steacie Institute for Molecular Sciences, National Research Council of Canada, Ottawa, Canada*

**Robin D. Rogers**  
*The Center for Green Manufacturing, The University of Alabama, Tuscaloosa, Alabama, U.S.A.*

**James H. R. Tucker**  
*School of Chemistry, University of Exeter, Exeter, United Kingdom*

**Michael Zaworotko**  
*Department of Chemistry, University of South Florida, Tampa, Florida, U.S.A.*





# List of Contributors

- Christer B. Aakeröy** / *Kansas State University, Manhattan, Kansas, U.S.A.*
- Rebecca J. Aarons** / *University of Manchester, Manchester, United Kingdom*
- Alaa S. Abd-El-Aziz** / *The University of Winnipeg, Winnipeg, Manitoba, Canada*
- Saad A. M. Ali** / *Smith & Nephew Group Research Centre, York, United Kingdom*
- Frank H. Allen** / *Cambridge Crystallographic Data Centre (CCDC), Cambridge, United Kingdom*
- Mark Allen** / *Montana State University, Bozeman, Montana, U.S.A.*
- David B. Amabilino** / *Institut de Ciència de Materials de Barcelona (CSIC), Cerdanyola del Vallès, Spain*
- Jörg Andrä** / *Research Center Borstel, Leibniz-Center for Medicine and Biosciences, Borstel, Germany*
- Marius Andruh** / *University of Bucharest, Bucharest, Romania*
- Eric V. Anslyn** / *University of Texas at Austin, Austin, Texas, U.S.A.*
- Jun-ichi Anzai** / *Tohoku University, Sendai, Japan*
- Pavel Anzenbacher, Jr.** / *Bowling Green State University, Bowling Green, Ohio, U.S.A.*
- Vladimir A. Azov** / *ETH Zürich, Zürich, Switzerland*
- Alan L. Balch** / *University of California, Davis, California, U.S.A.*
- Philip Ball** / *Nature, London, United Kingdom*
- Vincenzo Balzani** / *Università di Bologna, Bologna, Italy*
- Arindam Banerjee** / *Indian Association for the Cultivation of Science, Calcutta, West Bengal, India*
- José Osío Barcina** / *Universidad Complutense, Madrid, Spain*
- Francesco Barigelletti** / *Istituto per la Sintesi Organica e la Fotoreattività CNR-ISOF, Bologna, Italy*
- Craig E. Barnes** / *University of Tennessee, Knoxville, Tennessee, U.S.A.*
- Stuart R. Batten** / *Monash University, Clayton, Victoria, Australia*
- Derek A. Beauchamp** / *University of Windsor, Windsor, Ontario, Canada*
- Marc Bée** / *Université J. Fourier, Grenoble, France*
- Paul D. Beer** / *University of Oxford, Oxford, United Kingdom*
- Thomas W. Bell** / *University of Nevada, Reno, Nevada, U.S.A.*
- Andrew C. Benniston** / *University of Newcastle, Newcastle upon Tyne, United Kingdom*
- Katja E. Berg** / *Stanford University, Stanford, California, U.S.A.*
- Nicholas Blagden** / *Bradford University, Bradford, United Kingdom*
- Kristin Bowman-James** / *University of Kansas, Lawrence, Kansas, U.S.A.*
- Dario Braga** / *Università degli Studi di Bologna, Bologna, Italy*
- Klaus Brandenburg** / *Research Center Borstel, Leibniz-Center for Medicine and Biosciences, Borstel, Germany*
- Perla Breccia** / *Universidad Autónoma de Madrid, Madrid, Spain*
- Gareth J. Brown** / *The Queen's University of Belfast, Belfast, Northern Ireland*
- Andrew D. Burrows** / *University of Bath, Bath, United Kingdom*
- Daryle H. Busch** / *University of Kansas, Lawrence, Kansas, U.S.A.*
- Mino R. Caira** / *University of Cape Town, Rondebosch, Western Cape Province, South Africa*



- Salvatore Camiolo** / *University of Southampton, Southampton, United Kingdom*
- Jiří Čejka** / *Academy of Sciences of the Czech Republic, Prague, Czech Republic*
- Neil R. Champness** / *The University of Nottingham, Nottingham, United Kingdom*
- Gervais Chapuis** / *University of Lausanne, Lausanne, Switzerland*
- Da-Wei Chen** / *Achillian Pharmaceuticals Inc., New Haven, Connecticut, U.S.A.*
- Kihang Choi** / *Yale University, New Haven, Connecticut, U.S.A.*
- Alberto Ciferri** / *University of Genoa, Genoa, Italy*
- Anthony W. Coleman** / *Institut de Biologie et Chimie des Protéines, Lyon, France*
- James P. Collman** / *Stanford University, Stanford, California, U.S.A.*
- Ruud G. E. Coumans** / *University of Nijmegen, Nijmegen, The Netherlands*
- Robert H. Crabtree** / *Yale University, New Haven, Connecticut, U.S.A.*
- Peter J. Cragg** / *University of Brighton, Brighton, United Kingdom*
- Alberto Credi** / *Università di Bologna, Bologna, Italy*
- Leroy Cronin** / *The University of Glasgow, Glasgow, United Kingdom*
- Sheng Dai** / *Oak Ridge National Laboratory, Oak Ridge, Tennessee, U.S.A.*
- Ian Dance** / *University of New South Wales, Sydney, New South Wales, Australia*
- Eric Da Silva** / *Institut de Biologie et Chimie des Protéines, Lyon, France*
- Anthony P. Davis** / *University of Bristol, Bristol, United Kingdom*
- Steven De Feyter** / *Katholieke Universiteit Leuven (K.U.Leuven), Leuven, Belgium*
- Javier de Mendoza** / *Universidad Autónoma de Madrid, Madrid, Spain*
- Frans C. De Schryver** / *Katholieke Universiteit Leuven (K.U.Leuven), Leuven, Belgium*
- A. Prasanna de Silva** / *The Queen's University of Belfast, Belfast, Northern Ireland*
- Gautam R. Desiraju** / *University of Hyderabad, Hyderabad, Andhra Pradesh, India*
- Christian Detellier** / *University of Ottawa, Ottawa, Ontario, Canada*
- Bernard Dietrich** / *ISIS—Université Louis Pasteur, Strasbourg, France*
- Peter H. Dinolfo** / *Northwestern University, Evanston, Illinois, U.S.A.*
- Stefano Di Stefano** / *Università degli Studi di Roma La Sapienza, Roma, Italy*
- Dennis A. Dougherty** / *California Institute of Technology, Pasadena, California, U.S.A.*
- Trevor Douglas** / *Montana State University, Bozeman, Montana, U.S.A.*
- Yuri Alexseevich Dyadin (Deceased)** / *The Siberian Branch of the Russian Academy of Sciences, Novosibirsk, Russia*
- James L. Dye** / *Michigan State University, East Lansing, Michigan, U.S.A.*
- Claude Ecolivet** / *Université de Rennes, Rennes, France*
- Johannes A. A. W. Elemans** / *University of Nijmegen, Nijmegen, The Netherlands*
- Marco Evangelisti** / *Leiden University, Leiden, The Netherlands*
- John S. O. Evans** / *University of Durham, Durham, United Kingdom*
- Jean-Yves Exposito** / *Centre National de la Recherche Scientifique, Lyon, France*
- Luigi Fabbrizzi** / *Università di Pavia, Pavia, Italy*
- Stephen Faulkner** / *University of Manchester, Manchester, United Kingdom*
- Riccardo Ferdani** / *Washington University School of Medicine, St. Louis, Missouri, U.S.A.*
- Ben L. Feringa** / *University of Groningen, Groningen, The Netherlands*
- Eduardo J. Fernández** / *Universidad de La Rioja, UA—CSIC, Logroño, Spain*
- Michelle Flenniken** / *Montana State University, Bozeman, Montana, U.S.A.*
- Thomas M. Fyles** / *University of Victoria, Victoria, British Columbia, Canada*
- Philip A. Gale** / *University of Southampton, Southampton, United Kingdom*
- Peter Gans** / *The University of Leeds, Leeds, United Kingdom*
- Patrick Garidel** / *Martin-Luther-Universität, Halle/Wittenberg, Halle/Saale, Germany*

- Maria Gdaniec** / *Adam Mickiewicz University, Poznań, Poland*
- Bruce C. Gibb** / *University of New Orleans, New Orleans, Louisiana, U.S.A.*
- Hermann Gies** / *Ruhr-Universität Bochum, Bochum, Germany*
- Karsten Gloe** / *Technische Universität Dresden, Dresden, Germany*
- George W. Gokel** / *Washington University School of Medicine, St. Louis, Missouri, U.S.A.*
- Israel Goldberg** / *Tel Aviv University, Tel Aviv, Israel*
- Carl Henrik Görbitz** / *University of Oslo, Oslo, Norway*
- Fabrizia Grepioni** / *Università di Sassari, Sassari, Italy*
- Manuela Grotjahn** / *Technische Universität Dresden, Dresden, Germany*
- C. David Gutsche** / *Texas Christian University, Fort Worth, Texas, U.S.A.*
- Ionel Haiduc** / *Universitatea “Babeş-Bolyai,” Cluj-Napoca, Romania*
- Andrew D. Hamilton** / *Yale University, New Haven, Connecticut, U.S.A.*
- Tamara D. Hamilton** / *University of Iowa, Iowa City, Iowa, U.S.A.*
- Michael J. Hardie** / *University of Leeds, Leeds, United Kingdom*
- Michael Harmata** / *University of Missouri—Columbia, Columbia, Missouri, U.S.A.*
- Kenneth D. M. Harris** / *Cardiff University, Cardiff, Wales*
- Jeffrey H. Harwell** / *University of Oklahoma, Norman, Oklahoma, U.S.A.*
- Takashi Hayashi** / *Kyushu University, Fukuoka, Japan*
- Elizabeth J. Hayes** / *University of Oxford, Oxford, United Kingdom*
- Tino Hertzsch** / *University of Berne, Berne, Switzerland*
- Robert C. Hider** / *King’s College London, London, United Kingdom*
- Andrew Hinton** / *University of Edinburgh, Edinburgh, United Kingdom*
- John D. Holbreay** / *The University of Alabama, Tuscaloosa, Alabama, U.S.A.*
- K. Travis Holman** / *Georgetown University, Washington, District of Columbia, U.S.A.*
- Antony M. Hooper** / *Rothamsted Research, Harpenden, Hertfordshire, United Kingdom*
- Junhua Huang** / *Commonwealth Scientific and Industrial Research Organization (CSIRO), Melbourne, Victoria, Australia*
- Jürg Hulliger** / *University of Berne, Berne, Switzerland*
- Joseph T. Hupp** / *Northwestern University, Evanston, Illinois, U.S.A.*
- Bakhtiyar T. Ibragimov** / *Institute of Bioorganic Chemistry of Uzbekistan Academy of Sciences, Tashkent, Uzbekistan*
- Yoshihisa Inoue** / *Entropy Control Project, International Cooperative Research Project (ICORP), Toyonaka, Japan*
- Yasuhiro Ishida** / *The University of Tokyo, Tokyo, Japan*
- Toschitake Iwamoto** / *Iwaki Meisei University, Iwaki, Fukushima, Japan*
- Stuart L. James** / *Queen’s University Belfast, Belfast, Northern Ireland*
- Kim D. Janda** / *The Scripps Research Institute and The Skaggs Institute for Chemical Biology, La Jolla, California, U.S.A.*
- Sei-Hum Jang** / *University of Washington, Seattle, Washington, U.S.A.*
- Janarthanan Jayawickramarajah** / *University of Texas at Austin, Austin, Texas, U.S.A.*
- Gunnar Jeschke** / *Max Planck Institute for Polymer Research, Mainz, Germany*
- Gyan P. Johari** / *McMaster University, Hamilton, Ontario, Canada*
- Bart Kahr** / *University of Washington, Seattle, Washington, U.S.A.*
- Angel E. Kaifer** / *University of Miami, Coral Gables, Florida, U.S.A.*
- Gerd Kaupp** / *University of Oldenburg, Oldenburg, Germany*
- Jun-ichi Kikuchi** / *Nara Institute of Science and Technology, Nara, Japan*
- Hee-Joon Kim** / *Pohang University of Science and Technology, Pohang, Republic of Korea*
- Kimoon Kim** / *Pohang University of Science and Technology, Pohang, Republic of Korea*



- Eiichi Kimura** / *Hiroshima University, Hiroshima, Japan*
- Yoshiyaki Kobuke** / *Nara Institute of Science and Technology, Nara, Japan; Crest, Japan Science and Technology, Nara, Japan*
- Carolyn A. Koh** / *King's College London, London, United Kingdom*
- Tohru Koike** / *Hiroshima University, Hiroshima, Japan*
- Hiroki Kondo** / *Kyushu Institute of Technology, Fukuoka, Japan*
- Shin-ichi Kugimiya** / *Nara Institute of Science and Technology, Tokyo, Japan*
- Jayant Kumar** / *University of Massachusetts Lowell, Lowell, Massachusetts, U.S.A.*
- Antonio Laguna** / *Universidad de Zaragoza—CSIC, Zaragoza, Spain*
- Chi-Keung Lam** / *The Chinese University of Hong Kong, Hong Kong SAR, People's Republic of China*
- Dario Landini** / *Università degli Studi di Milano, Milano, Italy*
- Adrian J. Lapthorn** / *University of Glasgow, Glasgow, United Kingdom*
- Adina N. Lazar** / *Institut de Biologie et Chimie des Protéines, Lyon, France*
- Pavel Lhoták** / *Institute of Chemical Technology, Prague, Czech Republic*
- Li Li** / *Nankai University, Tianjin, People's Republic of China*
- Leonard F. Lindoy** / *The University of Sydney, Sydney, New South Wales, Australia*
- Petra Linnartz** / *Kekulé-Institut für Organische Chemie und Biochemie der Universität, Bonn, Germany*
- Karen J. Lipscomb** / *Cambridge Crystallographic Data Centre (CCDC), Cambridge, United Kingdom*
- Yu Liu** / *Nankai University, Tianjin, People's Republic of China*
- Zu Dong Liu** / *King's College London, London, United Kingdom*
- José M. Llinares** / *University of Kansas, Lawrence, Kansas, U.S.A.*
- Stephen J. Loeb** / *University of Windsor, Windsor, Ontario, Canada*
- José M. López-de-Luzuriaga** / *Universidad de La Rioja, UA—CSIC, Logroño, Spain*
- Ulrich Lüning** / *Universität Kiel, Kiel, Germany*
- Arne Lützen** / *University of Oldenburg, Oldenburg, Germany*
- Donal H. Macartney** / *Queen's University, Kingston, Ontario, Canada*
- Leonard R. MacGillivray** / *University of Iowa, Iowa City, Iowa, U.S.A.*
- Joseph M. Mahoney** / *University of Notre Dame, Notre Dame, Indiana, U.S.A.*
- Angelamaria Maia** / *Università degli Studi di Milano, Milano, Italy*
- Thomas C. W. Mak** / *The Chinese University of Hong Kong, Hong Kong SAR, People's Republic of China*
- Luigi Mandolini** / *Università degli Studi di Roma La Sapienza, Roma, Italy*
- Amedea Manfredi** / *CNR-Istituto di Scienze e Technologie Molecolari, Milano, Italy*
- Christian R. Marcilly** / *French Institute of Petroleum (IFP), Rueil Malmaison, France*
- Bernd Marler** / *Ruhr-Universität Bochum, Bochum, Germany*
- Michael J. Marsella** / *University of California, Riverside, California, U.S.A.*
- Antonio García Martínez** / *Universidad Complutense, Madrid, Spain*
- Takasuke Matsuo** / *Osaka University, Osaka, Japan*
- Karen R. Maxcy** / *IBM T.J. Watson Research Center, Yorktown Heights, New York, U.S.A.*
- J. Andrew McCammon** / *University of California—San Diego, La Jolla, California, U.S.A.*
- Gareth D. McClean** / *The Queen's University of Belfast, Belfast, Northern Ireland*
- Judith R. Meakin** / *University of Aberdeen, Foresterhill, Aberdeen, United Kingdom*
- Pierangelo Metrangola** / *Polytechnic of Milan, Milan, Italy*
- Robert M. Metzger** / *The University of Alabama, Tuscaloosa, Alabama, U.S.A.*
- Amaresh Mishra** / *University of Akron, Akron, Ohio, U.S.A.*
- Karycia D. D. Mitchell** / *University of Victoria, Victoria, British Columbia, Canada*
- Mikiji Miyata** / *Osaka University, Osaka, Japan*

- Sandra Monti** / *Istituto per la Sintesi Organica e la Fotoreattività CNR-ISOF, Bologna, Italy*
- Thomas S. Moody** / *The Queen's University of Belfast, Belfast, Northern Ireland*
- Charles N. Moorefield** / *University of Akron, Akron, Ohio, U.S.A.*
- Arvin Moser** / *University of Ottawa, Ottawa, Ontario, Canada*
- Ravi Mosurkal** / *University of Massachusetts Lowell, Lowell, Massachusetts, U.S.A.*
- Ashwini Nangia** / *University of Hyderabad, Hyderabad, India*
- Luigi R. Nassimbeni** / *University of Cape Town, Rondebosch, Western Cape Province, South Africa*
- George R. Newkome** / *University of Akron, Akron, Ohio, U.S.A.*
- Motorhiro Nishio** / *The CHPI Institute, Tokyo, Japan*
- Roeland J. M. Nolte** / *University of Nijmegen, Nijmegen, The Netherlands*
- Tomás C. O'Riordan** / *University College Cork, Cork, Ireland*
- Sijbren Otto** / *University of Cambridge, Cambridge, United Kingdom*
- Giannis S. Papaefstathiou** / *University of Iowa, Iowa City, Iowa, U.S.A.*
- Dmitri B. Papkovsky** / *University College Cork, Cork, Ireland*
- Gerard Parkin** / *Columbia University, New York, New York, U.S.A.*
- Alexandra L. Pickering** / *The University of Glasgow, Glasgow, United Kingdom*
- John A. Pickett** / *Rothamsted Research, Harpenden, Hertfordshire, United Kingdom*
- Lucidalva S. Pinheiro** / *Instituto de Química da Universidade de São Paulo, São Paulo, Brazil*
- Sebastian Polarz** / *Ruhr-University Bochum, Bochum, Germany*
- Gianluca Pozzi** / *CNR-Istituto di Scienze e Tecnologie Molecolari, Milano, Italy*
- Nicholas C. Price** / *University of Glasgow, Glasgow, United Kingdom*
- Sarah L. Price** / *University College London, London, United Kingdom*
- Silvio Quici** / *CNR-Istituto di Scienze e Tecnologie Molecolari, Milano, Italy*
- Torsten Rambusch** / *Technische Universität Dresden, Dresden, Germany*
- Alexander Rang** / *Kekulé-Institut für Organische Chemie und Biochemie der Universität, Bonn, Germany*
- Colin L. Raston** / *University of Western Australia, Crawley, Perth, Australia*
- Christopher I. Ratcliffe** / *National Research Council Canada, Ottawa, Ontario, Canada*
- Mikhail Rekharsky** / *Entropy Control Project, International Cooperative Research Project (ICORP), Osaka, Japan*
- Giuseppe Resnati** / *Polytechnic of Milan, Milan, Italy*
- Marcos Caroli Rezende** / *Universidad de Santiago de Chile, Santiago, Chile*
- John A. Ripmeester** / *National Research Council Canada, Ottawa, Ontario, Canada*
- Kari Rissanen** / *University of Jyväskylä, Jyväskylä, Finland*
- Michael A. J. Rodgers** / *Bowling Green State University, Bowling Green, Ohio, U.S.A.*
- Robin D. Rogers** / *The University of Alabama, Tuscaloosa, Alabama, U.S.A.*
- Alan E. Rowan** / *University of Nijmegen, Nijmegen, The Netherlands; NSRIM, University of Nijmegen, Nijmegen, The Netherlands*
- Dmitry M. Rudkevich** / *The University of Texas at Arlington, Arlington, Texas, U.S.A.*
- David A. Sabatini** / *University of Oklahoma, Norman, Oklahoma, U.S.A.*
- Kazuki Sada** / *Osaka University, Osaka, Japan*
- J. Timothy Sage** / *Northeastern University, Boston, Massachusetts, U.S.A.*
- Lynne A. Samuelson** / *U.S. Army RDECOM, Natick, Massachusetts, U.S.A.*
- Jeremy K. M. Sanders** / *University of Cambridge, Cambridge, United Kingdom*
- Muhunthan Sathiosatham** / *Eastman Kodak Company, Rochester, New York, U.S.A.*
- Abdelhamid Sayari** / *University of Ottawa, Ottawa, Ontario, Canada*
- John F. Scamehorn** / *University of Oklahoma, Norman, Oklahoma, U.S.A.*
- Franco Scandola** / *Università degli Studi di Ferrara, Ferrara, Italy*

- Christoph A. Schalley** / *Kekulé-Institut für Organische Chemie und Biochemie der Universität, Bonn, Germany*
- Franz P. Schmidtchen** / *Munich Institute of Technology, Garching, Germany*
- Hans-Jörg Schneider** / *Universität des Saarlandes, Saarbrücken, Germany*
- Robert A. Schoonheydt** / *Katholieke University Leuven, Leuven, Belgium*
- Martin Schröder** / *The University of Nottingham, Nottingham, United Kingdom*
- Paolo Scrimin** / *University of Padova, Padova, Italy*
- Nadrian C. Seeman** / *New York University, New York, New York, U.S.A.*
- Jonathan L. Sessler** / *University of Texas at Austin, Austin, Texas, U.S.A.*
- Corey Seward** / *Queen's University, Kingston, Ontario, Canada*
- John C. Sherman** / *University of British Columbia, Vancouver, British Columbia, Canada*
- George K. H. Shimizu** / *University of Calgary, Calgary, Alberta, Canada*
- Vladimir B. Shur** / *Russian Academy of Sciences, Moscow, Russia*
- Bradley D. Smith** / *University of Notre Dame, Notre Dame, Indiana, U.S.A.*
- John A. S. Smith** / *King's College London, London, United Kingdom*
- Dmitriy V. Soldatov** / *National Research Council Canada, Ottawa, Ontario, Canada*
- Piero Sozzani** / *Università di Milano—Bicocca, Milan, Italy*
- Scott K. Spear** / *The University of Alabama, Tuscaloosa, Alabama, U.S.A.*
- Jonathan W. Steed** / *University of Durham, Durham, United Kingdom*
- Ivan Stibor** / *Institute of Chemical Technology, Prague, Czech Republic*
- Shinji Sueda** / *Kyushu Institute of Technology, Fukuoka, Japan*
- Shih-Sheng Sun** / *Northwestern University, Evanston, Illinois, U.S.A.*
- Gerhard F. Swiegers** / *Commonwealth Scientific and Industrial Research Organization (CSIRO), Melbourne, Victoria, Australia*
- József Szejtli** / *CYCLOLAB, Cyclodextrin Research and Development Laboratory Ltd., Budapest, Hungary*
- Yuko Takata** / *Hiroshima University, Higashi-Hiroshima, Japan*
- Samat A. Talipov** / *Institute of Bioorganic Chemistry of Uzbekistan Academy of Sciences, Tashkent, Uzbekistan*
- Takashi Tatsumi** / *Yokohama National University, Yokohama, Japan*
- Paul Taylor** / *University of Edinburgh, Edinburgh, United Kingdom*
- Paolo Tecilla** / *University of Trieste, Trieste, Italy*
- Irina Sergeevna Terekhova** / *The Siberian Branch of the Russian Academy of Sciences, Novosibirsk, Russia*
- Carlo Thilgen** / *ETH Zürich, Zürich, Switzerland*
- Jim A. Thomas** / *University of Sheffield, Sheffield, United Kingdom*
- Pall Thordarson** / *The University of Sydney, Sydney, New South Wales, Australia*
- Irina A. Tikhonova** / *Russian Academy of Sciences, Moscow, Russia*
- Suzanne L. Tobey** / *University of Texas at Austin, Austin, Texas, U.S.A.*
- Toshinori Tsuru** / *Hiroshima University, Higashi-Hiroshima, Japan*
- James H. R. Tucker** / *University of Exeter, Exeter, United Kingdom*
- Konstantin A. Udachin** / *National Research Council of Canada, Ottawa, Ontario, Canada*
- Yoshio Umezawa** / *University of Tokyo, Tokyo, Japan*
- Alberto Vacca** / *Università degli Studi di Firenze, Sesto Fiorentino, Italy*
- Sabine Van Doorslaer** / *University of Antwerp, Wilrijk, Belgium*
- Jan H. van Esch** / *University of Groningen, Groningen, The Netherlands*
- Jaume Veciana** / *Institut de Ciència de Materials de Barcelona (CSIC), Cerdanyola del Vallès, Spain*
- Ramón Vilar** / *Imperial College of Science, Technology, and Medicine, London, United Kingdom*
- Malcolm D. Walkinshaw** / *University of Edinburgh, Edinburgh, United Kingdom*
- Suning Wang** / *Queen's University, Kingston, Ontario, Canada*

- Edwin Weber** / *Technische Universität Bergakademie Freiberg, Freiberg, Germany*
- Sheenagh M. Weir** / *The Queen's University of Belfast, Belfast, Northern Ireland*
- T. Richard Welberry** / *Australian National University, Canberra, Australia*
- Robin E. Westacott** / *Heriot-Watt University, Edinburgh, United Kingdom*
- Roger D. Willett** / *Washington State University, Pullman, Washington, U.S.A.*
- Chick C. Wilson** / *University of Glasgow, Glasgow, United Kingdom; Central Laboratory of the Research Councils (CLRC) Rutherford Appleton Laboratory, Oxon, United Kingdom*
- Chung F. Wong** / *University of California—San Diego, La Jolla, California, U.S.A.*
- Anatoly K. Yatsimirsky** / *Universidad Nacional Autónoma de México, Mexico City, Mexico*
- Nungruethai Yoswatthanant** / *Osaka University, Osaka, Japan*
- Mark Young** / *Montana State University, Bozeman, Montana, U.S.A.*
- Raoul Zana** / *Institut Charles Sadron (CNRS-ULP), Strasbourg, France*
- Heng-Yi Zhang** / *Nankai University, Tianjin, People's Republic of China*
- Mladen Žinić** / *Rudjer Bošković Institute, Zagreb, Croatia*





# Contents

<i>Preface</i> .....	xxi
<i>Foreword</i> .....	xxiii
<b>Alkali Metal Cations in Biochemistry</b> / Yoshiyaki Kobuke, Shin-ichi Kugimiya .....	1
<b>Alkalides and Electrides</b> / James L. Dye .....	12
<b>The Allosteric Effect</b> / Anatoly K. Yatsimirsky .....	20
<b>Amide- and Urea-Based Anion Receptors</b> / Philip A. Gale .....	31
<b>Amino Acids: Applications</b> / Arindam Banerjee .....	42
<b>Anion-Directed Assembly</b> / Ramón Vilar .....	51
<b>Annulenes</b> / Michael J. Marsella .....	59
<b>Anticrowns</b> / Vladimir B. Shur, Irina A. Tikhonova .....	68
<b>Artificial Enzymes</b> / Jun-ichi Kikuchi, Hiroki Kondo .....	76
<b>Aurophilic Interactions</b> / Antonio Laguna, Eduardo J. Fernández, José M. López-de-Luzuriaga .....	82
<b>Biological Ligands</b> / Andrew Hinton, Paul Taylor, Malcolm D. Walkinshaw .....	88
<b>Biological Models and Their Characteristics</b> / Paolo Scrimin, Paolo Tecilla .....	101
<b>Biomaterials</b> / Judith R. Meakin .....	110
<b>Biosensors</b> / Jun-ichi Anzai .....	115
<b>Bond-Stretch Isomerism</b> / Gerard Parkin .....	120
<b>Brillouin Scattering</b> / Claude Ecolivet .....	129
<b>Calixarenes and Their Analogues: Cation Complexation</b> / Anthony W. Coleman, Adina N. Lazar, Eric Da Silva .....	137
<b>Calixarenes and Their Analogues: Molecular Complexation</b> / Ivan Stibor, Pavel Lhoták .....	145
<b>Calixarenes: Synthesis and Historical Perspectives</b> / C. David Gutsche .....	153
<b>The Cambridge Structural Database</b> / Frank H. Allen, Karen J. Lipscomb .....	161
<b>Carbohydrates, Recognition of</b> / Arne Lützen .....	169
<b>Carbonic Anhydrase Models</b> / Tohru Koike, Eiichi Kimura .....	178
<b>Carboxypeptidase A</b> / Shinji Sueda, Hiroki Kondo .....	183
<b>Carcerands and Hemicarcerands</b> / Bruce C. Gibb .....	189
<b>Catalytic Antibodies</b> / Kim D. Janda, Da-Wei Chen .....	193
<b>Catenanes and Other Interlocked Molecules</b> / Alexander Rang, Christoph A. Schalley .....	206
<b>Cation-<math>\pi</math> Interactions</b> / Dennis A. Dougherty .....	214
<b>Cavitands</b> / Bruce C. Gibb .....	219
<b>Channel Inclusion Compounds</b> / Maria Gdaniec .....	223
<b>Chemical Topology</b> / David B. Amabilino .....	229
<b>Chiral Guest Recognition</b> / Anthony P. Davis .....	236
<b>Chiral Induction</b> / David B. Amabilino, Jaume Veciana .....	245
<b>Classical Descriptions of Inclusion Compounds</b> / Yuri Alexseevich Dyadin (Deceased), Irina Sergeevna Terekhova .....	253

<b>Classification and Nomenclature of Supramolecular Compounds</b> / Edwin Weber	261
<b>Clathrate Hydrates</b> / John A. Ripmeester, Christopher I. Ratcliffe, Konstantin A. Udachin	274
<b>Clathrate Hydrates: Occurrence, Uses, and Problems</b> / Christopher I. Ratcliffe, John A. Ripmeester	281
<b>Clathrate Inclusion Compounds, Phase Transitions in</b> / Takasuke Matsuo	289
<b>Collagens</b> / Jean-Yves Exposito	295
<b>Complexation of Fullerenes</b> / Colin L. Raston	302
<b>Concave Reagents</b> / Ulrich Lüning	311
<b>Concepts in Crystal Engineering</b> / Andrew D. Burrows	319
<b>Crown Ethers</b> / George W. Gokel	326
<b>Cryptands</b> / Bernard Dietrich	334
<b>Cryptophanes: Molecular Containers</b> / K. Travis Holman	340
<b>Crystal Deconstruction</b> / Fabrizia Grepioni, Dario Braga	349
<b>Crystal Engineering with Hydrogen Bonds</b> / Dario Braga, Fabrizia Grepioni	357
<b>Crystal Growth Mechanisms</b> / Nicholas Blagden	364
<b>Crystal Structure Prediction</b> / Sarah L. Price	371
<b>Crystalline Microporous Silicas</b> / Hermann Gies, Bernd Marler	380
<b>Cucurbituril, Its Homologues, and Derivatives</b> / Kimoon Kim, Hee-Joon Kim	390
<b>Cyclodextrins</b> / József Szejtli	398
<b>Cyclodextrins: Applications</b> / József Szejtli	405
<b>Cyclophanes: Definition and Scope</b> / Carlo Thilgen, Vladimir A. Azov	414
<b>Cyclophanes: Endoacidic, Endobasic, and Endolipophilic Cavities</b> / Andrew C. Benniston	424
<b>Dendrimers</b> / Charles N. Moorefield, George R. Newkome, Amaresh Mishra	432
<b>Deoxycholic, Cholic, and Apocholic Acids</b> / Mikiji Miyata, Kazuki Sada, Nungruethai Yoswathananont	441
<b>The Diphenylmethane Moiety</b> / Antonio García Martínez, José Osío Barcina	452
<b>Disorder and Diffuse Scattering</b> / T. Richard Welberry	457
<b>DNA as a Supramolecular Scaffold</b> / Alexandra L. Pickering, Leroy Cronin	467
<b>DNA Nanotechnology</b> / Nadrian C. Seeman	475
<b>Drug Delivery</b> / Saad A. M. Ali	484
<b>Drug Design</b> / Chung F. Wong, J. Andrew McCammon	490
<b>Dye Inclusion Crystals</b> / Bart Kahr, Sei-Hum Jang	497
<b>Electrochemical Sensors</b> / James H. R. Tucker	505
<b>Electron Paramagnetic Resonance Spectroscopy</b> / Gunnar Jeschke	520
<b>Emergence of Life</b> / Pall Thordarson	528
<b>Energy and Electron Transfer in Supramolecular Systems</b> / Jonathan L. Sessler, Janarthanan Jayawickramarajah, Muhunthan Sathiosatham	535
<b>Enzyme Mimics</b> / Anatoly K. Yatsimirsky	546
<b>Enzymes: Characteristics and Mechanisms</b> / Nicholas C. Price, Adrian J. Lapthorn	554
<b>Fluorescence Sensing of Anions</b> / Kihang Choi, Andrew D. Hamilton	566
<b>Fluorescent Sensors</b> / A. Prasanna de Silva, Gareth D. McClean, Thomas S. Moody	572
<b>Fullerenes as Encapsulating Hosts: Preparation, Detection, and Structures of Endohedral Fullerenes</b> / Alan L. Balch	579
<b>Gels</b> / Jan H. van Esch, Ben L. Feringa	586
<b>Glycoluril-Based Hosts</b> / Johannes A. A. W. Elemans, Alan E. Rowan, Roeland J. M. Nolte	597
<b>Gossypol</b> / Bakhtiyar T. Ibragimov, Samat A. Talipov	606
<b>Guanidinium-Based Anion Receptors</b> / Eric V. Anslyn, Suzanne L. Tobey	615

<b>Halogen Bonding</b> / <i>Pierangelo Metrangolo, Giuseppe Resnati</i> . . . . .	628
<b>Hemoglobins: O<sub>2</sub> Uptake and Transport</b> / <i>J. Timothy Sage</i> . . . . .	636
<b>Hofmann-Type Clathrates</b> / <i>Toschitake Iwamoto</i> . . . . .	645
<b>Homocalixarenes</b> / <i>Peter J. Cragg</i> . . . . .	649
<b>Hydrogen Bonding</b> / <i>Gautam R. Desiraju</i> . . . . .	658
<b>Hydrogen Bonds to Metals and Metal Hydrides</b> / <i>Robert H. Crabtree</i> . . . . .	666
<b>Hydrophobic Effects</b> / <i>Hans-Jörg Schneider</i> . . . . .	673
<b>Hydroquinone</b> / <i>Thomas C. W. Mak, Chi-Keung Lam</i> . . . . .	679
<b>Imaging and Targeting</b> / <i>Stephen Faulkner, Rebecca J. Aarons</i> . . . . .	687
<b>Inclusion Compounds: Selectivity, Thermal Stability, and Kinetics</b> / <i>Luigi R. Nassimbeni</i> . . . . .	696
<b>Inclusion Reactions and Polymerization</b> / <i>Mikiji Miyata</i> . . . . .	705
<b>Incommensurate and Commensurate Structures</b> / <i>Kenneth D. M. Harris</i> . . . . .	712
<b>Induced Fit</b> / <i>Yu Liu, Li Li, Heng-Yi Zhang</i> . . . . .	717
<b>Inelastic Neutron Scattering</b> / <i>Marc Bée</i> . . . . .	727
<b>Interpenetration</b> / <i>Stuart R. Batten</i> . . . . .	735
<b>Ion Channels and Their Models</b> / <i>Karycia D. D. Mitchell, Thomas M. Fyles</i> . . . . .	742
<b>Ion-Selective Electrodes</b> / <i>Yoshio Umezawa</i> . . . . .	747
<b>Ionic, Dipolar, and Interfacial Processes</b> / <i>Gyan P. Johari</i> . . . . .	753
<b>Ionophores</b> / <i>Riccardo Ferdani, George W. Gokel</i> . . . . .	760
<b>Isostructurality of Inclusion Compounds</b> / <i>Mino R. Caira</i> . . . . .	767
<b>Kinetics of Complexation</b> / <i>Donal H. Macartney</i> . . . . .	776
<b>Lariat Ethers</b> / <i>George W. Gokel</i> . . . . .	782
<b>Layered Supramolecular Solids and Their Intercalates</b> / <i>George K. H. Shimizu</i> . . . . .	791
<b>Light Scattering</b> / <i>Robin E. Westacott, Carolyn A. Koh</i> . . . . .	799
<b>Liquid Clathrates</b> / <i>Scott K. Spear, John D. Holbrey, Robin D. Rogers</i> . . . . .	804
<b>The Lock and Key Principle</b> / <i>Anatoly K. Yatsimirsky</i> . . . . .	809
<b>Luminescent Materials</b> / <i>Suning Wang, Corey Seward</i> . . . . .	816
<b>Luminescent Probes</b> / <i>Dmitri B. Papkovsky, Tomás C. O’Riordan</i> . . . . .	821
<b>Macrocycle Synthesis</b> / <i>Bernard Dietrich</i> . . . . .	830
<b>Mesoporous Materials</b> / <i>Sheng Dai, Craig E. Barnes</i> . . . . .	845
<b>Mesoporous Silica and Silica–Organic Hybrids</b> / <i>Abdelhamid Sayari</i> . . . . .	852
<b>Micelles and Vesicles</b> / <i>Raoul Zana</i> . . . . .	861
<b>Mineralomimetic Structures</b> / <i>Toschitake Iwamoto</i> . . . . .	868
<b>Modulated Structures</b> / <i>Gervais Chapuis</i> . . . . .	873
<b>Molecular Biomimetics</b> / <i>Philip Ball</i> . . . . .	879
<b>Molecular Clefts and Tweezers</b> / <i>Michael Harmata</i> . . . . .	887
<b>Molecular Logic Gates</b> / <i>Gareth J. Brown, A. Prasanna de Silva, Sheenagh M. Weir</i> . . . . .	893
<b>Molecular Modeling and Related Computational Techniques</b> / <i>Manuela Grotjahn, Torsten Rambusch, Karsten Gloe, Leonard F. Lindoy</i> . . . . .	901
<b>Molecular Squares, Boxes, and Cubes</b> / <i>Peter H. Dinolfo, Shih-Sheng Sun, Joseph T. Hupp</i> . . . . .	909
<b>Molecular Switches</b> / <i>Ruud G. E. Coumans, Alan E. Rowan</i> . . . . .	917
<b>Molecular Wires</b> / <i>Franco Scandola</i> . . . . .	925
<b>Molecular-Level Machines</b> / <i>Vincenzo Balzani, Alberto Credi</i> . . . . .	931
<b>Naked Anion Effect</b> / <i>Dario Landini, Angelamaria Maia</i> . . . . .	939
<b>Nanocasting Strategies and Porous Materials</b> / <i>Sebastian Polarz</i> . . . . .	950
<b>Neutron Diffraction</b> / <i>Chick C. Wilson</i> . . . . .	959

<b>Nomenclature in Crystal Engineering</b> / Ashwini Nangia	967
<b>Nonlinear Optical Materials</b> / Ravi Mosurkal, Lynne A. Samuelson, Jayant Kumar	973
<b>Nuclear Magnetic Resonance Spectroscopy</b> / Arvin Moser, Christian Detellier	981
<b>Nuclear Quadrupole Resonance Spectroscopy</b> / John A. S. Smith	989
<b>Organic Zeolites</b> / Tino Hertzsch, Jürg Hulliger, Edwin Weber, Piero Sozzani	996
<b>Organometallic Anion Receptors</b> / Paul D. Beer, Elizabeth J. Hayes	1006
<b>Organometallic Oligomers and Polymers</b> / Alaa S. Abd-El-Aziz	1014
<b>O<sub>2</sub> Uptake and Transport, Models of</b> / James P. Collman, Katja E. Berg	1023
<b>Peptide Nanotubes</b> / Carl Henrik Görbitz	1035
<b>Phase-Transfer Catalysis in Environmentally Benign Reaction Media</b> / Silvio Quici, Amedea Manfredi, Gianluca Pozzi	1042
<b>Photochemical Sensors</b> / Luigi Fabbrizzi	1053
<b>Photophysical and Photochemical Methods</b> / Pavel Anzenbacher, Jr., Michael A. J. Rodgers	1060
<b>Phthalocyanines</b> / Marco Evangelisti	1069
<b><math>\pi</math>-<math>\pi</math> Interactions: Theory and Scope</b> / Ian Dance	1076
<b><math>\pi</math>-<math>\pi</math> Stacking as a Crystal Engineering Tool</b> / Stuart L. James	1093
<b>Platonic and Archimedean Solids</b> / Leonard R. MacGillivray	1100
<b>Podands</b> / Edwin Weber	1106
<b>Polarity Formation: Markov Chain Model</b> / Jürg Hulliger	1120
<b>Polymorphism</b> / Mino R. Caira	1129
<b>Porphyrin Derivatives, Functional</b> / Mladen Žinić	1139
<b>Porphyrin-Based Clathrates</b> / Israel Goldberg	1150
<b>Preorganization and Complementarity</b> / John C. Sherman	1158
<b>Protein Supramolecular Chemistry</b> / Jörg Andrä, Patrick Garidel, Klaus Brandenburg	1161
<b>Protonated Aza-Macrocycles for Anion Complexation</b> / José M. Llinares, Kristin Bowman-James	1170
<b>Pyrrole- and Polypyrrole-Based Anion Receptors</b> / Philip A. Gale, Jonathan L. Sessler, Salvatore Camiolo	1176
<b>Racks, Ladders, and Grids</b> / Marius Andruh	1186
<b>Rotaxanes and Pseudorotaxanes</b> / Petra Linnartz, Christoph A. Schalley	1194
<b>Scanning Tunneling Microscopy</b> / Lucidalva S. Pinheiro	1202
<b>Second-Sphere Coordination</b> / Derek A. Beauchamp, Stephen J. Loeb	1209
<b>Secondary Bonding</b> / Ionel Haiduc	1215
<b>Selectivity: Thermodynamic and Kinetic</b> / Franz P. Schmidtchen	1225
<b>Self-Assembling Capsules</b> / Dmitry M. Rudkevich	1231
<b>Self-Assembling Catenanes</b> / Gerhard F. Swiegers, Junhua Huang	1240
<b>Self-Assembly: Definition and Kinetic and Thermodynamic Considerations</b> / Jim A. Thomas	1248
<b>Self-Assembly in Biochemistry</b> / Tamara D. Hamilton, Leonard R. MacGillivray	1257
<b>Self-Assembly: Terminology</b> / Gerhard F. Swiegers	1263
<b>Semiochemistry</b> / Antony M. Hooper, John A. Pickett	1270
<b>Siderophores</b> / Robert C. Hider, Zu Dong Liu	1278
<b>Simultaneous Binding of Cations and Anions</b> / Bradley D. Smith, Joseph M. Mahoney	1291
<b>Simultaneous Binding of Cations and Neutral Molecules</b> / Michael J. Hardie	1295
<b>Soft and Smart Materials</b> / Dmitriy V. Soldatov	1302
<b>Solid-State Nuclear Magnetic Resonance Spectroscopy</b> / John A. Ripmeester, Christopher I. Ratcliffe	1307



<b>Solid-State Reactivity/Topochemistry</b> / Leonard R. MacGillivray, Giannis S. Papaefstathiou . . . .	1316
<b>Solvation Effects in Guest Binding</b> / Mikhail Rekharzsky, Yoshihisa Inoue . . . . .	1322
<b>Solvatochromism</b> / Marcos Caroli Rezende . . . . .	1330
<b>Space Groups and Crystal Packing Modes</b> / Chick C. Wilson . . . . .	1337
<b>Spherands</b> / John C. Sherman . . . . .	1344
<b>Spontaneous Formation of Homochiral Supramolecular Architectures</b> / Yasuhiro Ishida . . . . .	1349
<b>Stability Constants: Definition and Determination</b> / Peter Gans, Alberto Vacca . . . . .	1360
<b>Steroid-Based Anion Complexation Agents</b> / Anthony P. Davis . . . . .	1365
<b>Strict Self-Assembly and Self-Assembly with Covalent Modifications</b> / Bruce C. Gibb . . . . .	1372
<b>Strong Hydrogen Bonds</b> / Christer B. Aakeröy . . . . .	1379
<b>Structural Engineering in Organic–Inorganic Perovskites</b> / Karen R. Maxcy, Roger D. Willett . . . . .	1387
<b>Supermicroscopy: AFM, SNOM, and SXM</b> / Steven De Feyter, Frans C. De Schryver . . . . .	1394
<b>Supramolecular Chemistry: Definition</b> / Jonathan W. Steed . . . . .	1401
<b>Supramolecular Electrochemistry</b> / Angel E. Kaifer . . . . .	1412
<b>Supramolecular Isomerism</b> / Martin Schröder, Neil R. Champness . . . . .	1420
<b>Supramolecular Libraries</b> / Sijbren Otto, Jeremy K. M. Sanders . . . . .	1427
<b>Supramolecular Photochemistry</b> / Sandra Monti, Francesco Barigelletti . . . . .	1434
<b>Supramolecular Polymers</b> / Alberto Ciferri . . . . .	1443
<b>Supramolecular Stabilization</b> / Dmitriy V. Soldatov, John A. Ripmeester . . . . .	1453
<b>Surfactants, Part I: Fundamentals</b> / John F. Scamehorn, David A. Sabatini, Jeffrey H. Harwell . . . . .	1458
<b>Surfactants, Part II: Applications</b> / John F. Scamehorn, David A. Sabatini, Jeffrey H. Harwell . . . . .	1470
<b>Swelling Clays (Smectites) and Nanofilms</b> / Robert A. Schoonheydt . . . . .	1478
<b>Tectons: Definition and Scope</b> / Pierangelo Metrangolo, Giuseppe Resnati . . . . .	1484
<b>The Template Effect</b> / Daryle H. Busch . . . . .	1493
<b>Thiourea Inclusion Compounds</b> / Kenneth D. M. Harris . . . . .	1501
<b>Torands</b> / Thomas W. Bell . . . . .	1508
<b>Tröger's Base Derivatives</b> / Gerd Kaupp . . . . .	1516
<b>Unimolecular Electronics and Unimolecular Rectifiers</b> / Robert M. Metzger . . . . .	1525
<b>Urea Inclusion Compounds</b> / Kenneth D. M. Harris . . . . .	1538
<b>van der Waals Forces</b> / Hans-Jörg Schneider . . . . .	1550
<b>Vibrational Spectroscopy</b> / Carolyn A. Koh . . . . .	1557
<b>Viruses as Host Assemblies</b> / Michelle Flenniken, Mark Allen, Mark Young, Trevor Douglas . . . . .	1563
<b>Vitamin B<sub>12</sub> and Heme Models</b> / Sabine Van Doorslaer . . . . .	1569
<b>Weak Hydrogen Bonds</b> / Motorhiro Nishio . . . . .	1576
<b>X-Ray Crystallography</b> / Kari Rissanen . . . . .	1586
<b>X-Ray and Neutron Powder Diffraction</b> / John S. O. Evans . . . . .	1592
<b>Zeolites in the Petroleum Industry</b> / Christian Marcilly (Retired) . . . . .	1599
<b>Zeolites: Catalysis</b> / Takashi Tatsumi . . . . .	1610
<b>Zeolites: Separation Science</b> / Toshinori Tsuru, Yuko Takata . . . . .	1617
<b>Zeolites: Structures and Inclusion Properties</b> / Jiří Čejka . . . . .	1623
<b>Zinc-Containing Enzymes and Their Models</b> / Takashi Hayashi . . . . .	1631
<b>Zwitterion Receptors</b> / Stefano Di Stefano, Luigi Mandolini, Perla Breccia, Javier de Mendoza . . . . .	1639





## Preface

Chemistry has witnessed a phenomenal change in the last decades of the twentieth century. Research in two areas in particular have driven the emergence and significance of supramolecular chemistry. Since the Nobel prize-winning work of Cram, Lehn, and Pedersen in the late 1960's and early 1970's, work in solution host guest compounds, and latterly self-assembling and self-organizing systems, has seen a veritable explosion. The older field of solid-state inclusion chemistry has, to a very great extent, paralleled these developments with a great deal of recent effort in crystal engineering being regarded as solid-state supramolecular synthesis. Both subfields rely crucially on an understanding of the noncovalent bond—the quintessence of supramolecular chemistry. The evolution of these areas underscores the dynamic growth of supramolecular research and the explosion of interest in the field.

Clearly one of the most important goals of the *Encyclopedia of Supramolecular Chemistry* then is to provide a broad-based overview of the discipline and to capture the significance of research in this area, with special emphasis on a synthesis of the concepts and language of supramolecular chemistry across a wide range of related disciplines. Furthermore, this Encyclopedia is not written by, nor written exclusively for “supramolecular chemists”; it is for students and practitioners of the chemistry (indeed science) of the noncovalent bond wherever it occurs. We have made specific efforts to direct the reader to the defining literature in the field and specifically included cross-references to help the researcher locate other entries of interest.

We hope that this two-volume work will become a useful and well-thumbed source of information and ideas, as well as a helpful teaching aid as courses in intermolecular interactions continue to grow. If browsing through this work stimulates a new idea or a new collaboration from an unusual combination of topics, or if it clarifies a point of confusion for an undergraduate or senior researcher, then we will have succeeded.

As editors, we would very much like to thank the very many contributors and the members of the Editorial Advisory Board who have donated their time and insights to this work. It is very much a community effort and we have spent more time listening and nodding, than talking. Finally, we would like to express our heartfelt thanks to the editorial and production staff at Marcel Dekker, Inc. who have organized the monumental task of gathering together all of the elements of such a diverse production. We are especially grateful to Oona Schmid not just for her extremely hard work, but also for her insight into the needs of this work and the community as a whole.

*Jerry L. Atwood*  
Columbia, Missouri, U.S.A.

*Jonathan W. Steed*  
Durham, United Kingdom  
July 2003



# Foreword

Molecular chemistry has, over many years, developed a wide range of very powerful procedures for constructing ever more sophisticated molecules from atoms linked by covalent bonds. Beyond molecular chemistry lies supramolecular chemistry which aims at setting up highly complex chemical systems from components interacting via noncovalent intermolecular forces.

The concept and the term supramolecular chemistry were introduced in 1978, in the words: "Just as there is a field of molecular chemistry based on the covalent bond, there is a field of supramolecular chemistry, the chemistry of molecular assemblies and of the intermolecular bond," reformulated on various occasions, e.g., "Supramolecular chemistry may be defined as 'chemistry beyond the molecule,' bearing on the organized entities of higher complexity that result from the association of two or more chemical species held together by intermolecular forces."

The breadth and especially the unifying power of the concept became progressively more and more apparent, so that recent years have seen an explosive growth, as measured by the increasing number of laboratories that join the field and whose work has been reported in a vast range of publications, books, journals, meetings, and research networks.

By the appropriate manipulation of noncovalent interactions, supramolecular chemistry became the chemistry of molecular information, involving the storage of information at the molecular level, in the structural features, and its retrieval, transfer, processing at the supramolecular level, through molecular recognition processes operating via specific interactional algorithms. A further step consisted of the design of systems undergoing self-organization, i.e., systems capable of spontaneously generating well-defined supramolecular architectures by self-assembly from their components under the control of the molecular information stored in the covalent framework of the components and read out at the supramolecular level through specific interactions. Self-organization processes thus represent the operation of programmed chemical systems leading to the specific generation of well-defined entities.

The design of such molecular information-controlled, "programmed," and functional self-organizing systems provides an original approach to nanoscience and nanotechnology, offering a powerful alternative/complement to nanofabrication and to nanomanipulation.

Supramolecular chemistry is also intrinsically a dynamic chemistry in view of the lability of the interactions connecting the molecular components of a supramolecular entity and the resulting ability of supramolecular species to exchange their constituents. Thus, in addition to self-organization by design, which strives to achieve full control over the output supramolecular entity by explicit programming, a new development resides in the implementation of self-organization by selection, operating on dynamic constitutional diversity in response to either internal or external factors to achieve adaptation.

From molecular recognition to self-organization, to programmed chemical systems, supramolecular chemistry progressively leads up the ladder of complexity and opens new horizons for chemistry toward a science of informed, organized, and adaptative matter.

Supramolecular chemistry is a highly interdisciplinary field of science. A major feature is the range of perspectives offered by the cross-fertilization of supramolecular chemical research

due to its location at the intersection of chemistry, biology, and physics. Drawing on the physics of organized condensed matter and extending to the complex entities and processes of biology, supramolecular chemistry expands into a supramolecular science. It has penetrated such diverse areas as for instance: polymer chemistry and materials science, solid-state chemistry and crystal engineering, species for nonlinear optics, biological interactions and drug design, sensor and diagnostic procedures, nanoscience and nanotechnology, etc.

Supramolecular chemistry has thus become a highly diverse but coherent and lively body of concepts and objects, generating and incorporating novel areas of investigation. Such wide horizons are a challenge and a stimulus to the creative imagination of the chemist.

As a new field of science emerges, grows, and matures, it generates novel terminology to name the concepts that define it and to describe the objects that constitute it. The language of supramolecular chemistry, its vocabulary, and syntax have been progressively developed, leading to the introduction of new terms or to the reappropriation of old ones.

Such conceptualizing and naming play a very important role, not only for shaping the field but also by the ground they offer to the creative imagination. Indeed, one may let one's imagination be carried by the magic of the word and pulled by the evocative and stimulating power of the concept.

It is clear that the time is ripe for an *Encyclopedia of Supramolecular Chemistry*, presenting its basic concepts, its various objects, and processes as well as its relations to other areas of basic and applied science. It will be of great value to the many practitioners in the field as well as to those, perhaps even more numerous newcomers, who wish to get acquainted with it and may wish to join the family and become part of the adventure!

The editors and authors deserve our warmest thanks for their timely work to the benefit of the common good.

*Jean-Marie Lehn*  
Strasbourg, France  
September 2003

#### *General references*

- Lehn, J.-M. *Supramolecular chemistry: Concepts and perspectives*. VCH Weinheim **1995**.
- Lehn, J.-M. *Supramolecular Chemistry/Science—Some Conjectures and Perspectives*. In *Supramolecular Chemistry: Where It Is and Where It Is Going*; Ungaro, R., Dalcanale, E., Eds.; Kluwer: Dordrecht, 1999; 287–304.
- Lehn, J.-M. Toward complex matter: Supramolecular chemistry and self-organization. *Proc. Natl. Acad. Sci. USA*, **2002**, 99, 4763.

# Alkali Metal Cations in Biochemistry

**Yoshiyaki Kobuke**

*Nara Institute of Science and Technology, Nara, Japan;  
CREST, Japan Science and Technology, Nara, Japan*

**Shin-ichi Kugimiya**

*Nara Institute of Science and Technology, Tokyo, Japan*

## INTRODUCTION

Alkali metals easily lose one electron at the outer *s*-shell to form singly charged cations. Among these, the  $\text{Na}^+$  and  $\text{K}^+$  ions play the most important biological roles. Because of the weak and nonspecific nature of the interaction with other ligands, the biological significance is determined primarily by the magnitude of the concentrations. Similar chemical principles are applicable in a series of alkaline earth metal cations, except these are doubly positively charged. Moreover, the sizes become smaller, because the biologically important  $\text{Mg}^{2+}$  (0.60 Å) and  $\text{Ca}^{2+}$  (1 Å) ions correspond to  $\text{Li}^+$  (0.6 Å) and  $\text{Na}^+$  (0.95 Å) ions, respectively. These concentrations of the alkali and alkaline earth metal ions reflect those of seawater, and this coincidence evidences that the first life was born in archeological seawater. Therefore, the “physiological salt solution” employs concentrations in which  $\text{Na}^+ > \text{K}^+ > \text{Mg}^{2+} > \text{Ca}^{2+}$ . This order, however, shows a discrepancy from the one found in the earth’s crust, where Ca, Na, K, and Mg occupy the fifth to the eighth elements in this order. The reason for this difference is that the  $\text{Ca}^{2+}$  ion is selectively eliminated from solution by the tendency to form insoluble precipitates such as  $\text{CaCO}_3$  or  $\text{Ca}_4(\text{PO}_4)_3$ . According to this tendency,  $\text{CaCO}_3$  is accumulated in rocks, and  $\text{Ca}_4(\text{PO}_4)_3$  is an important component of bone and tooth in the biological systems.

Dominant alkali metal ions,  $\text{Na}^+$  and  $\text{K}^+$ , are highly soluble in aqueous solution and are the most important components in maintaining the salt concentrations inside and outside the cell, necessary to keep homeostasis of biological cells. At the same time, their single charge is associated with relatively small solvation energies, 98.5 and 80.5 kcal mol<sup>−1</sup> for  $\text{Na}^+$  and  $\text{K}^+$  ions, respectively, reflecting the size difference on delocalizing the positive charges. These ions are most appropriately employed as messengers of biological signal transduction by mass (i.e., charge) transport across the membrane.<sup>[1]</sup> Compared to these ions,  $\text{Mg}^{2+}$  with two positive charges is constrained in a small atomic volume and must compensate by strong ion pairing with anionic counterparts of high charge densities. Phosphate anions are the most satisfactory as a

pair component, and Mg – phosphates behave like molecules in many chemical events. The high solvation energy of the  $\text{Mg}^{2+}$  ion (454 kcal mol<sup>−1</sup>) makes it difficult to use as the charge messenger of signal transduction.

The  $\text{Ca}^{2+}$  ion possesses properties that are intermediate, and it is associated with various biologically important roles. It does not favor any specific coordination structure but still interacts strongly with ligands, especially with an oxygen anion, to alter the charged state and geometrical structure of the ligands, just as transition metal ions do. At the same time, the  $\text{Ca}^{2+}$  ion can be transferred into the cell across the biological membrane, in spite of its high hydration energy (379 kcal mol<sup>−1</sup>), and plays a role as a second messenger in the cell. For example, acetylcholine is ejected into a synaptic crevasse triggered by the entry of a  $\text{Ca}^{2+}$  ion. However, the presence of the  $\text{Ca}^{2+}$  ion in the cell is hazardous because of its wide spectrum of actions and is eliminated from the inside cell and stored in endocellular cavities immediately after the completion of the specific role. When the  $\text{Ca}^{2+}$  concentration is monitored by, e.g.,  $\text{Ca}^{2+}$ -specific sensors, a  $\text{Ca}^{2+}$  wave can actually be observed. When this control system is destroyed, cells suffer fatal damage. For example, Alzheimer’s and other related diseases are believed to induce such an uncontrolled entry of  $\text{Ca}^{2+}$  ion and to cause fatal damage to nerve cells. The entry of the  $\text{Ca}^{2+}$  ion was demonstrated by single channel measurements, and its close relationship with diseases was invoked.<sup>[2]</sup>

## BIOLOGICAL ENERGY CONVERSION AND ION CHANNELS

A biological energy conversion system stores energy first in the form of a proton concentration gradient across the biological membrane via coupled electron and proton transport using the action of a photosynthetic or metabolic energy-producing pathway in many plants and animals.<sup>[3]</sup> This is a universal expression of energy storage, but it relies on the presence of the membrane as the separation barrier of the  $\text{H}^+$ -concentration gradient and must be

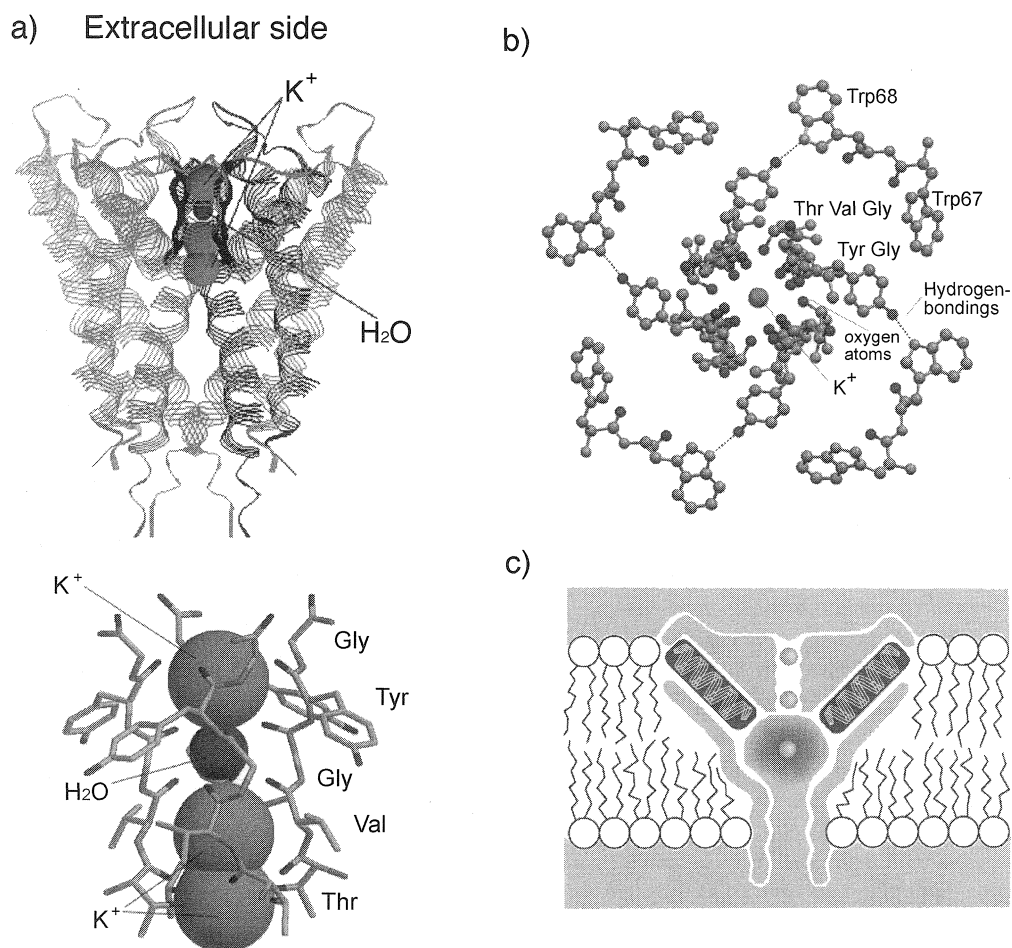


**Fig. 1** Crystal structure of  $K^+$  channel from *Streptomyces lividans*. a) Top: A ribbon representation of the KcsA tetramer viewed from the side. The four subunits are distinguished by color. Selectivity filter (black sticks) locates extracellular side in interface.  $K^+$  ions are represented by green spheres. Bottom: Selectivity filter with four chains represented are comprised of the signature sequence amino acids Thr, Val, Gly, Tyr, Gly running from bottom to top. Two  $K^+$  ions (green) are located at opposite ends of the selectivity filter, roughly 7.5 Å apart, with a single water molecule (red) in between. The inner  $K^+$  is in rapid equilibrium between adjacent coordination sites. b)  $K^+$  channel selectivity filter viewed from the extracellular side. Carbonyl oxygens of the main chain Thr75-Gly79, and the side chain of the Thr are shown as red spheres. The Tyr side chains are directed away from the ion conduction pathway. Blue dotted line represents hydrogen-bondings. c) Overall representation of  $K^+$  channel stabilizing a cation in the middle of the membrane. A large aqueous cavity stabilizes an ion (green) in the otherwise hydrophobic membrane interior. Oriented helices point their partial negative charge (carboxyl end, red) toward the cavity. Fig. 1a and b were produced with a PDB file (code: 1BL8.pdb from Ref. [5]) and Raswin Molecular Graphics (version 2.7.2, Glaxo Research and Development, U.K.).

converted to another form of stable energy in order to be transferred to the spot where energy is required. This transformation is accomplished by  $H^+$ -ATPase, where the vectorial proton flux across the membrane can produce adenosine triphosphate as molecular energy or the so-called “energy coin.” This energy in the form of pyrophosphate bonds can be transported to numerous energy-demanding organs. Around one-third to one-fourth of this ATP is then consumed for the generation of  $Na^+/K^+$  concentration gradient across the membrane of nerve cells through the action of  $Na^+/K^+$ -ATPase.<sup>[4]</sup>

Consumption of one molecule of ATP transports  $3Na^+$  and  $2K^+$  ions outside or inside the cell, respectively. These concentration gradients are maintained across the impermeable membrane, but large ionic fluxes are generated once these ions become permeable through the membrane. This ion-permeating device, the ion channel, is a molecular machine of signal transduction located in the brain and nervous systems.<sup>[1]</sup> Ion transport across the membrane, generally in a form of a large flux, induces a rapid change of membrane potentials. The opening and closing of the ion channels are controlled by



the gate systems equipped intrinsically in the channel. Ion channels can recognize cation and anion and  $K^+/Na^+$  ions with high selectivities. Once a  $Na^+$  channel is opened,  $Na^+$  ions accumulated outside the membrane enter into the cell, shifting the membrane potential toward a positive value. This channel is then inactivated and followed by the opening of a  $K^+$  channel to shift the potential toward a negative value by the outflux of  $K^+$  ions. The temporary shift of the membrane potential is large enough to induce the opening of a second  $Na^+$  channel, located close to the first channel, and a second cycle follows. In this way, the wave of membrane potential, termed an “action potential,” is transferred along the nerve axon. The ion channel is regarded, therefore, as a molecular device of signal transduction, relying on  $Na^+$ ,  $K^+$ ,  $Ca^{2+}$ , and  $Cl^-$  ions as the predominant messengers.

The chemistry of alkali and alkaline earth metal ions is understood most comprehensively through analyzing the function of ion channels, especially mechanisms of ion selectivity and gating. An ion channel with a typical conductance of 10 pS allows the passage of  $5 \times 10^6$  ions per second through a single molecular pore. Even operating at such large ionic fluxes, ion channels generally discriminate between different ionic species, for example, cation and anion and  $K^+/Na^+$ , by passing them through the selectivity filter. Permeability ratios,  $P_{Na}/P_K$ , for several  $K^+$  channels are less than  $0.01 \sim 0.07$ .<sup>[1]</sup> This remarkable selectivity of  $K^+$  may be understood by examining how the structure of a selectivity filter manages different

hydration energies and ionic radii. In this article, recent advances in this area will be described in light of mechanisms of high selectivity and gating based on x-ray crystallographies. Furthermore, approaches to the construction of artificial ion channels are focused on these specific functions.

## STRUCTURE OF ION CHANNELS

### X-Ray Analysis of Selectivity Filter and Ion-Conducting Mechanism

The first x-ray crystal structure of an ion channel appeared in 1998 from MacKinnon's group (Fig. 1).<sup>[5]</sup> The structure of the selectivity filter forced scientists to abandon the previous hypothesis that  $K^+$  ion should be stabilized by cation- $\pi$  interactions in the aromatic cage when surrounded by four tyrosine residues. In the selectivity filter located near the extracellular surface, one Thr OH and four main-chain amide carbonyls from Val-Gly-Tyr-Gly are lined up in a 12 Å length. Because the  $K^+$  channel is composed of four identical subunits, this provides four consecutive spherical cavities for  $K^+$  binding by wrapping each  $K^+$  with eight neutral oxygen atoms. This mode of binding is reminiscent of valinomycin and sandwiched crown complexes. The Tyr unit does not contribute to the direct stabilization, but it is directed outwardly toward the pore and interacts with a Trp residue by a phenolic

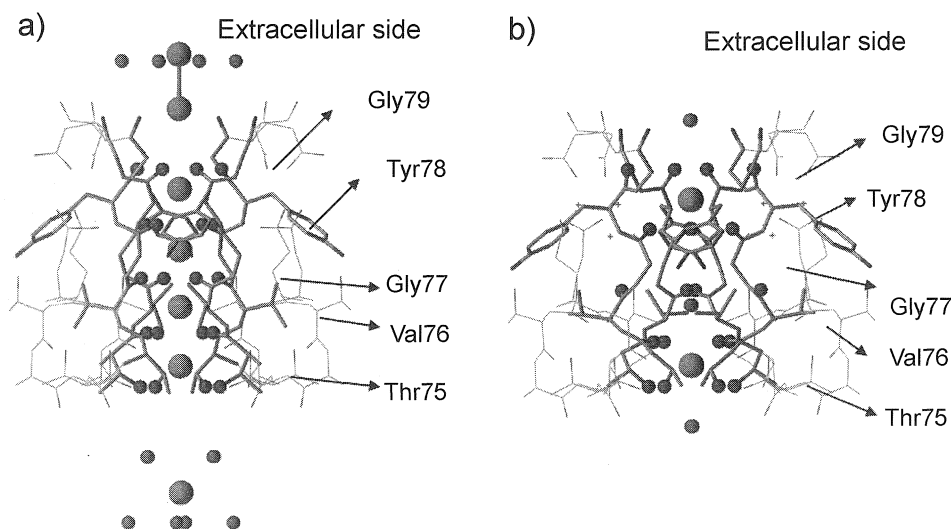


**Fig. 2** Crystal structures of  $K^+$  ion channel with different  $K^+$  concentrations. a)  $K^+$  channel selectivity filter with high concentration of  $K^+$  ions (green spheres) along the ion pathway, and water molecules (pink spheres) in the vicinity. b)  $K^+$  channel selectivity filter with low  $K^+$  concentration of  $K^+$  ion (green spheres). Main-chains of the selectivity filter are disordered. Fig. 2a and b were produced with PDB files (code: 1K4C and 1K4D from Ref. [8]) and ViewerLite (version 5.0 Accelrys. Inc., U.K.).

$\text{OH} \cdots \text{N}$  (indolyl) hydrogen bond (Fig. 1b). This unit may keep the pore wide and contribute to the  $\text{K}^+/\text{Na}^+$  selectivity through decreasing the stabilizing power for a smaller  $\text{Na}^+$  ion. The selectivity filter is composed completely of neutral oxygen atoms in favor of stabilizing the  $\text{K}^+$  rather than the  $\text{Na}^+$  ion, which demands stronger electrostatic interactions. The selectivity filter of the  $\text{Na}^+$  ion is believed to contain ionic pairs,<sup>[6]</sup> and its structural elucidation is highly desirable. Furthermore, the selectivity ratio  $P_{\text{K}}/P_{\text{Na}}$  of this  $\text{K}^+$  channel KcsA shows only a moderate value of 11,<sup>[7]</sup> and it is interesting to imagine how highly selective  $\text{K}^+$  channels introduce any additional recognition principle(s). Another characteristic point of this x-ray structure is that the transmembrane pore contains a large water pool in the middle of the membrane, to which helical negative dipoles direct. Further, the inner half of the conduction pathway is lined with hydrophobic side chains and is wide enough to be filled completely with water molecules. These are thought to be features that allow a high throughput of  $\text{K}^+$  ions (Fig. 1c).

The above selectivity filter constrained two  $\text{K}^+$  ions about 7.5 Å apart. This configuration was thought to promote ion conduction by electrostatic repulsion. With an increased resolution, MacKinnon also determined two crystal structures at high and low  $\text{K}^+$  concentration states.<sup>[8]</sup> At the high concentration, they found four  $\text{K}^+$  ions in the selectivity filter instead of two, and two more hydrated  $\text{K}^+$  ions at its extracellular entryway. Further-

more, the  $\text{K}^+$  ion in the central cavity was fully surrounded by eight water molecules. All of these  $\text{K}^+$  ions were embedded in a square antiprismatic geometry by water, carbonyl, and hydroxyl oxygen-donor ligand groups (Fig. 2). These ordered water molecules make dehydration and hydration interconversion processes of  $\text{K}^+$  ion at both entryways easy. The similarity of the coordination structures, one at the central cavity, four in the selectivity filter, and two at the extracellular entryway, can promote the smooth structural interconversion and explain the rapid transport of  $\text{K}^+$  ion through the  $\text{K}^+$  channel.

The  $\text{Cl}^-$  channel is a physiological counterpart of cation channels, and the analysis of  $\text{Cl}^-$  selectivity may contribute to the true understanding of the whole series of ion selectivities. In the x-ray crystal structure of the closed state of the  $\text{Cl}^-$  channel, two  $\text{Cl}^-$  ions detected inside the pore were stabilized by hydrogen bonding with main-chain amide NH and side-chain hydroxyl groups of Ser and Tyr (Fig. 3).<sup>[9,10]</sup>

### Gating Mechanisms of Ion Channels

Gating is one of the principal functions of ion channels. Ion permeation occurs only when the corresponding ion channels open on accepting their own stimuli. This gating information is classified into three types: voltage across the membrane (voltage-gated); binding of ligands such as neurotransmitters or second messengers (ligand-gated); and membrane deformation (mechanosensitive). In any event, in opening the gate, massive mechanical variations of channel structure must be performed when responding to the sensor unit. Recent developments in crystallographic structure determination enabled the identification of the open and closed states of several ion channels and discussion of the mechanisms based on these experimental structures.

In voltage-dependent  $\text{K}^+$  channels, the number of gating charges amounts to 12–14 electron charges as a result of the assembly of four identical subunits having 3–3.5 charges. This large gating charge responds sharply to change of the membrane voltage. X-ray analysis elucidated the movement of this gating charge across the membrane, as shown in Fig. 4.<sup>[11,12]</sup> Here, the sensor units are composed of a highly conserved Arg-rich domain in the S4 helix. Its movement across almost the entire membrane can deform the channel geometry from trapezoidal to cylindrical forms and open the central pore (Fig. 4b). This new proposal differs from the conventional hypothesis of charge movement within the “gating pore.”<sup>[13]</sup>

Voltage-dependent  $\text{K}^+$  channels close by a process called “inactivation,” rapidly after opening. In *Drosophila* mutant  $\text{K}^+$  channels, the cytoplasmic amino terminus in its own channel forms the inactivation gate. The central

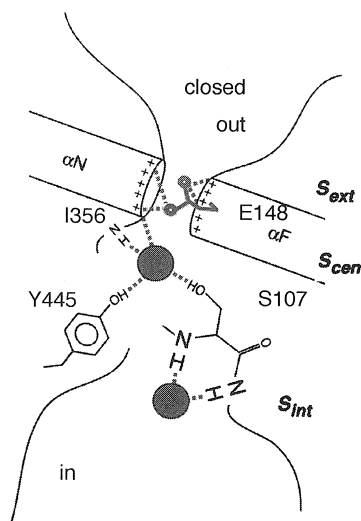


**Fig. 3** Schematic illustration of the closed conformation of a ClC chloride channel. The ion-binding sites  $S_{\text{int}}$  and  $S_{\text{cen}}$  are occupied by chloride ions (red sphere) stabilized by  $\text{Cl}^- \cdots \text{H}$  hydrogen bondings (dashed lines). The external ion-binding site  $S_{\text{ext}}$  constitutes the gate and is blocked by the side chain of Glu148 (red).

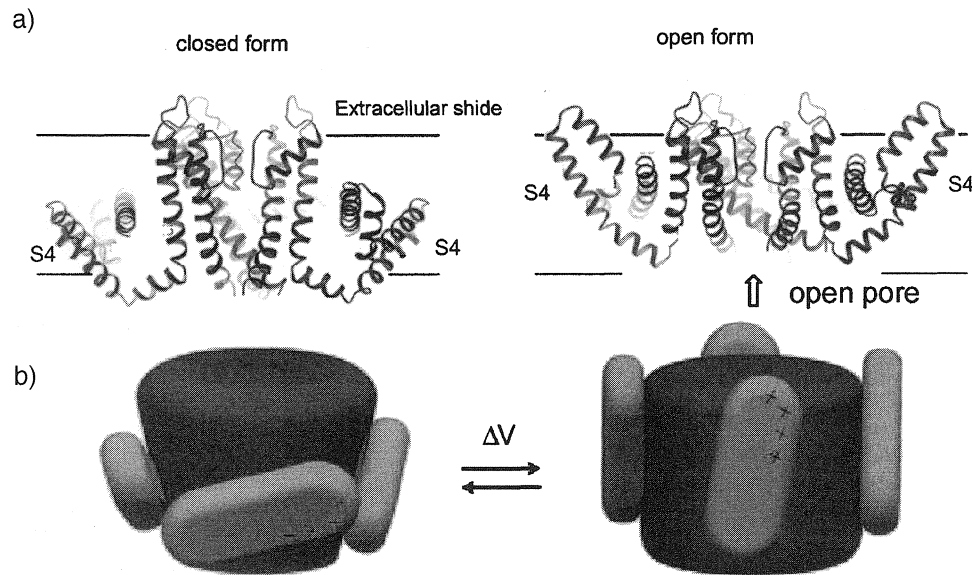


**Fig. 4** Movement of voltage-sensor in voltage-gated  $K^+$  channel. a) Positions within the membrane of the voltage-sensor paddles S4 (red) during closed and opened conformations, with coupling to pore opening. b) Gating charges (red plus signs) are carried through the membrane from inside (bottom) to outside (top) by movements of the voltage-sensor paddles against the lipid membrane and the open pore.

cavity and the inner pore of the  $K^+$  channel provide the receptor site for the inactivation gate and inhibitors such as hydrophobic quaternary ammonium ions (Fig 5a).<sup>[14]</sup> The inactivation occurs by a sequential reaction, in which

the gate peptide is bound initially to the cytoplasmic channel surface and then enters the pore (Fig. 5b).

The structural basis of ligand gating was reported for a  $Ca^{2+}$ -gated  $K^+$  channel. Here, eight RCK (regulator of  $K^+$

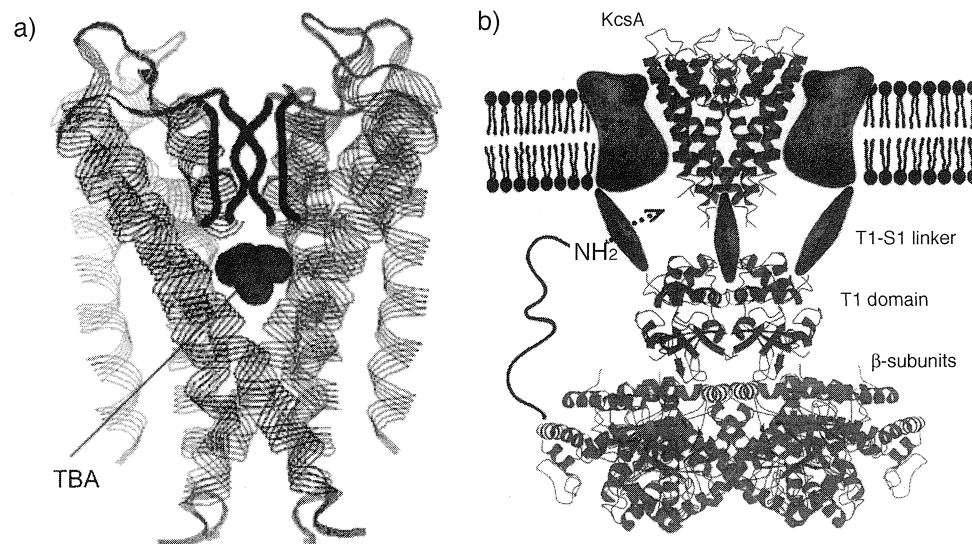


**Fig. 5** Inactivation of  $K^+$  channel. a) Crystal structure of KcsA  $K^+$  channel with a hydrophobic cation, tetrabutylammonium TBA. b) Composite model of a voltage-dependent  $K^+$  channel. The  $\alpha$ -subunit is shown in blue and the  $\beta$ -subunit in red. The pore is represented by the KcsA  $K^+$  channel (5) and the T1- $\beta$  complex (15). The structures of the linker (T1-S1) connecting the voltage sensors to the T1 domain are unknown. An N-terminal inactivation gate is shown entering a lateral opening to gain access to the pore. Fig. 5a was produced with a PDB file (1J95.pdb from Ref. [14]) and Raswin Molecular Graphics (version 2.7.2, Glaxo Research and Development, U.K.).

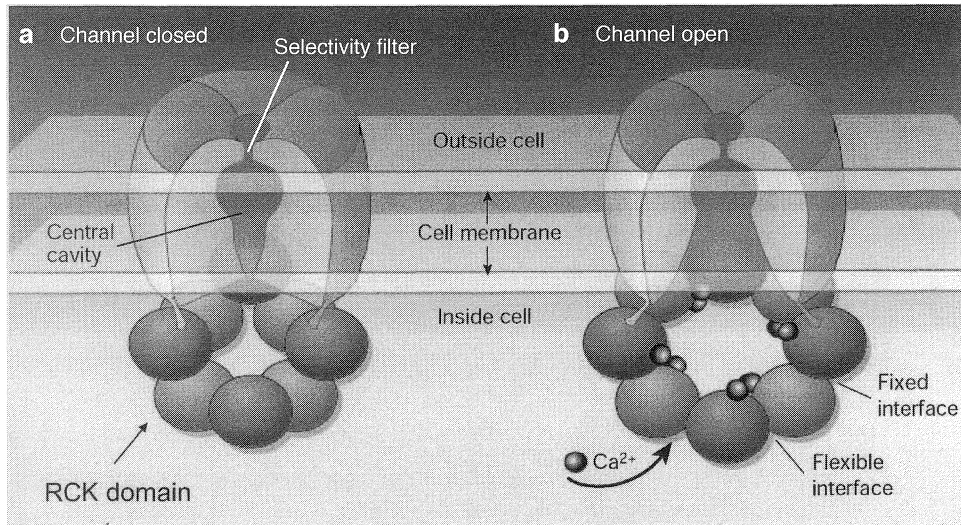


**Fig. 6** Schematic model for the gating and opening of a bacterial  $\text{Ca}^{2+}$ -gated  $\text{K}^+$  channel. a) The closed and b) the open conformations. Three of the four subunits of a  $\text{K}^+$  channel are shown in brown. The purple and red circles represent the eight RCK domains, which, after binding  $\text{Ca}^{2+}$ , are thought to deform with respect to each other, causing changes in the pore in the center of the channel.

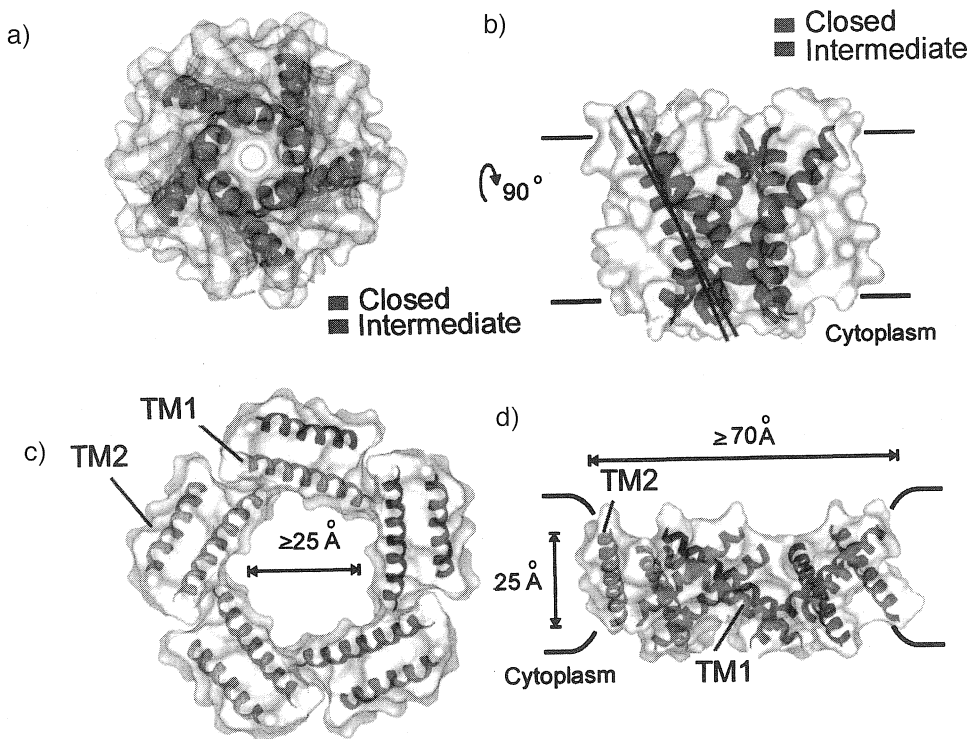


**Fig. 7** Modeling structure of the MscL transmembrane segments. a) Top view (from extracellular) and b) side view in the intermediate closed state (orange ribbon) compared with closed structure (green ribbon). Not much difference between closed and intermediate states. c) Top view of open form (from extracellular) with a wide open pore. d) Side view of the open form.

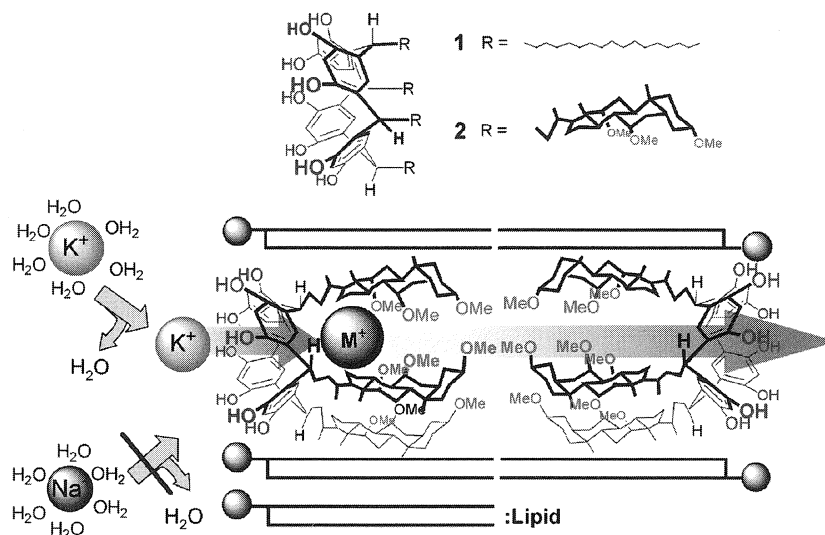


**Fig. 8** Chemical structures of molecular ion channels with K<sup>+</sup> ion selectivity, **1**, **2**. Schematic illustration of expected structures of a tail-to-tail dimer. The side chain opposite to the reader is eliminated for clarity.

conductance) domains assemble to form a large gating ring at the intracellular membrane surface. The cooperative binding of eight  $\text{Ca}^{2+}$  ions from the intracellular solution induces conformational change of the gating ring in such a way that it can open the inner helices of the pore to permit ion conduction. The gating behavior is shown schematically in Fig. 6, where the upper part forms an ion conduction pore in the membrane. The lower part from solution represents the RCK domain, where eight  $\text{Ca}^{2+}$  ions are bound allosterically.<sup>[16,17]</sup>

The open and closed conformations on binding ligands to the nicotinic acetylcholine receptor channel were already trapped and observed by electron microscopy. Here again, the cooperative binding of ligands induces large rotational movements of the pore-defining subunits.<sup>[18]</sup>

Mechanosensitive ion channels act as membrane-embedded mechanoelectrical switches that open a large pore in response to membrane deformations. It is a way of biological signal transformation of physical stresses such as touch and hearing to changes into electrochemical responses. The gating mechanism of a large-conductance mechanosensitive pentameric channel (MscL) was elucidated as shown in Fig. 7.<sup>[19,20]</sup> Transitions from the closed or intermediate state to the open states upon application of tension to the membrane are accompanied by massive rearrangements of the two transmembrane helices TM1 and TM2. The inner TM1, creating the bulk hydrophilic pore containing Thr, Lys, and Asp units, rotates along its principal axis and shifts away from the symmetrical axis to open the water-filled pore of 30–40 Å, leading to conductance at nano-Siemens levels (Figs. 7c,d).

## ARTIFICIAL ION CHANNELS

Construction of artificial ion channels according to simple principles<sup>[21,22]</sup> is interesting for obtaining molecular devices that mimic the biological signal transduction system. There are two ways to prepare ion-conducting artificial pores—molecular and supramolecular methodologies, along with modification of ionophoric antibiotics.

## Molecular Ion Channels

A macrocyclic resorcin[4]arene with four hydrophobic substituents in the axial position provides an ion-conducting molecular pore by tail-to-tail dimerization.<sup>[23]</sup> Because the pore size and characteristics of the entryway are defined explicitly by the molecule, only one conductance level is observed. The relatively simple structure is amenable to systematic structural modifications and is, therefore, appropriate in establishing the structure–function relationships. When a methyl ether derivative of cholic acid was employed as the axial substituent,<sup>[24]</sup> the conductance was increased by 50% to 9.9 *pS*, compared with the value 6.1 *pS* observed for **1** with simple alkyl substituents.<sup>[23]</sup> The cation and anion selectivity ratio  $P_K/P_{Cl}$  was 20 for **2**, showing a significantly larger selectivity factor compared to 8 for **1**. A hydrophilic molecular plane of methoxy substituents certainly contributes to the increase of conductance and a higher cation and anion selectivity by the arrangement of a more hydrophilic environment at the central pore. Both ion channels exhibited moderate  $K^+$  preferences compared to  $Na^+$  by a factor of ca. 3. The aromatic moiety provides a weak electric field



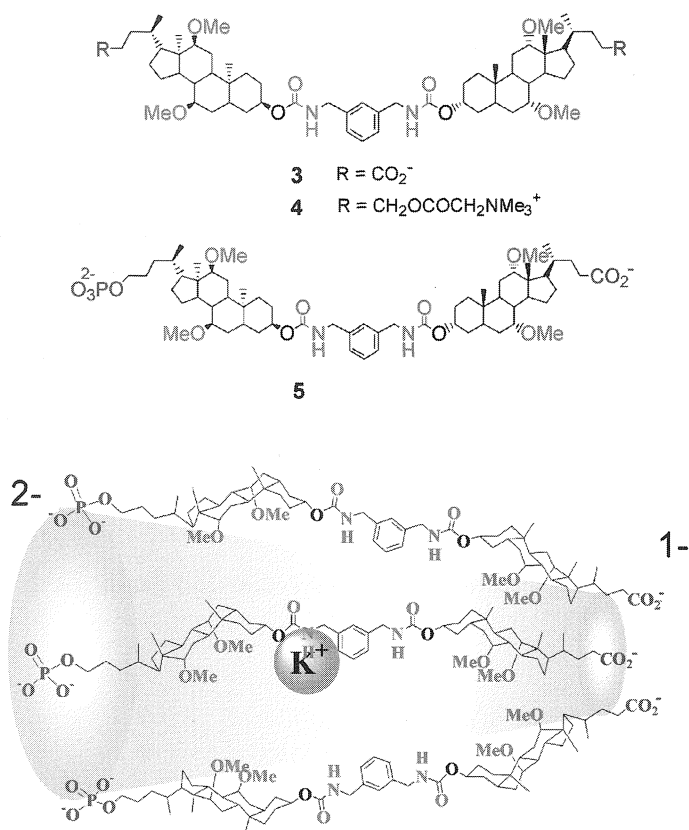


**Fig. 9** Chemical structure of supramolecular ion channels with K<sup>+</sup> ion selectivity, **3**, **4** and with voltage-dependent properties **5**. Schematic illustration of supramolecular ion channels **5** with different mouth diameters in bilayer lipid membranes.

that can desolvate the K<sup>+</sup> ion with a lower dehydration energy to pass through the cavity but can only partly desolvate the more hydrophilic Na<sup>+</sup> ion (Fig. 8). The inverse selectivities, a preference for Na<sup>+</sup> and Cl<sup>-</sup>, were not yet obtained, and their embodiment remains a challenging target in this field.

### Supramolecular Ion Channels

Besides synthesizing a molecular pore of a definite diameter, supramolecular pore formation provides an attractive alternative. This methodology is also adopted in Nature for the formation of the K<sup>+</sup> and acetylcholine receptor channels as homotetramer and heteropentamer, respectively.<sup>[1]</sup> The assembly number of artificial supramolecular channels is generally not controlled, and various levels of conductance are usually observed. Two cholic acid methyl ether derivatives were connected via bisurethane linkages to obtain a membrane-penetrating component in its extended conformation. The carboxylate **3** and ammonium **4** head groups provide supramolecular

ion channels showing stable open durations.<sup>[25,26]</sup> Both channels are cation selective, irrespective of different charges of head groups. The cation and anion selectivity values  $P_K/P_{Cl}$  were 17 and 7.9 for **3** with negative head groups, and **4** with positive head groups, respectively. Therefore, the terminal charges reasonably perturbed the entry of the cation relative to the anion. The discrimination factor between K<sup>+</sup> and Na<sup>+</sup> ions was again moderate,  $P_K/P_{Na}$  being three for both channels. The metal ion selectivity is determined primarily at the critical domain of the pore environment and is separated substantially from the charged head groups.

Two head groups of carboxylic and phosphoric acids were introduced to displace different charges at the ends of the membrane-penetrating cholic acid dimer unit **5**.<sup>[27]</sup> The head group charges should be asymmetric under basic conditions (-1/-2 at pH 8.2). When **5** was introduced into a planar bilayer membrane under an application of the asymmetric voltage to facilitate the vectorial incorporation of the channel, the current values at a positive voltage range were larger than the corresponding values at the negative one. The current-voltage plots were fitted by curves passing through a zero point to show clear rectification properties. Without asymmetric voltage application, the current observed was symmetric. The rectification currents observed seem to be a result of the different radii of the channel mouths controlled by the displacement of different charge numbers at the molecular terminals, as shown in Fig. 9.

Ion channels can produce large ionic fluxes across the bilayer lipid membrane. Because living cells, including bacteria, rigorously maintain ionic concentrations and rely on the ion impermeability of the biological membrane, incorporation of foreign ion channels disrupts such osmotic balance. Recently, antibiotic activities of artificial ion channels were demonstrated independently by Ghadiri<sup>[28]</sup> and Gokel.<sup>[29]</sup> Supramolecular assembly of cyclic oligopeptides increased ion permeability in bacterial membranes, induced the collapse of the transmembrane ionic potentials, and finally caused rapid death of the cell. Similar activities were observed for crown-ether-based artificial ion channels against the bacterium *Escherichia coli*. These are thought to have considerable potential against the rapid emergence of drug-resistant bacterial infections.

### Antibiotic-Based Ion Channels

Gramicidin antibiotics form a head-to-head dimer in a bilayer lipid membrane to afford a stable cation-selective ion channel. A half-gramicidin unit was introduced into an inner half-membrane with anchoring on gold surface and the other half counterpart was incorporated into the outer half membrane as a mobile unit.<sup>[30]</sup> The diffusion of the mobile half gramicidin unit carrying a guest molecule

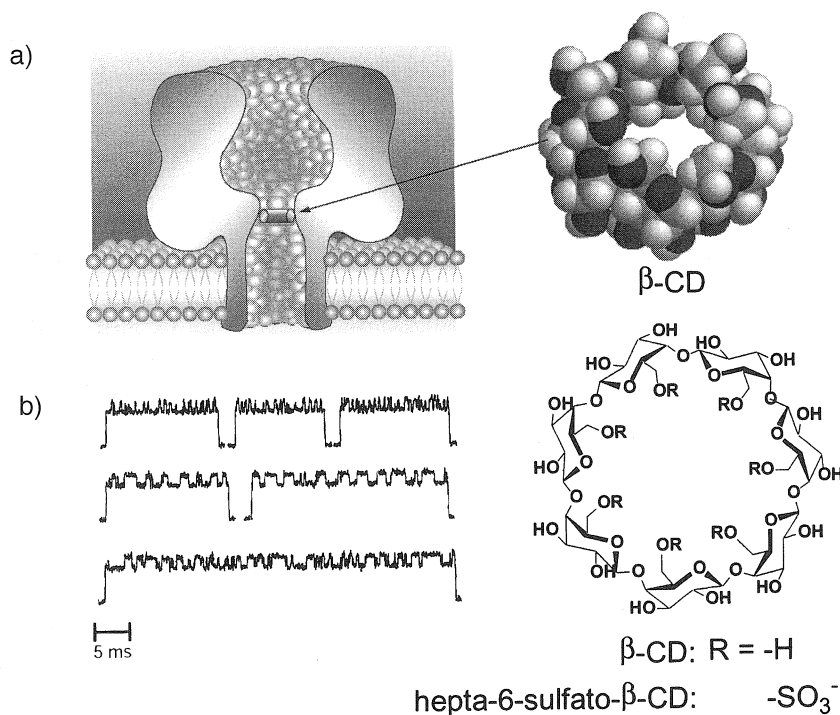


**Fig. 10** Artificial ion channel with *staphylococcal*  $\alpha$ -hemolysin ( $\alpha$ HL) with a molecular adaptor. a) Schematic of the  $\alpha$ HL pore showing  $\beta$ CD lodged in the lumen of the channel with adapters,  $\beta$ CD and hepta-6-sulfato- $\beta$ -cyclodextrin. b) Detection of organic molecules by stochastic sensing. The pore contains a noncovalent  $\beta$ CD adapter, which is capable of carrying out host-guest chemistry while lodged in the lumen. Upper trace, promethazine; middle trace, imipramine; lower trace, mixture of promethazine (100  $\mu$ M), and imipramine (100  $\mu$ M).

within the outer half of the membrane was switched off by an interaction with a receptor immobilized at the membrane surface. This prevented the gramicidin dimer formation and decreased the ionic currents across the membrane. The addition of competitive guests recovered the conductance state. In this way, the population of molecular ion channels could be switched on and off by recognition events mimicking biological sensory functions.

$\alpha$ -Hemolysin ( $\alpha$ HL) is a heptameric assembly of  $\beta$ -sheet turns to make a mushroom-shaped large pore (near 30 Å diameter) surrounded by 14  $\beta$ -sheets in a biological membrane. Through this cavity, a large ionic flux can be generated, and  $\alpha$ -HL is a highly toxic material. This cavity interestingly can accommodate  $\beta$ -cyclodextrin ( $\beta$ -CD) to make an ion channel of a moderate pore size, therefore, affording moderate conductivities.<sup>[31,32]</sup> Weakly anion-selective  $\alpha$ -HL becomes more anion selective when  $\beta$ -CD is accommodated in the middle of the channel pore due to a favorable interaction of  $\beta$ -CD with anions. By contrast, hepta-6-sulfato- $\beta$ -cyclodextrin carrying high negative charges produces reversed cation selectivities. It is noteworthy that this molecular adapter system can generate high permeability ratios ( $P_K/P_{Cl}$ ) over a 200-fold range.<sup>[33]</sup>

As  $\beta$ -CD is an effective host for various substrates, the binding of guests in the cavity modifies the mode of ionic flux of the  $\beta$ -CD adapter channel. Depending on the binding characteristics of the guests, the conductance and time profiles of open-closed transitions can be modified. Because an ion channel is a molecular device used to amplify events at a single molecular level into a massive ionic flux, it affords a highly sensitive stochastic sensor for guest molecules (Fig. 10).

## CONCLUSION

Alkali metal ions carry important messages and biological signals by their movements. By controlling the ionic species (Na<sup>+</sup>, K<sup>+</sup>, along with Ca<sup>2+</sup> and Cl<sup>-</sup> ions), magnitude of the flux (conductivity), triggering signals (voltage variation, ligand binding, and membrane deformation), and dynamic behavior (duration of open-closed times), ion channels play critical roles in biological processes in the brain and nervous system. The mode of information transfer is totally different from the electronic systems we developed for computer systems. Although the achievements of dry electronic systems are magnificent,

the wet biological system is still far advanced in many respects. However, the use of wet systems in vitro is far less developed, and we need to gain an understanding of numerous principles of such biological systems. The construction of artificial ion channels may help scientists develop ways to comprehend these basic units and their systems. With further exploration to be undertaken in this area, the future picture can not easily be foreseen.

## ARTICLES OF FURTHER INTEREST

*The Allosteric Effect*, p. 20  
*Biological Ligands*, p. 88  
*Biological Models and Their Characteristics*, p. 101  
*Calixarenes and Their Analogues: Cation Complexation*, p. 137  
*Calixarenes: Synthesis and Historical Perspectives*, p. 153  
*Cation- $\pi$  Interactions*, p. 214  
*Crown Ethers*, p. 326  
*Cryptands*, p. 334  
*Cyclodextrins*, p. 398  
*Induced Fit*, p. 717  
*Ion Channels and Their Models*, p. 742  
*Ionophores*, p. 760  
*Lariat Ethers*, p. 782  
*Molecular Logic Gates*, p. 893  
*Preorganization and Complementarity*, p. 1158  
*Protein Supramolecular Chemistry*, p. 1161  
*Spherands*, p. 1344  
*X-Ray Crystallography*, p. 1586

## REFERENCES

- Hill, B. *Ionic Channels of Excitable Membranes*, 3rd Ed.; Sinauer Associate: Sunderland, MA, 2001.
- Lin, H.; Zhu, Y.J.; Lal, R. Amyloid protein (1–40) forms calcium-permeable,  $\text{Zn}^{2+}$ -sensitive channel in reconstituted lipid vesicles. *Biochem.* **1999**, *38* (34), 11189–11196.
- Alberts, B.; Johnson, A.; Lewis, J.; Raff, M.; Robert, K.; Walter, P. *Molecular Biology of The Cell*, 4th Ed.; Garland Science: New York, 2001.
- Nicholls, D.G.; Freguson, S.J. *Bioenergetics 3*; Academic Press: San Diego, 2003.
- Doyle, D.A.; Cabral, J.M.; Pfuetzner, R.A.; Kuo, A.; Gulbis, J.M.; Cohen, S.L.; Chait, B.T.; MacKinnon, R. The structure of the potassium channel: Molecular basis of  $\text{K}^+$  conduction and selectivity. *Science* **1998**, *280* (5360), 69–77.
- Favre, I.; Moczydlowski, E.; Schild, L. On the structural basis for ionic selectivity among  $\text{Na}^+$ ,  $\text{K}^+$ , and  $\text{Ca}^{2+}$  in the voltage-gated sodium channel. *Biophys. J.* **1996**, *71* (6), 3110–3125.
- Meuser, D.; Splitt, H.; Wagner, R.; Schrempf, H. Exploring the open pore of the potassium channel from *Streptomyces lividans*. *FEBS Lett.* **1999**, *462* (3), 447–452.
- Zhou, Y.; Morais-Cabral, J.H.; Kaufman, A.; MacKinnon, R. Chemistry of ion coordination and hydration revealed by a  $\text{K}^+$  channel-Fab complex at 2.0 Å resolution. *Nature* **2001**, *414* (6859), 43–48.
- Dutzler, R.; Campbell, E.B.; Cadene, M.; Chait, B.T.; MacKinnon, R. X-ray structure of a CIC chloride channel at 3.0 Å reveals the molecular basis of anion selectivity. *Nature* **2002**, *415* (6869), 287–294.
- Dutzler, R.; Campbell, E.B.; MacKinnon, R. Gating the selectivity filter in CIC chloride channels. *Science* **2003**, *300* (5616), 108–112.
- Jiang, Y.; Lee, A.; Chen, J.; Ruta, V.; Cadene, M.; Chait, B.T.; MacKinnon, R. X-ray structure of a voltage-dependent  $\text{K}^+$  channel. *Nature* **2003**, *423* (6935), 33–41.
- Jiang, Y.; Ruta, V.; Chen, J.; Lee, A.; MacKinnon, R. The principle of gating charge movement in a voltage-dependent  $\text{K}^+$  channel. *Nature* **2003**, *423* (6935), 42–47.
- Horn, R. Coupled movements in voltage-gated ion channels. *J. Gen. Physiol.* **2002**, *120* (4), 449–453.
- Zhou, M.; Cabral, J.H.M.; Mann, S.; MacKinnon, R. Potassium channel receptor site for the inactivation gate and quaternary amine inhibitors. *Nature* **2001**, *411* (6838), 657–661.
- Gulbis, J.M.; Zhou, M.; Mann, S.; MacKinnon, R. Structure of the cytoplasmic  $\beta$  subunit-T1 assembly of voltage-dependent  $\text{K}^+$  channels. *Science* **2000**, *289* (5476), 123–127.
- Jiang, Y.; Lee, A.; Chen, J.; Cadene, M.; Chait, B.T.; MacKinnon, R. Crystal structure and mechanism of a calcium-gated potassium channel. *Nature* **2002**, *417* (6888), 515–522.
- Schumacher, M.; Adelman, J.P. An open and shut case. *Nature* **2002**, *417* (6888), 501–502.
- Unwin, N. Acetylcholine receptor channel imaged in the open state. *Nature* **1995**, *373* (6509), 37–43.
- Chang, G.; Spencer, R.H.; Lee, A.T.; Barclay, M.T.; Rees, D.C. Structure of the MscL homolog from *Mycobacterium tuberculosis*: A gated mechanosensitive ion channel. *Science* **1998**, *282* (5397), 2220–2226.
- Perozo, E.; Cortes, D.M.; Sompompisut, P.; Kloda, A.; Martinac, B. Open channel structure of MscL and the gating mechanism of mechanosensitive channels. *Nature* **2002**, *418* (6901), 942–948.
- Kobuke, Y. Artificial Ion Channels. In *Advances in Supramolecular Chemistry*; Gokel, G.W., Ed.; JAI Press: New York, 1997; Vol. 4, 163–209.
- Kobuke, Y.; Tanaka, Y.; Sokabe, M. Artificial Non-Peptide Single Ion Channels. In *Towards Biophysics of Ion Channels, Progress in Cell Research*; Sokabe, M., Ed.; Elsevier: Amsterdam, 1997; Vol. 6, 167–188.
- Tanaka, Y.; Kobuke, Y.; Sokabe, M. Non-peptidic ion channel with  $\text{K}^+$  selectivity. *Angew. Chem., Int. Ed. Engl.* **1995**, *34* (6), 693–694.
- Yoshino, N.; Satake, A.; Kobuke, Y. Artificial ion channel by macrocyclic resorcin[4]arene having amphiphilic cholic

- acid ethers. *Angew. Chem., Int. Ed.* **2001**, *40* (2), 457–459.
25. Kobuke, Y.; Nagatani, T. A supramolecular ion channel based on amphiphilic cholic acid derivatives. *Chem. Lett.* **2000**, *4*, 298–299.
26. Kobuke, Y.; Nagatani, T. Transmembrane ion channels constructed of cholic acid derivatives and characterizations by single channel current measurements. *J. Org. Chem.* **2001**, *66* (15), 5094–5101.
27. Goto, C.; Yamamura, M.; Satake, A.; Kobuke, Y. Artificial ion channels showing rectified current behavior. *J. Am. Chem. Soc.* **2001**, *123* (49), 12152–12159.
28. Fernandez-Lopez, S.; Kim, H.S.; Choi, E.C.; Delgado, M.; Granja, J.R.; Khasanov, A.; Kraehenbuehl, K.; Long, G.; Weinberger, D.A.; Wilcoxon, K.M.; Ghadiri, M.R. Antibacterial agents based on the cyclic D,L- $\alpha$ -peptide architecture. *Nature* **2001**, *412* (6845), 452–455.
29. Leevy, W.M.; Donato, G.M.; Ferdani, R.; Goldman, W.E.; Schlesinger, P.E.; Gokel, G.W. Synthetic hydrophile channels of appropriate length kill *Escherichia coli*. *J. Am. Chem. Soc.* **2002**, *124* (31), 9022–9023.
30. Cornell, B.A.; Braach-Maksyitis, V.L.B.; King, L.G.; Osman, P.D.J.; Raguse, B.; Wiczorek, L.; Pace, R.J. A biosensor that uses ion-channel switches. *Nature* **1997**, *387* (6633), 580–583.
31. Gu, L.-Q.; Braha, O.; Conlan, S.; Cheley, S.; Bayley, H. Stochastic sensing of organic analytes by a pore-forming protein containing a molecular adapter. *Nature* **1999**, *398* (6729), 686–690.
32. Gu, L.-Q.; Serra, M.D.; Vincent, J.B.; Vigh, G.; Cheley, S.; Braha, O.; Bayley, H. Reversal of charge selectivity in transmembrane protein pores by using noncovalent molecular adapters. *Proc. Natl. Acad. Sci. U. S. A.* **2000**, *97* (8), 3959–3964.
33. Bayley, H.; Cremer, P.S. Stochastic sensors inspired by biology. *Nature* **2001**, *413* (6852), 226–230.

# Alkalides and Electrides

James L. Dye

Michigan State University, East Lansing, Michigan, U.S.A.

## INTRODUCTION

Crystalline alkalides are salts with alkali metal anions ( $\text{Na}^-$ ,  $\text{K}^-$ ,  $\text{Rb}^-$ , or  $\text{Cs}^-$ ) that have been known since 1974, when the first sodide was synthesized.<sup>[1]</sup> The first crystalline electride, in which trapped electrons serve as the anions, was first fully characterized in 1986.<sup>[2]</sup> The key to the formation of both classes of materials is complexation of the countercation ( $\text{Li}^+$  through  $\text{Cs}^+$ ) by organic macrocyclic or macrobicyclic molecules such as crown ethers and cryptands. Seven electrides and 37 alkalides have now been synthesized and their structures were determined by single crystal x-ray crystallography.<sup>[3]</sup> Their properties were studied by a number of methods, including optical, electron paramagnetic resonance (EPR), and nuclear magnetic resonance (NMR) spectroscopy, magnetic susceptibility, conductivity, and differential scanning calorimetry (DSC).

Both alkalides and electrides are powerful reducing agents; so powerful, in fact, that most cannot survive, even in vacuo at temperatures above about  $-30^\circ\text{C}$ . The organic complexant is irreversibly destroyed by cleavage of the O—C or N—C bonds of the complexant. This reducing ability of alkalides is, however, useful in organic synthesis when a powerful two-electron reducing agent is needed.<sup>[4]</sup> Alkalides and electrides in solution are able to reduce nearly all metallic cations to form nanoscale metal particles.<sup>[5]</sup>

In this overview of alkalides and electrides, the methodologies and special techniques used will be briefly described, and the structural features and electronic, optical and magnetic properties will be summarized. The reference list is far from complete, but the information given can provide many additional references to the original literature in this field.

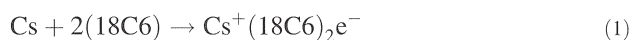
## EXPERIMENTAL METHODS

The major concern in the preparation and study of alkalides and electrides is their extreme sensitivity to air, moisture, and especially elevated temperatures. Thus, ordinary glove box procedures do not suffice without provision to keep the samples cold (below about  $-40^\circ\text{C}$ ) at all times during and after synthesis. It should be noted,

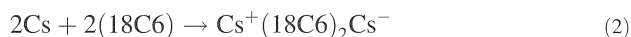
however, that the formation and use of alkalides such as  $\text{K}^+(\text{15-crown-5})_2\text{Na}^-$  in solution (in THF, for example) can be carried out at room temperature in a glove box, Schlenk line, or by syringe techniques. Thus, organic synthetic methods that need a powerful two-electron reducing agent need not be as rigorous as those required to prepare crystalline alkalides and electrides.

Synthesis is simple and straightforward in principle. One merely needs to prepare a solution of the complexant and alkali metal in a pure aprotic solvent such as methylamine ( $\text{MeNH}_2$ ) or dimethyl ether ( $\text{Me}_2\text{O}$ ), filter the solution through a porous glass frit into a second compartment of a K-cell,<sup>[6]</sup> and add a less polar cosolvent such as diethyl ether ( $\text{Et}_2\text{O}$ ) or trimethylamine ( $\text{Me}_3\text{N}$ ). Then the more polar primary solvent is removed by evaporation until the solution is saturated at about  $-40^\circ\text{C}$ . Slow cooling over a 1- or 2-day period (sometimes with temperature cycling back to the starting temperature to dissolve small crystals) results in crystal growth. The crystals can then be washed with the secondary solvent by pouring the liquid back through the frit and redistilling it for further washes. Finally, vacuum evaporation of all solvents leaves dry crystals for study. In some cases, solvent molecules are included in the crystal structure so that wet crystals must be harvested.

In practice, things are not as simple as indicated above. Because the metal solutions are thermodynamically unstable, all glassware used must be rigorously cleaned, and solvents must be free of reducible impurities. Control of the stoichiometry can sometimes determine whether an electride or an alkalide (or a mixture of the two) is formed. For example, the preparation of an electride or a ceside can be controlled by the relative amounts of 18-crown-6 (18C6) and cesium metal according to



or



By using a slight excess of 18C6, the electride is formed, while an excess of cesium gives the ceside. Because cesium metal is insoluble in  $\text{Me}_2\text{O}$ , this solvent can be used as a primary solvent. When preparing the electride, excess 18C6 is removed by washing with the secondary

solvent. Again, complications often occur. It is easy to use cryptand[2.2.2], (C222) to prepare  $K^+(C222) Na^-$  by using a mixture of K and Na metals and to prepare  $Na^+(C222)Na^-$  with just sodium. But, we have never been able to make crystalline  $Na^+(C222)e^-$ . Whenever sodium is present in solution, regardless of the complexant used, a sodide is formed. Another complication that can occur, especially with  $MeNH_2$  and either  $Et_2O$  or  $Me_3N$ , is phase separation of the liquid solutions. One gets a concentrated  $MeNH_2$ -rich phase and a more dilute cosolvent-rich phase. Also, of course, the growth of high-quality crystals remains more an art than a science; we frequently obtain apparently well-formed crystals that do not diffract x-rays well enough to permit structure determination. In the descriptions of structures and properties that constitute the balance of this article, only alkalides and electrides of known structure will be considered. Many other polycrystalline alkalides and electrides were prepared and studied, but without a structure, one can never be confident that a pure compound was prepared. This is particularly true of electrides, which are frequently contaminated with alkali metal anions.

In this article, we will not describe in detail the experimental equipment used to determine the optical, electronic, and magnetic properties of these materials. Standard instruments were used for EPR, ENDOR, solid-state NMR, SQUID susceptibility, powder conductivity, optical reflectance and transmittance, and DSC, although some home-built instruments were involved. The specific equipment used is described in the references. The major consideration in designing and using equipment is the need to keep the samples cold and away from air and moisture at all times.

## ALKALIDES

### Origin and Synthesis

The synthesis of crystalline alkalides had its origins in the study of alkali metal solutions in amines and ethers. Although genuine alkali metal anions apparently do not form in metal-ammonia solutions, they are ubiquitous in less-polar solvents. A great deal of confusion in early work was removed when Hurley, Tuttle, and Golden<sup>[7]</sup> showed that  $Na^+$  in sodium borosilicate glass was readily exchanged by other alkali cations in solution. This exchange yielded the peak of  $Na^-$ , even when no sodium was added to the solution. The optical absorption spectra of alkali metal solutions in ethylenediamine at room temperature (shown in Fig. 1) (corrected for  $Na^-$  contamination when necessary) were obtained by Dewald and Dye in 1964.<sup>[8]</sup> Later work<sup>[9]</sup> clearly identified the

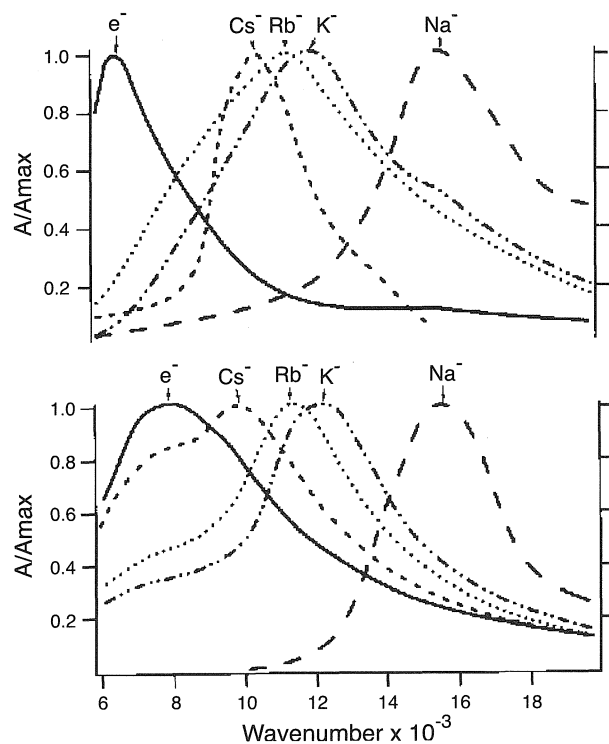


**Fig. 1** Optical spectra of alkali metal solutions in ethylenediamine (8), corrected for sodide absorption (bottom) and from thin solvent-free films (top). The solution spectrum labeled  $e^-$  is that of lithium. Note also the shoulder due to  $e^-_{solv}$  in Cs, Rb, and K solutions.

peaks of  $e^-$ ,  $Cs^-$ ,  $Rb^-$ ,  $K^-$ , and  $Na^-$ , as labeled in the figure. Note the absence of  $Li^-$ , a result of the high solvation energy of  $Li^+$ .

The study of more concentrated alkali metal solutions in a variety of solvents became possible in 1970, when crown ethers were used<sup>[10]</sup> to enhance the solubility of the metal. The use of crown ethers and cryptands permitted extensive studies of the optical spectra of solvated electrons and alkali metal anions in solution. After the isolation of the first sodide salt in 1974,<sup>[11]</sup> the optical spectra of polycrystalline films of various alkalides and electrides were determined by rapid evaporation of all solvent from a liquid film on the walls of the optical cell.<sup>[11]</sup> Displayed in Fig. 1 are the optical spectra obtained in this way. Clearly, there is a 1:1 correspondence between the spectra in solution and in the solid state. Although the peak positions shift somewhat with temperature and with the complexant used, the optical peaks can be used to verify the presence of particular alkali metal anions or trapped electrons. In addition to rapid solvent evaporation, solvent-free alkalide and electride films can be made by codeposition of the complexant and alkali metal in high vacuum ( $10^{-8}$  torr).<sup>[12]</sup> This permitted the study of optical



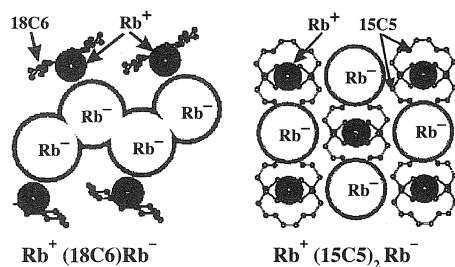


**Fig. 2** Examples of  $M^-$  chain formation (left) and isolated  $M^-$  (right) in two rubidium rubridides. The  $Rb^+$  and  $Rb^-$  ions are drawn to scale, while ball-and-stick models are used for 18C6 and 15C5.

transmission spectra, conductivity, and thermionic electron emission.<sup>[13]</sup>

## Structural Features

Alkali metal anions are large and highly polarizable. With two electrons sharing the outer  $s$ -orbital, expansion occurs to yield radii of about 2.8, 3.1, 3.2, and 3.5 Å for  $Na^-$ ,  $K^-$ ,  $Rb^-$ , and  $Cs^-$ , respectively.<sup>[14]</sup> Crystal structure determination permitted the identification of a variety of structural motifs. In addition to isolated anions, various structures include contact ion pairs between  $M^+$  and  $M^-$ , dimers of the anions,  $(M^-)_2$ , and anionic chains,  $(M^-)_n$ .<sup>[14]</sup> Although one might think that coulomb repulsion would prevent dimerization of  $M^-$ , a theoretical study<sup>[15]</sup> showed that such dimers can be stabilized by adjacent cations. Dimers and chains presumably form by partial hybridization of the diffuse  $s$ -orbital with empty  $p$ - or  $d$ -orbitals.

Two extremes are shown in Fig. 2. Isolated anions, separated from the cations by the complexant, are present in  $Rb^+(15C5)_2Rb^-$ , while chains of  $Rb^-$  in close contact with  $Rb^+$  form in  $Rb^+(18C6)Rb^-$ . The cesides,  $Li^+(C211)Cs^-$  and  $Cs^+(C222)Cs^-$  also form chains of anions, while anionic dimers are present in  $K^+(C222)K^-$  and  $Rb^+(C222)Rb^-$ . In most alkalides, the alkali metal anions are isolated from one another and from the cations. However, cation–anion contact pairs are present in  $M^+$  (hexamethyl hexacyclen)  $Na^-$ , with  $M=K, Rb, Cs$ .<sup>[16]</sup>

## Properties

Many properties of alkalide crystals, powders, and films were measured. The original alkalide,  $Na^+(C222)Na^-$ , has been most thoroughly studied, in part because of the high stability of pure samples. In contrast to most alkalides, single crystals and vapor-deposited films of this sodide are stable in vacuo for many hours, even at room temperature. In addition to the crystal structure, we measured the thermodynamics of formation by an EMF method, optical

transmission spectra of polycrystalline films, reflectance spectra of single crystals, single-crystal fluorescence spectra, EPR of defect electrons,  $^{23}Na$ -NMR spectra of powder and oriented single crystals, powder- and single-crystal conductivity, exciton formation and mobility, photoelectron emission spectra, and multiphoton photobleaching. Only limited sets of such measurements were made on other alkalides;  $Na^+(C222)Na^-$  could be viewed as the best-understood model of an alkalide with isolated alkali metal anions.

## Optical spectra

The optical transmission spectra of polycrystalline films are shown in Fig. 1. The spectrum clearly arises primarily from an  $np \leftarrow ns$  transition. The peak positions correlate well with the corresponding dissociation transitions in the gas phase. The anisotropy in the solid leads to a small orientation dependence of the peak position in the single-crystal reflectance spectrum of  $Na^+(C222)Na^-$ .<sup>[12]</sup> Recent unpublished work in our laboratory showed that the effect is much larger in  $Li^+(C211)Cs^-$ , which forms extended chains of ceside anions.<sup>[17]</sup> This orientation dependence is a natural consequence of the removal of excited  $p$ -state degeneracy in the anisotropic solid.

Pure alkalides are diamagnetic insulators or semiconductors. It is practically impossible, however, to avoid the incorporation of defect electrons in the structure. They are easily detectable by EPR spectroscopy and contribute to defect conductivity and a “Curie tail” in the magnetic susceptibility. When defect electrons in  $Na^+(C222)Na^-$  are photoexcited, they remain for many minutes in states near the vacuum level and can be photoejected with infrared (IR) photons.<sup>[18]</sup> The effect is completely absent in defect-free crystals of this sodide.

## NMR spectra

Alkali metal NMR spectroscopy provides a good diagnostic tool for isolated alkali metal anions in solution and in solid alkalides. The chemical shifts are close to those calculated for the gaseous anions, much more diamagnetic (negative) than the reference state of  $M^+(aq.)$ . In solution, the chemical shifts of  $M^-$  are about  $-62$ ,  $-100$ ,  $-190$ , and  $-290$  ppm for  $M=Na, K, Rb$ , and  $Cs$ , respectively, compared with calculated gas-phase values of  $-63$ ,  $-103$ ,  $-214$ , and  $-346$  ppm.<sup>[19]</sup> The values in solid alkalides are somewhat dependent on the compound, but for salts with isolated anions, the values are about  $-61$ ,  $-105$ ,  $-190$ , and  $-220$  ppm, in agreement with the solution values and, at least for  $Na$  and  $K$ , nearly the same as the gas-phase chemical shifts. The absence of significant shifts from those of gaseous  $M^-$  is a consequence of the large size of the anions and their nearly spherical shape. Shifts in the paramagnetic direction (Ramsey

shifts) are caused by mixing of the unoccupied orbitals of the alkali metals with those of surrounding molecules. The large size of the alkali metal anions tends to minimize such shifts.

When dimers or chains of alkali metal atoms are present, the anion chemical shift is considerably more paramagnetic, even to the extent of having the shift of  $\text{Cs}^-$  confused with that of  $\text{Cs}^+$  in early work.<sup>[19]</sup> Recent studies indicate that dimer or chain formation can shift the peaks of  $\text{K}^-$ ,  $\text{Rb}^-$ , and  $\text{Cs}^-$  by hundreds of ppm. The mixing of *p* or *d* orbitals to provide some bonding between adjacent anions would introduce considerable spin-orbit coupling that would result in a pronounced paramagnetic shift.

Because the alkali metal nuclei have quadrupole moments, the lines are considerably broader than those of nuclei with spin 1/2. The effect is small for  $^7\text{Li}$  and  $^{133}\text{Cs}$  and only moderate for  $^{23}\text{Na}$ . With  $^{39}\text{K}$ ,  $^{85}\text{Rb}$ , and  $^{87}\text{Rb}$ , quadrupole broadening makes solid-state NMR studies difficult, but even in these cases, the static line shapes can provide considerable information about the quadrupole coupling constants, asymmetry parameters, and chemical shifts.<sup>[20]</sup>

## Stability

The tendency of alkalides to decompose above about  $-30^\circ\text{C}$  made the study of their properties difficult. The decomposition mode with crown ethers and cryptands is the rupture of  $\text{O}-\text{C}$  bonds. For example,  $M_a^+(\text{C222})M_b^-$  (with  $M_a$  and  $M_b$  the same or different alkali metals) releases ethylene from the  $-\text{O}-\text{CH}_2-\text{CH}_2-\text{O}-$  moiety with formation of alkoxide units.<sup>[21]</sup> The  $\text{N}-\text{C}$  bonds in perazacryptands and cyclens is considerably more resistant to reduction. We recently prepared the sodide and potasside of fully methylated perazacryptand [2.2.2] and found them to be stable at room temperature for months.<sup>[22]</sup> The flip-side of this story is that aza complexants have generally much poorer complexing ability for alkali cations. When a complex forms, it frequently dissociates at elevated temperatures to yield the metal and free complexant. Thus, a synthetic challenge in this field is to find peraza complexants with just the right size and lone pair orientation to form strong complexes with alkali cations.

## ELECTRIDES

### Background and Definitions

In contrast to alkali metal anions, which were first positively identified as solution species in 1970, solvated and trapped electrons have been known for more than a century.<sup>[23]</sup> With the advent of pulse radiolysis, the solvated electron has become probably the most widely

studied species in chemistry. Electrons trapped at defect sites in crystals (F-centers and clusters) have also been studied extensively for over a century.<sup>[24]</sup> Alkali metal incorporation in aluminosilicate zeolites to yield electrons trapped near clusters of cations has been the subject of many experimental and theoretical studies<sup>[25]</sup> since first observed in 1966.<sup>[26]</sup> Even simple alkali metals, with a “sea” of electrons filling the space between cations, have one electron per cation. What then distinguishes true electrides from all these other materials?

As the “-ide” ending suggests, the electrons in electrides take on the role of anions.<sup>[27]</sup> This implies that electrides are crystalline ionic compounds with one electron per cation. They could be viewed as salts that contain stoichiometric F-centers, with electrons as the only anions. But because one cannot suppress the quantum nature of electrons, these “anions” are special. The line between localized weakly interacting electrons and delocalized, or metallic electrons is blurred, and both extremes are encountered in electrides. Because most of the electron density in electrides is present in otherwise empty, well-defined pseudo-one-dimensional cavities and channels, they could also be viewed as forming low-dimensional correlated electron gasses.

### General Structural Features

Except for zeolite-based electrides, to be considered later, the cations in all electrides synthesized to date are alkali cations,  $\text{Li}^+$ ,  $\text{K}^+$ ,  $\text{Rb}^+$ , or  $\text{Cs}^+$ , sequestered inside a cryptand cage or sandwiched between two crown ether molecules. Thus, the cations are well shielded from the electrons. The temperature dependence of the  $^{133}\text{Cs}$ -NMR chemical shift (Knight shift) in two electrides shows that the unpaired electron density at the  $\text{Cs}^+$  cation is less than 0.1% of the value for the isolated atom.<sup>[28]</sup> The structures of the complexed cations are practically identical to those of corresponding alkalides and normal salts. Because the electron density of the trapped electrons is too low to detect by x-ray crystallography, the major structural difference between an electride and the corresponding alkalide is that the former has large voids at the anionic sites. To a first approximation, then, the electrons could be viewed as particles in adjacent, nearly spherical boxes. The common feature of an intense optical absorption band in the near IR at 1200–1500 nm, with a long tail into the visible, is the counterpart of the optical behavior of solvated electrons. The optical bands of solvated electrons were attributed, for many years, to electrons trapped in otherwise empty cavities.<sup>[23]</sup> The similarity to electrons in electride cavities is striking.

A complication that caused confusion in the study of electrides is structural polymorphism. Each of the electrides  $\text{Cs}^+(\text{18C6})_2\text{e}^-$ ,  $\text{Cs}^+(\text{15C5})_2\text{e}^-$ ,  $\text{Li}^+(\text{C211})\text{e}^-$ , and  $\text{Rb}^+(\text{C222})\text{e}^-$  exists in at least two polymorphs.<sup>[3]</sup> Only

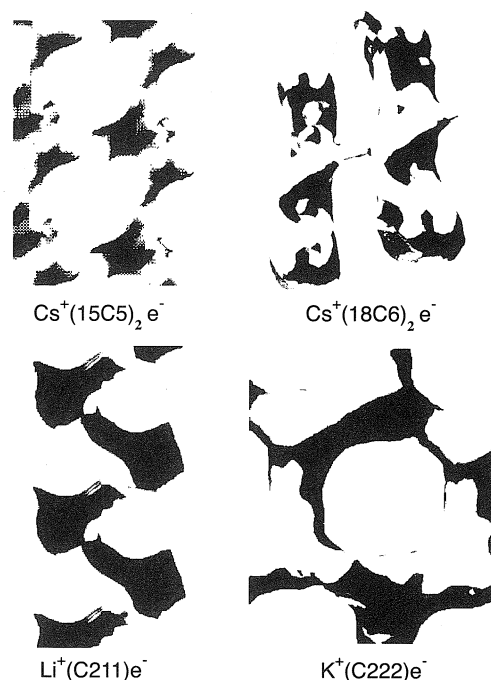


Fig. 3 Channel structures of four electrides. The general shapes of the cavities and channels are represented. (From Ref. [29].)

one form of each electride has a known structure, but the properties of the two forms are different. The factors that determine which form precipitates from solution are not known, and transitions between the types are slow. In the case of  $\text{Rb}^+(\text{C}222)\text{e}^-$ , mixtures of the two forms were usually produced, and it was necessary to use the magnetic properties to determine the amount of each present.<sup>[3]</sup>

### Electron–Electron Interactions

The cavities and channels left by close-packing of the complexed cations tend to form uniform one-dimensional chains, like beads on a string, in five of the seven electrides of known structure.<sup>[29]</sup> The electrons are coupled antiferromagnetically, and the magnetic susceptibilities are well-fit by the Heisenberg linear-chain model, with a single negative coupling constant,  $J$ .<sup>[30]</sup> The mixed crown ether electride,  $[\text{Cs}^+(15\text{C}5)(18\text{C}6)\text{e}^-]_6 \cdot (18\text{C}6)$ , has a complex structure,<sup>[31]</sup> while  $\text{K}^+(\text{C}222)\text{e}^-$  has a two-dimensional channel-cavity structure with open channels in one direction and constricted channels in a second direction.<sup>[32]</sup> As with the corresponding potasside  $\text{K}^+(\text{C}222)\text{K}^-$ , this electride has open dumbbell-shaped cavities that contain two electrons.<sup>[32]</sup> The coupling is so strong in this case that the electride is nearly diamagnetic.

The temperature dependence of the susceptibility is well-described by the alternating chain antiferromagnetic Heisenberg model.

The correlation between the magnetic coupling constant,  $J$ , and the geometry of the cavity-channel systems is remarkable. It provides strong experimental evidence for the theoretical finding that the excess electron density resides primarily in the cavities and channels.<sup>[33]</sup> The geometry of the channels in three electrides is shown in Fig. 3. Because the distance between cavity centers only slightly varies from one electride to another, the major effect on the interelectron coupling is the size of the connecting channel. Shown in Fig. 4 is the strong correlation between the magnitude of the coupling constant and the cross-sectional area at the minimum diameter of the channel. Clearly, the overlap of the electronic wave functions is strongly influenced by the available void space between the electrons. This behavior of a well-defined, one-dimensional correlated electron gas of electrons should be a fruitful area for theoretical treatment.

### Optical and Electrical Properties

The intense near-IR absorption of electride films (Fig. 1) is characteristic of localized electrons with little inter-

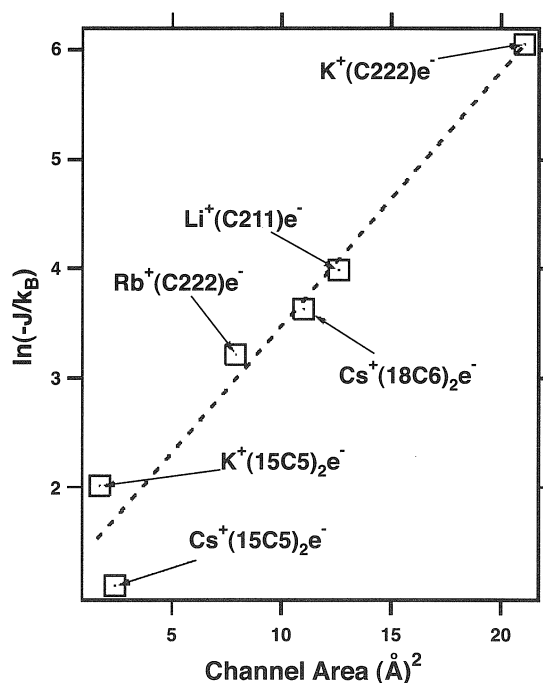


Fig. 4 Correlation of the antiferromagnetic coupling constants of electrides with the minimum cross-sectional area of the channels that connect the cavities. Reprinted with permission from Ref. [30]. Copyright 1997, American Chemical Society.

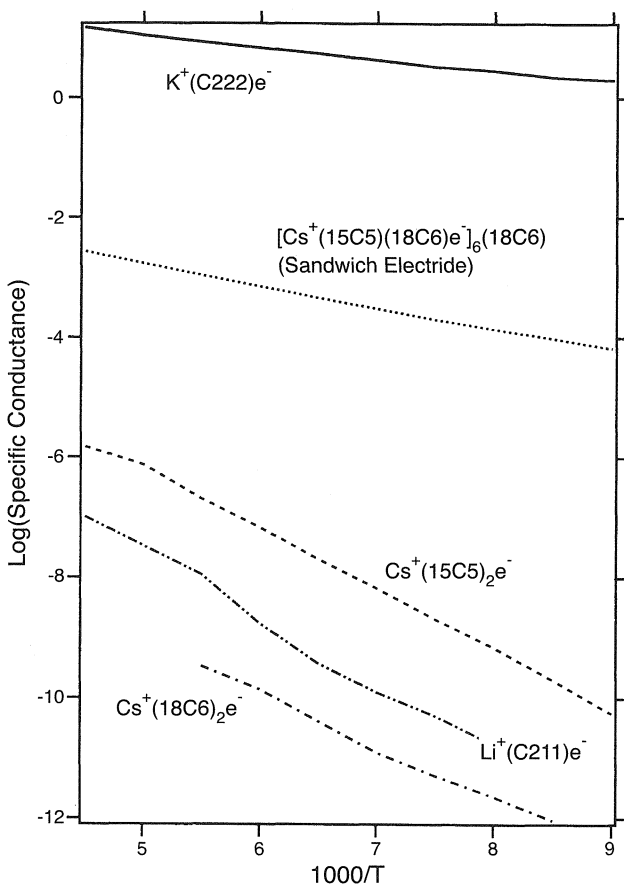


Fig. 5 Comparison of the conductivities of various electrides as functions of temperature. Reprinted with permission from Ref. [3]. Copyright 1997, American Chemical Society.

electron coupling. The electride  $\text{K}^+(\text{C222})\text{e}^-$  has a more open structure and far stronger coupling between electrons. This also has a profound effect on the optical spectrum and conductivity. Films of this electride, formed by high vacuum codeposition of K metal and cryptand [2.2.2] in 1:1 stoichiometry were extensively studied by optical transmission spectroscopy and four-probe conductivity.<sup>[34]</sup>

Freshly prepared films show the absorption peak of  $\text{K}^-$ . This tends to anneal with time to a combination of a localized electron peak at  $\sim 1250$  nm and an absorbance that rises steadily with increasing wavelength. The spectra are remarkably similar to those of concentrated metal–ammonia solutions as they move through the nonmetal to metal transition.<sup>[35]</sup> The rising absorbance is attributed to the plasma edge that is characteristic of metallic behavior. The electrical conductivity of powders and films of this electride is far greater than that of other electrides, as shown in Fig. 5. Whether these conductivities are intrinsic or defect-dominated is uncertain, but clearly, the open-channel nature of

$\text{K}^+(\text{C222})\text{e}^-$  has a profound effect, bringing this electride to the threshold of metallic behavior. Four-probe single crystal studies show that the conductivity is highly anisotropic.<sup>[36]</sup> It is nearly metallic along one direction in the plane of the channels and insulating perpendicular to this plane.

### The Search for Stable Electrides

It is likely that the study of electrides would be more widespread if thermal stability at room temperature could be achieved. The recent success in synthesizing a sodide and potasside that are stable at room temperature<sup>[22]</sup> provided the incentive to find aza-based complexants that will permit the crystallization of stable electrides. The cation of choice would be  $\text{Li}^+$ , because there would be no competition from  $\text{Li}^-$ , an alkalide that has never been made. A number of candidates were tried, from methylated cyclens to fully methylated azacryptands to adamanzane-like complexants. Thus far, none produced a crystalline electride of known structure. When the cation is kinetically able to leave the complexant, dissociation without decomposition occurs. The aza complexants used to date apparently do not form strong enough complexes to yield thermodynamically stable electrides, although alkalides can be made in some cases. The search for the ideal aza complexant continues.

### Inorganic Electrides

F-centers in alkali halides are stable. In 1966 Kasai and coworkers found that electrons could be trapped in a zeolite by incorporation of sodium from the vapor phase.<sup>[26]</sup> They identified the species  $\text{Na}_4^{3+}$ , an electron trapped by a cluster of four sodium cations. Since that time, a great deal of work was done on the inclusion of alkali metals in various aluminosilicates,<sup>[25]</sup> including the formation of a stoichiometric sodium sodalite that has  $\text{Na}_4^{3+}$  units inside every sodalite cage.<sup>[37]</sup> In common with electrides, these paramagnetic centers are coupled antiferromagnetically and undergo a Néel transition at 48 K. While these metal adducts to zeolots could be (and have been) called “electrides,”<sup>[25]</sup> they differ from the organic electrides by having several cations for each electron.

We recently added alkali metals from the vapor phase to two pure silica zeolots to yield adducts that have a 1:1 stoichiometry of cations to electrons.<sup>[38]</sup> The properties strongly point to ionization to yield alkali cations that interact with the  $\text{Si—O—Si}$  units that line the zeolite channels. Apparently, the released electrons occupy the open spaces of the channels, which have diameters of  $\sim 7$  Å. The electrons are strongly coupled to form nearly diamagnetic materials. These inorganic electrides are stable to at least  $100^\circ\text{C}$ . Potentially, zeolite-based systems

might be made that would have an even closer relationship to organic electrides. If a pure silica zeolite could be made that contains open channels and separate cation-trapping sites, it should be possible to prepare a stoichiometric electride with trapped cations and electrons that are free to roam the channels. Such systems might have interesting properties, including, perhaps, metallic conductivity.

## CONCLUSION

Although we studied alkalides and electrides for nearly 30 years, there is much that remains to be done to make them useful members of the chemistry-physics communities. We hope that the existence of stable, easy-to-prepare alkalides and electrides will prompt a number of other researchers to enter this intriguing field.

## ARTICLES OF FURTHER INTEREST

*Crown Ethers*, p. 326

*Cryptands*, p. 334

*Electron Paramagnetic Resonance Spectroscopy*, p. 520

*Energy and Electron Transfer in Supramolecular Systems*, p. 535

*Inclusion Compounds: Selectivity, Thermal Stability, and Kinetics*, p. 696

*Macrocyclic Synthesis*, p. 830

*Molecular Modeling and Related Computational Techniques*, p. 901

*Nuclear Magnetic Resonance Spectroscopy*, p. 981

*Solid-State Nuclear Magnetic Resonance Spectroscopy*, p. 1307

*Space Groups and Crystal-Packing Modes*, p. 1337

*X-Ray Crystallography*, p. 1586

*X-Ray and Neutron Powder Diffraction*, p. 1592

## REFERENCES

1. Dye, J.L.; Ceraso, J.M.; Lok, M.T.; Barnett, B.L.; Tehan, F.J. A crystalline salt of the sodium anion ( $\text{Na}^-$ ). *J. Am. Chem. Soc.* **1974**, *96*, 608–609.
2. Dawes, S.B.; Ward, D.L.; Huang, R.H.; Dye, J.L. First electride crystal structure. *J. Am. Chem. Soc.* **1986**, *108*, 3534–3535.
3. Xie, Q.; Huang, R.H.; Ichimura, A.S.; Phillips, R.C.; Pratt, W.P., Jr.; Dye, J.L. Structure and properties of a new electride,  $\text{Rb}^+(\text{cryptand}[2.2.2]\text{e}^-)$ . *J. Am. Chem. Soc.* **2000**, *122*, 6971–6978.
4. Jedlinski, Z. Novel electron-transfer reactions mediated by alkali metals complexed by macrocyclic ligand. *Acc. Chem. Res.* **1998**, *31*, 55–61.
5. Tsai, K.L.; Dye, J.L. Nanoscale metal particles by homogeneous reduction with alkalides or electrides. *J. Am. Chem. Soc.* **1991**, *113*, 1605–1652.
6. Wagner, M.J.; Dye, J.L. Alkalides and Electrides. In *Molecular Recognition: Receptors for Cationic Guests*, 1st Ed.; Gokel, G.W., Ed.; Pergamon Press: Oxford, U.K., 1996; 477–510.
7. Hurley, I.; Tuttle, T.R.J.; Golden, S. Origin of the 660-mu band in the spectra of alkali-metal-amine solutions. *J. Chem. Phys.* **1968**, *48*, 2818–2819.
8. Dewald, R.R.; Dye, J.L. Absorption spectra of the alkali metals in ethylenediamine. *J. Phys. Chem.* **1964**, *68*, 121–127.
9. Lok, M.T.; Tehan, F.J.; Dye, J.L. Spectra of  $\text{Na}^-$ ,  $\text{K}^-$  and  $\text{e}_{\text{solv}}^-$  in amines and ethers. *J. Phys. Chem.* **1972**, *76*, 2975–2981.
10. Dye, J.L.; DeBacker, M.G.; Nicely, V.A. Solubilization of alkali metals in tetrahydrofuran and diethyl ether by use of a cyclic polyether. *J. Am. Chem. Soc.* **1970**, *92*, 5226–5228.
11. Dye, J.L.; Yemen, M.R.; DaGue, M.G.; Lehn, J.-M. Optical spectra of alkali metal anion and ‘electride’ films. *J. Chem. Phys.* **1978**, *68*, 1665–1670.
12. Hendrickson, J.E.; Kuo, C.T.; Xie, Q.; Pratt, W.P., Jr.; Dye, J.L. Optical absorption and reflection spectra of  $\text{Na}^+(\text{C222})\text{Na}^-$ . *J. Phys. Chem.* **1996**, *100*, 3395–3401.
13. Phillips, R.C.; Dye, J.L. Thermionic emission from cold electride films. *Chem. Mater.* **2000**, *12*, 3642–3647.
14. Huang, R.H.; Ward, D.L.; Dye, J.L. Alkali-metal-anion dimers and chains in alkalide structures. *J. Am. Chem. Soc.* **1989**, *111*, 5707–5708.
15. Tientega, F.; Dye, J.L.; Harrison, J.F. The electronic structure of  $\text{K}_2^{-2}$ . *J. Am. Chem. Soc.* **1991**, *113*, 3206–3208.
16. Kuchenmeister, M.E.; Dye, J.L. Synthesis and structures of two thermally stable sodides with the macrocyclic complexant hexamethyl hexacyclen. *J. Am. Chem. Soc.* **1989**, *111*, 935–938.
17. Ichimura, A.S. Unpublished results, this laboratory.
18. Kuo, C.-T.; Dye, J.L.; Pratt, W.P., Jr. Effect of laser pulses on the photoelectron emission from  $\text{Na}^+(\text{C222})\text{Na}^-$ . *J. Phys. Chem.* **1994**, *98*, 13575–13582.
19. Dawes, S.B.; Ellaboudy, A.S.; Dye, J.L. Cesium-133 solid state nuclear magnetic resonance spectroscopy of alkalides and electrides. *J. Am. Chem. Soc.* **1987**, *109*, 3508–3513.
20. Kim, J.; Eglin, J.L.; Ellaboudy, A.S.; McMills, L.E.H.; Huang, S.; Dye, J.L.  $^{87}\text{Rb}$ ,  $^{85}\text{Rb}$ , and  $^{39}\text{K}$  NMR studies of alkalides, electrides and related compounds. *J. Phys. Chem.* **1996**, *100*, 2885–2891.
21. Cauliez, P.M.; Jackson, J.E.; Dye, J.L. An unusual reduction of ethylene occurring during the thermal decomposition of alkalides and electrides. *Tetrahedron Lett.* **1991**, *32*, 5039–5042.
22. Kim, J.; Ichimura, A.S.; Huang, R.H.; Redko, M.; Phillips, R.C.; Jackson, J.E.; Dye, J.L. Crystalline salts of  $\text{Na}^-$  and  $\text{K}^-$  that are stable at room temperature. *J. Am. Chem. Soc.* **1999**, *121*, 10666–10667.
23. Thompson, J.C. *Electrons in Liquid Ammonia*; Oxford Univ. Press: Oxford, 1976.

24. Markham, J.J. *F-Centers in Alkali Halides*; Academic Press: New York, 1966.
25. Edwards, P.P.; Anderson, P.A.; Thomas, J.M. Dissolved alkali metals in zeolites. *Acc. Chem. Res.* **1996**, *29*, 23–29.
26. Rabo, J.A.; Angell, P.H.; Kasai, P.H.; Schomaker, V. Studies of cations in zeolites: Adsorption of carbon monoxide; formation of Ni ions and  $\text{Na}_4^{3+}$  centres. *Discuss. Faraday Soc.* **1966**, *41*, 328–349.
27. Dye, J.L. Electrides: Ionic salts with electrons as the anions. *Science* **1990**, *247*, 663–668.
28. Dawes, S.B.; Eglin, J.L.; Moeggenborg, K.J.; Kim, J.; Dye, J.L.  $\text{Cs}^+(15\text{-crown-5})_2\text{e}^-$ , a crystalline antiferromagnetic electride. *J. Am. Chem. Soc.* **1991**, *113*, 1605–1609.
29. Dye, J.L.; Wagner, M.J.; Overney, G.; Huang, R.H.; Nagy, T.F.; Tomanek, D. Cavities and channels in electrides. *J. Am. Chem. Soc.* **1996**, *118*, 7329–7336.
30. Dye, J.L. Electrides: From 1D Heisenberg chains to 2D pseudo-metals. *Inorg. Chem.* **1997**, *36*, 3816–3826.
31. Wagner, M.J.; Huang, R.H.; Eglin, J.L.; Dye, J.L. An electride with a giant 6-electron ring. *Nature* **1994**, *368*, 726–729.
32. Huang, R.H.; Faber, M.K.; Moeggenborg, K.J.; Ward, D.L.; Dye, J.L. Structure of  $\text{K}^+(\text{cryptand}[2.2.2])$  electride and evidence for trapped electron pairs. *Nature* **1988**, *331*, 599–601.
33. Singh, D.J.; Krakauer, H.; Haas, C.; Pickett, W.E. Theoretical determination that electrons act as anions in the electride  $\text{Cs}^+(15\text{-crown-5})_2\text{e}^-$ . *Nature* **1993**, *365*, 39–42.
34. Hendrickson, J.E.; Pratt, W.P., Jr.; Phillips, R.C.; Dye, J.L. Optical spectra and conductivities of thin films of the electride  $\text{K}^+(\text{C222})\text{e}^-$ . *J. Phys. Chem., B* **1998**, *102*, 3917–3926.
35. Beckman, T.A.; Pitzer, K.S. The infrared spectra of marginally metallic systems: Sodium-ammonia solutions. *J. Phys. Chem.* **1961**, *65*, 1527–1532.
36. Ichimura, A.S.; Wagner, M.J.; Dye, J.L. Anisotropic charge transport and spin–spin interactions in  $\text{K}^+(\text{cryptand}[2.2.2])$  electride. *J. Phys. Chem., B* **2002**, *106*, 11196–11202.
37. Srdanov, V.I.; Stucky, G.D.; Lippma, E.; Engelhardt, G. Evidence for an antiferromagnetic transition in a zeolite-supported cubic lattice of F-centers. *Phys. Rev. Lett.* **1998**, *80*, 2449–2452.
38. Ichimura, A.S.; Dye, J.L.; Camblor, M.A.; Villaescusa, L.A. Toward inorganic electrides. *J. Am. Chem. Soc.* **2002**, *124*, 1170–1171.



# The Allosteric Effect

Anatoly K. Yatsimirsky

Universidad Nacional Autónoma de México, Mexico City, Mexico

## INTRODUCTION

The allosteric regulation of ligand binding to proteins is the principal regulatory mechanism in living systems on the molecular level.<sup>[1-3]</sup> The allosteric effect means the situation when the binding of one ligand at its binding site is influenced by the occupation of another binding site by another identical (homotropic effect) or different (heterotropic effect) ligand (effector). In biological systems, the allosteric effect is usually considered for oligomeric proteins, e.g., hemoglobin, and reflects interactions between subunits. In chemistry, it is studied with low-molecular-weight receptors possessing two or more binding sites, the interaction between which is mediated by conformational changes induced in the receptor upon occupation of one site. The positive allosteric effect, when the occupation of one site increases the affinity to the ligand on the other site, leads to positive cooperativity in ligand binding and may be used for amplification of the signal produced by the effector.<sup>[4,5]</sup> Allosteric regulation is a possible way to operate molecular switches, and it is important for the functioning of molecular machines.<sup>[4]</sup>

## BINDING ISOTHERMS FOR ALLOSTERIC SYSTEMS

In a general case of a receptor possessing  $N$  binding sites, the stepwise stoichiometric formation constants are defined as follows:

$$K_i = [RL_i]/([RL_{i-1}][L])$$

where  $1 \leq i \leq N$ , and the overall formation constants are defined as

$$\beta_i = K_1 K_2 \dots K_{i-1} K_i$$

In addition, one can define a single-site binding constant  $Q$  as

$$Q = [\text{occupied single site}]/([\text{free single site}][L])$$

The expression for the degree of complexation (or degree of saturation)  $Y$  is defined as follows:

$$Y = \frac{\text{(concentration of occupied sites)}}{\text{(total concentration of binding sites)}}$$

It has the following form:

$$Y = \frac{\sum_{i=1}^N i\beta_i[L]^i}{N\left(1 + \sum_{i=1}^N \beta_i[L]^i\right)} \quad (1)$$

Another useful function for the analysis of binding is the Bjerrum complex formation function  $\bar{n}$ , which gives an average number of ligand molecules bound per receptor:

$$\bar{n} = YN$$

In the case when the receptor possesses  $N$  identical and independent sites:

$$K_i = Q(N - i + 1)/i$$

and the ratio of two successive stability constants is<sup>[6]</sup>

$$K_{i+1}/K_i = i(N - i)/((i + 1)(N - i + 1)) \quad (2)$$

Evidently each next stability constant is smaller than the preceding one due to only statistical factors. Any deviation from the statistical ratio  $K_{i+1}/K_i$  implies a nonequivalence of binding sites or some sort of interaction between sites, in particular due to the allosteric effect. In the latter case, deviations from statistical binding are commonly referred to as cooperativity, which can be positive or negative, depending on whether the ratio of successive stability constants is higher or lower than the statistically expected value.<sup>[6]</sup>

The binding isotherm for the statistical binding takes a form of Eq. 3:

$$Y = Q[L]/(1 + Q[L]) \quad (3)$$

A modified linear form<sup>[6]</sup> of Eq. 3 is as below:

$$\bar{n}/[L] = NQ - \bar{n}Q \quad (4)$$

This is known as the Scatchard equation. Eq. 3 describes a simple hyperbolic binding isotherm, like in a case of a 1:1 complexation. The cooperative binding, however, modifies to a smaller or greater extent the shape of the isotherm, in particular, positive cooperativity leads to "sigmoid" binding isotherms. The oldest and still popular way to diagnose cooperativity by the analysis of the shape of the binding isotherm is to calculate the so-called Hill

coefficient  $h$ , which is the slope of the plot of  $\log(Y/(1-Y))$  versus  $\log[L]$ .<sup>[6]</sup>

$$h = d \log(Y/(1-Y)) / d \log[L] \quad (5)$$

The Hill equation was derived originally for a complexation process, which involves only one equilibrium between  $R$  and  $h$  molecules of  $L$  affording the single complex  $RL_h$ . The degree of saturation is given in this case by the following equation:

$$Y = [RL_h]/[R]_t = \beta_h [L]^h / (1 + \beta_h [L]^h) \quad (6)$$

which for  $h > 1$  describes a sigmoid-binding isotherm. Usually a linearized form given by Eq. 7 is used for the data fitting:

$$\log(Y/(1-Y)) = h \log[L] + \log \beta_h \quad (7)$$

Evidently this equation implies an infinite cooperativity when the binding constants for all complexation processes with  $i < h = N$  equal to zero. In real cases, the value of  $h$  defined as in Eq. 5 is approximately constant only in a restricted range of concentrations of  $L$ , typically around 50% of saturation. It approaches  $N$  when the positive cooperativity is high, equals unity for statistical binding, and is smaller than unity for negative cooperativity.

Typical sigmoid isotherms are shown in Fig. 1 for cooperative binding of dicarboxylic acids **16** and **17** to a double-decker porphyrin with pyridine substituents **15a** (see below, Fig. 5). The Hill coefficient for these systems  $h=4$  equals the total number of bound guests as a result of a strong positive allosteric effect.<sup>[4]</sup>

Classical models for the cooperative binding to oligomeric proteins, which are formally applicable also for synthetic receptors, include the symmetry model of

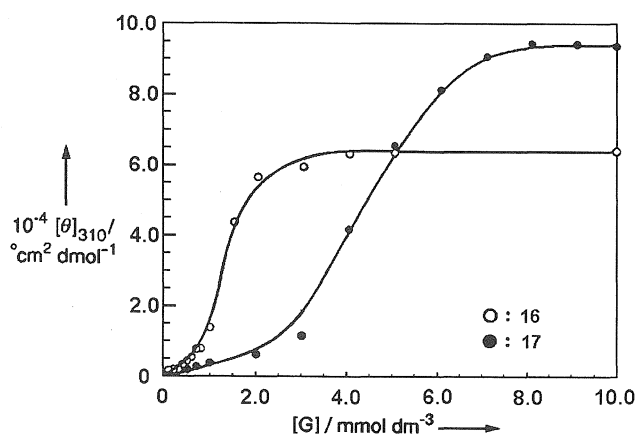
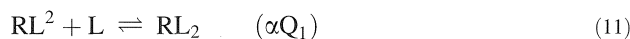
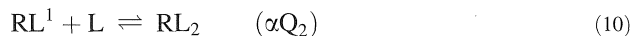


**Fig. 1** Binding isotherms of Guests **16** and **17** to Receptor **15a** (see Fig. 5) followed by the complexation-induced circular dichroism.<sup>[4,25]</sup> Reprinted with permission from Ref. [4]. Copyright 2001 by American Chemical Society.

Monod–Wyman–Changeux (MWC model)<sup>[7]</sup> and the sequential or induced-fit model of Koshland–Nemethy–Filmer (KNF model).<sup>[8]</sup> In the MWC model, the positive cooperativity is due to a mechanism that does not involve any positive site interactions. It results from the complexation-induced shift of preequilibrium between two states of the receptor, in which all binding sites have different conformations possessing different affinities to the ligand [the tense (T) or relaxed (R) state in hemoglobin]. In the KNF model, ligand binding induces a conformational change in the receptor-binding site, which is transmitted to other binding sites. If the interaction between sites is strong, the conformational change may occur in a concerted manner involving all binding sites and, in this case, the model formally coincides with the MWC model.

A large number of allosteric systems discussed below involve a receptor  $R$  possessing two binding sites for two different ligands (heterotropic system). Analysis of such a system is straightforward: one can measure the single-site binding constant for any ligand in the absence of the other ligand and then compare it with the binding constant determined in the presence of the other ligand. Analysis of homotropic systems is more complicated. Eqs. 8–11 describe such a system:



Here, superscripts 1 and 2 refer to first and second binding sites;  $Q_1$  and  $Q_2$  are the respective single-site binding constants; and  $\alpha$  is the interaction factor that shows how the binding constant for a given site changes upon occupation of the other site. Note that the interaction factor is the same for both binding sites. The stepwise stoichiometric formation constants equal:

$$K_1 = Q_1 + Q_2 \quad (12)$$

$$K_2 = \alpha Q_1 Q_2 / (Q_1 + Q_2) \quad (13)$$

Obviously, in this case, the single-site binding constants and the site interaction factor cannot be calculated from the experimentally determined constants  $K_1$  and  $K_2$  without making additional assumptions concerning possible equivalence or mutual dependence of the binding sites. In the case of statistical binding,  $Q_1 = Q_2 = Q$  and  $\alpha = 1$ ; therefore  $K_1 = 2Q$ ,  $K_2 = Q/2$ , and the ratio  $K_2/K_1 = 1/4$ . If the binding sites are equivalent ( $Q_1 = Q_2 = Q$ ) but not independent ( $\alpha \neq 1$ ), one observes positive ( $K_2/K_1 > 1/4$ ) or negative ( $K_2/K_1 < 1/4$ ) cooperativity when  $\alpha$  is larger or smaller than unity, respectively. Alternatively, if the

binding sites are nonequivalent ( $Q_1 \neq Q_2$ ) but independent ( $\alpha=1$ ), the ratio  $K_2/K_1$  equals

$$\begin{aligned} K_2/K_1 &= Q_1 Q_2 / (Q_1 + Q_2)^2 \\ &= (Q_2/Q_1) / (1 + Q_2/Q_1)^2 \end{aligned} \quad (14)$$

Predicted with Eq. 14 is that  $K_2/K_1$  has the maximum value of 1/4 at  $Q_2/Q_1=1$ , and, therefore, at all nonequal values of  $Q_1$  and  $Q_2$ , the ratio  $K_2/K_1$  is less than 1/4. In this case, a negative cooperativity without negative interaction between the binding sites is observed.

It should be noted that cooperativity does not necessarily result from site interaction. Often, the mutual attraction or repulsion of bound ligands leads to positive or negative cooperativity, respectively. For example, highly cooperative binding of four molecules of *n*-octyl  $\beta$ -D-glucopyranoside to the resorcinol cyclic tetramer in  $\text{CHCl}_3$ , which is characterized by the Hill coefficient  $h=4$ , results from intracomplex guest-guest hydrogen bonding involving the 5- $\text{CH}_2\text{OH}$  and 2-OH groups of adjacent glucopyranoside molecules.<sup>[9]</sup>

## ALLOSTERIC SYSTEMS BASED ON CROWN ETHERS AND PODANDS

The earliest examples of synthetic allosteric systems involved modification of binding properties of crown ethers by changing their conformations as a result of complexation with another metal cation at an adjacent binding site. For example, complexation of a bipyridine moiety of **1** (Fig. 2) with  $\text{W}(\text{CO})_4$  changes the selectivity of the crown ether from preferable binding of  $\text{K}^+$  over  $\text{Na}^+$  to preferable binding of  $\text{Na}^+$  over  $\text{K}^+$ .<sup>[10]</sup> In a more recent study of the cooperative binding of  $\text{K}^+$  or  $\text{Ca}^{2+}$  and monosaccharides to Receptor **2** (Fig. 2), reminiscent by its design of **1**, a negative allosteric effect was reported.<sup>[11]</sup> Cation-induced changes in the macrocycle conformation produced a disposition of boronic acids unfavorable for the saccharide complexation.

The *bis*-crown ether **3** (Fig. 2) showed a negative cooperativity in binding two  $\text{K}^+$  or  $\text{Na}^+$  cations, which resulted, however, from mutual repulsion of metal ions rather than from a negative allosteric effect.<sup>[12]</sup> Binding of two neutral Lewis acids, e.g.,  $\text{Hg}(\text{CN})_2$  showed a positive cooperativity with the Hill coefficient  $h=1.5$ .<sup>[12]</sup> This was interpreted as a result of positive allosteric effect due to the reduction of the conformational freedom of the second macrocycle favorable for complexation conformation upon binding of the first  $\text{Hg}(\text{CN})_2$  molecule.

A strong negative allosteric effect was found for the complexation of diquat dication by *bis*-crown receptor **4**

(Fig. 2) in the presence of transition metal complexes like  $\text{Cr}(\text{CO})_4$  and  $\text{Ru}(\text{Bipy})_2^{2+}$ .<sup>[13]</sup> Binding of these complexes to a bipyridine moiety of **4** induces rotation of the aromatic rings and formation of a planar structure, which does not bind diquat dication.

A large group of receptors showing a positive cooperativity in metal ion complexation is based on polyether (podand) compounds bearing terminal groups capable of chelation of transition metal ions.<sup>[14]</sup> As an example, in Fig. 2 (**5**), a complexation-induced cyclization of a podand bearing  $\beta$ -diketone terminal groups is shown.<sup>[15]</sup> The resulting complex is capable of complexation of alkali metal cations. Other examples of such pseudocrown ethers can be found in Ref. [14]. As pointed out in the preceding section, the interaction factor must be the same for two binding sites of a receptor. Therefore, one should expect that the complexation of a podand with an alkali metal cation in its turn must promote the interaction between the terminal groups. Such an effect was demonstrated for system **6** (Fig. 2).<sup>[16]</sup> A podand bearing two  $\text{Zn}(\text{II})$  porphyrin complexes recognizes diamines by sandwiching them between two metal centers. The addition of sodium cations increases by a factor of 2 the affinity of the receptor to 1,2-diaminocyclohexane.

The allosteric regulation of the binding of an organic guest by complexation with alkali cations is illustrated by the molecular clip **7a**, Fig. 2.<sup>[17]</sup> It exists in three conformations *ss*, *sa*, and *aa*, interconverting slowly on the NMR time scale. The predominant conformer *sa* (as well as a minor conformer *sa*) converts upon uptake of a potassium ion in the crown ether bottom unit to *aa* conformer, which then binds an aromatic guest, such as 1,3-dinitrobenzene, about four times better than without  $\text{K}^+$  (Fig. 2, **7b**).

The allosteric effect also plays a role in the cooperative binding of anions and cations by some ditopic receptors, such as in the case of Receptor **8**, Fig. 2.<sup>[18]</sup> The positive cooperativity in the binding of  $\text{Cl}^-$  in the presence of  $\text{K}^+$  partly results from the electrostatic attraction between oppositely charged ions. But, at the same time, binding of  $\text{H}_2\text{PO}_4^-$  shows a negative cooperativity with  $\text{K}^+$ , and this specificity to the type of anion indicates a contribution of some nonelectrostatic, most probably, conformational effects.

## ALLOSTERIC SYSTEMS BASED ON CYCLOPHANES

A cyclophane possesses a hydrophobic cavity suitable for complexation of nonpolar organic guests. Several heterotropic allosteric systems based on cavity formation induced by complexation with transition metal cations were reported. The idea is generally similar to metal-induced

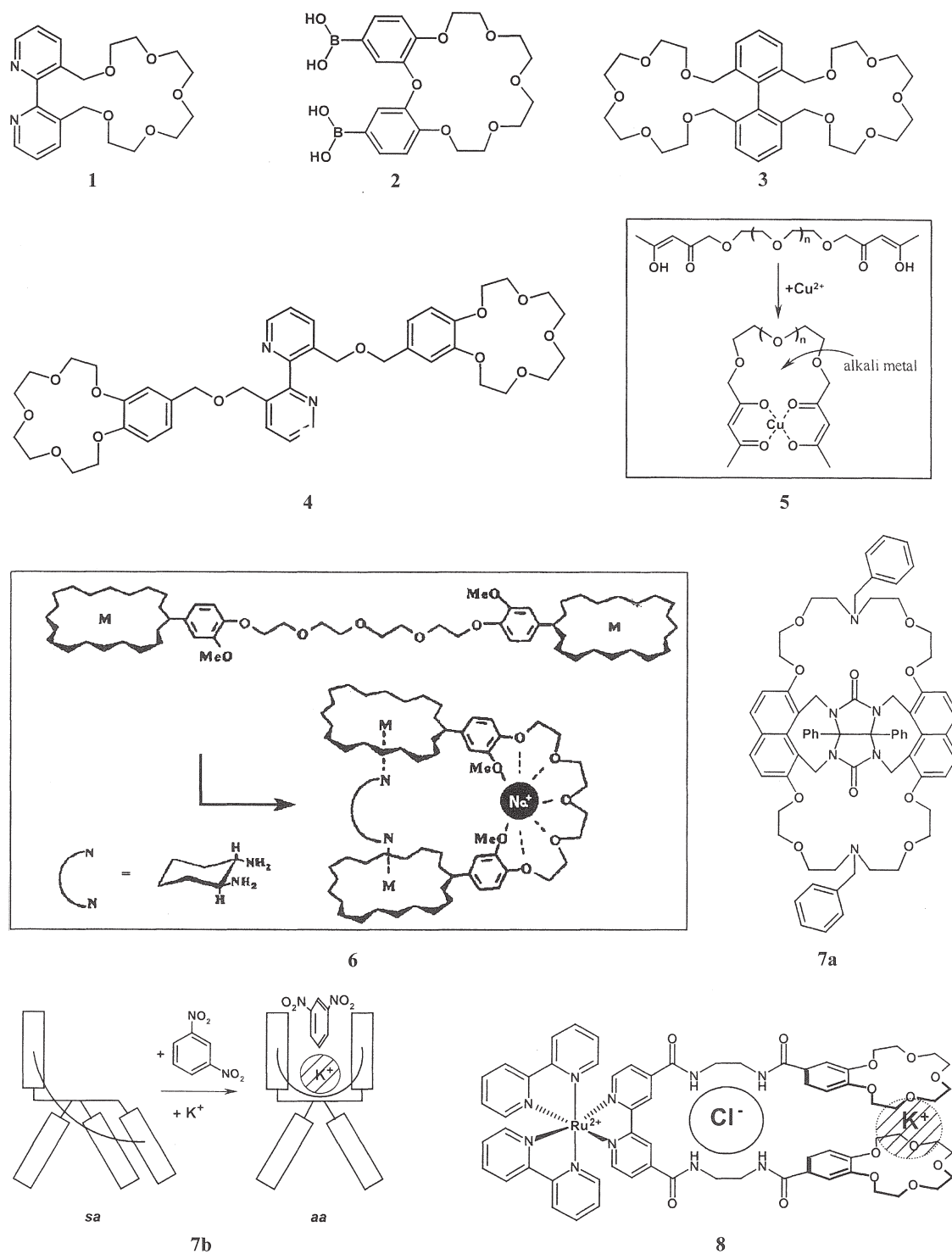


**Fig. 2** Allosteric systems based on complexation with crown ethers and podands. Entry 6. From Ref. [16]. Reproduced by permission of The Royal Society of Chemistry (RSC) on behalf of the Centre National de la Recherche Scientifique (CNRS).

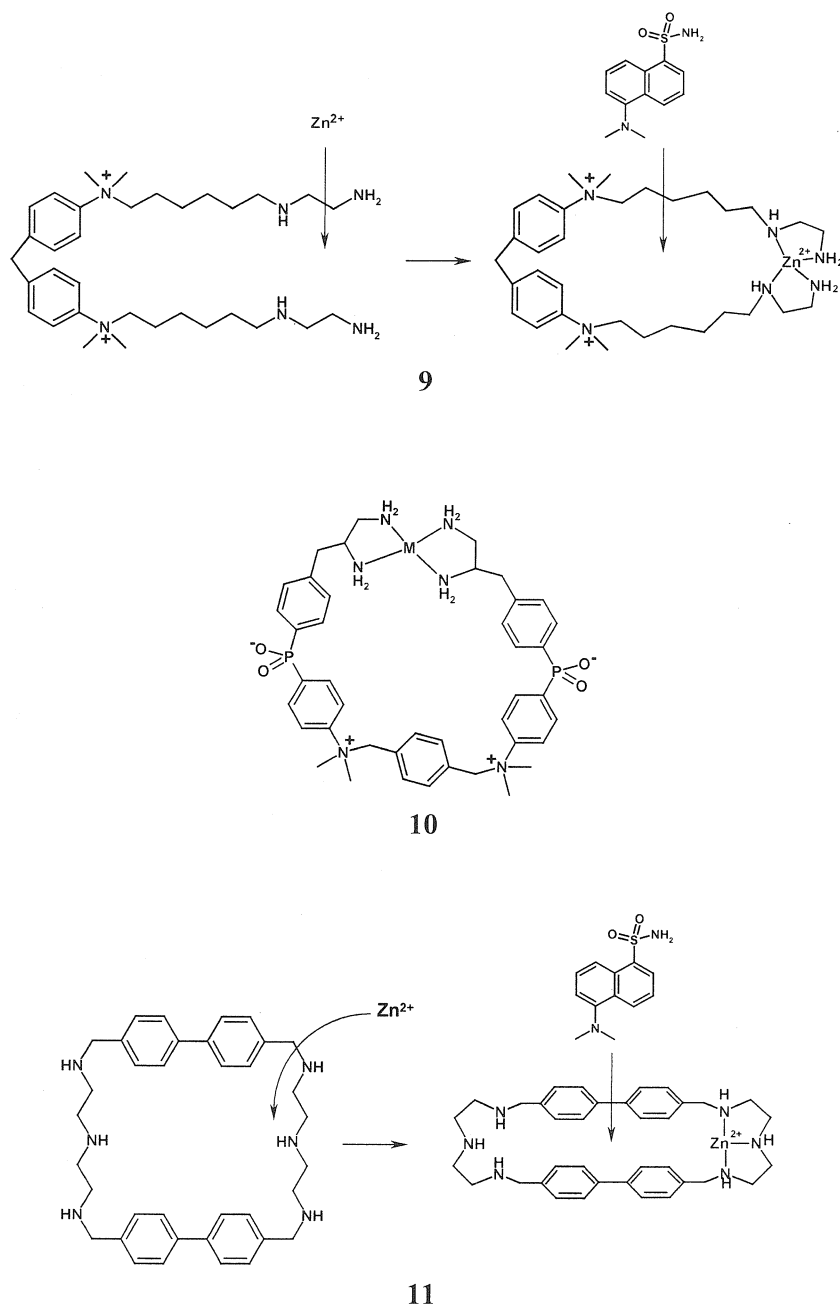


Fig. 3 Allosteric systems based on complexation with cyclophanes.

cyclization of podands described in the preceding section [see Fig. 2 (5) as an example], but instead of leading to cooperativity between binding of two different metal ions, it leads to the cooperativity between binding of a metal ion and an organic molecule. Illustrated in Fig. 3 (9) is a cooperative complexation of  $Zn(II)$  or  $Cu(II)$  and a fluorescent indicator dansylamide to an open cyclophane precursor bearing ethylenediamine terminal groups.<sup>[19]</sup> Addition of the metal ion closes the cavity and allows the

indicator to form an inclusion complex with the stability constant ca.  $10\text{ M}^{-1}$  in water. This is ca. 100 times less than the stability constant for inclusion of the same guest in a normal azaniacyclophane of the same size, but the important thing is that in the absence of metal ions, the open host does not bind the indicator.

A similar principle was applied for the construction of metallocyclophanes 10, Fig. 3.<sup>[20]</sup> For this system, it was shown that the shape of the hydrophobic cavity depends

on the type of metal cation: when  $M=Zn$ , the host more strongly binds a guest that is a naphthalene derivative than a guest that is a biphenyl derivative, but when  $M=Cu$ , the binding preference is inverted. Thus, the distinct coordination geometries of these metals differently affect the shape of the cavity.

Another principle operates in System **11** (Fig. 3).<sup>[21]</sup> Here, the metal binding leads to the ring contraction and better accommodation of the organic guest in the cavity, which is too large. The stability constant for guest inclusion increases by a factor of 100.

### ALLOSTERIC SYSTEMS BASED ON CALIXARENES

Calix[4]arenes are conformationally flexible hosts particularly suitable for design of allosteric receptors due to a possible communication between binding sites situated at the upper and lower rims.<sup>[5,22]</sup> Positive and negative heterotropic allosterism was demonstrated by using a calix[4]arene with the metal-binding lower rim and the sugar-binding upper rim created by introducing two boronic acid groups.<sup>[22]</sup> Additions of hard cations ( $Ca^{2+}$ ,  $Mg^{2+}$ , or  $Na^+$ ) decreased, but additions of soft cations like  $K^+$ ,  $Rb^+$ , or  $Cs^+$  increased the sugar binding. This switch from a negative to a positive heterotropic allosteric effect, depending on the type of metal cation within a series of cations, which are similar by their chemical natures, demonstrates a possibility of a fine tuning of the binding site conformation of calixarene hosts.

Receptor **12** (Fig. 4) binds urea derivatives in  $CHCl_3$  via hydrogen bonding to two aryl carboxylate groups with a positive allosteric effect based on the conformation change induced by complexation of  $Na^+$  with the crown ether fragment of the receptor.<sup>[23]</sup> In the free receptor, carboxylic groups are at a short distance, favoring intramolecular hydrogen bonding. The addition of  $Na^+$  leads to a larger separation between the carboxylic groups, favoring the intermolecular hydrogen bonding with the guest.

A similar effect of metal-induced conversion of a calixarene conformation with intramolecularly bound amide groups (closed form unable to bind guest molecules) into a conformation with more separated unbound amide groups (open form) capable of complexation with amide guests operates in the allosteric regulation of the host **13** (Fig. 4).<sup>[5]</sup>

Widening the opposite side of a calixarene upon complexation of small cations to the oxygen atoms of a calixarene lower rim leads to the positive heterotropic allosteric effect in the inclusion of [60]fullerene in a cage molecule **14** (Fig. 4) derived from two calix[3]aryl esters by complexation of their pyridine groups with  $Pd(II)$ .<sup>[24]</sup>

Receptor **14** binds [60]fullerene in  $CHCl_2CHCl_2$  with the stability constant  $K=39\text{ M}^{-1}$ . The addition of  $Li^+$  cations induces flattening of the cage and an increase in  $K$  up to  $2100\text{ M}^{-1}$ . Interestingly, the addition of  $Na^+$  cations produces a strong negative allosteric effect.

### DIMERIC PORPHYRINS

Face-to-face dimeric metalloporphyrins represent a new class of homotropic allosteric receptors that show strong positive cooperativity in binding different guests.<sup>[4,5,25]</sup> As an example, in Fig. 5, the cerium(IV) *bis*[tetrakis(4-pyridyl)-porphyrinate] double decker is shown, with **15a** designed for complexation of dicarboxylic acids **16** and **17**. The addition of any of these guests to **15a** in dichloromethane/ethyl acetate (30/1) leads to the appearance of circular dichroism spectra. The value of  $[\theta]_{\max}$  at 310 nm was found to be proportional to the amount of complexed receptor. Shown in Fig. 1 are the respective plots of  $[\theta]_{\max}$  versus guest concentration, which have typical sigmoid shape and give  $h=4$  in the Hill coordinates. The binding mode of the guests is illustrated in Fig. 5 (**18**). It is proposed that successive binding of guest molecules reduces the degree of free rotation of porphyrin rings in the double decker, which makes the binding of each next guest more energetically favorable. Binding of the same guests to **15b**, which can bind only one guest molecule, is too weak to be detectable in agreement with weak binding of the first guest to **15a** required for high cooperativity.

Interestingly, a similarly designed double decker for the complexation of saccharide guests, **19** (Fig. 5), shows negative cooperativity: only one guest can be bound to the receptor. The difference between these two systems is that in the case of **15a**, binding of the guests does not change the basic structure of the double decker. But in the case of **19**, binding of the first guest induces deformation of the receptor structure, which makes more distant other boronic acid groups and thus precludes the binding of additional guests.

### ALLOSTERIC REGULATION OF REACTIVITY AND CATALYSIS

Enzyme regulation is one of the most important biological applications of the allosteric effect. There is, however, little progress in reproducing regulation of reactivity and catalysis in chemical systems. Earlier works demonstrated a possibility of allosteric regulation of reactivity in several simple systems possessing a 2,2'-bipyridyl unit as a regulatory switch relevant to allosteric receptors of type **1**.<sup>[26]</sup>



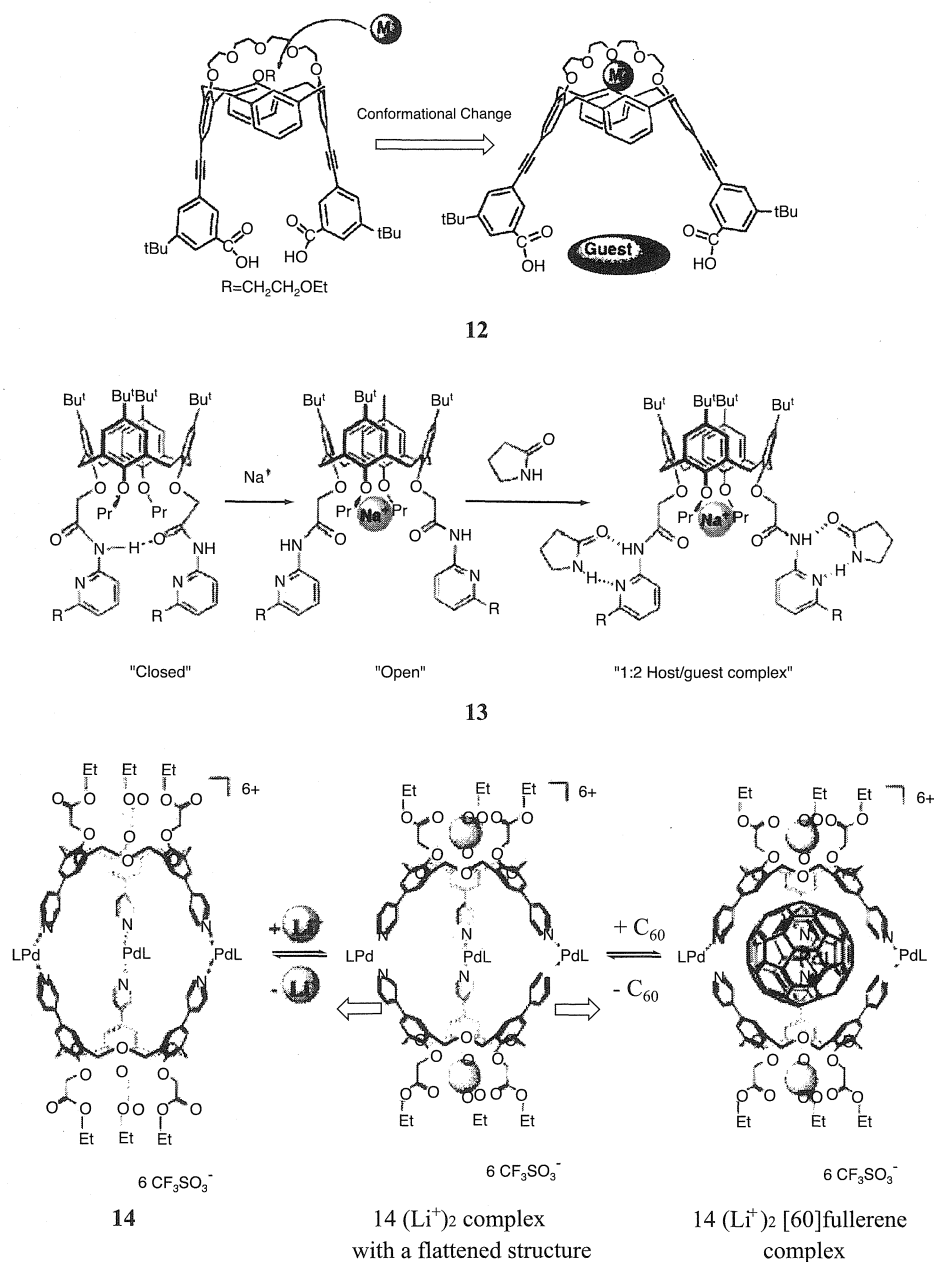


**Fig. 4** Positive heterotropic allosteric regulation of complexation with calixarene hosts. Entry **12**: Reprinted from Ref. [23]. Copyright 1998, with permission from Elsevier; Entry **13**: Reprinted with permission from Ref. [5]. Copyright 2001 by American Chemical Society; Entry **14**: Reprinted from Ref. [24]. Copyright 2000, with permission from Elsevier.

For example, rate of cyclization of **20** strongly increases in the presence of  $\text{Ni(II)}$  cations. Rates of nucleophilic substitution in and elimination from **21** strongly increase in the presence of  $\text{Pd(II)}$  (Fig. 6). These systems, however, did not allow a clear separation of conformational and electronic, in particular, inductive effects.

The allosteric 30-fold acceleration of the reduction of a podand bearing a quinone group by 1-propyl-1,4-dihydronicotinamide in the presence of potassium cations<sup>[27]</sup> is illustrated in Fig. 6 (**22**). The system is based on the same

principle as **6** (Fig. 2). A different approach was proposed for the allosteric regulation of a catalyst for the phosphodiester cleavage, **23** (Fig. 6).<sup>[28]</sup> The catalyst is a trinuclear metal complex with two functional metal ions ( $M_F$ ), which activate the phosphodiester substrate, and one structural ion ( $M_S$ ), which has the regulatory function. With  $M_F = \text{Cu(II)}$ , variation in  $M_S = \text{Cu(II)}$ ,  $\text{Ni(II)}$ , or  $\text{Pd(II)}$  leads to significant changes in the catalytic activity attributed to subtle differences in the ionic radius and coordination geometry of the allosteric metal ion.

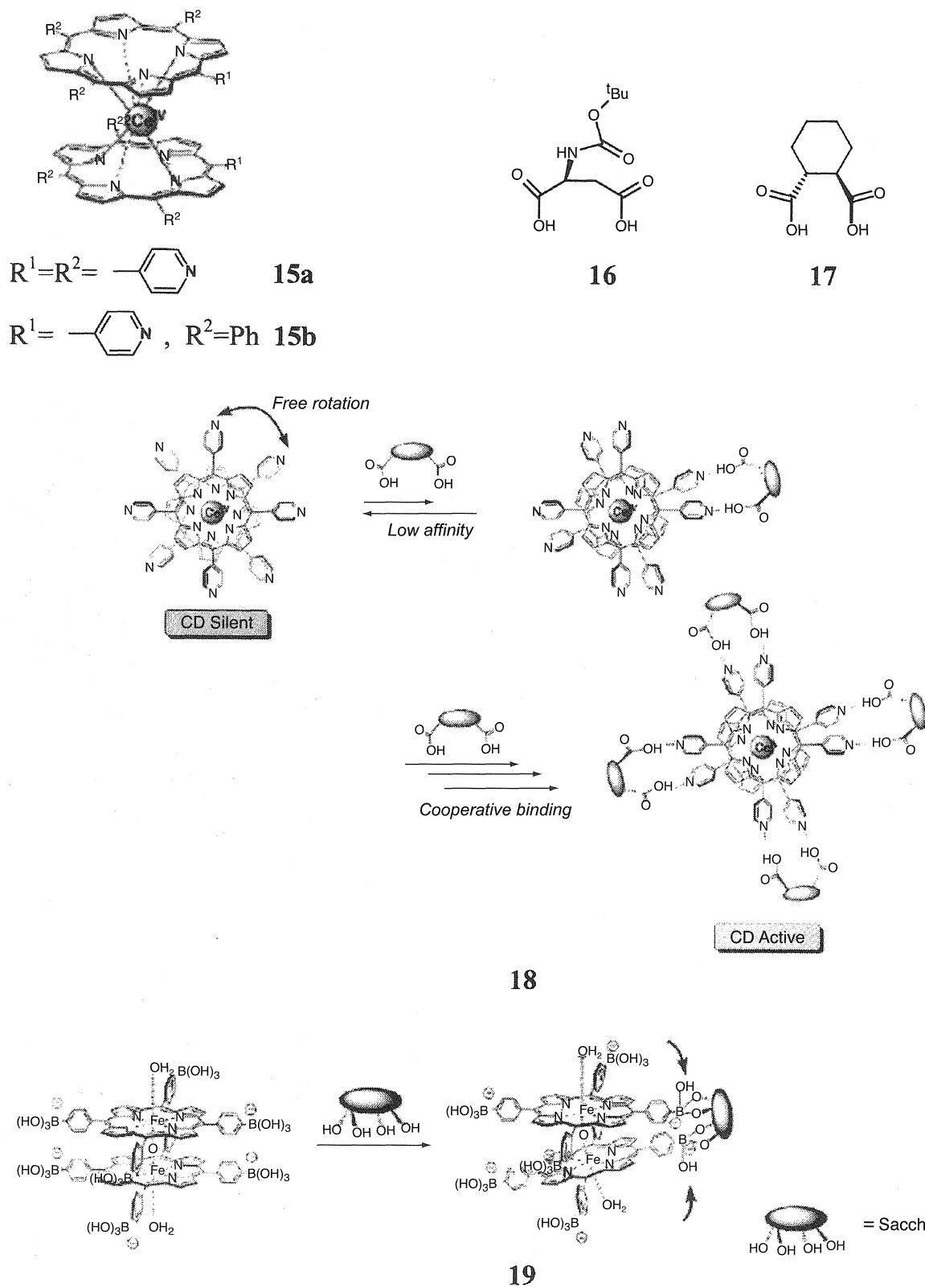


**Fig. 5** Allosteric systems based on porphyrin face-to-face dimers. Entries **18** and **19**: Reprinted with permission from Ref. [4]. Copyright 2001 by American Chemical Society.

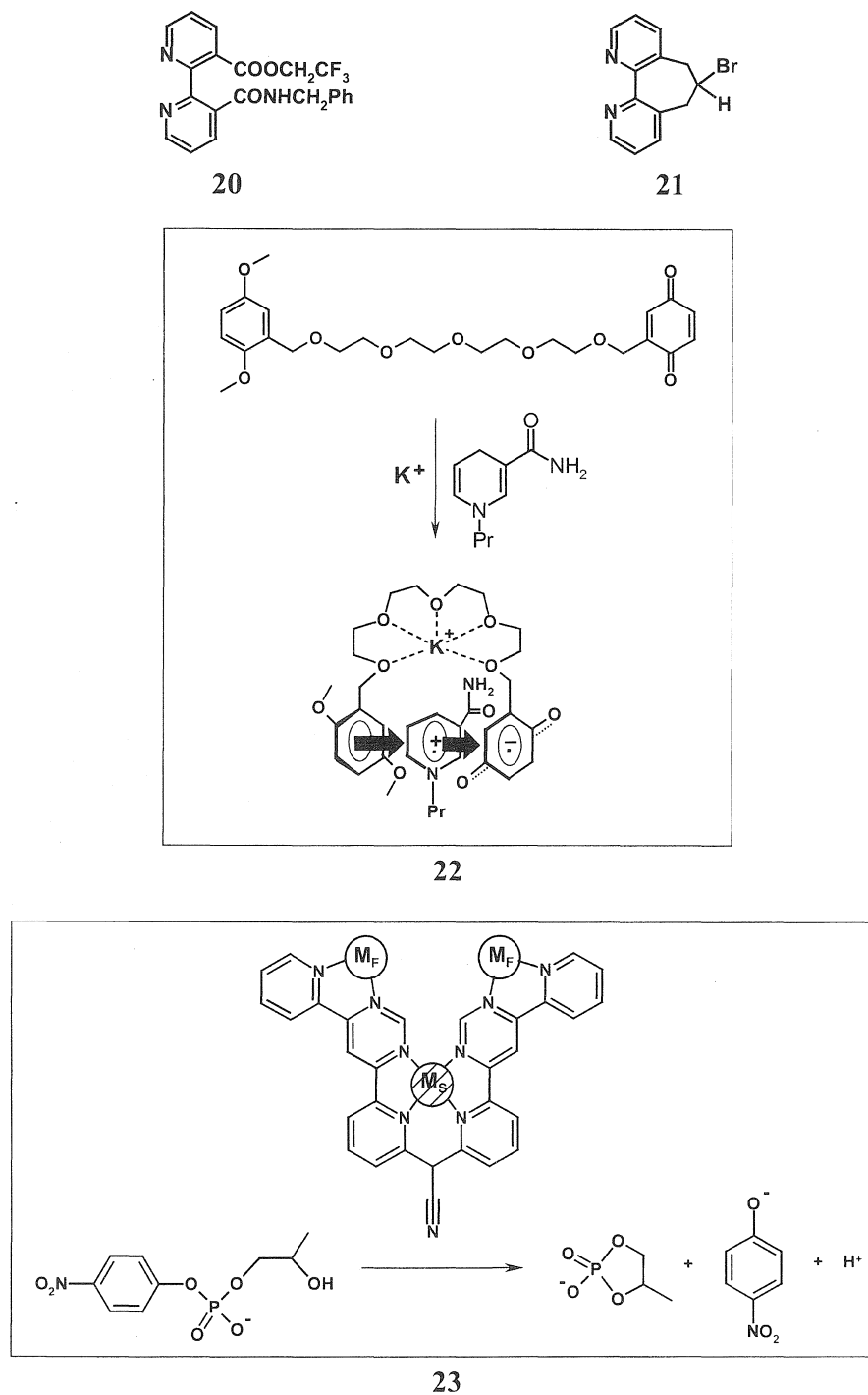


Fig. 6 Allosteric regulation of reactivity.

### MISCELLANEOUS ALLOSTERIC SYSTEMS

Not unexpectedly, many attempts were made to imitate the cooperativity of oxygen binding by hemoglobin, e.g., by using *bis*-metalloporphyrin complexes.<sup>[29]</sup> Allosteric

preorganization of oligobipyridine ligands by coordination with Cu(I) leads to self-assembly of interesting metal helicates with strand characteristics of DNA.<sup>[30]</sup> A similar effect was reported in complexation of Fe(III) with tripodal hydroxamate ligands: each next step in the consecutive

complexation of three metal ions has a larger stability constant.<sup>[31]</sup> Strong cooperativity between cation and anion binding to a cyclopeptide in  $\text{CHCl}_3$  was attributed at least partially to the allosteric effect.<sup>[32]</sup>

## CONCLUSION

Allosteric regulation requires a certain conformational flexibility of the receptor. The positive allosteric effect may be considered a preorganization of one binding site by a conformational change induced by the occupation of the other binding site. Many widely used types of synthetic hosts, such as crown ethers, cyclophanes, and calixarenes, have suitable conformational dynamic properties, but the recent discovery of other highly efficient allosteric systems based on, e.g., porphyrin double-decker structures points to the possibility of using receptors of different structural types. It should be noted that the actual mechanism of the allosteric effect in many systems remains essentially hypothetical. With oligomeric proteins, binding sites are separated by large distances, excluding any mutual interaction between bound guests. In synthetic hosts, binding sites are close enough to expect some contribution of such interaction to the observed cooperativity, which is difficult to separate from the purely conformational effect. Practically, further development of allosteric systems promises considerable progress in the creation of new receptors and catalysts with tunable properties, as well as new analytical and other devices with improved sensitivity and selectivity.

## ARTICLES OF FURTHER INTEREST

*Hemoglobins: O<sub>2</sub> Uptake and Transport*, p. 636

*Induced Fit*, p. 717

*The Lock and Key Principle*, p. 809

*Molecular Switches*, p. 917

*Molecular-Level Machines*, p. 931

*O<sub>2</sub> Uptake and Transport, Models of*, p. 1023

*Preorganization and Complementarity*, p. 1158

## REFERENCES

1. Fersht, A. *Enzyme Structure and Mechanism*, 2nd Ed.; W. H. Freeman: New York, 1985.
2. Levitzki, A. *Quantitative Aspects of Allosteric Mechanism*; Springer: New York, 1978.
3. Perutz, M.F. Mechanisms of cooperativity and allosteric regulation in proteins. *Q. Rev. Biophys.* **1989**, *22*, 139–236.
4. Shinkai, S.; Ikeda, M.; Sugasaki, A.; Takeuchi, M. Positive allosteric systems designed on dynamic supramolecular scaffolds: Toward switching and amplification of guest affinity and selectivity. *Acc. Chem. Res.* **2001**, *34* (6), 494–503.
5. Takeuchi, M.; Ikeda, M.; Sugasaki, A.; Shinkai, S. Molecular design of artificial molecular and ion recognition systems with allosteric guest responses. *Acc. Chem. Res.* **2001**, *34* (11), 865–873.
6. Perlmutter-Hayman, B. Cooperative binding to macromolecules. A formal approach. *Acc. Chem. Res.* **1986**, *19* (3), 90–96.
7. Monod, J.; Wyman, J.; Changeux, J. D. On the nature of allosteric transitions: A plausible model. *J. Mol. Biol.* **1965**, *12* (1), 88–118.
8. Koshland, D.E.; Nemethy, G.; Filmer, D. Comparison of experimental binding data and theoretical models in proteins containing subunits. *Biochemistry* **1966**, *5* (1), 365–385.
9. Kikuchi, Y.; Tanaka, Y.; Sutarto, S.; Kobayashi, K.; Toi, H.; Aoyama, Y. Highly cooperative binding of alkyl glucopyranosides to the resorcinol cyclic tetramer due to intracomplex guest–guest hydrogen-bonding: Solvophobicity/solvophilicity control by an alkyl group of the geometry, stoichiometry, stereoselectivity, and cooperativity. *J. Am. Chem. Soc.* **1992**, *114* (26), 10302–10306.
10. Rebek, J., Jr.; Wattlely, R.V. Allosteric effects. Remote control of ion transport selectivity. *J. Am. Chem. Soc.* **1980**, *102* (14), 4853–4854.
11. Deng, G.; James, T. D.; Shinkai, S. Allosteric interaction of metal ions with saccharides in a crowned diboronic acid. *J. Am. Chem. Soc.* **1994**, *116* (11), 4567–4572.
12. Rebek, J., Jr.; Costello, T.; Marshall, L.; Wattlely, R.; Gadwood, R.C.; Onan, K. Allosteric effects in organic chemistry: Binding cooperativity in a model of subunit interactions. *J. Am. Chem. Soc.* **1985**, *107* (25), 7481–7487.
13. Beer, P.D.; Rothin, A.B. A new allosteric bis crown ether ligand that displays negative binding cooperativity of the diquaternary by the complexation of a transition metal guest. *J. Chem. Soc. Chem. Commun.* **1988**, (1), 52–54.
14. Nabeshima, T. Regulation of ion recognition by utilizing information at the molecular level. *Coord. Chem. Rev.* **1996**, *148*, 151–169.
15. Kobuke, Y.; Satoh, Y. Positive cooperativity in cation binding by novel polyether bis( $\beta$ -diketone) hosts. *J. Am. Chem. Soc.* **1992**, *114* (2), 789–790.
16. Monti, D.; La Monica, L.; Scipioni, A.; Mancini, G. Effect of the inclusion of sodium cations on the binding properties of a switchable diporphyrin receptor. *New. J. Chem.* **2001**, *25*, 780–782.
17. Sijbesma, R.P.; Nottle, R.J.M. A molecular clip with allosteric binding properties. *J. Am. Chem. Soc.* **1991**, *113* (17), 6695–6696.
18. Beer, P.D.; Dent, S.W. Potassium cation induced switch in anion selectivity exhibited by heteroditopic ruthenium(II) and rhenium(I) bipyridyl bis(benzo-15-crown-5) ion pair receptors. *Chem. Commun.* **1998**, (7), 825–826.
19. Schneider, H.-J.; Ruf, D. A synthetic allosteric system with high cooperativity between polar and hydrophobic binding

- sites. *Angew. Chem. Int. Ed. Engl.* **1990**, *29* (10), 1159–1160.
20. Wang, F.; Schwabacher, A.W. Metal control of non-polar binding shape selectivity. *Tetrahedron Lett.* **1999**, *40* (43), 7641–7644.
21. Baldes, R.; Schneider, H.-J. Complexes from polyazacyclophanes, fluorescent indicators, and metal cations—An example of allostereism through ring contraction. *Angew. Chem. Int. Ed. Engl.* **1995**, *34* (3), 321–323.
22. Ohseto, F.; Yamamoto, H.; Matsumoto, H.; Shinkai, S. Allosteric communication between the metal-binding lower rim and the sugar-binding upper rim in a calix[4]crown platform. *Tetrahedron Lett.* **1995**, *36* (38), 6911–6914.
23. Haino, T.; Katsutani, Y.; Akii, H.; Fukazawa, Y. Allosteric receptor based on monodeoxycalix[4]arene crown ether. *Tetrahedron Lett.* **1998**, *39* (44), 8133–8136.
24. Ikeda, A.; Udzu, H.; Yoshimura, M.; Shinkai, S. Inclusion of [60]fullerene in a self-assembled homocalix[3]arene-based dimeric capsule constructed by a Pd(II)-pyridine interaction. The Li<sup>+</sup> binding to the lower rims can improve the inclusion ability. *Tetrahedron* **2000**, *56* (13), 1825–1832.
25. Takeuchi, M.; Imada, T.; Shinkai, S. A strong positive allosteric effect in the molecular recognition of dicarboxylic acids by a cerium(IV) *bis*[tetrakis(4-pyridyl)-porphyrinate] double decker. *Angew. Chem. Int. Ed. Engl.* **1998**, *37* (15), 2096–2099.
26. Rebek, J., Jr. Binding forces, equilibria, and rates: New model for enzymic catalysis. *Acc. Chem. Res.* **1984**, *17*, 258–264.
27. Pierre, J.-L.; Gagnaire, G.; Chautemps, P. An artificial allosteric system: Regulation of a biomimetic reduction (NADH model) by potassium ions. *Tetrahedron Lett.* **1992**, *33* (2), 217–220.
28. Fritsky, I.O.; Ott, R.; Pritzkow, H.; Krämer, R. An allosteric synthetic catalyst: Metal ions tune the activity of an artificial phosphodiesterase. *Chem. Eur. J.* **2001**, *7* (6), 1221–1231.
29. Tabushi, I. Artificial allosteric systems. *Pure Appl. Chem.* **1988**, *60* (4), 581–586.
30. Pfeil, A.; Lehn, J.-M. Helicate self-organization: Positive cooperativity in the self-assembly of double-helical metal complexes. *Chem. Commun.* **1992**, 838–840.
31. Blanc, S.; Yakirevich, P.; Laize, E.; Meyer, M.; Libman, J.; Dorsselaer, A.V.; Albrecht-Gary, A.-M.; Shanzer, A. Allosteric effects in polynuclear triple-strand ferric complexes. *J. Am. Chem. Soc.* **1997**, *119* (21), 4934–4944.
32. Kubik, S. Large increase in cation binding affinity of artificial cyclopeptide receptors by an allosteric effect. *J. Am. Chem. Soc.* **1999**, *121* (25), 5846–5855.

# Amide- and Urea-Based Anion Receptors

Philip A. Gale

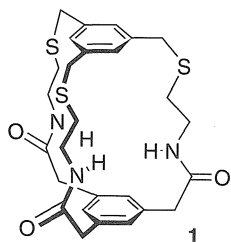
University of Southampton, Southampton, United Kingdom

## INTRODUCTION

Among the armory of functional groups capable of binding anions,<sup>[1–4]</sup> the amides and the ureas are the most commonly employed anion binding sites in neutral organic anion receptor species (Fig. 1a, b). Oxyanion binding in proteins occurs through hydrogen bond donation from, most commonly, the peptide backbone NH groups and from arginine.<sup>[5,6]</sup> One challenge that has been increasingly well met by the supramolecular chemistry community over the last 15 years, has been to design anion receptors with increasing selectivity for particular anionic guests. Of course, the supramolecular chemist does not (yet) have the precise control over the positioning of functional groups in three-dimensional space offered by the tertiary structure of a protein. In spite of this, great progress has been made in the design of neutral anion receptors, with systems now displaying exceptionally high association constants with anions. One of the major design criteria used in developing these systems is to prevent self-association (Fig. 1c) that competes with anion complexation and, hence, lowers association constants.

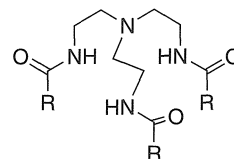
## AMIDES

The first synthetic amide-based anion receptor **1** was reported in 1986 by Pascal Jr. and coworkers.<sup>[7]</sup> This neutral cyclophane-type receptor was synthesized by reaction of 1,3,5-*tris*-(bromomethyl)benzene with three equivalents of cysteamine to form a triamine which was then clipped with one equivalent of the *tris*-acid chloride of 1,3,5-benzenetriacetic acid. The receptor contains three amide NH groups that may be directed into the center of

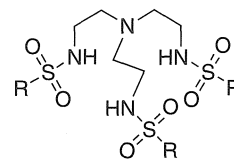


the receptor to form a binding site for smaller anions. Preliminary <sup>1</sup>H- and <sup>19</sup>F-NMR studies in DMSO-*d*<sub>6</sub> suggested that there was an interaction with fluoride anions in solution.

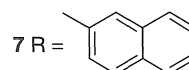
In early work, *tris*-amide-based anion receptors were also prepared by the groups of Reinhoudt and Beer. Reinhoudt and coworkers prepared a series of *tris*-amides and sulfonamides (**2–7**) that are selective for dihydrogenphosphate.<sup>[8]</sup> The receptors were synthesized from *tris*-(aminoethyl)amine (tren) by reaction with an appropriate acid chloride in the presence of triethylamine and were purified by recrystallization from methanol with isolated yields ranging from 70–90%. Association constants were determined with tetrabutylammonium dihydrogen phosphate, hydrogen sulfate, and chloride in acetonitrile by conductometry. The receptors show the selectivity trend  $\text{H}_2\text{PO}_4^- > \text{Cl}^- > \text{HSO}_4^-$ , with receptor **7** having the highest affinity for dihydrogen phosphate (presumably due to the increased acidity of the sulfonamide NH group and  $\pi$ -stacking effects of the naphthalene groups.) Beer and coworkers also synthesized tren-based anion receptors in the early 1990s.<sup>[9]</sup> These systems



- 2** R = CH<sub>2</sub>Cl  
**3** R = (CH<sub>2</sub>)<sub>4</sub>CH<sub>3</sub>  
**4** R = C<sub>6</sub>H<sub>5</sub>  
**5** R = 4-MeOC<sub>6</sub>H<sub>4</sub>



- 6** R = 4-MeC<sub>6</sub>H<sub>4</sub>





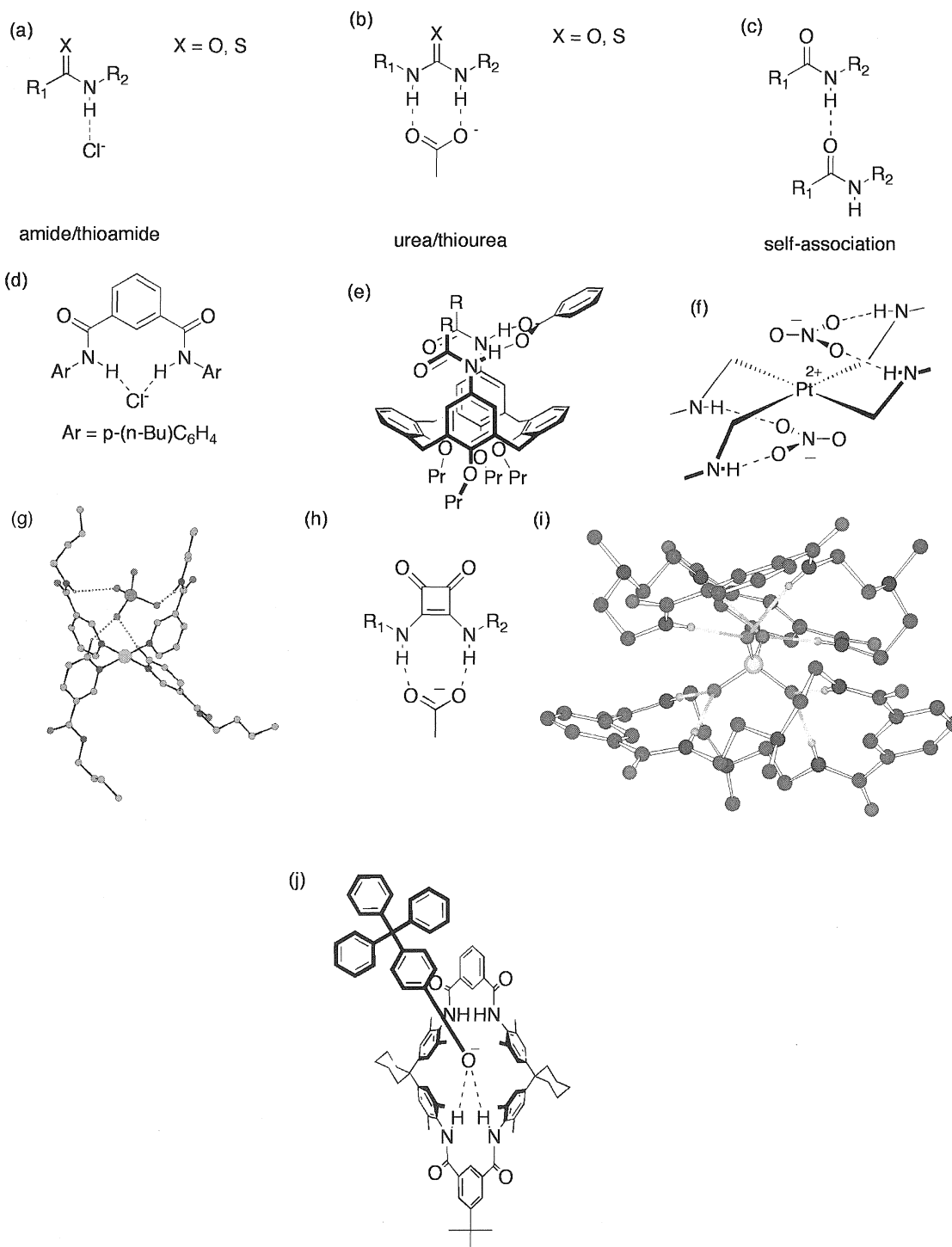
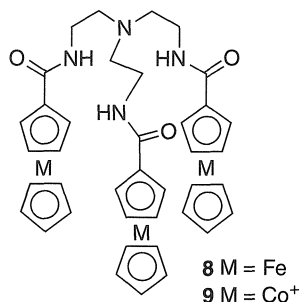
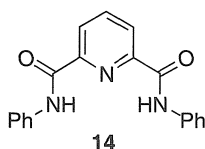
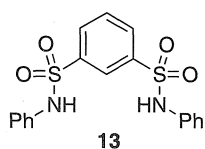
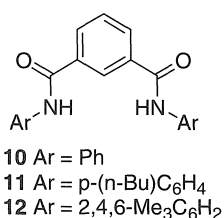


**Fig. 1** (a) Amides and thioamides are excellent hydrogen bond donors to anions; (b) ureas and thioureas are complementary hydrogen bond donors for carboxylates; (c) amides can self-associate so lowering their affinity for anions; (d) Crabtree's isophthalamide **11**–chloride complex; (e) Loeb's upper-rim amide functionalized calix[4]arene–benzoate complex; (f) a schematic diagram of Gale and Loeb's receptor **18** forming a 1:2 receptor:nitrate complex; (g) crystal structure of the perrhenate complex of receptor **18**; (h) a squaramide–acetate complex; (i) crystal structure of the sulfate sandwich formed by receptor **20** and the anion; (j) a phenolate anion bound to a tetralactam macrocycle—a precursor to rotaxane formation. (View this art in color at [www.dekker.com](http://www.dekker.com).)



contained ferrocene **8** or cobaltocenium **9** moieties that act as electrochemical reporter groups and, in the case of **9**, add an electrostatic component to the anion complexation.<sup>[9]</sup> These systems show similar anion selectivity trends as those shown by receptors **2–7**, in addition to being able to sense the presence of anions via cathodic shifts in the metallocenes' redox potentials. Receptor **8**, for example, is capable of detecting dihydrogen phosphate anions in the presence of 10-fold excesses of chloride and hydrogen sulfate.

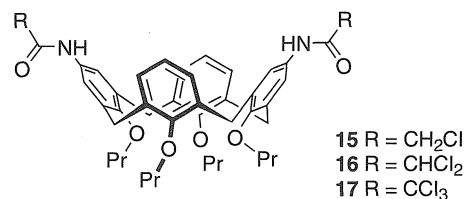
More recently, some simple and yet highly effective amide-cleft-based anion receptors were synthesized by Crabtree and coworkers.<sup>[10]</sup> Receptors **10–14** are based upon benzene or pyridine rings that are substituted in the 1- and 3-positions, or in the case of pyridine 2- and 6-positions, with either amide or sulfonamide groups. Proton NMR titrations in dichloromethane-*d*<sub>2</sub> were used to determine the association constants of the receptors with halide anions and acetate. All the receptors displayed solely 1:1 receptor:anion complex stoichiometry in solution, except receptor **13** that showed behavior consistent



with the formation of 1:1 and 1:2 receptor:anion complexes with fluoride and acetate. Among the halides, the receptors have association constants following the trend Cl<sup>−</sup> > Br<sup>−</sup> > I<sup>−</sup> with fluoride and acetate binding being either stronger or weaker than chloride binding depending upon the nature of the receptor. The highest association constant observed with this set of receptors was that of the chloride complex of **11** ( $K_a = 61,000 \text{ M}^{-1}$ ; Fig. 1d). Interestingly, the presence of the pyridine nitrogen lone pair in receptor **14** serves to decrease the affinity of larger anions for this receptor and so increases the selectivity for smaller anions. For example, fluoride and chloride bind to **14** with association constants of 24,000 and 1500 M<sup>−1</sup>, respectively, compared to 31,000 and 61,000 M<sup>−1</sup> for fluoride and chloride binding to receptor **11**.

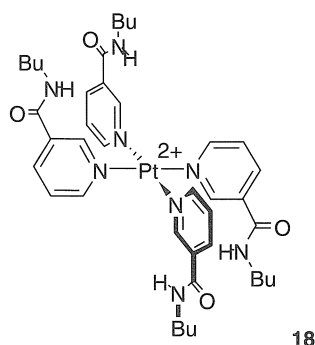
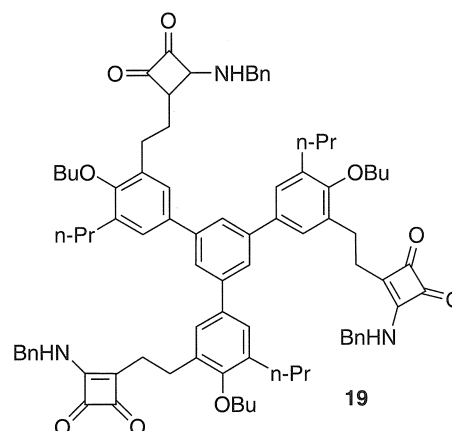
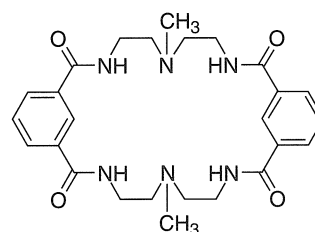
By arranging two amide groups in a parallel arrangement in space, Cameron and Loeb developed a set of receptors that are selective for Y-shaped carboxylate anions over tetrahedral or pseudotetrahedral oxo-anions.<sup>[11]</sup> Calix[4]arenes **15**, **16**, and **17** were synthesized by reaction of the upper-rim calix[4]arene *bis*-amine with mono-, di-, or trichloroacetyl chloride. Receptor **16** proved to have the highest affinity for anionic guests. For example, receptor **15** binds benzoate in chloroform-*d* with a stability constant of 107 M<sup>−1</sup>, whereas the receptor **16**–benzoate complex has an association constant of 5160 M<sup>−1</sup>. This increase in binding strength is attributed to the increased electron withdrawing effect of the dichloromethyl group in **16** compared to the monochloromethyl group in **15**. Compound **17** did not interact with anions, which model studies suggest is due to the steric bulk of the trichloromethyl groups that prevent the putative anionic guest approaching the upper-rim anion-binding site. These receptors proved to be selective for carboxylates over tetrahedral anions such as perrhenate. The stronger binding of Y-shaped anions is attributed to the calixarene adopting a so-called “pinched cone” conformation, with the calixarene rings attached to the two amide groups becoming parallel, so allowing the amide groups to align in a complementary manner to the carboxylate guest (Fig. 1e).

As we have seen, calix[4]arenes offer an organic scaffold upon which receptors may be constructed. Gale, Loeb, and coworkers also used a platinum tetrapyridine complex as an inorganic scaffold with which to arrange amide groups in space.<sup>[12]</sup> The square planar Pt(II)



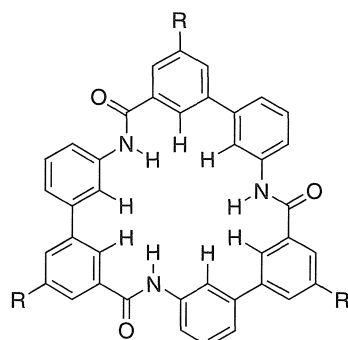
complex was prepared by reaction of one equivalent of  $\text{PtCl}_2(\text{EtCN})_2$  with four equivalents of *n*-butylnicotinamide and two equivalents of  $\text{AgPF}_6$  in acetonitrile. The anion complexation properties of  $\mathbf{18}[\text{PF}_6]_2$  were studied using  $^1\text{H}$ -NMR titration techniques. Unfortunately, a variety of solvent conditions were required due to solubility problems during the titrations, and therefore, association constants are not directly comparable. It was found that tetrahedral or pseudotetrahedral anions such as  $\text{ReO}_4^-$ ,  $\text{CF}_3\text{SO}_3^-$ , and  $\text{HSO}_4^-$  form exclusively 1:1 receptor:anion complexes with receptor **18**. However flat anions such as acetate and nitrate form 1:2 receptor:anion complexes (shown schematically in Fig. 1f). Of particular note is the fact that acetate anions are relatively strongly bound even in the very polar 9:1 DMSO/acetonitrile solvent mixture. The fact that  $K_2$  ( $491 \text{ M}^{-1}$ ) is greater than  $K_1$  ( $230 \text{ M}^{-1}$ ) infers that binding of the first anion has a positive allosteric effect, which favors binding of the second. The 1:1 receptor:anion binding observed for the weakly coordinated  $\text{ReO}_4^-$ ,  $\text{CF}_3\text{SO}_3^-$ , and  $\text{HSO}_4^-$  anions is supported by the x-ray structure of  $\mathbf{18}[\text{ReO}_4]_2$ . In particular, it can be seen that in order to try and maximize hydrogen bonding, the relatively acidic nicotinamide CHs from the ligands on the opposite side of the square plane form hydrogen bonds to the perrhenate anion (Fig. 1g). To do this, the complex must significantly distort from centrosymmetry, a fact that presumably disfavors the interaction with a second anion, resulting in the observation of 1:1 binding in solution (Fig. 1g).

In a different approach to carboxylate complexation, squaramide (i.e., 3,4-diamino-cyclobutene-1,2-dione) derivatives have been used by Prohens et al. as selective receptors (Fig. 1h).<sup>[13]</sup> These receptors possess a parallel ditopic hydrogen bond donor array (c.f. urea) that show good to moderate association constants with acetate anions. A variety of mono-, di-, and tritopic receptors were synthesized, including the *tris*-squaramide receptor **19** that forms strong complexes with *tris*-carboxylates such as trimesoate and *cis*-cyclohexentricarboxylate ( $K_a = 3.9 \times 10^3 \text{ M}^{-1}$  and  $7.7 \times 10^3 \text{ M}^{-1}$ , respectively, in 10%  $\text{D}_2\text{O}/\text{DMSO}$ .)

**18****19****20**

Bowman-James and coworkers showed that receptor **20**, a tetraamide-bisamine macrocycle, forms strong complexes with oxo-anions in chloroform solution.<sup>[14]</sup> Proton NMR titration experiments show that hydrogen sulfate binds with an association constant  $\log K$  of 4.50, while dihydrogen phosphate has an association constant  $\log K$  of 4.66. In these cases, a broadening of the NMR spectrum during the titration may be indicative of the anions protonating the amine moieties present in the macrocycle. Therefore, the simple 1:1 solution-binding model used to calculate the stability constants may no longer be valid. In contrast, aprotic anions such as nitrate, perchlorate, chloride, and iodide are bound more weakly (of these anions, chloride is most strongly bound  $\log K_a = 2.70$ .) Most notably, the receptor forms a sandwich complex with sulfate in the solid state. This complex was formed by slow diffusion of diethylether into a chloroform solution of **20** and tetrabutylammonium hydrogensulfate. The sulfate anion is bound by eight hydrogen bonds from the eight amide groups in the sandwich (Fig. 1i).

Receptors **21** and **22**, reported by Choi and Hamilton, show a particularly high affinity for iodide and oxo-anions such as nitrate.<sup>[15]</sup> The receptor features a central hole of around 5 Å diameter lined with three amide NH groups and six aryl CH groups. The receptors are skewed in a way that allows the three NH groups to form a complementary hydrogen-bonding site suitable for pseudo-tetrahedral anions (e.g., *p*-tosylate.) Proton NMR spectroscopic titration studies were carried out in the

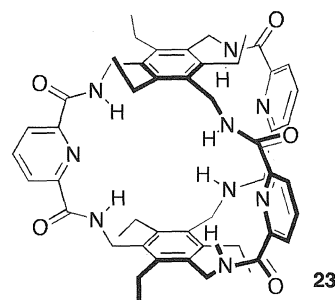
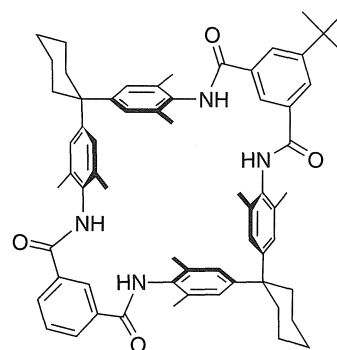


**21** R = CO<sub>2</sub>Et  
**22** R = NHBoc

case of both receptors using either 2% DMSO-*d*<sub>6</sub>/CDCl<sub>3</sub> or pure DMSO-*d*<sub>6</sub> as the solvent. The results revealed that the best-bound anion substrates, namely I<sup>−</sup>, NO<sub>3</sub><sup>−</sup>, and TsO<sup>−</sup>, are bound with affinity constants that are on the order of 10<sup>5</sup> M<sup>−1</sup>. Both receptors were found to display similar affinities for anions, indicating that the functional groups on the periphery of the macrocycles do not serve to modulate anion binding selectivity or affinity. Proton NMR titration curves involving tosylate anion and subsequent Job plot analysis revealed the exclusive formation of a 1:1 receptor:tosylate complex in the case of both receptors. However, other anions displayed more complex binding behavior. For example, the shift of the amide NH resonance of **22** observed upon the addition of iodide anions reflected the formation of a 2:1 receptor:iodide complex during the initial phases of the titration (i.e., an iodide sandwich complex in solution), with the equilibrium at higher iodide concentrations being pushed in favor of a 1:1 receptor:iodide complex.

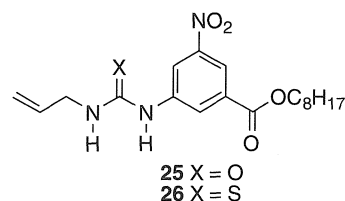
Anslyn and coworkers used receptor **23**, a trigonal box containing six convergently arranged amide NH groups designed to hydrogen bond to the  $\pi$ -clouds of included guests, to examine the role of hydrogen bonding in the stabilization of enolate intermediates.<sup>[16]</sup> In particular, the role of hydrogen bonding to the enolate  $\pi$ -cloud versus binding to the enolate oxygen atom lone pairs was examined by comparing the p*K*<sub>a</sub> shifts of a variety of ketones in the presence of **23** and also in the presence of another receptor designed to form hydrogen bonds only to the enolates' oxygen atoms. It was found that NH- $\pi$  hydrogen bonding has a greater effect on carbon acidity than hydrogen bonding to oxygen lone-pair electrons.

Vögtle and coworkers employed anion complexation in new strategies for high-yielding rotaxane syntheses.<sup>[17]</sup> These workers discovered that phenolate anions, when bound to tetralactam macrocycles (Fig. 1j) such as **24**, are capable of reacting with acid chlorides and therefore may be used to form ester rotaxanes. A variety of different rotaxanes were synthesized via this method, including systems with carbonate and acetyl axles.

**23****24**

## UREA

While an amide group can donate a single hydrogen bond, urea can donate two in a parallel fashion, and so it is complementary to oxyanions such as carboxylates (Fig. 1b). One of the earliest examples of anion complexation to urea-based receptors (e.g., **25** and **26**) was reported in 1992 by Wilcox and coworkers.<sup>[18]</sup> Although receptor **26** (the thiourea) proved to have a higher affinity for carboxylates than the urea-based receptor **25**, the binding properties of **25** were studied in detail, as thioureas are more susceptible to electrophilic and nucleophilic attacks. NMR experiments revealed large downfield shifts of the urea NH protons upon addition of oxyanions such as carboxylates, sulfonates, and phosphates (as their tetrabutylammonium salts in chloroform-*d*), however, the association constants were too high to be accurately determined by <sup>1</sup>H-NMR titration methods. Therefore, ultraviolet/visible (UV/Vis) titration experiments were employed. It was found that of the oxyanions used, receptor **25** binds benzoate most strongly (*K*<sub>a</sub> = 2.7 × 10<sup>4</sup> M<sup>−1</sup>).



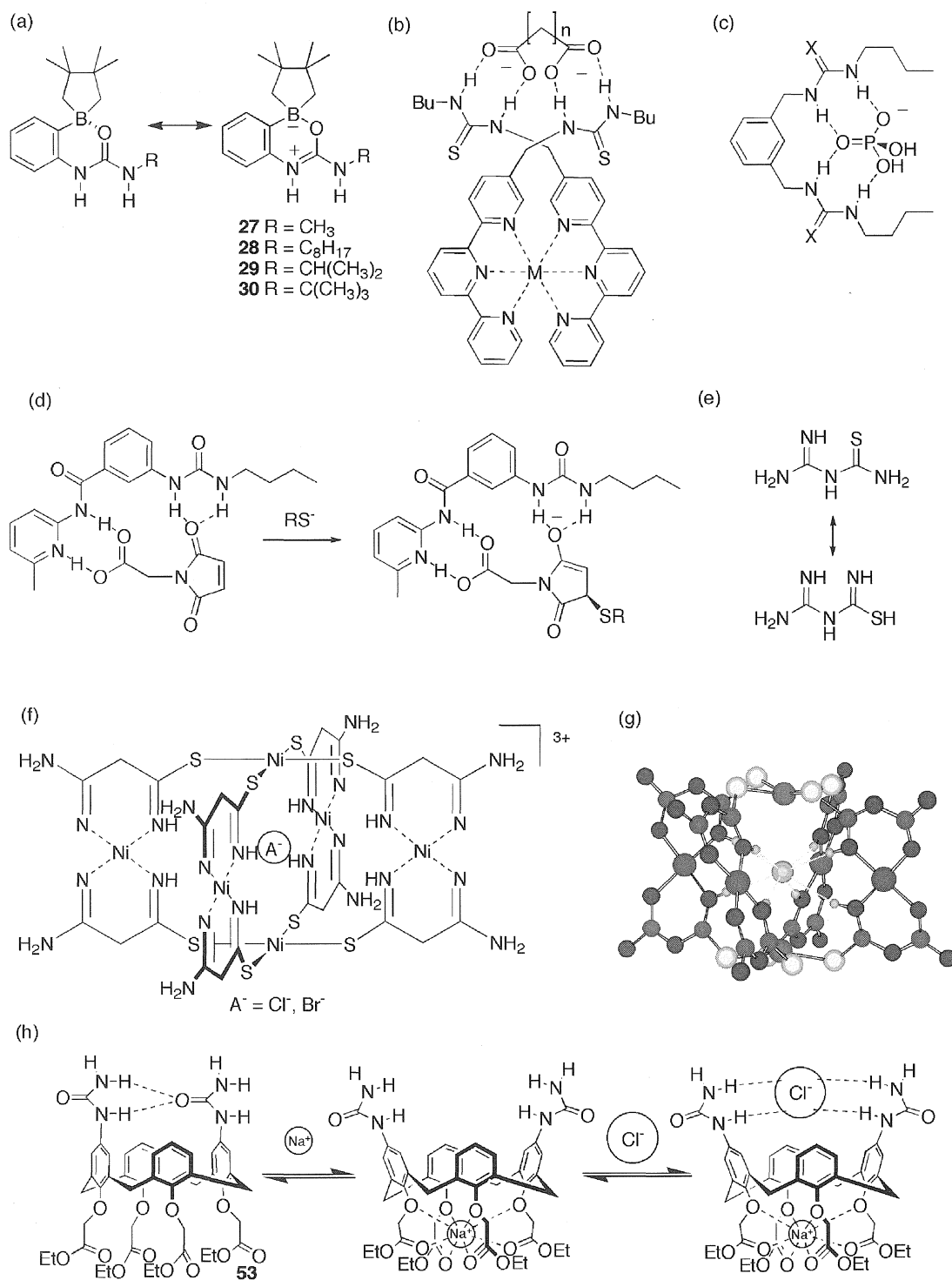
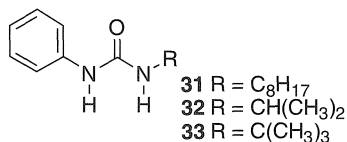
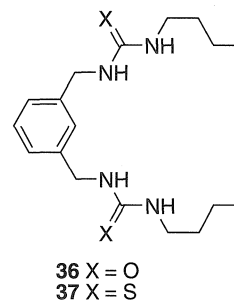
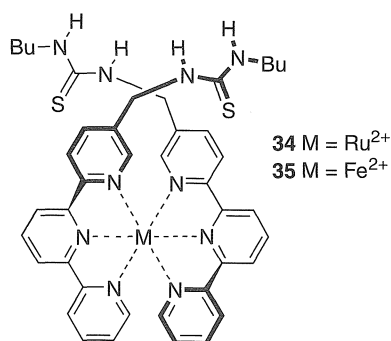


**Fig. 2** (a) A boronate group enhances the acidity of the urea NH protons in Smith's receptors; (b) a dicarboxylate complex of Hamilton's combinatorial type ditopic terpy based receptor **34**; (c) the dihydrogen phosphate complex of receptors **36** and **37** ( $X = O, S$ ); (d) an example of catalysis by stabilization of an anionic intermediate by receptor **49**; (e) amidinothiourea; (f) Mingo's anion templated nickel-amidinothiourea cage and (g) the crystal structure of this complex; (h) Reinhoudt's metal ion switched chloride receptor **53**. (View this art in color at [www.dekker.com](http://www.dekker.com).)



Smith and coworkers increased the affinity of both amides and ureas for anions by polarizing the hydrogen bond donor site using an intramolecular interaction from a boronate group.<sup>[19]</sup> A variety of receptors were synthesized, including receptors **27–30** (Fig. 2a). Proton NMR titrations in DMSO-*d*<sub>6</sub> with acetate anions were conducted with receptors **28–30** and analogues **31–33** which do not contain a boronate group. The following association constants (M<sup>-1</sup>) were determined: **28/31**  $K_a = 7 \times 10^3 / 3.7 \times 10^2$ , **29/32**  $K_a = 6.9 \times 10^3 / 3.1 \times 10^2$ , **30/33**  $K_a = 7.1 \times 10^3 / 2.6 \times 10^2$ . These results clearly show the enhanced carboxylate complexation properties of the boronate receptors as compared to the regular urea systems **31–33**. Similar results were observed with amide-based receptors.

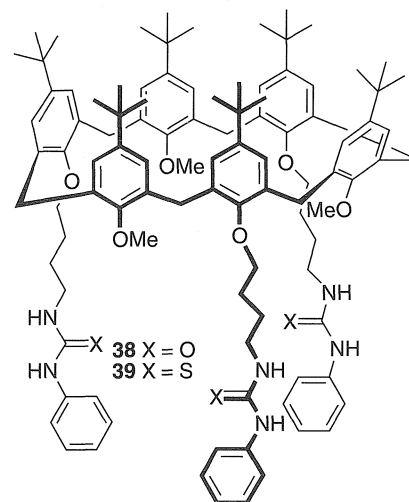
A number of research groups synthesized ditopic receptors containing two urea moieties for the complexation of dicarboxylates. Hamilton and coworkers used metal-templated receptors for this purpose.<sup>[20]</sup> A thiourea-substituted terpyridine was synthesized from methylterpyridine by bromination with *N*-bromosuccinimide (NBS) followed by Gabriel amine synthesis and finally treatment with butyl isothiocyanate. The ruthenium complex **34** was obtained by heating the ligand with 0.5 equivalent of RuCl<sub>2</sub>(DMSO)<sub>4</sub> in ethylene glycol and the iron complex **35** by mixing aqueous solutions of the receptor and Fe(NH<sub>4</sub>)<sub>2</sub>(SO<sub>4</sub>)<sub>2</sub>. Both complexes were isolated as their PF<sub>6</sub> salts. Upon addition of dicarboxylates to receptor **35**, displacement of the terpyridine ligands occurred. However, in the case of the inert ruthenium receptor **34**, displacement did not occur, instead the dicarboxylate anions bound to the thiourea groups (Fig. 2b). Association constants were determined in 5% D<sub>2</sub>O/DMSO-*d*<sub>6</sub>. Similar association constants were obtained for a variety of guests



(glutarate  $K_a = 8.3 \times 10^3$  M<sup>-1</sup>, adipate  $K_a = 2.9 \times 10^3$  M<sup>-1</sup>, and pimelate  $K_a = 6.0 \times 10^3$  M<sup>-1</sup>), suggesting a degree of flexibility in the anion-binding site.

By producing a ditopic receptor containing urea or thiourea groups in close proximity, Umezawa and coworkers produced dihydrogenphosphate selective receptors.<sup>[21]</sup> Receptors **36** and **37** are selective for dihydrogenphosphate over a variety of other oxo-anions. The two urea groups present in the receptor can simultaneously coordinate to the same dihydrogen phosphate anion (Fig. 2c). Thus, NMR titration studies in DMSO-*d*<sub>6</sub> revealed receptors **36** and **37** bind H<sub>2</sub>PO<sub>4</sub><sup>-</sup> with association constants of 110 and 820 M<sup>-1</sup>, respectively, while non-complementary anions such as acetate are bound with association constants of 43 and 470 M<sup>-1</sup>, respectively.

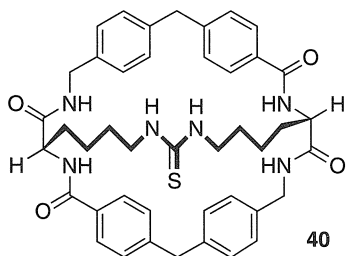
Reinhoudt, Ungaro, and coworkers synthesized calix[6]arenes **38** and **39** that are substituted at the lower rim with three urea or thiourea groups linked via alkyl chains.<sup>[22]</sup> The threefold symmetry of the receptor imparts a selectivity for threefold symmetric tricarboxylates such as 1,3,5-benzenetricarboxylate. This anion was bound by receptor **39** with an association constant of 290,000 M<sup>-1</sup> in chloroform-*d*<sub>3</sub>, while benzoate was bound with an association constant of 1400 M<sup>-1</sup>.



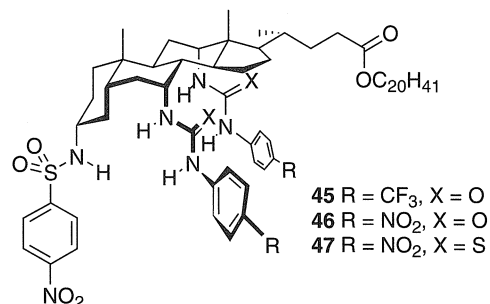
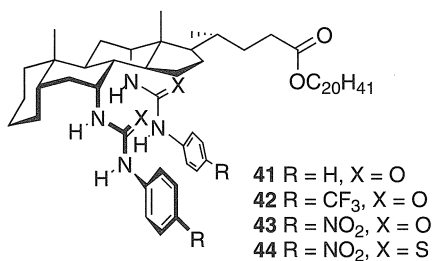


## RECEPTORS THAT UTILIZE AMIDES AND UREAS

The complexation of biologically important amino acid derivatives has been the driving force behind Kilburn and coworkers' research in this area.<sup>[23]</sup> By combining thiourea and amide moieties in cryptand-like macrobicyclic structures, e.g., **40**, Kilburn and coworkers synthesized receptors for amino acid derivatives that show selectivity for particular side-chain residues. Extraction methods were used to calculate association constants with a number of *N*-protected tetrabutylammonium amino acid salts in chloroform. Receptor **40** is selective for *N*<sup>α</sup>-Ac-L-lysine ( $K_a = 13 \times 10^4 \text{ M}^{-1}$ ) over *N*-Ac-L-glycine ( $K_a = 68,600 \text{ M}^{-1}$ ), *N*-Ac-L-alanine ( $K_a = 16,900 \text{ M}^{-1}$ ), and several other protected amino-acid carboxylate salts. Kilburn showed that D-amino acid substrates bind predominantly on the outside of the macrocycle, whereas L-amino acid derivatives bind within the cavity of the receptor with the acetyl amide in a *cis*-configuration, the energetic penalty for forming the *cis* configuration being offset by the formation of hydrogen bonds between the *cis* amide and the rim of the macrocycle.

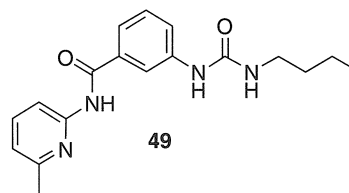
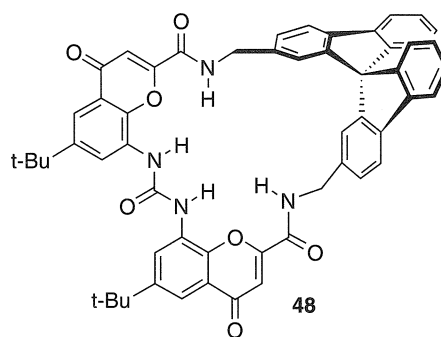


Over recent years, Davis and coworkers produced a variety of anion receptors based upon cholic acid. Recently, new urea derivatized receptors termed "chola-pods" have been synthesized that form remarkably strong complexes with bromide and chloride anions in water-saturated chloroform solution.<sup>[24]</sup> Receptors **41–44** contain two urea or thiourea groups with electron withdrawing substituents linked to the cholic acid skeleton, while



**45–47** contain an additional sulfonamide group. The attachment of the hydrogen bonding groups to the steroid skeleton largely prevents the formation of intramolecular hydrogen bonding, while the electron-withdrawing units serve to increase the acidity of the urea moieties and, hence, increase their affinity for anions. This is reflected in the very high association constants with chloride ( $K_a = 1.03 \times 10^{11} \text{ M}^{-1}$  with receptor **47**). These molecules may show excellent phase-transfer properties as well as display biological activity possibly as membrane transport agents for chloride.

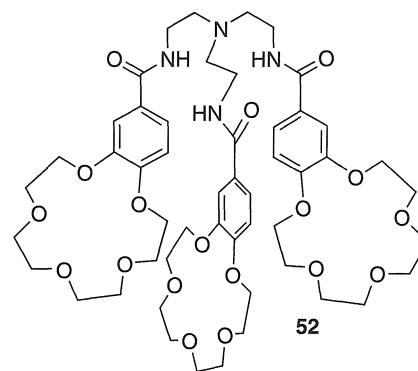
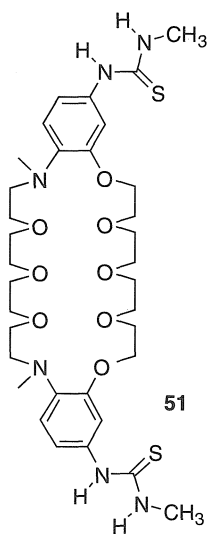
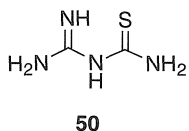
Morán and coworkers also combined urea and amide moieties, in this case, in chiral receptors that are recognized chiral hydroxycarboxylates such as lactic or mandelic acid.<sup>[25]</sup> Receptor **48** combines a *bis*-chromenylurea with a spirobifluorenone linker in a macrocyclic structure and is capable of resolving a racemic mixture of the tetramethylammonium salt of mandelic acid by thin-layer chromatography. Proton NMR titrations in DMSO-*d*<sub>6</sub> gave association constants for lactic acid [(*R*)-lactic acid  $K_a = 3.5 \times 10^4 \text{ M}^{-1}$ , (*S*)-lactic acid  $K_a = 3.5 \times 10^3 \text{ M}^{-1}$ ].



Hamilton used an anion-binding strategy with an amidourea receptor (**49**) to stabilize an oxyanion transition state and so catalyze the 1,4-addition reaction of a thiol to maleimide (Fig. 2d).<sup>[26]</sup> The enolate intermediate is stabilized via two hydrogen bonds to the urea group in **49**, to a greater extent than the carbonyl oxygen present in the starting material. Therefore, the transition state of this reaction is stabilized relative to the starting material, and the reaction is accelerated.

### ION PAIR COMPLEXATION BY AMIDE- AND UREA-BASED RECEPTORS

Finally we will briefly examine receptors for ion pairs that contain amide or urea groups. An elegant self-assembly process of an amidinothiourea (**50**) (Fig. 2e) with  $\text{NiCl}_2$  has been reported by Mingos and coworkers.<sup>[27]</sup> Complexation of  $\text{NiCl}_2$  by amidinothiourea in methanol yields crystals of a cage complex (Fig. 2f). The cage  $[\text{Ni}_6(\text{atu})_8\text{Cl}]\text{Cl}_3$  consists of eight amidinothiourea units that coordinate six nickel ions through both nitrogen and sulfur donor atoms. A chloride anion is encapsulated within the cage by eight  $\text{NH}\cdots\text{Cl}$  hydrogen bonds (as revealed by the crystal structure shown in Fig. 2g). An analogous complex can be formed between amidinothiourea and  $\text{NiBr}_2$ , however, when nickel salts containing noncage complementary anions such as nitrate,



acetate, or perchlorate salts are used, the simple monomer  $[\text{Ni}(\text{atu})_2]^{2+}$  complexes are formed. Interestingly, if chloride anions are subsequently added to these complexes, the cage complex spontaneously assembles.

Kubo and coworkers synthesized a *bis*-thiourea functionalized dibenzo-diaza-30-crown-10 **51** that wraps around potassium cations, so bringing the two thiourea groups into close proximity, forming an anion binding site.<sup>[28]</sup> NMR titration experiments with  $(\text{PhO})_2\text{P}(\text{O})\text{O}^-$  anions (which form both 1:1 and 1:2 receptor:anion complexes with **51**) in acetonitrile- $d_3$  solution in the absence and presence of potassium cations show an increase in  $K_1$  from 490 to  $9200 \text{ M}^{-1}$  upon addition of three equivalents of potassium cations.

In the area of amidic receptors, the *tris*-crown-ether tren-based receptor **52**, synthesized by Beer and coworkers was recently shown to efficiently extract pertechnetate anions from simulated nuclear waste streams in the presence of sodium cations.<sup>[29]</sup>

Reinhoudt and coworkers produced a switchable anion receptor.<sup>[30]</sup> Receptor **53** (Fig. 2h) is a calix[4]arene substituted at the lower rim with cation-binding ester groups and at the upper rim with two distally arranged urea groups. In chloroform solution, intramolecular hydrogen bonds between the urea moieties block the potential anion-binding site. Upon addition of sodium cations, the lower rim of the calixarene contracts as the sodium ions are bound by the four ester groups. This conformational rearrangement separates the two urea groups at the upper rim, so disrupting the intramolecular hydrogen bonding and, therefore, allowing anions such as chloride to complex the receptor (Fig. 2h).

### CONCLUSION

Amides and ureas have proven to be excellent anion receptor groups, widely employed by the supramolecular

A

chemistry community in receptors for anions and ion pairs. This is due in no small part to their ease of synthesis and stability. The roles amides play in binding to anions in protein structures is being revealed by protein crystallography, and these structures are inspiring new generations of synthetic receptors containing peptide groups capable of functioning as anion receptors in aqueous solutions.<sup>[31]</sup> There is much yet to be explored in this fascinating area of supramolecular chemistry. For more information, the reader is directed to reviews<sup>[1–4]</sup> that provide entry to the extensive literature in this area.

## ACKNOWLEDGMENT

The author would like to acknowledge the Royal Society for a University Research Fellowship.

## ARTICLES OF FURTHER INTEREST

*Anion-Directed Assembly*, p. 51

*Guanidinium-Based Anion Receptors*, p. 615

*Hydrogen Bonding*, p. 658

*Organometallic Anion Receptors*, p. 1006

*Protonated Aza-Macrocycles for Anion Complexation*, p. 1170

*Pyrrole- and Polypyrrole-Based Anion Receptors*, p. 1176

*Simultaneous Binding of Cations and Anions*, p. 1291

## REFERENCES

- Gale, P.A. Anion receptor chemistry: Highlights from 1999. *Coord. Chem. Rev.* **2001**, *213*, 79–128.
- Beer, P.D.; Gale, P.A. Anion recognition and sensing: The state of the art and future perspectives. *Angew. Chem., Int. Ed.* **2001**, *40* (3), 486–516.
- Schmidtchen, F.P.; Berger, M. Artificial organic host molecules for anions. *Chem. Rev.* **1997**, *97* (5), 1609–1646.
- Antonisse, M.M.G.; Reinhoudt, D.N. Neutral anion receptors: Design and application. *Chem. Commun.* **1998**, (4), 443–448.
- Chakrabarti, P. Anion binding sites in protein structures. *J. Mol. Biol.* **1993**, *234* (2), 463–482.
- Mangani, S.; Ferraroni, M. Natural Anion Receptors: Anion Recognition by Proteins. In *Supramolecular Chemistry of Anions*, 1st Ed.; Bianchi, A., Bowman-James, K., García-España, E., Eds.; WILEY-VCH: New York, 1997; 63–78.
- Pascal, R.A., Jr.; Spergel, J.; Van Engen, D. Synthesis and x-ray crystallographic characterisation of a (1,3,5) cyclophane with three amide NH groups surrounding a central cavity. A neutral host for anion complexation. *Tetrahedron Lett.* **1986**, *27* (35), 4099–4102.
- Valiyaveetil, S.; Engbersen, J.F.J.; Verboom, W.; Reinhoudt, D.N. Synthesis and complexation studies of neutral anion receptors. *Angew. Chem., Int. Ed. Engl.* **1993**, *32* (6), 900–901.
- Beer, P.D. Transition-metal receptor systems for the selective recognition and sensing of anionic guest species. *Acc. Chem. Rec.* **1998**, *31* (2), 71–80.
- Kavallieratos, K.; Bertao, C.M.; Crabtree, R.H. Hydrogen bonding in anion recognition: A family of versatile non-preorganised neutral and acyclic receptors. *J. Org. Chem.* **1999**, *64* (5), 1675–1683.
- Cameron, B.R.; Loeb, S.J. Bis(amido)calix[4]arenes in the pinched cone conformation as tuneable hydrogen-bonding anion receptors. *Chem. Commun.* **1997**, (6), 573–574.
- Bondy, C.R.; Gale, P.A.; Loeb, S.J. Platinum(II) nicotinamide complexes as receptors for oxo-anions. *Chem. Commun.* **2001**, (8), 729–730.
- Prohens, R.; Tomás, S.; Morey, J.; Deyà, P.M.; Ballester, P.; Costa, A. Squaramido-based receptors: Molecular recognition of carboxylate anions in highly competitive media. *Tetrahedron Lett.* **1998**, *39* (9), 1063–1066.
- Hossain, Md.A.; Llinares, J.M.; Powell, D.; Bowman-James, K. Multiple hydrogen bond stabilisation of a sandwich complex of sulfate between two macrocyclic tetraamides. *Inorg. Chem.* **2001**, *40* (13), 2936–2937.
- Choi, K.; Hamilton, A.D. Selective anion binding by a macrocycle with convergent hydrogen bonding functionality. *J. Am. Chem. Soc.* **2001**, *123* (10), 2456–2457.
- Snowden, T.S.; Bisson, A.P.; Anslyn, E.V. A comparison of NH- $\pi$  versus lone pair hydrogen bonding effects on carbon acid pK<sub>a</sub> shifts. *J. Am. Chem. Soc.* **1999**, *121* (26), 6324–6325.
- Reuter, C.; Wienand, W.; Hübner, G.M.; Seel, C.; Vögtle, F. High-yield synthesis of ester, carbonate, and acetal taxanes by anion template assistance and their hydrolytic dethreading. *Chem. Eur. J.* **1999**, *5* (9), 2692–2697.
- Smith, P.J.; Reddington, M.V.; Wilcox, C.S. Ion pair binding by a urea in chloroform solution. *Tetrahedron Lett.* **1992**, *33* (41), 6085–6088.
- Hughes, M.P.; Smith, B.D. Enhanced carboxylate binding using urea and amide-based receptors with internal Lewis acid coordination: A cooperative polarization effect. *J. Org. Chem.* **1997**, *62* (13), 4492–4499.
- Goodman, M.S.; Jubian, V.; Hamilton, A.D. Metal templated receptors for the effective complexation of dicarboxylates. *Tetrahedron Lett.* **1995**, *36* (15), 2551–2554.
- Nishizawa, S.; Bühlmann, P.; Iwao, M.; Umezawa, Y. Anion recognition by urea and thiourea groups: Remarkably simple neutral receptors for dihydrogenphosphate. *Tetrahedron Lett.* **1995**, *36* (36), 6483–6486.
- Scheerder, J.; Engbersen, J.F.J.; Casnati, A.; Ungaro, R.; Reinhoudt, D.N. Complexation of halide anions and tri-carboxylate anions by neutral urea-derivatized *p*-tert-butylcalix[6]arenes. *J. Org. Chem.* **1995**, *60* (20), 6448–6454.

23. Pernía, G.J.; Kilburn, J.D.; Essex, J.W.; Mortishire-Smith, R.J.; Rowley, M. Stabilization of a *cis* amide bond in a host–guest complex. *J. Am. Chem. Soc.* **1996**, *118* (42), 10220–10227.
24. Ayling, A.J.; Pérez-Payán, M.N.; Davis, A.P. New “cholapod” anionophores: High-affinity halide receptors derived from cholic acid. *J. Am. Chem. Soc.* **2001**, *123* (50), 12716–12717.
25. Tejada, A.; Oliva, A.I.; Simón, L.; Grande, M.; Caballero, Ma.C.; Morán, J.R. A macrocyclic receptor for the chiral recognition of hydrocarboxylates. *Tetrahedron Lett.* **2000**, *41* (23), 4563–4566.
26. Fan, E.; Vicent, C.; Hamilton, A.D. Molecular recognition and catalysis: Incorporation of an “oxyanion hole” into a synthetic receptor. *New J. Chem.* **1997**, *21* (1), 81–85.
27. Vilár, R.; Mingos, D.M.P.; White, A.J.P.; Williams, D.J. Anion control in the self-assembly of a cage coordination complex. *Angew. Chem., Int. Ed.* **1998**, *37* (9), 1258–1261.
28. Tozawa, T.; Misawa, Y.; Tokita, S.; Kubo, Y. A regioselectivelybis(thiourea)-substituted dibenzo-diaza-30-crown-10: A new strategy for the development of multi-site receptors. *Tetrahedron Lett.* **2000**, *41* (27), 5219–5223.
29. Beer, P.D.; Hopkins, P.K.; McKinney, J.D. Cooperative halide, perrhenate anion–sodium cation binding and pertechnetate extraction and transport by a novel tripodal tris-(amido benzo-15-crown-5) ligand. *Chem. Commun.* **1999**, (13), 1253–1254.
30. Scheerder, J.; van Duynhoven, J.P.M.; Engbersen, J.F.J.; Reinhoudt, D.N. Solubilization of NaX salts in chloroform by bifunctional receptors. *Angew. Chem., Int. Ed. Engl.* **1996**, *35* (10), 1090–1093.
31. Kubik, S.; Kirchner, R.; Nolting, D.; Seidel, J. A molecular oyster: A neutral anion receptor containing two cyclopeptide subunits with a remarkable sulfate affinity in aqueous solution. *J. Am. Chem. Soc.* **2002**, *124* (43), 12752–12760.

# Amino Acids: Applications

Arindam Banerjee

*Indian Association for the Cultivation of Science, Calcutta, West Bengal, India*

## INTRODUCTION

J.M. Lehn first introduced the term “supramolecular chemistry” in the literature in 1969 while he was studying the inclusion complexes of  $\text{Eu}^{3+}$  with its receptor-molecule cryptands. Lehn defined supramolecular chemistry as “the chemistry of intermolecular bonds”; in a supramolecular system, the same or different chemical compounds are held together by various noncovalent interactions. Amino acids, the building blocks of proteins and peptides, are useful in constructing various supramolecular architectures and forming inclusion complexes with different receptor molecules, including cyclodextrins and calixarenes. Amino acid derivatives also form host-guest inclusion complexes with structurally different receptor molecules, such as chiral crown ethers and cyclodextrines.  $\alpha$ -Amino-acid-derived lipids become supramolecular receptors through self-assembly, and they host styryl dyes. Many  $\alpha$ -amino acids form complexes with various types of transition metals, including  $\text{Pt}^{2+}$  and lanthanides, leading to the formation of different supramolecular architectures.

Peptides composed of various coded and noncoded amino acid residues self-assemble to form various types of supramolecular architectures, including supramolecular helices and sheets, nanotubes, nanorods, nanovesicles, and nanofibers. The higher-order self-assembly of supramolecular  $\beta$ -sheets or supramolecular helices composed of short synthetic acyclic peptides leads to the formation of amyloid-like fibrils. Synthetic cyclic peptides were used in supramolecular chemistry as molecular scaffolding for artificial receptors, so as to host various chiral and achiral ions and other small neutral substrates. Cyclic peptides also self-assemble like their acyclic counterparts to form supramolecular structures, including hollow nanotubes. Self-assembling cyclic peptides can be served as artificial ion channels, and some of them exhibit potential antimicrobial activities against drug-resistant bacteria.

## SYNTHETIC CYCLIC PEPTIDES AS RECEPTORS

Artificial receptor design is an important aspect of supramolecular chemistry. Synthetic cyclic peptides were

not used extensively so far, probably due to their usual relative flexibility compared to other macrocycles that contain a rigid framework or backbone (e.g., crown ethers, calixarenes, etc.). In spite of their cyclic structure, they are hardly able to bind guests in a well-defined cavity. However, cyclic peptides with conformationally constrained subunits like aromatic or alicyclic backbones or those containing rigid subunits were used for binding substrate molecules such as amino acid derivatives,<sup>[1]</sup> aromatic compounds,<sup>[2]</sup> or dicarboxylic acids.<sup>[3]</sup> Following this approach, Ishida and his colleagues demonstrated the complexation of phosphate ions with cyclic oligopeptides (with six to 14 residues) containing 3-aminobenzoic acid (AB) and protein amino acids in an alternating sequence.<sup>[4]</sup> Kubik established that a cyclic hexapeptide composed of alternating L-glutamic and 3-aminobenzoic acids binds to quaternary ammonium ions in  $\text{CHCl}_3$  through cation- $\pi$  interactions.<sup>[5]</sup> The cation-binding property of this cyclic peptide was enhanced by a factor of  $10^3$ – $10^4$  in presence of certain anions (e.g., tosylate or phenyl phosphonate). This is due to the allosteric effects of these anions from binding to the cyclopeptide NH groups and stabilizing the receptor structure, which is essentially appropriate for interactions with positively charged ions.<sup>[5]</sup> The introduction of L-Pro in the cyclic peptide backbone was shown to rigidify the cyclic peptide structure and to increase the cation-and anion-binding affinities. Kubik and his coworkers established that  $\text{cyclo}[(\text{L-Pro-AB})_3]$  has greater cation and anion affinity than the receptor molecule  $\text{cyclo}[(\text{L-Glu-AB})_3]$ .<sup>[6]</sup> This is because anion complexation is reduced to a great extent. As in the latter peptide, the amide NH groups in the L-Glu residues are involved in strong intramolecular hydrogen bonds, and are, therefore, not available for binding with host anions. Consequently, the stability of the cation complex also decreases. Using different amino acid subunits in the cyclic peptide backbone can regulate the solution conformation of these cyclic hexapeptides, which, in turn, can tune receptor properties. All these above-mentioned cyclic oligopeptides exhibit ditopic receptor properties for simultaneous complexation of cations and anions. Kubik and his coworkers improved the cation-binding affinity and incurred a significant loss of anion-binding ability by using intramolecular conformational control in a cyclic hexapeptide containing alternating L-proline and

substituted 3-aminobenzoic acid residues.<sup>[7]</sup> The presence of methoxy carbonyl groups in the fourth-position of the aromatic ring of the 3-aminobenzoic acid subunits helps to form hydrogen bonds to adjacent amide NH protons, inducing the orientation of an amide group parallel to the aromatic rings. This causes the amide protons to point away from the central cavity and to be unavailable for binding with anions. The investigation of the optimum ring size required for good cation binding revealed that cyclotetrapeptides with alternating L-Pro and 3-aminobenzoic acid possess a lower affinity toward cations than the corresponding hexapeptides.<sup>[8]</sup> It was observed that the phenyl urea substituted at the benzene ring of cyclotetrapeptide can be used as the anion (iodide or acetate) receptor in DMSO-*d*<sub>6</sub> solution.<sup>[8]</sup> Artificial receptors that discriminate between two enantiomers of a given substrate are important in bioorganic and supramolecular chemistry. Recently, Kubik and his coworkers achieved the enantioselective recognition of a chiral quaternary ammonium ion (e.g., *N,N,N*-trimethyl,1-phenyl ethyl ammonium cation) using C<sub>3</sub> symmetric cyclic hexapeptides composed of L-proline and substituted 3-aminophenyl benzoic acid in 0.1% DMSO-*d*<sub>6</sub>-CDCl<sub>3</sub> solution.<sup>[9]</sup>

### INCLUSION COMPLEXES OF AMINO ACIDS AND THEIR DERIVATIVES WITH THEIR HOSTS

Host-guest complexation, by cyclodextrins for example, plays an important role in biomimetic and supramolecular chemistry. Cyclodextrins (CDs) are barrel-shaped cyclic carbohydrate molecules composed of six, seven or eight glucose residues, which are termed  $\alpha$ ,  $\beta$ , or  $\gamma$  cyclodextrin, respectively. Due to the presence of an internal cavity, CDs can be used as versatile hosts. Amino acids form gas-phase inclusion complexes with CDs and they can be detected using ES-MS and a gas-phase guest exchange reaction.<sup>[10]</sup> Chiral discrimination of amino acid guests in CDs hosts was also achieved in the gas phase. The  $\alpha$ CDs and  $\beta$ CDs form inclusion complexes with coumarin-6-sulfonyl amino acid derivatives in water. Theoretical modeling and fluorescence experimental results suggest the possibility of forming 1:2 guest-host complexes for  $\beta$ CD.<sup>[11]</sup> A recent report described the complexation of native L- $\alpha$ -amino acids with aliphatic or aromatic side chains by water-soluble substituted calix[4]arenes.<sup>[12]</sup> The host-guest complexation was studied using <sup>1</sup>H-NMR experiments. The upfield shift of some specific aromatic protons (H *meta* and H *para*) of the guest molecules compared to the free guest, due to the ring current effect of the aromatic nuclei of the host, confirms the formation of an inclusion complex. The inclusion of aliphatic or

aromatic apolar amino acid residues within the calix[4]-arene cavity occurs either by CH- $\pi$  interaction (for L-Val and L-Leu) or by  $\pi$ - $\pi$  interaction (for L-Phe, L-His, L-Trp.). Another macrocyclic receptor, cyclotetrachromotryptylene, forms 1:1 host-guest complexes with various native  $\alpha$ -amino acids in water at pH 7 and 25°C. This phenomenon was studied using <sup>1</sup>H-NMR spectroscopy.<sup>[13]</sup> Sometimes host-guest complexation helps in useful chemical transformations like hydrolysis. A recent study indicated the formation of inclusion complexes of  $\gamma$ -CD and various amino acid methyl esters. This formation eventually leads to hydrolysis of host molecules. In the entire process, a high stereoselectivity was observed.<sup>[14]</sup>

### METAL ION-AMINO ACID COMPLEXATION IN SUPRAMOLECULAR CHEMISTRY

A pentadecanuclear complex of Eu<sup>III</sup> with tyrosine at high pH provides a novel supramolecular architecture, which involves 15 Eu<sup>III</sup> ions and 10 tyrosine ligands plus hydroxo and aquo ligands associated with hydrolysis. In this structure, the europium(III) ions are assembled into three parallel layers, and each of the layers contains five Eu<sup>III</sup> ions that occupy the vertical positions of a nearly perfect pentagon. The 10 tyrosine ligands can be grouped into two equivalent classes, each of which extends its 4-hydroxybenzyl side chains orthogonal to the crystallographically imposed C<sub>2</sub> axis.<sup>[15]</sup> The side chains do not take part in coordination, while the amino and the carboxylate groups of each tyrosine residue participate in metal ion chelation, making each of the 10 tyrosinate groups become a tetradentate ligand. Near physiological pH (which is 6–7), multinuclear lanthanide complexes of various  $\alpha$ -amino acids (e.g., Gly, Ala, Val, Glu) form a cubane-like cluster core that assembles to form 3D porous framework structures.<sup>[16]</sup>

### SELF-ASSEMBLY OF $\alpha$ -AMINO-ACID-DERIVED LIPIDS

Study of the inclusion behaviors of the cavity of many commonly known macrocyclic receptors like calixarenes, cyclodextrins and cyclic oligopeptides draws considerable interest in supramolecular chemistry. However, the construction of inclusion compounds using self-assembly of  $\alpha$ -amino-acid-derived lipids is relatively rare.<sup>[17–20]</sup> L-Glutamic-acid-derived anionic lipids act as supramolecular receptors and provide specific hydrophobic cavities for accommodating cationic dyes.<sup>[17,18]</sup> Cationic dyes are incorporated inside, due to their molecular planarity. Hachisako and his coworkers studied various types

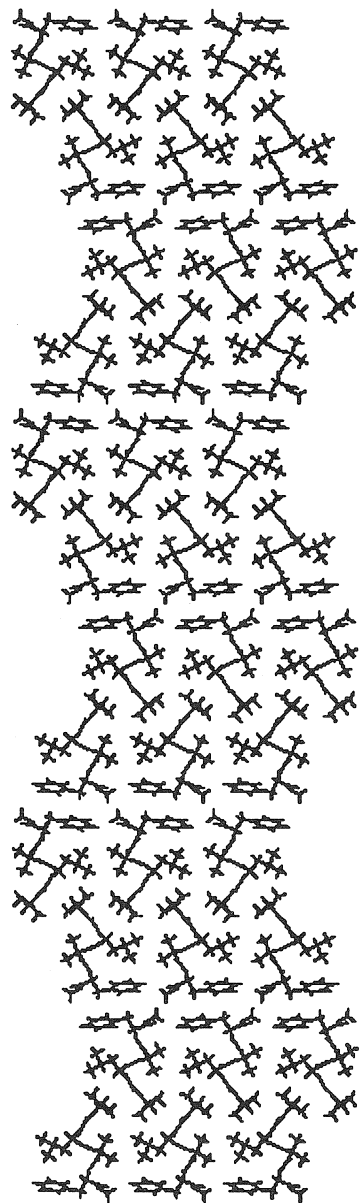
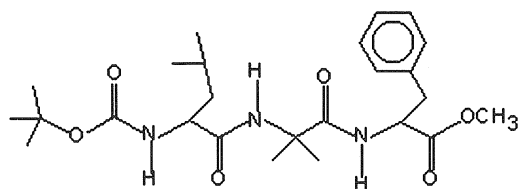


**Fig. 1** Packing diagram of individual columns of the tripeptide Boc-Leu-Aib-Phe-OMe in the *c* projection, illustrating the formation of a highly ordered supramolecular helical assembly via van der Waals' interactions.

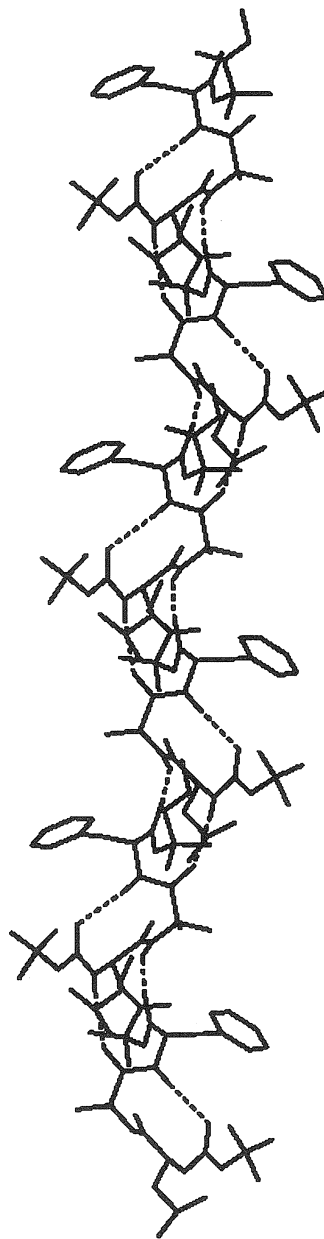
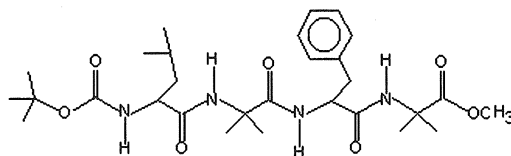


**Fig. 2** The packing diagram of the tetrapeptide Boc-Leu-Aib-Phe-Aib-OMe showing a higher-ordered supramolecular helical assembly as determined by x-ray crystal structure analysis along the *b* axis. Hydrogen bonds are shown as dotted lines. Side chains of Leu, Phe, and nonhydrogen-bonded hydrogen atoms are omitted for clarity.



of  $\alpha$ -amino-acid-derived cationic lipids containing multiple amide linkages per molecule, to probe the role of  $\alpha$ -amino-acid residues and the chemical structural requirements needed to form specific hydrophobic cavities of supramolecular receptors in aqueous solution.<sup>[20]</sup> The role of amino acid residues on inclusion and molecular recognition were examined using structurally related cationic styryl dyes like 4-[4-(dimethylamino)styryl]-*N*-methyl pyridinium iodide, 2-[4-(dimethylamino)styryl]-*N*-ethyl pyridinium iodide, and 2-[4-(dimethylamino)styryl]-*N*-methyl pyridinium iodide. These dyes not only act as host molecules but also serve as microenvironmental probes due to their solvatochromic nature.

## SELF-ASSEMBLY OF CYCLIC AND ACYCLIC SYNTHETIC PEPTIDES

### Supramolecular Peptide Helices

The design and construction of monomolecular peptide helical structures using appropriate, conformationally restricted amino acid residues were extensively studied. However, relatively less attention was paid to the construction of a supramolecular peptide helix. In biological systems, supramolecular helices with various levels of self-organization and self-assembly of the peptide backbone are common. My research group is involved in constructing various supramolecular helical structures from acyclic oligopeptides containing noncoded amino acids with appropriate conformations, which can act as subunits for self-assembly.<sup>[21–25]</sup>

The majority of the backbone torsion angles of the terminally blocked tripeptide Boc-Leu-Aib-Phe-OMe [Aib:  $\alpha$ -aminoisobutyric acid] falls within the helical region, and it fails to form any intramolecularly hydrogen-bonded turn structures. However, this helps to form a supramolecular helical structure (Fig. 1) through noncovalent interactions in the solid state.<sup>[21]</sup> The scanning electron microscopic (SEM) picture of the tripeptide Boc-Leu-Aib-Phe-OMe shows the filamentous ribbon-like fibrillar morphology that is reminiscent of neurodegenerative disease-causing amyloid fibrils.

The terminally protected tetrapeptide Boc-Leu-Aib-Phe-Aib-OMe adopts a consecutive double-bend conformation with two successive  $\beta$ -turns. It self-assembles through various noncovalent interactions, including intermolecular hydrogen bonds, to form a supramolecular helical structure in crystals (Fig. 2).<sup>[22]</sup> Similarly, another double-bend-forming peptide Boc-Ala-Aib-Leu-Aib-OMe self-associates to form a supramolecular helix via intermolecular hydrogen bonding in the crystal structure.<sup>[23]</sup> However, the tetrapeptide Boc- $\beta$ -Ala-Aib-Leu-Aib-OMe [ $\beta$ -Ala:  $\beta$ -alanine] adopts a new type of consecutive

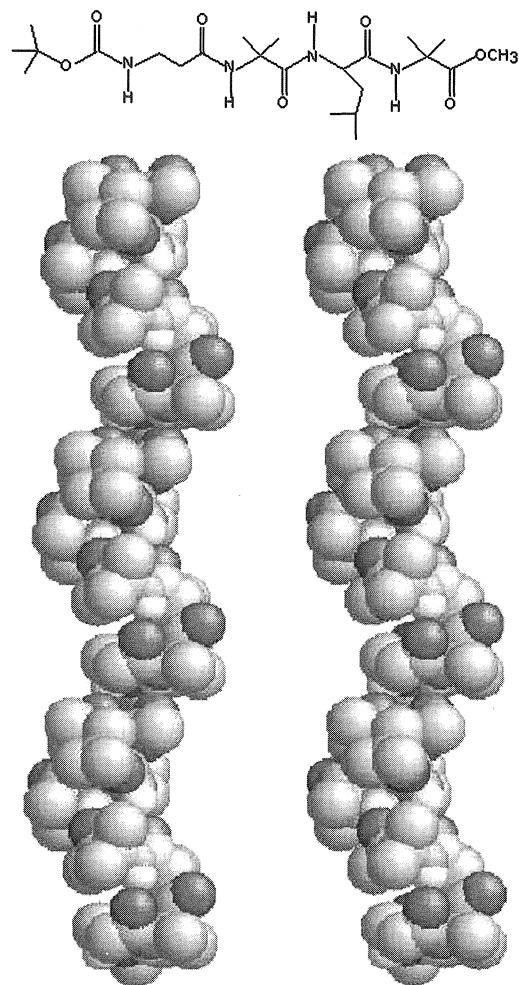


**Fig. 3** A cross-eye stereo, space-filling representation of the tetrapeptide Boc- $\beta$ -Ala-Aib-Leu-Aib-OMe showing a higher-ordered supramolecular helical assembly, as determined by single-crystal x-ray diffraction studies. Nitrogen atoms are blue, oxygen atoms are red, and carbon atoms are gray. Nonhydrogen-bonded hydrogen atoms and side chains of Leu are omitted for clarity. (View this art in color at [www.dekker.com](http://www.dekker.com).)

double-turn structure, which self-associates to form a unique supramolecular helix (Fig. 3).<sup>[24]</sup> The terminally protected tetrapeptide Boc-Aib-Val-Aib- $\beta$ -Ala-OMe adopts a double-turn molecular conformation that self-assembles to form an anisotropic intermolecularly hydrogen-bonded supramolecular helix with an average diameter of 1 nm in the crystal (Fig. 4). This supramolecular helical structure further self-assembles to form polydisperse nanorods with diameters ranging from 10–40 nm.<sup>[25]</sup>

### Supramolecular Acyclic Peptide $\beta$ -Sheets

The design and construction of acyclic oligopeptide molecules, which form supramolecular  $\beta$ -sheet structures,

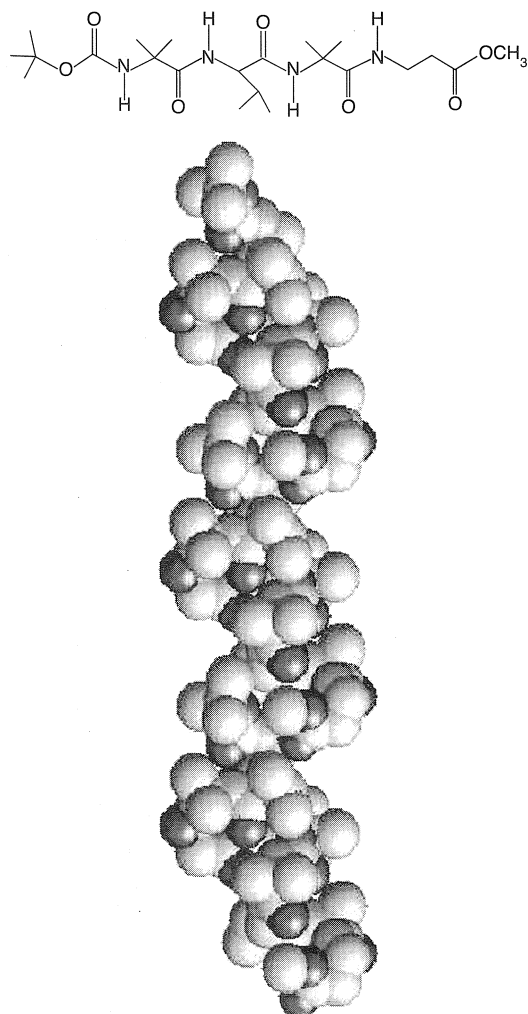


**Fig. 4** Space-filling model of the supramolecular helical array of the tetrapeptide Boc-Aib-Val-Aib- $\beta$ -Ala-OMe showing the staking of subunits maintaining proper registry, generating a helical structure as determined by x-ray crystallographic analysis. Nitrogen atoms are blue, oxygen atoms are red, and carbon atoms are gray. Hydrogen atoms are omitted for clarity. (View this art in color at [www.dekker.com](http://www.dekker.com).)

comprise an emerging field. Formation of supramolecular  $\beta$ -sheet structures using various noncovalent interactions and their further self-association into highly ordered fibrillar structures are responsible for causing many fatal progressive neurodegenerative amyloid diseases, like Alzheimer's and Parkinson's. To understand the molecular bases of pathogenesis and therapeutics of these diseases, it is important to construct supramolecular peptide  $\beta$ -sheet assemblage. There are many reports of  $\beta$ -sheet stabilization involving unimolecular  $\beta$ -sheet formation and subsequent stabilization by only intramolecular interactions.<sup>[26,27]</sup> However, there are limited reports elucidating peptide  $\beta$ -sheet formation and stabilization in

crystals and in solution by purely intermolecular interactions.<sup>[28–32]</sup> My research group is actively engaged in constructing amyloid-like fibril-forming supramolecular  $\beta$ -sheets.<sup>[28–32]</sup> The terminally blocked tripeptide containing noncoded amino acids [viz.,  $\beta$ -alanine ( $\beta$ -Ala) and  $\alpha$ -aminoisobutyric acid (Aib)], Boc- $\beta$ -Ala-Aib- $\beta$ -Ala-OMe, adopts a  $\beta$ -strand structure with an overall extended backbone conformation with a slight kink at the middle. It self-assembles to form a supramolecular parallel  $\beta$ -sheet structure in crystal (Fig. 5) and amyloid-like fibrils in the solid state.<sup>[28]</sup> The supramolecular  $\beta$ -sheet structure is formed by various noncovalent interactions, including intermolecular hydrogen bonding. This is the first crystallographic evidence of an amyloid-like fibril-forming parallel  $\beta$ -sheet assemblage of a synthetic tripeptide composed of only nonprotein amino acids. A recent report describes that components of a series of terminally protected dipeptides, composed of 3-aminophenyl acetic acid and Aib/Val/Pro, share a common structural feature—an extended backbone conformation—and they self-assemble to form an intermolecularly hydrogen-

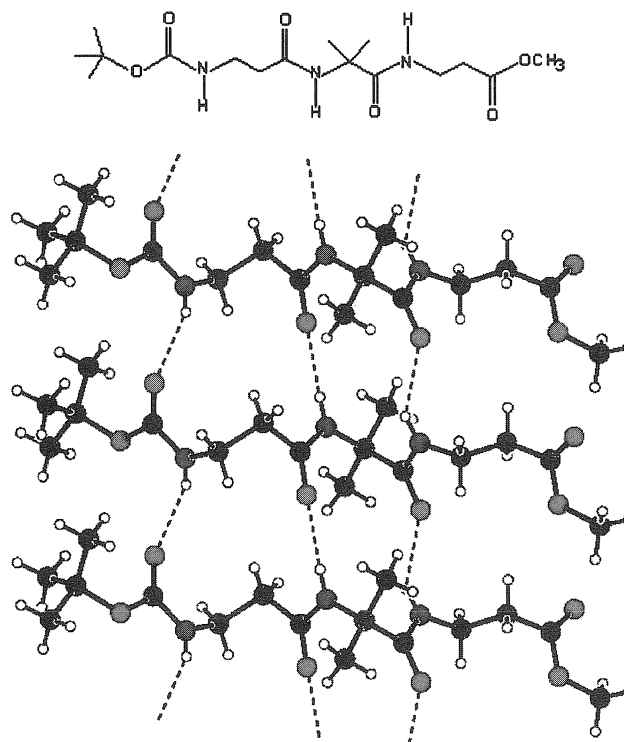


**Fig. 5** Packing diagram of the terminally protected tripeptide Boc- $\beta$ -Ala-Aib- $\beta$ -Ala-OMe in the *b* projection, illustrating intermolecular hydrogen bonding in solid state and formation of the supramolecular  $\beta$ -sheet. Nitrogen atoms are blue, oxygen atoms are red, carbon atoms are black, and hydrogen atoms are white circles. Dashed lines indicate hydrogen bonds. (View this art in color at [www.dekker.com](http://www.dekker.com).)

bonded supramolecular  $\beta$ -sheet structure and show amyloid-like fibrillar morphology in the solid state.<sup>[29]</sup> Similarly, other terminally protected tripeptides Boc-Ala-Gly- $\beta$ -Ala-OMe<sup>[30]</sup> and Boc-Leu-Aib-Leu-OMe<sup>[31]</sup> self-assemble through intermolecular hydrogen bonding to form supramolecular  $\beta$ -sheet structures in crystals. Both tripeptides form the antiparallel  $\beta$ -sheet structure. The tripeptide Boc-Leu-Aib- $\beta$ -Ala-OMe adopts an intramolecularly hydrogen-bonded  $\beta$ -turn conformation in the crystals. There are two molecules in the asymmetric unit to form a molecular dimer of two different conformers.<sup>[32]</sup> This peptide self-assembles by intermolecular hydrogen

bonds and other noncovalent interactions to form a supramolecular  $\beta$ -sheet structure in crystals (Fig. 6). This is the first example of a  $\beta$ -turn forming short acyclic peptide, which forms the supramolecular  $\beta$ -sheet structure in crystals instead of a supramolecular helix.

### Self-Assembling Cyclic Peptides

Cyclic peptides with an even number of alternating D- and L- $\alpha$ -amino acids adopt flat ring-shaped structures in which the backbone amide groups are arranged perpendicular to the side chains and the plane of the ring conformation.

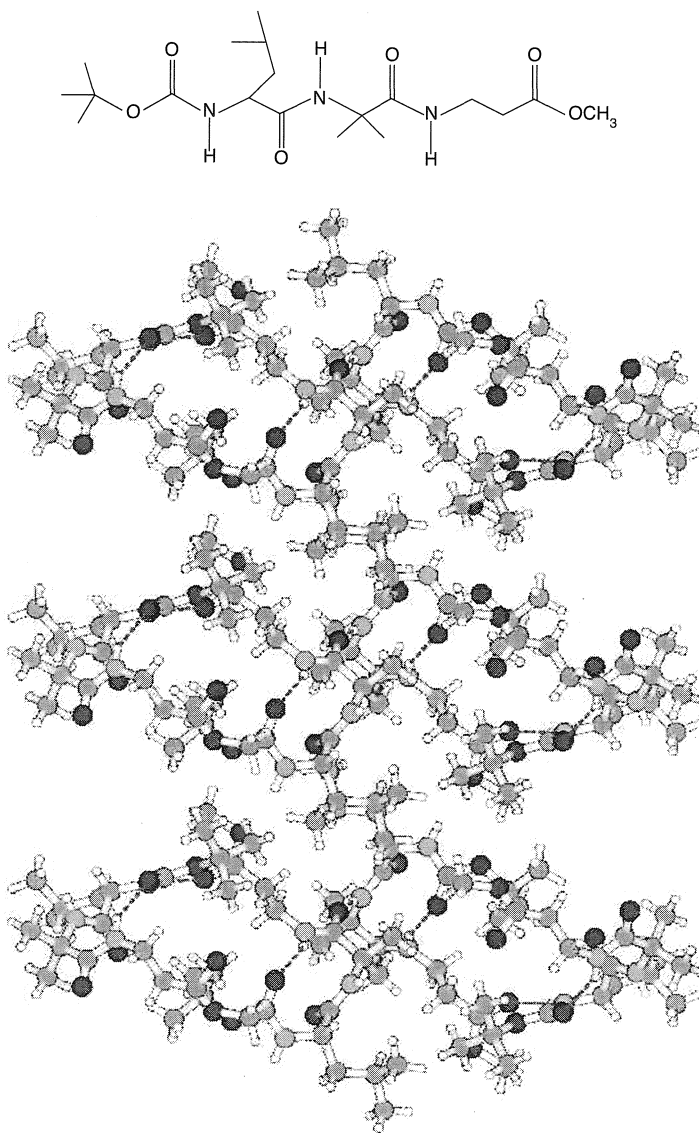


**Fig. 6** The packing of the terminally protected tripeptide Boc-Leu-Aib- $\beta$ -Ala-OMe, showing the formation of a continuous  $\beta$ -sheet column along the crystallographic  $b$  axis via intermolecular hydrogen bonds and van der Waals' interactions in the crystal. Dashed lines indicate hydrogen bonds. Nitrogen atoms are blue, oxygen atoms are red, carbon atoms are green, and hydrogen atoms are white. (View this art in color at [www.dekker.com](http://www.dekker.com).)

Under favorable conditions, these cyclic peptide rings self-assemble through intermolecular hydrogen bonding to form open-ended hollow  $\beta$ -sheet-like nanotubular structures, keeping the amino acid side chains outside the surface of the ensemble. In a pioneering work, Ghadiri and his coworkers demonstrated the formation of hollow tubular supramolecular structures with an appropriate internal diameter of 7 Å from a self-assembling cyclic octapeptide cyclo-[(-L-Glu-D-Ala-L-Glu-D-Ala-)<sub>2</sub>].<sup>[33]</sup> The internal diameter of cyclic peptide nanotubes can be altered by varying the peptide ring size. The 12-residue peptide cyclo-[(-L-Glu-D-Ala-L-Glu-D-Ala-)<sub>3</sub>]<sup>[34]</sup> was shown to undergo proton-triggered self-assembly, which leads to the formation of a nanotubular structure of an enhanced van der Waals' diameter of 13 Å. A remarkable feature of these cyclic peptide nanotubes is that the surface properties of the tubular structures can be varied by appropriately selecting the amino acid side chains. Cyclic D, L-peptides with appropriate hydrophobic side chains can be partitioned in nonpolar lipid bilayers and undergo self-association to form transmembrane ion channels. In 1994, Ghadiri and his coworkers demonstrated the formation of a transmembrane ion channel based on a self-assembled, cyclic D,L-octapeptide.<sup>[35]</sup> Single-channel conductance measurements and fluorescence proton transfer assays were used to examine the channel-forming properties of cyclic D,L-peptides. These ion channels exhibit transport activity for Na<sup>+</sup> and K<sup>+</sup> greater than 10<sup>7</sup> ions s<sup>-1</sup>. The cyclic decapeptide cyclo-[(-L-Trp-D-Leu)<sub>4</sub>-L-Gln-D-Leu] with an internal van der Waals diameter of 10 Å, was shown to transport glucose molecules across the lipid bilayer membrane.<sup>[36]</sup> A report from Seebach and his group noted that cyclic tetrapeptides containing only chiral  $\beta^3$ -amino acids can form hollow tubes similar to those exhibited by cyclic D,L- $\alpha$ -peptides.<sup>[37]</sup> Ghadiri et al. demonstrated the formation of ion channels by two self-assembling cyclic  $\beta^3$ -peptides.<sup>[38]</sup> Described in recent report from Ghadiri's group was that self-assembling cyclic D,L- $\alpha$ -peptides composed of six and eight residues can serve as potent antibacterial agents against drug-resistant bacteria<sup>[39]</sup> by enhancing the membrane permeability, collapsing the transmembrane potential, and eventually causing rapid cell death. These antibacterial cyclic oligopeptides were found to be nontoxic in mice, and they hold considerable promise in combating many drug-resistant bacterial infections in human beings.

## CONCLUSION

The applications of amino acids in supramolecular chemistry are multipurpose. One purpose is to make inclusion complexes with common macrocyclic hosts, like

CDs or calixarenes. Other applications include complexations of metal ions with amino acids, leading to various supramolecular architectures. In addition, various amino acids are used to synthesize cyclic and acyclic peptides that have wide applications in supramolecular chemistry, such as creating nonself-assembling cyclic oligopeptides with well-defined cavities that can be used as hosts for various cations (including the chiral one), anions, and electroneutral substrates. Finally, self-assembling cyclic and acyclic peptides not only form various supramolecular architectures, but also, cyclic oligopeptides can be used as artificial ion channels and antibacterial agents.

## ACKNOWLEDGMENTS

I am thankful to Debashis Haldar, Arijit Banerjee, Apurba Kumar Das, Sudipta Ray, and Partha Pratim Bose for their help in the preparation of the entire manuscript. I am very grateful to my collaborator Prof. M.G.B. Drew, The University of Readings, Whiteknights, U.K., for solving numerous crystal structures of my peptides that are cited within this article.

## ARTICLES OF FURTHER INTEREST

*Alkali Metal Cations in Biochemistry*, p. 1  
*Artificial Enzymes*, p. 76  
*Biological Ligands*, p. 88  
*Biological Models and Their Characteristics*, p. 101  
*Channel Inclusion Compounds*, p. 223  
*Cyclodextrins*, p. 398  
*Emergence of Life*, p. 528  
*Enzyme Mimics*, p. 546  
*Hydrogen Bonding*, p. 658  
*Ion Channels and Their Models*, p. 742  
*Peptide Nanotubes*, p. 1035  
*Protein Supramolecular Chemistry*, p. 1161

## REFERENCES

1. Miyake, H.; Yamashita, T.; Kojima, Y.; Tsukube, H. Enantioselective transport of amino acid ester salts by macrocyclic pseudopeptides containing N,N'-ethylene-bridged-di-peptide units. *Tetrahedron Lett.* **1995**, 36, 7669–7672.
2. Garcia, M.E.; Gavin, J.A.; Deng, N.; Andrievsky, A.A.; Mallouk, T.E. Combinatorial synthesis of modular chiral cyclophanes. *Tetrahedron Lett.* **1996**, 37, 8313–8316.
3. Ranganathan, D.; Haridas, V.; Karle, I.L. Cystinophanse, a novel family of aromatic-bridged cystine cyclic peptides:

- Synthesis, crystal structure, molecular recognition, and conformational studies. *J. Am. Chem. Soc.* **1998**, *120*, 2695–2702.
4. Ishida, H.; Suga, M.; Donowaki, K.; Ohkubo, K. Highly effective binding of phosphomonoesters with neutral cyclic peptides which include a non-natural amino acid. *J. Org. Chem.* **1995**, *60*, 5374–5375.
  5. Kubik, S. Large increase in cation binding affinity of artificial cyclopeptide receptors by an allosteric effect. *J. Am. Chem. Soc.* **1999**, *121*, 5846–5855.
  6. Kubik, S.; Goddard, R. A new cyclic pseudopeptide composed of (L)-proline and 3-aminobenzoic acid subunits as a ditopic receptor for the simultaneous complexation of cations and anions. *J. Org. Chem.* **1999**, *64*, 9475–9486.
  7. Kubik, S.; Goddard, R. Intermolecular conformational control in a cyclic peptide composed of alternating L-proline and substituted 3-aminobenzoic acid subunits. *Chem. Commun.* **2000**, 633–634.
  8. Pohl, S.; Goddard, R.; Kubik, S. A new cyclic peptide composed of alternating L-proline and 3-aminobenzoic acid subunits. *Tetrahedron Lett.* **2001**, *42*, 7555–7558.
  9. Heinrichs, G.; Vial, L.; Lacour, L.; Kubik, S. Enantioselective recognition of a chiral quaternary ammonium ion by  $C_3$  symmetric cyclic hexapeptides. *Chem. Commun.* **2003**, 1252–1253.
  10. Ramirez, J.; He, F.; Lebrilla, C.B. Gas-phase chiral differentiation of amino acid guests in cyclodextrin hosts. *J. Am. Chem. Soc.* **1998**, *120*, 7387–7388.
  11. Al-Kindy, S.M.Z.; Suliman, F.E.O.; Al-Hamadi, A.A. Fluorescence enhancement of coumarin-6-sulfonyl chloride amino acid derivatives in cyclodextrin media. *Anal. Sci.* **2001**, *17*, 539–543.
  12. Arena, G.; Contino, A.; Gulino, F.G.; Margi, A.; Sansone, F.; Scitto, D.; Ungaro, R. Complexation of native L- $\alpha$ -amino acids by water soluble calix[4]arenes. *Tetrahedron Lett.* **1999**, *40*, 1597–1600.
  13. Poh, B.L.; Tan, C.M. Complexation of amino acids by cyclotetrachromotriptylene in aqueous solution—Importance of CH- $\pi$  and  $\pi$ - $\pi$  interactions. *Tetrahedron* **1994**, *50*, 3453–3462.
  14. Goto, K.; Nakamisha, K.; Tanone, O.; Nakushina, S.; Toudo, I.; Imamuro, C.; Ihara, Y.; Matsumoto, Y.; Ueoka, R. Cyclodextrin-mediated deacylation of amino acid esters with marked stereoselectivity. *Chem. Pharm. Bull.* **2002**, *50*, 1283–1285.
  15. Wang, R.; Zheng, Z.; Jin, T.; Staples, R.J. Coordination chemistry of lanthanides at “high” pH: Synthesis and structure of the pentadecanuclear complex of europium (III) with tyrosine. *Angew. Chem., Int. Ed.* **1999**, *38*, 1813–1815.
  16. Wang, R.; Liu, H.; Carducci, M.D.; Jin, T.; Zheng, C.; Zheng, Z. Lanthanide coordination with  $\alpha$ -amino acids under near physiological pH conditions: Polymetallic complexes containing the cubane like  $[\text{Ln}_4(\mu_3\text{-OH})_4]^{8+}$  cluster core. *Inorg. Chem.* **2001**, *40*, 2743–2750.
  17. Hachisako, H.; Yamazaki, T.; Ihara, H.; Hirayama, C.; Yamada, K. Formation of specific hydrophobic sites for incorporation of methylene blue by laterally arranged L-glutamate residue in crystalline bilayer aggregates. *J. Chem. Soc., Perkin Trans.* **1994**, (2), 1671–1680.
  18. Hachisako, H.; Motozato, Y.; Murakani, R.; Yamada, K. Extraordinary monomer–dimer transition of methylene blue induced by the phase transition of telomer-bilayer membranes formed from dialkyl L-glutamate amphiphiles with oligo acrylic acid head group. *Chem. Lett.* **1992**, 219–222.
  19. Hachisako, H.; Yamazaki, T.; Ihara, H.; Hirayama, C.; Yamada, K. Recognition of molecular planarity of cationic dyes by anionic crystalline bilayer aggregates: Evidence using metachromatic and solvchromatic properties. *J. Chem. Soc., Perkin Trans.* **1994**, (2), 1681–1690.
  20. Hachisako, H.; Murata, Y.; Ihara, H. Supramolecular receptors from  $\alpha$ -amino acid-derived lipids. *J. Chem. Soc., Perkin Trans.* **1999**, (2), 2569–2577.
  21. Haldar, D.; Maji, S.K.; Sheldrick, W.S.; Banerjee, A. First crystallographic signature of the highly ordered supramolecular helical assemblage from a tripeptide containing a non-coded amino acid. *Tetrahedron Lett.* **2002**, *43*, 2653–2656.
  22. Haldar, D.; Maji, S.K.; Drew, M.G.B.; Banerjee, A.; Banerjee, A. Self-assembly of a short peptide monomer into the continuous hydrogen bonded supramolecular helix: The crystallographic evidence. *Tetrahedron Lett.* **2002**, *43*, 5465–5468.
  23. Maji, S.K.; Banerjee, A.; Drew, M.G.B.; Haldar, D.; Banerjee, A. Self-assembly of a tetrapeptide in which a unique supramolecular helical structure is formed via intermolecular hydrogen bonding in the solid state. *Tetrahedron Lett.* **2002**, *43*, 6759–6762.
  24. Banerjee, A.; Maji, S.K.; Drew, M.G.B.; Haldar, D.; Banerjee, A. Supramolecular peptide helix from a novel double turn forming peptide containing a  $\beta$ -amino acid. *Tetrahedron Lett.* **2003**, *44*, 699–702.
  25. Haldar, D.; Banerjee, A.; Drew, M.G.B.; Das, A.K.; Banerjee, A. First crystallographic signature of an acyclic peptide nanorod: Molecular mechanism of nanorod formation by a self-assembled tetrapeptide. *Chem. Commun.* **2003**, 1406–1407.
  26. Fisk, J.D.; Gellman, S.H. A parallel  $\beta$ -sheet model system that folds in water. *J. Am. Chem. Soc.* **2001**, *123*, 343–344.
  27. Das, C.; Raghothama, S.; Balaram, P. A designed three stranded  $\beta$ -sheet peptide as a multiple  $\beta$ -hairpin model. *J. Am. Chem. Soc.* **1998**, *120*, 5812–5813, and references cited therein.
  28. Maji, S.K.; Drew, M.G.B.; Banerjee, A. First crystallographic signature of amyloid-like fibril forming  $\beta$ -sheet assemblage from a tripeptide with non-coded amino acids. *Chem. Commun.* **2001**, 1946–1947.
  29. Maji, S.K.; Haldar, D.; Banerjee, A.; Banerjee, A. Fibril-forming model synthetic peptides containing 3-aminophenyl acetic acid. *Tetrahedron* **2002**, *58*, 8695–8702.
  30. Maji, S.K.; Malik, S.; Drew, M.G.B.; Nandi, A.K.; Banerjee, A. A synthetic tripeptide as a novel organogelator: A structural investigation. *Tetrahedron Lett.* **2003**, *44*, 4103–4107.
  31. Banerjee, A.; Maji, S.K.; Drew, M.G.B.; Haldar, D.; Banerjee, A. Amyloid-like fibril forming antiparallel

- supramolecular  $\beta$ -sheet from a synthetic tripeptide : A crystallographic signature. *Tetrahedron Lett.* **2003**, *44*, 6741–6744.
32. Banerjee, A.; Maji, S.K.; Drew, M.G.B.; Haldar, D.; Banerjee, A. Amyloid-like fibril-forming supramolecular  $\beta$ -sheet from a  $\beta$ -turn forming tripeptide containing non-coded amino acids: The crystallographic signature. *Tetrahedron Lett.* **2003**, *44*, 335–339.
33. Ghadiri, M.R.; Granja, J.R.; Milligan, R.A.; Mcree, D.E.; Khazanovich, N. Self-assembling organic nanotubes based on a cyclic peptide architecture. *Nature* **1993**, *366*, 324–327.
34. Khazanovich, N.; Granja, J.R.; McRee, D.E.; Milligan, R.A.; Ghadiri, M.R. Nanoscale tubular ensembles with specified internal diameters. Design of a self-assembled nanotube with a 13 Å pore. *J. Am. Chem. Soc.* **1994**, *116*, 6011–6012.
35. Ghadiri, M.R.; Granja, J.R.; Buehler, L.K. Artificial transmembrane ion channels from self-assembling peptide nanotubes. *Nature* **1994**, *369*, 301–304.
36. Granja, J.R.; Ghadiri, M.R. Channel-mediated transport of glucose across lipid bilayers. *J. Am. Chem. Soc.* **1994**, *116*, 10785–10786.
37. Seebach, D.; Mathews, J.L.; Meden, A.; Wessels, T.; Baerlocher, C.; McCusker, L.B. Cyclo-[ $\beta$ ]-peptides: Structure and tubular stacking of cyclic tetramers of 3-aminobutanoic acid as determined from powder diffraction data. *Helv. Chim. Acta* **1997**, *80*, 173–182.
38. Clark, T.D.; Buehler, L.K.; Ghadiri, M.R. Self-assembling cyclic  $\beta^3$ -peptide nanotubes as artificial transmembrane ion channels. *J. Am. Chem. Soc.* **1998**, *120*, 651–656.
39. Fernandez-Lopez, S.; Kim, H.S.; Chot, E.C.; Delgado, M.; Granja, J.R.; Khasnov, A.; Krachenbuehl, K.; Long, G.; Weinbeger, D.A.; Wilcoxon, K.M.; Ghadiri, M.R. Antibacterial agents based on the cyclic D, L- $\alpha$ -peptide architecture. *Nature* **2001**, *412*, 452–455.

# Anion-Directed Assembly

Ramón Vilar

Imperial College of Science, Technology, and Medicine,  
London, United Kingdom

A

## INTRODUCTION

There is great current interest in developing strategies for the synthesis of complex molecular architectures with novel properties and potential in a wide range of applications. During the past few years, supramolecular chemistry provided important advances in this direction. The increased control over the assembly of molecular components led to the rational synthesis of novel species such as molecular cages, helicates, rotaxanes, and catenanes, among several others. A common strategy used to prepare such assemblies involves the use of chemical templates. As defined by Busch, "A chemical template organizes an assembly of atoms, with respect to one or more geometric loci, in order to achieve a particular linking of atoms" (p. 389).<sup>[1]</sup> When there are several potential ways of linking a group of molecular components, the template provides the instructions for the formation of a single product. In the presence of another template, a different assembly is expected, and as a consequence, a different product should be formed. In general, after the template has directed the formation of the assembly, it can be removed to yield the template-free product. However, this is not possible if the templating agent is an integral part of the final product. In this entry, a template (or directing agent) will be considered to be any species that organizes an assembly of atoms or molecules for specific linking and is either removed from the final product or kept as an integral part of it.

## ANIONS AS TEMPLATES

In contrast to the well-studied templating properties of cationic and neutral species,<sup>[2,3]</sup> anions have been largely neglected as templating agents until recently. Up to 1996 there were only a handful of examples of anion-directed assemblies, the first ones being reported in the early 1990s.<sup>[4,5]</sup> The relative lack of anion-templated assemblies has been partially attributed to intrinsic properties of anions, such as their diffuse nature (i.e., small charge-to-radius ratio), pH sensitivity, and their relative high solvation-free energies.<sup>[9]</sup> However, as demonstrated over

the past few years, these limitations can be overcome by appropriately modifying the experimental conditions, and several anion-directed assemblies have now been reported. The importance of anions as templates is also seen in biological processes where, for example, anions have been identified as directing agents in protein folding.<sup>[6]</sup>

This entry provides a compilation of anion-directed assemblies and analyzes some of the factors that have made these syntheses possible. This is the first time that the subject is specifically reviewed, even though Beer and Gale incorporated a section on this topic in their three reviews on supramolecular chemistry of anions.<sup>[7–9]</sup> The current entry will be divided into two main sections: anion-directed synthesis of metalla-assemblies, and anion-directed assembly in organic synthesis. While in the first type of assemblies the anions use mainly electrostatic and Lewis-acid–base interactions to direct the syntheses, in the second case hydrogen bonds play a very important role. The size and geometry of the templating anions are also essential in dictating the final structure to be formed (as it is in any other templated reaction). Due to space limitations, this entry will concentrate on anion-directed assemblies that yield well-defined molecular species. The anion-directed assembly of polymeric materials, although an important area within supramolecular chemistry, is out of the scope of this review.

## ANION-DIRECTED SYNTHESIS OF METALLA-ASSEMBLIES

### Metalla-Macrocycles and Circular Helicates

One of the first anion-directed assemblies is the [12]mercuracarborand-4 (1) reported by Hawthorne in 1991, which can be prepared in high yields by reacting 1,2-dilithio-carborane with mercuric chloride (see Fig. 1).<sup>[4]</sup> This compound consists of four bivalent 1,2-carborane cages linked by four mercury atoms forming a macrocycle with a chloride ion located at its center. The anion displays strong Lewis-acid–base interactions with the four mercury atoms of the macrocycle. Such interactions play an important role in directing the formation of the cyclic



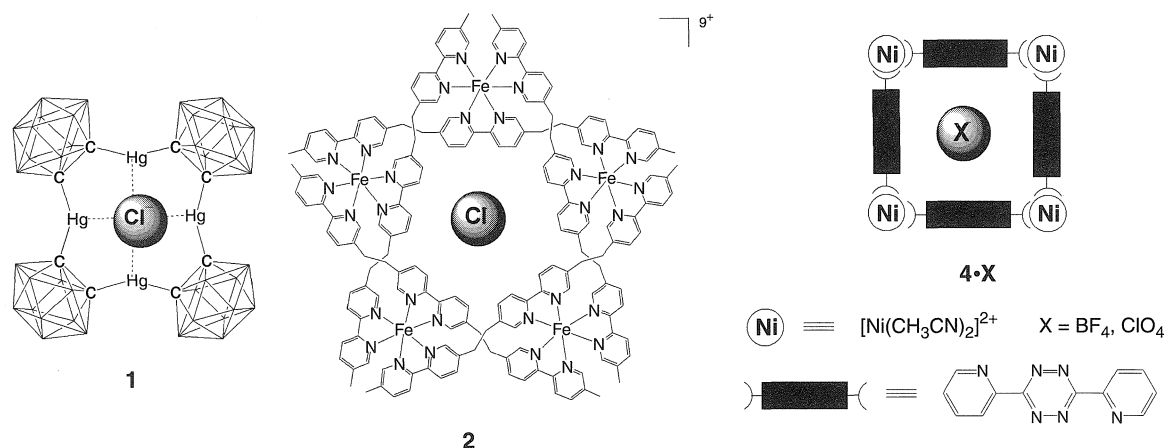


**Fig. 1** The anion-templated assemblies reported by Hawthorne,<sup>[4,10]</sup> Lehn,<sup>[11,12]</sup> and Dunbar.<sup>[14,15]</sup> (View this art in color at [www.dekker.com](http://www.dekker.com).)

structures as opposed to the noncyclic ones. The same authors later showed that an analogous cyclic tetramer is obtained when mercuric iodide is used for the cyclization reaction but, in contrast, an acyclic polymer is formed in the presence of mercuric acetate.<sup>[10]</sup>

Elegant examples of anion-templated synthesis are the penta- and hexanuclear circular helicates reported by Lehn (see Fig. 1).<sup>[11,12]</sup> In this work it was demonstrated that the self-assembly of iron(II) salts and a *tris*-bipyridyl ligand (L) is highly dependent on the presence of specific anions. With FeCl<sub>2</sub>, the pentanuclear circular helicate [Fe<sub>5</sub>L<sub>5</sub>Cl]<sup>9+</sup> (**2**) is obtained, while the hexanuclear analogue [Fe<sub>6</sub>L<sub>6</sub>(SO<sub>4</sub>)]<sup>10+</sup> (**3**) is formed in quantitative yields with FeSO<sub>4</sub> [hexanuclear systems are also formed with Fe(BF<sub>4</sub>)<sub>2</sub> and FeSiF<sub>6</sub>]. The structural characterization of [Fe<sub>5</sub>L<sub>5</sub>Cl]<sup>9+</sup> demonstrated it to be a circular double helix with an inner cavity radius of 1.75 Å. The chloride ion is contained within this cavity (which provides an excellent size match for this halide) and is tightly bound thanks to the 10 positive charges from the five iron(II) centers located in the periphery. By increasing the size of the templating anion, it is then possible to assemble structures with larger cavities such as [Fe<sub>6</sub>L<sub>6</sub>(SO<sub>4</sub>)]<sup>10+</sup>. In these examples, electrostatic interactions and good ion-to-cavity size match are the directing forces behind the anion-templated self-assembly process. Using a similar approach, McCleverty and Ward reported the synthesis of the cyclic supramolecular complex [Co<sub>8</sub>L<sub>12</sub>(ClO<sub>4</sub>)]<sup>3+</sup> (where L = *bis* {3-(2-pyridyl)pyrazol-1-yl} dihydroborate) with a perchlorate anion encapsulated in the central cavity.<sup>[13]</sup> The anion is likely to play an important role in the selective formation of this structure.

More recently, Dunbar demonstrated that the structures resulting from the self-assembly of metal cations with the *bis*-chelating ligand 3,6-*bis*(2-pyridyl)1,2,4,5-tetrazine (bptz) are strongly dependant on the anions present in

the reaction mixture.<sup>[14,15]</sup> In the presence of BF<sub>4</sub><sup>-</sup> and ClO<sub>4</sub><sup>-</sup>, the molecular squares [Ni<sub>4</sub>(bptz)<sub>4</sub>(CH<sub>3</sub>CN)<sub>8</sub>][X]<sub>8</sub> (**4·X**) (X = BF<sub>4</sub><sup>-</sup>, ClO<sub>4</sub><sup>-</sup>) are formed in approximately 75% yield (see Fig. 1), while in the presence of SbF<sub>6</sub><sup>-</sup>, the molecular pentagon [Ni<sub>5</sub>(bptz)<sub>5</sub>(CH<sub>3</sub>CN)<sub>10</sub>][SbF<sub>6</sub>]<sub>10</sub> (**5**) is obtained (in 60–70% yields). The structural characterization of the molecular square **4·BF<sub>4</sub>** showed that it has a void space with an approximate diameter of 4.6 Å, which is of the ideal size match for the BF<sub>4</sub><sup>-</sup> anion. In the case of the pentagon, the void space at its center is larger, providing a better size match for larger anions such as SbF<sub>6</sub><sup>-</sup>. The structures observed in the solid state are retained in solution, as demonstrated by ESI mass spectrometry.

Examples of metalla-macrocycles where hydrogen bonding (in addition to electrostatic and Lewis-acid–base interactions) is used by the templating anion to direct the assembly are the Ni/Pd boxes reported by Vilar (see Fig. 2).<sup>[16]</sup> The Ni(atu)<sub>2</sub> fragment (atu = deprotonated amidinothiourea) reacts with PdX<sub>2</sub>(PPh<sub>3</sub>)<sub>2</sub> to selectively form the metalla-macrocycles [Pd<sub>2</sub>Ni<sub>2</sub>(atu)<sub>4</sub>(PPh<sub>3</sub>)<sub>4</sub>X]<sup>3+</sup> (**6·X**) (X = Cl, Br, and I) in 55–74% yields. In the presence of other anions such as triflate, nitrate, or acetate, the formation of the macrocycle is not observed, and instead monometallic species are obtained. Interestingly, if stoichiometric amounts of chloride, bromide, or iodide are added to these mixtures, the corresponding macrocycles are formed quantitatively, confirming the templating role of the halide anions. The structural characterization of these macrocycles demonstrates that, in the solid state, the halides located at their center form hydrogen bonds with four NH groups from the amidinothiourea ligands and with several C–H groups from the phenyl rings of the phosphines. The halides also interact with the palladium centers in a Lewis-acid–base fashion. <sup>31</sup>P-NMR studies revealed that the halides

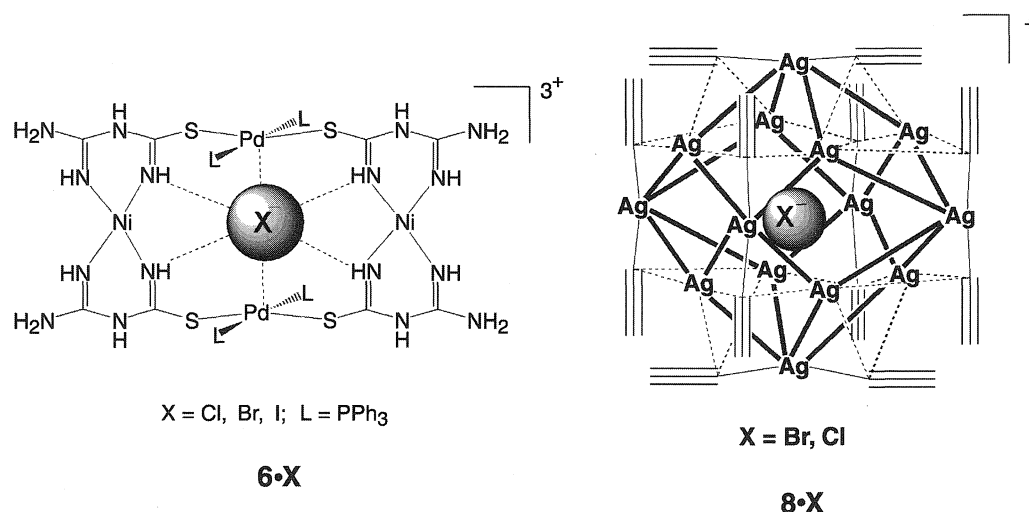


**Fig. 2** Anion-templated metalla-macrocycles **6·X**<sup>[16]</sup> and silver-alkynyl cages **8·X**<sup>[21]</sup> (View this art in color at [www.dekker.com](http://www.dekker.com).)

bound to the metalla-macrocycles can be exchanged in solution.

### Metalla-Cages

The first examples of metalla-cages synthesized by anion-directed processes are a series of polyoxometallates reported by Müller.<sup>[5,17]</sup> In these species, anions control the aggregation of  $V^{n+}O_x$  polyhedra into cage-type structures such as  $[HV_{18}O_{44}(NO_3)]^{10+}$ ,  $[HV_{22}O_{54}(SCN)]^{6+}$ , and  $[H_4V_{15}O_{40}(PO_4)]^{7+}$ , in which the anions are situated inside the cavity of the cages. With other anions such as acetate, V–O aggregates are formed in which the anions are located on the outer surface of the shell. Similarly, Zubieta reported that the synthesis of a series of oxovanadium-organophosphates such as  $[(VO)_6(tBuPO_3)_8Cl]$  may be directed by the encapsulated chloride anion.<sup>[18]</sup>

An interesting example of anion-directed assembly is the “super-adamatoid” silver cage  $[Ag_6(triphos)_4X_4]^{2+}$  (**7·X**) [**X** =  $O_3SCF_3$ ,  $ClO_4$ , and  $NO_3$ ; tripfos =  $(PPh_2CH_2)_3CMe$ ] reported by James and Mingos.<sup>[19]</sup> The formation of these cages is anion-specific, because they are only obtained in the presence of the above-mentioned anions. When other species such as  $BF_4^-$  and  $SbF_6^-$  were used, the corresponding rigid cages were not formed but instead, more labile products in which the phosphines dissociate were obtained. These results indicate that, in order to form the silver cages, a nucleophilic anion with the appropriate geometry to bridge three silver atoms is essential. This process has been further exploited by James to prepare metallo-dendrimers by using benzylsulfate dendrons to direct the assembly of the silver cage.<sup>[20]</sup>

Another example of silver assemblies obtained by anion-directed synthesis<sup>[21]</sup> are the silver cages  $[Ag_{14}(C\equiv C^tBu)_{12}X]^+$  (**8·X**) (**X** = F, Cl, Br). The reaction of *t*-butylalkyne and  $AgBF_4$  in the presence of a base yields the organometallic polymer  $[Ag(C\equiv C^tBu)]_n$ , which is converted (in high yields) into the cages  $[Ag_{14}(C\equiv C^tBu)_{12}X]^+$  (see Fig. 2) upon addition of fluoride, chloride, or bromide salts (but not when other anions such as triflate or tosylate are used). Their structural characterization demonstrated cages **8·X** to have a rhombohedral geometry with the corresponding halide encapsulated at their center. The cavity generated by this specific assembly is of the right geometry and dimensions to encapsulate spherical anions with a maximum radius of approximately 2.0 Å. Electrospray ionization mass spectrometry (ESI-MS) and solution state infrared (IR) studies demonstrated that the cage-type structure is retained in solution. The silver atoms are held together by the bridging alkynyls and a combination of metallophilic attractions between the silver centers and Lewis-acid–base interactions between the silver atoms and the encapsulated halide.

Fujita reported a wide range of systems formed by the self-assembly of several nitrogen-donor ligands and palladium and platinum centers.<sup>[22]</sup> In the assembly of some of these systems, the templating properties of anions play an important role. When the square planar complex  $[Pd(en)_2(NO_3)_2]$  is reacted with 1,3,5-*tris*(4-pyridylmethyl)benzene in the presence of anionic species having a hydrophobic moiety (such as 4-methoxyphenylacetate), the nearly quantitative formation of the cage structure **9** is observed (see Fig. 3).<sup>[23]</sup> In the absence of the anionic/hydrophobic species, this reaction gives rise to a considerable amount of polymeric material. Similarly, the

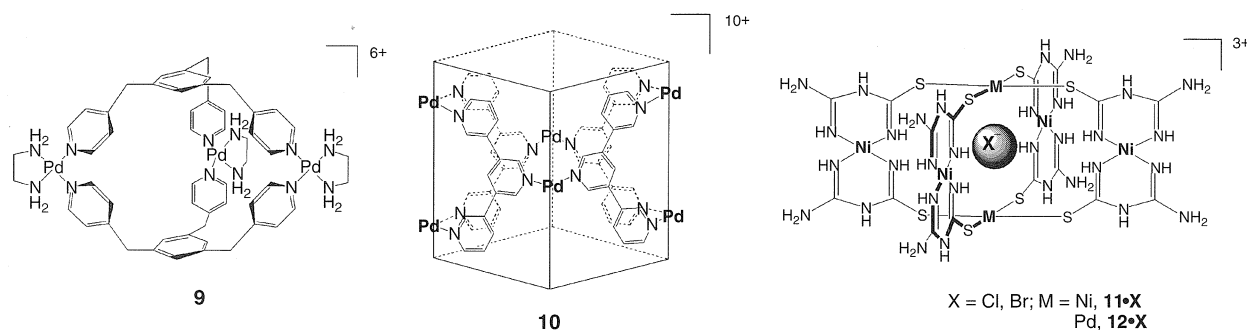


**Fig. 3** Anion-directed cages **9**, **11·X**, **12·X**,<sup>[23,25,26]</sup> and Fujita's nanochannels.<sup>[24]</sup> (View this art in color at [www.dekker.com](http://www.dekker.com).)

quantitative formation of coordination channels such as **10** has been reported to occur when  $[\text{Pd}(\text{en})_2(\text{NO}_3)_2]$  is reacted with oligo(3,5-oligopyridine)s in the presence of rod-like anion species such as 4,4'-biphenylenedicarboxylate (see Fig. 3).<sup>[24]</sup> In these examples, the template directs the assembly not only through electrostatic interactions but also through  $\pi$ - $\pi$  stacking and the use of hydrophobic effects.

A combination of metal··anion and hydrogen-bonding interactions has been used in the anion-directed synthesis of a series of hexametal cages.<sup>[25,26]</sup> The nickel complexes  $[\text{Ni}_6(\text{atu})_8\text{X}]^{3+}$  (**11·X**) can be prepared by mixing stoichiometric amounts of  $\text{NiX}_2$  and Hatu (X = Cl, Br; Hatu = amidinothiourea) in methanol. The structural characterization of the resulting compounds demonstrated that the six nickel atoms are assembled in an octahedral geometry around a central anion and are linked by eight deprotonated Hatu ligands. The corresponding halide anion is encapsulated at the center of the cage and forms eight H-bonds with the ligands' NH groups. There is also an important attraction between the  $\text{NiS}_4$  units located at the poles of the cage and the central anion. The analogous hexanuclear cages  $[\text{Ni}_2\text{Pd}_2(\text{atu})_8\text{X}]^{3+}$

(**12·X**) (X = Cl, Br) can be prepared by reacting four equivalents of the preformed  $\text{Ni}(\text{atu})_2$  complex and two equivalents of  $\text{Pd}(\text{PhCN})_2\text{X}_2$ . In the presence of other anions (such as  $\text{I}^-$ ,  $\text{ClO}_4^-$ ,  $\text{OAc}^-$ , or  $\text{NO}_3^-$ ), the hexanuclear cages do not form, indicating the important geometrical constraints (both regarding their volume and spherical shape) imposed by the templating halides for the formation of these specific structures.

## ANION-DIRECTED ASSEMBLY IN ORGANIC SYNTHESIS

### Macrocycles

Cation-directed synthesis of organic macrocycles such as crown ethers is a well-established procedure that has been widely utilized for many years. However, the use of anionic species for this purpose has only recently begun to be exploited. One of the first examples of anion-directed organic synthesis is the oligopyrrolic macrocycle **13** reported by Sessler (see Fig. 4).<sup>[27]</sup> This macrocycle was

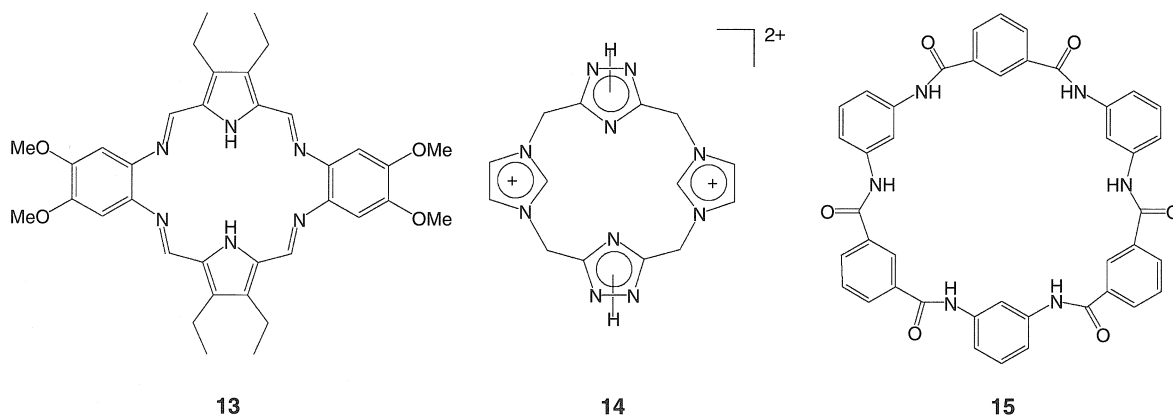


**Fig. 4** Products of the anion-directed macrocyclization reactions reported by Sessler,<sup>[27]</sup> Alcalde,<sup>[28]</sup> and Kim.<sup>[29]</sup>

prepared quantitatively using  $\text{HNO}_3$  (rather than  $\text{HCl}$ ) as acid catalyst for the cyclization. Under these conditions, the nitrate salt of the protonated macrocycle precipitated out of the reaction mixture. These results led the authors to suggest a possible templating effect exerted by the anionic species. Similarly, Alcalde recently reported<sup>[28]</sup> the chloride-directed synthesis of a series of [14]imidazoliophanes such as **14** (see Fig. 4). The macrocyclization reaction leading to these species was studied in the presence of a wide range of anions and demonstrated to give greatly increased yields when chloride (and in some cases, bromide) was used. In the presence of larger anions (such as  $\text{BF}_4^-$ ,  $\text{PF}_6^-$ , and  $\text{H}_2\text{PO}_4^-$ ), the yields were considerably lower, suggesting a good size-match between the cavity of the macrocycles and the two halides.

Another example in which anions seem to play an important directing role is in the synthesis of oligoamide macrocycles.<sup>[29]</sup> Following observations that certain salts (such as  $\text{LiCl}$  and  $\text{CaCl}_2$ ) have an influence on the formation of polyamides, Kim engaged in studying the influence of such salts in model macrocyclic compounds. Specifically, the high dilution reaction between isophthalic acid chloride and *m*-phenylenediamine was studied and reported to yield a complex mixture of cyclic and oligomeric species. However, when this reaction was repeated in the presence of  $\text{CaCl}_2$ , the main product obtained was the cyclic hexamer **15** (see Fig. 4) in preference to the other cyclic and oligomeric species. Structural characterization of **15** demonstrated it to have a  $\text{CaCl}_3^-$  anion (formed in situ from  $\text{CaCl}_2$  and free chloride) positioned in the inner cavity of the macrocycle. These results suggested a directing effect of the anion,

because in its absence, the main product of the reactions was not the hexamer **15** but oligomers and rings of different sizes.

## Rotaxanes and Pseudorotaxanes

The interest in rotaxanes, pseudorotaxanes, and catenanes (i.e., molecules that contain non-covalently interlocked components) stems from their potential use as building blocks in molecular devices. Their syntheses usually rely on some sort of template assistance, such as the preorganization of the assembly's components around a metal center. While cationic templates have been widely used in this context, only a few examples of anion-directed synthesis of interlocked molecules have been reported. In fact, although rotaxanes and pseudorotaxanes have been prepared in this way (as discussed in this section), to date there is no reported example of anion-directed synthesis of catenanes.

Stoddart and Williams reported the first example of anion-assisted self-assembly of a pseudorotaxane.<sup>[30]</sup> By mixing four equivalents of  $[\text{NH}_2(\text{CH}_2\text{Ph})_2][\text{PF}_6]$  with one equivalent of a large macrocycle (tetrakis-*p*-phenylene [68]crown-20), the pseudorotaxane (**16**) shown in Fig. 5 was obtained. This superstructure was structurally characterized, revealing the presence of the  $\text{PF}_6^-$  anion at its center, which forms multiple  $\text{C}-\text{H} \cdots \text{F}$  hydrogen bonds with the hydroquinone methine and the benzylic methylene hydrogen atoms. The presence of an encapsulated  $\text{PF}_6^-$  and its multiple interactions with the receptor suggest that it plays an important directing role in the self-assembly of this superstructure. Further studies in

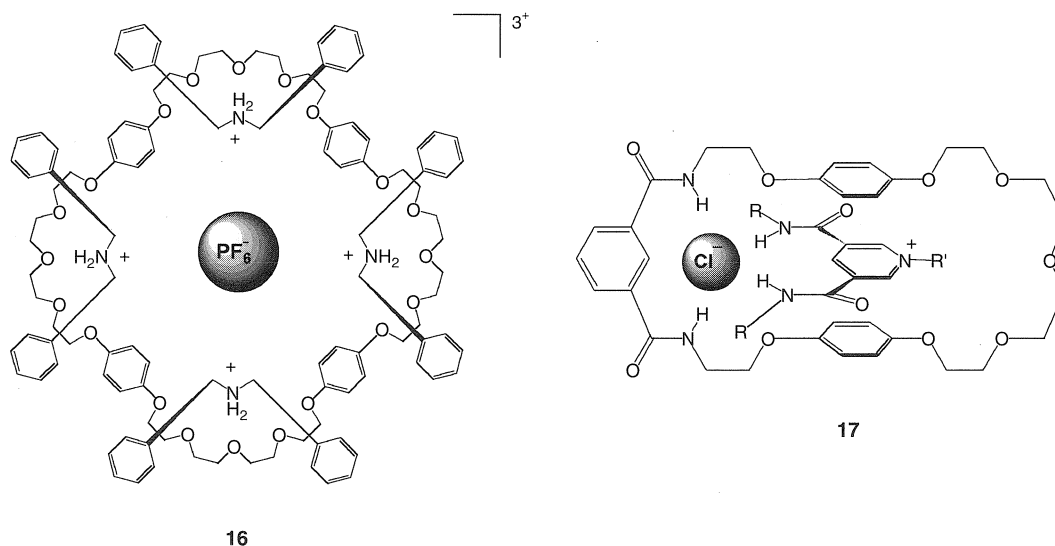


**Fig. 5** Two examples of pseudorotaxanes reported by Stoddart and Williams<sup>[30]</sup> and by Beer.<sup>[31]</sup> (View this art in color at [www.dekker.com](http://www.dekker.com).)

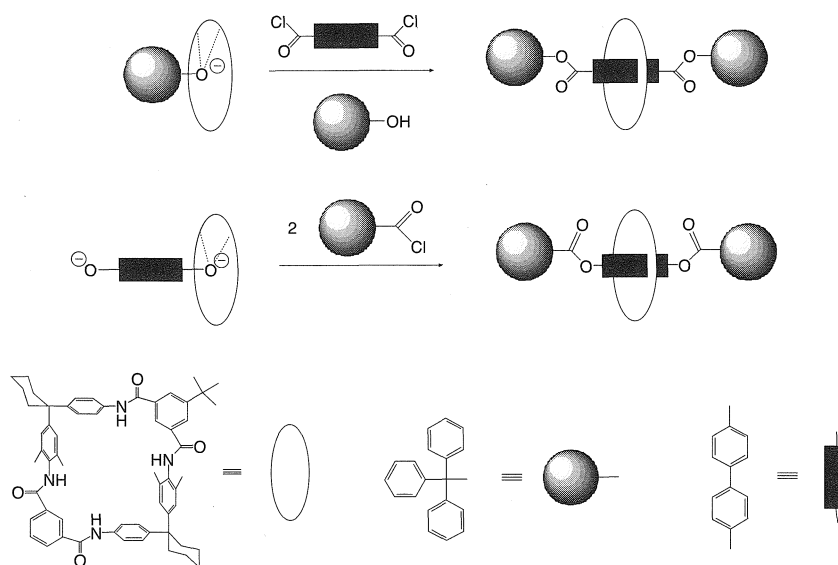


**Fig. 6** Reaction scheme for the anion-directed synthesis of Vögtle's rotaxanes.<sup>[32]</sup> (View this art in color at [www.dekker.com](http://www.dekker.com).)

the presence of other anions would provide interesting insight into this reaction.

Beer recently reported the anion-directed assembly of the [2]pseudorotaxane **17**.<sup>[31]</sup> In this system (see Fig. 5), a chloride anion has been employed as the central core about which two ligands (the macrocycle and the liner species) are orthogonally disposed by means of H-bonding to the anion. The formation of **17** was studied in solution by UV/Vis spectroscopy and <sup>1</sup>H-NMR and confirmed in the solid state by an x-ray crystal structure. While chloride was demonstrated to be a good directing agent for the formation of **17**, other anions such as Br<sup>−</sup>, I<sup>−</sup>, and PF<sub>6</sub><sup>−</sup> proved to be poor templates. This demonstrates the importance of the geometries and dimensions of the templating anion for the formation of a specific assembly.

In 1999 Vögtle reported the first example of anion-directed synthesis of rotaxanes.<sup>[32]</sup> The first step in this synthesis consisted of forming a strong host–guest complex between a tetralactam macrocycle and a phenolate anion (see Fig. 6). With this, the anion (also a good nucleophile) is properly positioned to further react with the adequate component to form a rotaxane. Using this methodology, different rotaxanes were prepared depending on whether the phenolic functionality was located at the stopper component or at the axle precursor.

## Helicates

In contrast to the well-documented assembly of helicates around metal centers, there are only two examples of

well-identified anion-assembled helicates. De Mendoza reported the first in 1996,<sup>[33]</sup> while Kruger and Martin only recently published the second.<sup>[34]</sup> The former reported that a tetraguanidinium strand self-assembled around a sulfate anion to produce a double helical structure. The formation of this assembly was proposed on the basis of NMR and CD spectroscopic studies. More recently, Kruger and Martin structurally characterized a double helicate formed by assembling a diammonium-*bis*-pyridinium salt around two chloride anions. In both of these examples, the directing forces to form the assemblies are based on H-bonding interactions between the anions and the N–H groups present in the ligands.

## CONCLUSION AND OUTLOOK

Important developments in the supramolecular chemistry of anions were seen in the last few years. As a consequence, anion-directed assemblies have started to emerge, providing synthetic chemists with a new approach for the synthesis of complex molecular architectures. The anion-directed assembly of macrocycles, molecular cages, nanotubes, helicates, rotaxanes, and pseudorotaxanes is already a reality. These examples have established the foundations for a systematic and rational approach to the anion-directed synthesis of novel supramolecular (and molecular) structures. Moreover, they suggest that even in well-known reactions, the participation of anions might have been ignored until now. In the years to come, we will certainly see an increasing number of assemblies prepared through anion-directed

approaches, which will provide new methodologies for synthetic chemistry.

## ACKNOWLEDGMENTS

Daniela Rais and Joachim Steinke are thanked for proofreading this manuscript and for providing valuable suggestions for improving it.

## ARTICLES OF FURTHER INTEREST

*Amide- and Urea-Based Anion Receptors*, p. 31  
*Fluorescence Sensing of Anions*, p. 566  
*Guanidium-Based Anion Receptors*, p. 615  
*Halogen Bonding*, p. 628  
*Macrocyclic Synthesis*, p. 830  
*Molecular Squares, Boxes, and Cubes*, p. 909  
*Naked Anion Effect*, p. 939  
*Organometallic Anion Receptors*, p. 1006  
*Rotaxanes and Pseudorotaxanes*, p. 1194  
*Self-Assembly: Definition and Kinetic and Thermodynamic Considerations*, p. 1248  
*The Template Effect*, p. 1493

## REFERENCES

- Busch, D.H. Structural definition of chemical templates and the prediction of new and unusual materials. *J. Inclusion Phenom.* **1992**, *12* (1–4), 389–395.
- Anderson, S.; Anderson, H.L.; Sanders, J.K.M. Expanding roles for templates in synthesis. *Acc. Chem. Res.* **1993**, *26* (9), 469–475.
- Hoss, R.; Vögtle, F. Template synthesis. *Angew. Chem., Int. Ed. Engl.* **1994**, *33* (4), 375–384.
- Yang, X.; Knobler, C.B.; Hawthorne, M.F. “[12]Mercuracarborand-4”, the first representative of a new class of rigid macrocyclic electrophiles: The chloride ion complex of a charge-reversed analogue of [12]crown-4. *Angew. Chem., Int. Ed. Engl.* **1991**, *30* (11), 1507–1508.
- Müller, A.; Penk, M.; Rohlfing, R.; Krickemeyer, E.; Döring, J. Topologically interesting cages for negative ions with extremely high “coordination number”: An unusual property of V–O clusters. *Angew. Chem., Int. Ed. Engl.* **1990**, *29* (8), 926–927.
- Henkels, C.H.; Kurz, J.C.; Fierke, C.A.; Oas, T.G. Linked folding and anion binding of the *Bacillus subtilis* ribonuclease P protein. *Biochemistry* **2001**, *40* (9), 2777–2789.
- Gale, P.A. Anion receptor chemistry: Highlights from 1999. *Coord. Chem. Rev.* **2001**, *213*, 79–128.
- Gale, P.A. Anion coordination and anion-directed assembly: Highlights from 1997 and 1998. *Coord. Chem. Rev.* **2000**, *199*, 181–233.
- Beer, P.D.; Gale, P.A. Anion recognition and sensing: The state of the art and future perspectives. *Angew. Chem., Int. Ed.* **2001**, *40* (3), 487–516.
- Zheng, Z.; Knobler, C.B.; Hawthorne, M.F. Stereoselective anion template effects: Syntheses and molecular structures of tetraphenyl [12]mercuracarborand-4 complexes of halide ions. *J. Am. Chem. Soc.* **1995**, *117* (18), 5105–5113.
- Hasenknopf, B.; Lehn, J.-M.; Kneisel, B.O.; Baum, G.; Fenske, D. Self-assembly of a circular double helicate. *Angew. Chem., Int. Ed. Engl.* **1996**, *35* (16), 1838–1840.
- Hasenknopf, B.; Lehn, J.-M.; Boumediene, N.; Dupont-Gervais, A.; Van Dorsselaer, A.; Kneisel, B.O.; Fenske, D. Self-assembly of tetra- and hexanuclear circular helicate. *J. Am. Chem. Soc.* **1997**, *119* (45), 10956–10962.
- Jones, P.L.; Byrom, K.J.; Jeffery, J.C.; McCleverty, J.A.; Ward, M.D. A cyclic supramolecular complex containing eight metal ions, twelve bridging ligands, and an anion encapsulated in the central cavity. *Chem. Commun.* **1997**, 1361–1362.
- Campos-Fernández, C.S.; Clérac, R.; Dunbar, K.R. A one-pot, high yield synthesis of a paramagnetic nickel square from divergent precursors by anion template assembly. *Angew. Chem., Int. Ed.* **1999**, *38* (23), 3469–3477.
- Campos-Fernández, C.S.; Clérac, R.; Koomen, J.M.; Russell, D.H.; Dunbar, K.R. A fine-tuning the ring-size of metallacyclophanes: A rational approach to molecular pentagons. *J. Am. Chem. Soc.* **2001**, *123* (4), 773–774.
- Cheng, S.-T.; Doxiadi, E.; Vilar, R.; White, A.J.P.; Williams, D.J. Anion templated synthesis of Ni/Pd containing metalla-macrocycles. *J. Chem. Soc. Dalton Trans.* **2001**, 2239–2244.
- Müller, A.; Rohlfing, R.; Krickemeyer, E.; Bögge, H. Control of the linkage of inorganic fragments of V–O compounds: From cluster shells as carcerands via cluster aggregates to solid-state structures. *Angew. Chem., Int. Ed. Engl.* **1993**, *32* (6), 909–912.
- Salta, J.; Chen, Q.; Chang, Y.-D.; Zubieta, J. The oxovanadium-organophosphonate system: Complex cluster structures  $[(VO)_6(rBuPO_3)_8Cl]$ ,  $[(VO)_4\{PhP(O)_2-OP(O)_2Ph\}_4Cl]^-$ , and  $[V_{18}O_{25}(H_2)_2(PhPO_3)_{20}Cl_4]^{4-}$  with encapsulated chloride anions prepared from simple precursors. *Angew. Chem., Int. Ed. Engl.* **1994**, *33* (7), 757–760.
- James, S.L.; Mingos, D.M.P.; White, A.J.P.; Williams, D.J. Anion-templated formation of a unique inorganic ‘superadamantoid’ cage  $[Ag_6(tripho)_4(O_3SCF_3)_4]^{2+}$  [tripho =  $(PPh_2CH_2)_3CMe$ ]. *Chem. Commun.* **1998**, (2323–2324).
- Xu, X.; MacLean, E.J.; Teat, S.J.; Nieuwenhuyzen, M.; Chambers, M.; James, S.L. Labile co-ordination dendrimers. *Chem. Commun.* **2002**, 78–79.
- Rais, D.; Yau, J.; Mingos, D.M.P.; Vilar, R.; White, A.J.P.; Williams, D.J. Anion-templated syntheses of rhombohedral silver-alkynyl cage compounds. *Angew. Chem., Int. Ed.* **2001**, *40* (18), 3464–3467.
- Fujita, M. Metal-directed self-assembly of two- and three-dimensional synthetic receptors. *Chem. Soc. Rev.* **1998**, *27* (6), 417–425.

23. Fujita, M.; Nagao, S.; Ogura, K. Guest-induced organization of a three-dimensional palladium(II) cage-like complex. A prototype for "induced-fit" molecular recognition. *J. Am. Chem. Soc.* **1995**, *117* (5), 1649–1650.
24. Aoyagi, M.; Biradha, K.; Fujita, M. Quantitative formation of coordination nanotubes templated by rodlike guests. *J. Am. Chem. Soc.* **1999**, *121* (32), 7457–7458.
25. Vilar, R.; Mingos, D.M.P.; White, A.J.P.; Williams, D.J. Anion control in the self-assembly of a cage coordination complex. *Angew. Chem., Int. Ed.* **1998**, *37* (9), 1258–1261.
26. Vilar, R.; Mingos, D.M.P.; White, A.J.P.; Williams, D.J. Aufbau synthesis of a mixed-metal anion receptor cage. *Chem. Commun.* **1999**, 229–230.
27. Sessler, J.L.; Mody, T.D.; Lynch, V. Synthesis and x-ray characterization of a unranyl(VI) Schiff base complex derived from 2:2 condensation product of 3,4-diethylpyrrole-2,5-dicarbaldehyde and 1,2-diamino-4,5-dimethoxybenzene. *Inorg. Chem.* **1992**, *31* (4), 529–531.
28. Alcalde, E.; Ramos, S.; Pérez-García, L. Anion template-directed synthesis of dicationic [1<sub>4</sub>]imidazoliophanes. *Org. Lett.* **1999**, *1* (7), 1035–1038.
29. Kim, Y.H.; Calabrese, J.; McEwen, C. CaCl<sub>2</sub> or Ca<sub>2</sub>Cl<sub>4</sub> complexing cyclic aromatic amide. Template effect on cyclization. *J. Am. Chem. Soc.* **1996**, *118* (6), 1545–1546.
30. Fyfe, M.C.T.; Glink, P.T.; Menzer, S.; Stoddart, J.F.; White, A.J.P.; Williams, D.J. Anion-assisted self-assembly. *Angew. Chem., Int. Ed. Engl.* **1997**, *36* (19), 2068–2070.
31. Wisner, J.A.; Beer, P.D.; Drew, M.G.B. A demonstration of anion templation and selectivity in pseudorotaxane formation. *Angew. Chem., Int. Ed.* **2001**, *40* (19), 3606–3609.
32. Reuter, C.; Wienand, W.; Hübner, G.M.; Seel, C.; Vögtle, F. High-yield synthesis of ester, carbonate, and acetal rotaxanes by anion template assistance and their hydrolytic dethreading. *Chem. Eur. J.* **1999**, *5* (9), 2692–2697.
33. Sánchez-Quesada, J.; Seel, C.; Prados, P.; de Mendoza, J. Anion helicates: Double strand helical self-assembly of chiral bicyclic guanidinium dimers and tetramers around sulfate templates. *J. Am. Chem. Soc.* **1996**, *118* (1), 277–278.
34. Keegan, J.; Kruger, P.E.; Nieuwenhuyzen, M.; O'Brien, J.; Martin, N. Anion directed assembly of a dinuclear double helicate. *Chem. Commun.* **2001**, 2192–2193.



# Annulenes

Michael J. Marsella

University of California, Riverside, California, U.S.A.

A

## INTRODUCTION

The  $[n]$ annulenes may be defined as cyclic polyalkenes possessing a closed circuit of  $n$   $\pi$ -conjugated  $p_z$ -orbitals. The first three small annulenes are shown in Fig. 1 and include [4]annulene (cyclobutadiene), [6]annulene (benzene), and [8]annulene (cyclooctatetraene). The bracketed number,  $n$ , can be classified as either a  $4n+2$  (Hückel aromatic/Möbous antiaromatic) or  $4n$  (Hückel antiaromatic/Möbius aromatic) delocalized  $\pi$ -electron species. That said, it is not surprising that the concept of aromaticity<sup>[1]</sup> is closely associated with the annulenes. Indeed, the first three annulenes listed cover the concepts of Hückel aromatic, antiaromatic, and nonaromatic properties (see Fig. 1).

Given that the annulene literature is vast and has already been covered within many excellent reviews,<sup>[2,3]</sup> this work is not intended to be comprehensive. Instead, this review will reflect a sampling of current annulene chemistry, focusing on representative aspects of [4]-, [6]-, [8]-, [12]-, [14]-, [16]-, and [18]annulenes.

## DEFINITIONS AND ACRONYMS

For convenience, definitions of key terms and acronyms used in this review are provided below:

**ACID (Anisotropy of the Current-Induced Density):** A theoretical method for visualizing, as an isosurface, delocalization of electrons in molecules.

**$[n]$ Annulene:** A cyclic polyalkene possessing a closed circuit of  $n$   $\pi$ -conjugated  $p_z$ -orbitals.

**Antiaromaticity:** A property associated with  $[n]$ annulenes possessing either  $4n$  electrons (Hückel) or  $4n+2$  electrons (Möbius), such that the acyclic homologue is more stable than the cycle. A paratropic compound.

**Aromaticity:** A property associated with  $[n]$ annulenes possessing either a  $4n+2$  (Hückel) or  $4n$  (Möbius) number of delocalized  $\pi$ -electrons capable of sustaining a ring current.<sup>[1]</sup>

**Hückel aromaticity:** An aromatic annulene composed of a continuous circuit of  $p_z$ -orbitals oriented along the same axis (or plane) and possessing  $4n+2$  electrons.

**Möbius Aromaticity:** An aromatic annulene composed of a continuous array of  $p_z$ -orbitals containing a  $4n$

number of  $\pi$ -electrons, arranged such that an (ideal)  $180^\circ$  twist occurs within the orbital circuit.

**BLE (Bond Localization Energy):** The energy necessary to localize a common bond between two cyclic  $\pi$ -systems. See the work of Mitchell, cited herein.<sup>[4,5]</sup>

**Diatropic ring current ( $^1\text{H-NMR}$ ):** An induced ring current within the annulene  $\pi$ -circuit that opposes the applied magnetic field, resulting in a downfield shift of protons on the outside of an aromatic annulene.

**Frost's circle:** A simple, geometrical approach to approximating the HMO energy levels for planar annulenes. The lowest energy MO has an HMO energy of  $\alpha+2\beta$ .

**HMO theory (Hückel Molecular Orbital theory):** A simple molecular orbital theory applied to planar  $\pi$ -conjugated systems. A key simplification involves treatment of the  $\pi$ -system independently from the  $\sigma$ -system. The HMO molecular orbital energies are in terms of  $\alpha$  and  $\beta$ , where  $\alpha$  is equated with the energy of an isolated  $p_z$  orbital, and  $\beta$  is the resonance integral, equated to the energy associated with having electrons shared by atoms. As reference, benzene is  $4\beta$  more stable than an isolated  $p_z$  orbital.

**Homoaromaticity:** Cyclic conjugation of a  $\pi$ -system that bypasses one (or more) saturated atoms.

**NICS (Nucleus-Independent Chemical Shifts):** A theoretical method for determining the ring current at the center (or any position in space) of an annulene or other delocalized system.

**Paratropic ring current ( $^1\text{H-NMR}$ ):** An induced ring current within the annulene  $\pi$ -circuit that aligns with the applied magnetic field, resulting in an upfield shift of affected protons.

## [4]ANNULENES

The instability of [4]annulene (a neutral  $4n$   $\pi$ -electron annulene) can be gleaned from either Frost's Circle<sup>[6]</sup> or HMO theory.<sup>[7]</sup> As shown in Fig. 2, the former predicts an open-shell triplet, implicating instability. The latter reports no gain in energy ( $0\beta$ ) relative to its acyclic analogue, butadiene. Experimental evidence shows that cyclobutadiene is, in fact, a closed shell species, with alternate single and double bonds. Regardless, as predicted, [4]annulene proved to be an unstable compound.

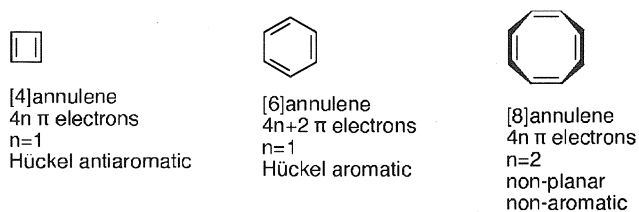


**Fig. 1** Depicting the first three simple  $[n]$ annulenes along with their  $\pi$ -electron count and Hückel aromatic/antiaromatic/non-aromatic classification.

[4]annulene:  
cyclobutadiene

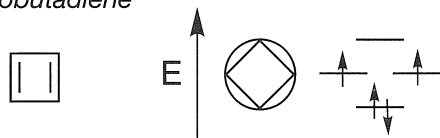
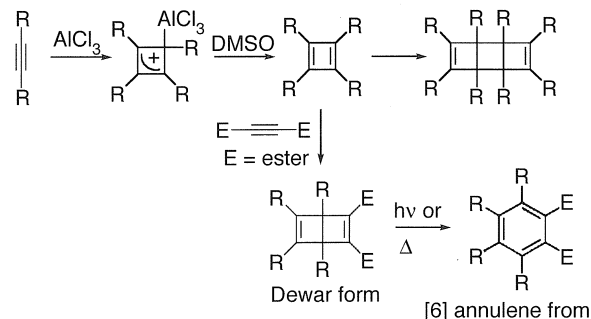


**Fig. 2** Frost's circle applied to [4]annulene.

Harnessing the reactivity of [4]annulenes has allowed for their controlled use in  $[4\pi_s + 2\pi_s]$  cycloaddition reactions, playing the role of diene, dienophile, or both.<sup>[8–11]</sup> Transient tetraalkylcyclobutadienes can be readily prepared via DMF-promoted decomposition of the corresponding tetraalkylcyclobutadiene-aluminum trichloride complex. The complex is stable and can be readily prepared by reaction of aluminum trichloride with a dialkylacetylene. In the absence of a good dienophile, the reactive tetraalkylcyclobutadienes undergo dimerization to yield 1,2,3,4,5,6,7,8-octaalkyl-tricyclo[4.2.0.0<sup>0,0</sup>]octa-3,7-dienes (Scheme 1). In the presence of a good dienophile, such as acetylenedicarboxylic acid or its corresponding esters, the Diels–Alder adduct can be isolated in high yield.<sup>[10,11]</sup> It is noteworthy to mention that the product of this  $[4\pi + 2\pi]$  reaction is a substituted Dewar benzene, itself a high-energy isomer of [6]annulene. Thus, from a synthetic standpoint, a substituted [4]annulene can be converted to its isomeric [6]annulene via two pericyclic reactions: a thermal  $[4\pi_s + 2\pi_s]$  followed by a pho-



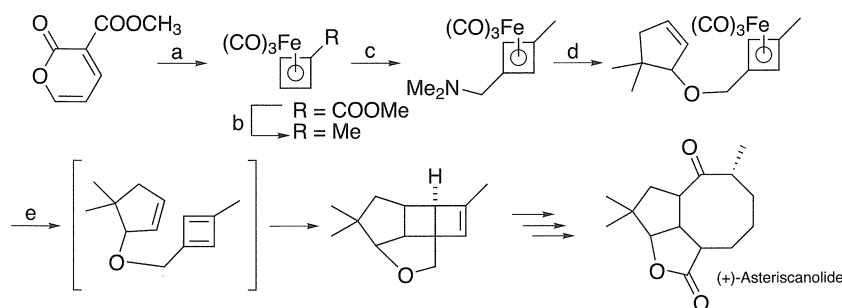
**Scheme 1** Synthesis of a [6]annulene via its Dewar benzene isomer. The Dewar form is prepared via a  $[4\pi + 2\pi]$  cycloaddition with [4]annulene and a substituted acetylene.

tochemical  $4\pi$  electrocyclic ring opening (Scheme 1). Due to this fact, Dewar benzene was proposed as a supramolecular protecting group for aromatic rings, preventing aryl–aryl stacking interactions from biasing solid-state properties.<sup>[11]</sup>

An elegant use of [4]annulene chemistry utilizes the stable tricarbonylcyclobutadiene iron complex as a protected cyclobutadiene.<sup>[8,9]</sup> One advantage over the aluminum cyclobutadiene complex is the ability of the tricarbonylcyclobutadiene iron complex to be amenable to synthetic modifications of the four-membered ring. Typically, ceric ammonium nitrate (CAN; or other oxidants) may be used to oxidize the iron and liberate free cyclobutadiene. An example of this methodology is shown in Scheme 2, as applied to the synthesis of (+)-asteriscanolide. Further examples of reactions utilizing this chemistry are shown in Table 1.

## [6]ANNULENES

Benzene embodies aromaticity and is the standard by which the property of aromaticity is measured. Given that fact, it is worthwhile to provide an overview of recent techniques that attempt to quantify the property of aromaticity.



**Scheme 2** (a)  $h\nu$ ,  $C_6H_6$ ;  $Fe_2(CO)_9$ ,  $50^\circ C$  (64%); (b) LAH,  $BF_3 \cdot OEt_2$  (93%); (c)  $Me_2NCH_2NMe_2$ ,  $H_3PO_4$ ,  $CH_3CO_2H$ ,  $100^\circ C$  (67%); (d) MeI, THF; NaH, 5,5-dimethyl-cyclopent-2-enol, THF/DMF (50%); and (e)  $Me_3NO$ , acetone,  $56^\circ C$  (63%).

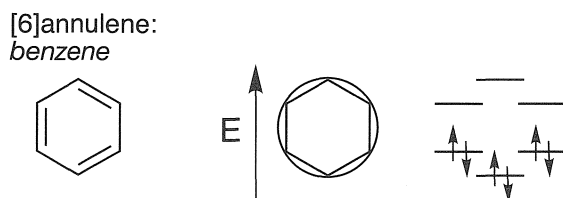
**Table 1** Showing substrate and cycloadduct product from the intramolecular  $[4\pi+2\pi]$  cycloaddition involving the  $[4]$ annulene moiety

Substrate	Cycloadduct	Substrate	Cycloadduct

From a theoretical standpoint, simple analysis via Frost's circle yields a closed-shell system, implying stability (compare to cyclobutadiene) (Fig. 3). The HMO theory renders benzene ca. 1  $\beta$  more stable than its acyclic analogue, hexatriene. Although these pen and paper methods cannot compare to modern computational methods presently available for a desktop computer, they are elegant in their simplicity and qualitative predictive power. However, given the interest in quantifying some measure of aromaticity (or antiaromaticity) among different annulenes,<sup>a</sup> much higher levels of theory are desired and have been developed. Recently, two new techniques were reported that integrate the power of *ab initio* calculations with simple protocols that are generally applicable to a wide variety of annulenes and related compounds. Both methods can take advantage of the popular Gaussian<sup>[12]</sup> suite of computational chemistry programs. Given their generality, availability, and ease of setup, they were highlighted in brief below.

### NICS

Proton chemical shifts of annulenes have long been utilized as probes of ring currents.<sup>[13]</sup> For example, protons outside and inside of an aromatic annulene will

**Fig. 3** Frost's circle applied to  $[6]$ annulene.

shift downfield and upfield, respectively, as a function of the induced ring current. In general, those protons at (or above) the annulene center experience a greater magnitude of shift than those outside the annulene ring. One synthetic/experimental limitation of this "internal probe" technique is the ability to place an NMR active nucleus at a ring center. A theoretical technique designed to overcome this problem places a ghost atom at the ring center (or any position in space). Absolute magnetic shieldings can then be calculated using available computational chemistry programs. This facile technique, known as Nucleus-Independent Chemical Shifts (NICS), is established as an effective aromaticity criterion. Some values are given in Table 2 (note that negative NICS values denote aromaticity, and positive NICS values denote antiaromaticity).

### ACID

The ACID method (anisotropy of the current-induced density) provides a method to visualize, as an isosurface, delocalization of electrons in molecules.<sup>[14-16]</sup> One major advantage of this method is its invariance with respect to the relative orientation between molecule and magnetic

**Table 2** Nics values for several aromatic and antiaromatic species

Annulene	Point group	NICS ( $6-31+G^*$ )
Benzene	$D_{6h}$	-9.7
[8]Annulene dianion	$D_{8h}$	-13.9
[4]Annulene	$D_{2h}$	+27.6
Naphthalene	$D_{2h}$	-9.9

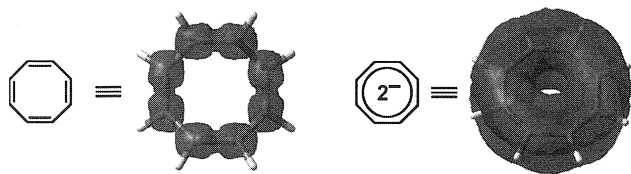


**Fig. 4** ACID surface mapped onto the localized, tub conformer of [8]annulene (left), and the planar, delocalized [8]annulene dianion (right). Discontinuous surfaces imply no delocalization at those corresponding points in space (with respect to the selected isosurface value; here set at 0.05). (View this art in color at [www.dekker.com](http://www.dekker.com).)

field. Furthermore, it is not a simple function of the electron density, and it utilizes the same symmetry as the wave function. In the proverbial sense that “one picture is worth a thousand words,” the ACID technique is best summarized by direct visualization of such an isosurface. As such, illustrated in Fig. 4 is an ACID isosurface mapped onto both the (localized) tub conformer and (delocalized) planar conformer of [8]annulene and its aromatic dianion, respectively.

In addition to the classical [6]annulene, benzene, neutral in-plane trishomoaromatic “benzene” frameworks (such as that depicted in Fig. 5) were also studied.<sup>[17]</sup> Although not yet synthesized, these compounds were collectively studied using a variety of computational techniques. Unique from benzene, the six over-

lapping *p*-orbitals lie in-plane (as opposed to orthogonal). Given that this arrangement constitutes a closed circuit of  $4n+2$   $\pi$ -electrons, the system, according to the definition provided herein, constitutes a (homo-) [6]annulene. Within the reported series, a maximum NICS value of  $-30.1$  ppm was found at the ring center. Ultimately, it was determined that such in-plane annulenes may possess more than one third the aromatic stabilization energy of benzene, thus constituting the best candidates yet proposed for a neutral *trishomoaromatic* compound.

## [8]ANNULENES

[8]Annulene is a  $4n$   $\pi$ -electron system, and thus, the (neutral) planar form would be expected to exhibit antiaromatic behavior. Indeed, Frost’s circle analysis predicts an open-shell species (as with [4]annulene; see Figs. 2 and 6). Extensive studies of cyclooctatetraene were performed,<sup>[18,19]</sup> and it was established that the neutral state avoids the problem of antiaromaticity by adopting a tub conformation. Both the anion and dianion are known to exist in a planar conformation, the latter being aromatic.<sup>[19]</sup> This fact is also predicted by simple analysis of the [8]annulene dianion by Frost’s circle (see Fig. 6). It is predicted that the planar [8]annulene dianion is a closed-shell system.

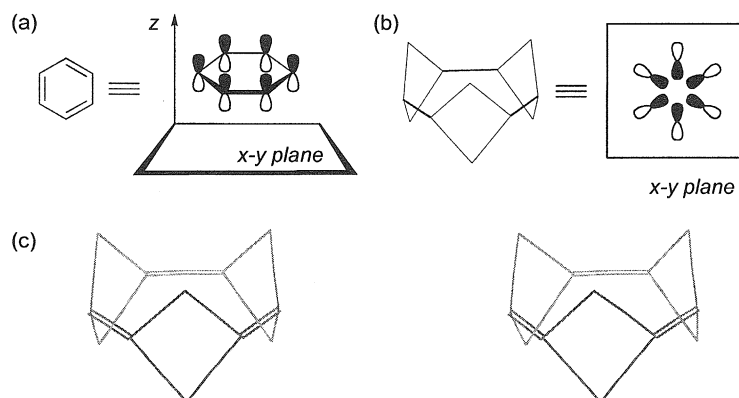


**Fig. 5** (a) Benzene *p*-orbitals are orthogonal to the *x-y* plane. (b) In an in-plane benzene, six *p*-orbitals lie in-plane. (c) Stereoview (cross-eye) of an in-plane benzene skeleton.

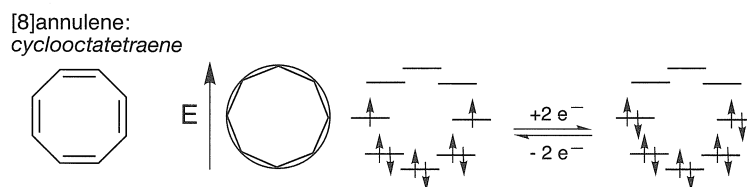


**Fig. 6** Frost’s circle applied to [8]annulene and its dianion.

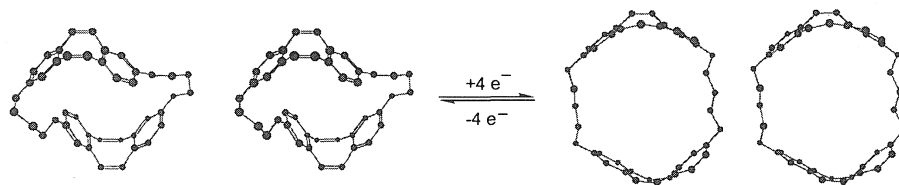


**Fig. 7** Stereoviews (cross-eye) of a shape-changing cyclophane composed of two [8]annulene moieties. The stereoviews were modeled at the PM3 level of theory and optimized only for illustrative purposes (structures may not correspond to true global minima).

At the *ab initio* level of theory, a NICS calculation of the dianion yields an (aromatic) value of  $-13.9^{[13]}$  (see Table 2), and ACID<sup>[14]</sup> clearly illustrates the corresponding shift from the localized neutral tub conformer to the delocalized planar dianion (see Fig. 4).

The redox-induced conformational change associated with [8]annulene was utilized as the key element in the design of shape-changing molecules. A shape-changing cyclophane was reported,<sup>[20]</sup> likely capable of functioning as a redox-triggered two-state host (Fig. 7). In an analogous manner, a polymer composed of tetra[2,3-thienylene] monomers (a thiophene-fused [8]annulene) was also reported,<sup>[21–23]</sup> a design intended to translate additive tub-to-planar conformational changes into an overall perturbation of polymer chain length (i.e., a polymeric electromechanical actuator or molecular muscle, see Fig. 8a,b and Table 3). In contrast to the aforementioned conformationally dynamic [8]annulenes, oxidation of the constrained tub conformer of octamethoxytetraphenylene (an *o*-dialkoxybenzene-fused [8]annulene), yields electrochromic switching via redox-triggered reversible carbon–carbon bond formation (Fig. 8c).<sup>[24]</sup>

Tetra[2,3-thienylene] was also utilized as a rigid unit, a double-helical scaffold.<sup>[25]</sup> Specifically, a racemic mix-

ture of the corresponding octaaryl double helix, shown in Fig. 9, crystallizes to yield homochiral, supramolecular polymer chains extending in the direction of the long crystal axis. Edge-to-face stacking of neighboring (intermolecular) terminal phenyl groups dominated the homochiral supramolecular assembly (Fig. 9). Similarly, tetraphenylene was also used as a scaffold for the synthesis of octaaryl double-helical monomers (Fig. 10).<sup>[26]</sup>

### MöBIUS [4*n*]ANNULENES: [12]-, [16]-, AND [20]ANNULENE

Although the concept of Möbius aromaticity was put forth in 1964,<sup>[27]</sup> no neutral [4*n*]annulene exhibiting a Möbius strip conformation (Fig. 11) and Möbius aromatic character has yet been prepared. It was originally predicted that all [4*n*]annulenes  $\geq$  [20]annulene should be capable of accommodating a Möbius strip conformation with minimal strain. Recent theoretical studies revealed that the [4*n*]annulenes, [12]-, [16]-, and [20]annulene, exhibit Möbius conformers (local minima) and corresponding aromatic character (NICS values of  $-14.6$ ,  $-15.6$ , and  $-10.2$  ppm at ring center, respectively), although the lowest-energy conformers (global minima), in all cases, are of Hückel topology.<sup>[28]</sup> Clearly, control of conformation via the targeted synthetic design of a [4*n*]annulene

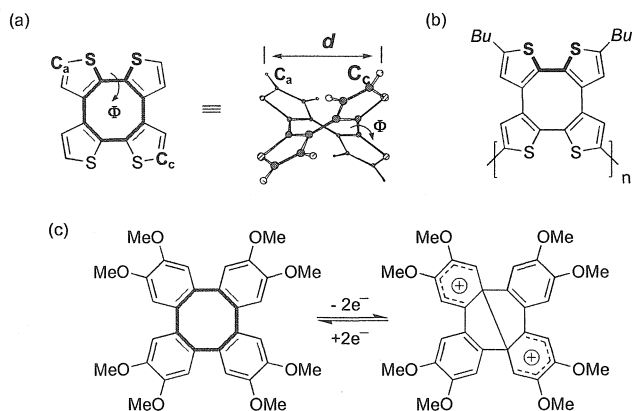


**Fig. 8** (a) Depicting tetra(2,3-thienylene) and corresponding descriptors,  $\Phi$  and  $d$  (see Table 3). (b) Poly(tetra[2,3-thienylene]), a putative molecular muscle. (c) Depicting redox-induced reversible carbon–carbon bond formation in octamethoxytetraphenylene.

**Table 3** Reporting the redox-induced perturbation of S–C–C–S dihedral angle,  $\Phi$ , and corresponding dimensional change,  $d$  (see Fig. 8a)

Compound	Charge	$\Phi$ (deg)	$d$ (Å)	$\Delta d$ (%)
Monomer	0	49.5	6.87	—
Monomer	1+	34.8	7.27	5.69
Dimer	0	48.9	6.90	—
Dimer	1+	38.6	7.14	3.54
Dimer	2+	31.4	7.33	5.92

Charges were determined via electrochemical analysis of tetra(2,3-thienylene) monomer and dimer, and conformer data was calculated at the B3LYP/6-31G(*d,p*) level of theory.

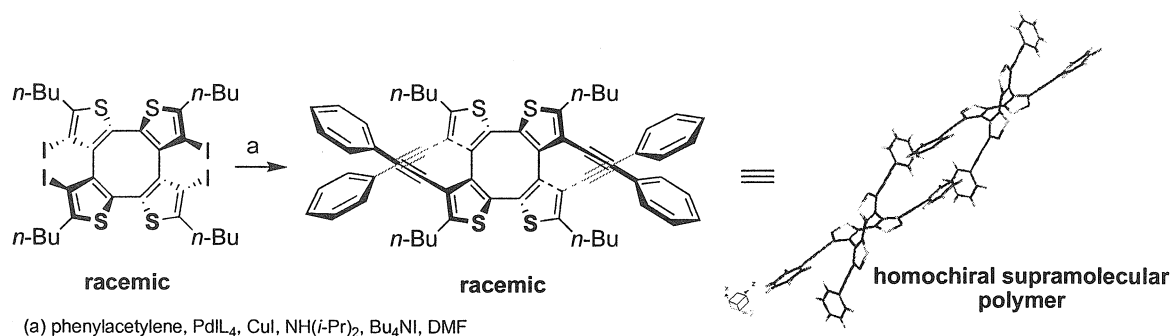


**Fig. 9** Synthesis of a racemic octaaryl double helix utilizing tetra[2,3-thienylene] as a core. Supramolecular self-assembly of the racemic mixture yields homochiral supramolecular polymers (dimer repeat shown).

with true Möbius topology will be required to provide supporting experimental data to this study.

#### [14]ANNULENE: DIHYDROPYRENE VALENCE TAUTOMERISM AND APPLICATIONS DERIVED THEREFROM

The [14]annulene, dimethyldihydropyrene (DHP), exhibits rich chemistry that was reviewed elsewhere in detail.<sup>[2,29]</sup> A key reaction of this annulene is the symmetry-allowed photochemical transformation between the closed [14]annulene form, and the open metacyclopentadiene form (CPD; see Scheme 3a). The transition between colorless and colored forms, the perturbations in conjugation pathways, and the <sup>1</sup>H-NMR shift associated with the two methyl groups poised near the ring center (thus, reporting changes in ring currents) made DHP an excellent scaffold from which to design photochromic switches and other  $\pi$ -functional molecules.

The current state-of-the-art DHP photochromic switch is capable of accessing three unique states (CPD–CPD, CPD–DHP, and DHP–DHP; see Scheme I3b).<sup>[29,30]</sup> This multistate photochromic switch was prepared by fusion of two benzo[*e*]dimethyldihydropyrene moieties. The states can be optically read and written, although the DHP–DHP

state rapidly converts back to the CPD–DHP state via a thermal (symmetry forbidden) process.

The DHP to CPD interconversion also perturbs conjugation pathways around the perimeter of the molecule. This fact was capitalized upon to yield an optoelectronic redox switch (Scheme 3c).<sup>[31]</sup> Specifically, the 16- $\pi$  linear circuit extending from thiophene A through DHP to thiophene B is interrupted upon conversion to Th-CPD-Th. This process is reversible, and only the DHP form exhibits anodic activity within a window of 0.0–0.75 V. Thus, the state of the photochromic switch can be written photochemically and read electrochemically (the CPD form is redox silent, and the DHP form is redox active).

In addition to functioning as a switch, DHP also serves as a tool with which to probe aromatic character by NMR (via monitoring the “reporter” methyl groups).<sup>[4]</sup> It was shown that the BLE of any aromatic annulene benzannulated onto DHP (i.e., [*n*]annulene, shown in Fig. 3d) can be determined by the following equation:

$$\text{BLE} = [4.18 + \delta(\text{Ar})]/2.59$$

where  $\delta(\text{Ar})$  is the average chemical shift of the internal methyl groups.

This equation is true due to the sensitivity of the methyl groups to the ring current of the DHP skeleton, as well as to the fact that annulated DHPs can be dissected into two  $\pi$ -circuits (i.e., red and blue according to Scheme 3d). The

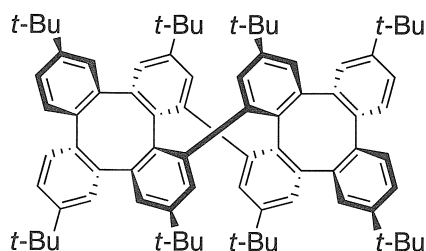


**Fig. 10** An octaaryl double helix formed from the fusion of two tetraphenylene units.

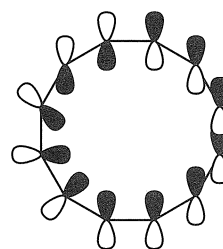
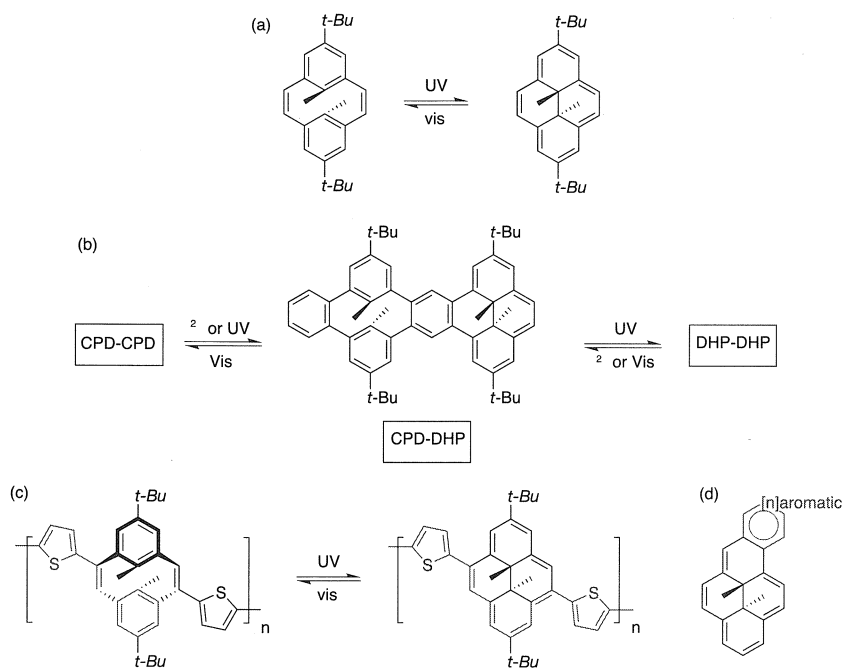


**Fig. 11** A conceptual illustration of 12  $p_z$  orbitals arranged in a Möbius strip conformation.



**Scheme 3** (a) The DHP-CPD photochemical interconversion; (b) a DHP-based three-way switch; (c) a thiophene-DHP copolymer capable of attenuating effective conjugation length via the DHP-CPD photochemical interconversion; and (d) the two  $\pi$ -circuits in a benzannulated-DHP: blue corresponds to the DHP skeleton, and red corresponds to a benzannulated aromatic. (View this art in color at [www.dekker.com](http://www.dekker.com).)

larger the resonance energy in the red fragment, the less delocalization in the blue circuit (i.e., DHP), hence, the smaller the diatropic shift of the methyl groups. Of course, one drawback of this method is that it requires covalent attachment between the DHP “probe” and the aromatic  $[n]$ annulene to be studied.

### [16]- AND [18]ANNULENE

The [16]-annulene and [18]annulene are the smallest annulenes (antiaromatic and aromatic, respectively), possessing internal protons to be thermodynamically stable at room temperature (Fig. 12). Not surprisingly,

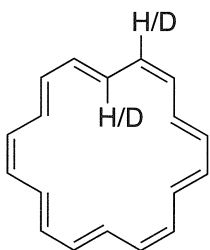


**Fig. 12** [18]Annulene, emphasizing internal versus external H/D environments.

steric interactions between internal protons affect the conformer distribution of these systems. Perdeuterated [16]- and [18]annulenes were synthesized in an effort to attenuate these internal sterics, given that C–D bonds are shorter than C–H bonds.<sup>[32]</sup> The results demonstrated increased ring currents in both of the perdeuterated annulenes, as determined by  $^1\text{H}$ -NMR analysis (paratropic and diatropic, respectively). It is proposed that the shorter C–D versus C–H bond reduces internal sterics, allowing the  $\sigma$ -framework of the annulenes to achieve near ideal ( $120^\circ$ ) C–C=C bond angles, and thus increasing the enforcement of  $\pi$ -delocalization. It should be emphasized that achieving near ideal bond angles was determined to be more important than achieving complete planarity (i.e., all internal H/D atoms in the same plane).

### CONCLUSION

Selected examples of recent properties and applications of  $[n]$ annulenes ( $n=4, 6, 8, 12, 14, 16$ , and  $18$ ) were presented. Despite years of investigation, it is apparent that these cyclic  $\pi$ -systems possess intrinsic properties that remain relevant to even the most “modern” of applications (for example, molecular devices). Furthermore, some interesting properties of as-yet unprepared



annulenes were predicted from accurate levels of ab initio theory. When coupling these facts and recognizing that the area of annulene chemistry extends far beyond this review, it is clear that interest in these systems will remain keen for many years to come.

## ARTICLES OF FURTHER INTEREST

*Calixarenes: Synthesis and Historical Perspectives*, p. 153

*Cation- $\pi$  Interactions*, p. 214

*Chemical Topology*, p. 229

*Cyclophanes: Definition and Scope*, p. 414

*Molecular Switches*, p. 917

*Molecular Wires*, p. 925

*Nuclear Magnetic Resonance Spectroscopy*, p. 981

*$\pi$ - $\pi$  Interactions: Theory and Scope*, p. 1076

*Spherands*, p. 1344

*Supramolecular Photochemistry*, p. 1434

## REFERENCES

1. Aromaticity, C. Aromaticity. *Chem. Rev.* **2001**, *101*, 1115–1566.
2. Garratt, P.J. *Aromaticity*; John Wiley and Sons: New York, 1986.
3. Kennedy, R.D.; Lloyd, D.; McNab, H. Annulenes, 1980–2000. *J. Chem. Soc., Perkin Trans. 1* **2002**, 1601–1621.
4. Mitchell, R.H.; Iyer, V.S.; Khalifa, N.; Mahadevan, R.; Venugopalan, S.; Weerawarna, S.A.; Zhou, P.Z. An experimental estimation of aromaticity relative to that of benzene: The synthesis and NMR properties of a series of highly annelated dimethyldihydropyrenes—Bridged benzannulenes. *J. Am. Chem. Soc.* **1995**, *117*, 1514–1532.
5. Mitchell, R.H.; Iyer, V.S.; Khalifa, N.; Mahadevan, R.; Venugopalan, S.; Weerawarna, S.A.; Zhou, P.Z. An experimental estimation of aromaticity relative to that of benzene—The synthesis and NMR properties of a series of highly annelated dimethyldihydropyrenes—Bridged benzannulenes. *J. Am. Chem. Soc.* **1995**, *117*, 1514.
6. Frost, A.A.; Musulin, B.J. Mnemonic device for molecular-orbital energies. *Chem. Phys.* **1953**, *21*, 572.
7. Yates, K. *Hückel Molecular Orbital Theory*; Academic Press, Inc.: Orlando, 1978.
8. Limanto, J.; Tallarico, J.A.; Porter, J.R.; Khuong, K.S.; Houk, K.N.; Snapper, M.L. Intramolecular cycloadditions of cyclobutadiene with olefins. *J. Am. Chem. Soc.* **2002**, *124*, 14748–14758.
9. Limanto, J.; Snapper, M.L. Sequential intramolecular cyclobutadiene cycloaddition, ring-opening metathesis, and cope rearrangement: Total syntheses of (+)- and (–)-asteriscanolide. *J. Am. Chem. Soc.* **2000**, *122*, 8071–8072.
10. Koster, J.B.; Timmermans, G.J.; van Bekkum, H. Reaction of the tetramethylcyclobutadiene-aluminum chloride complex with dienophilic esters. *Synthesis* **1971**, 139.
11. Marsella, M.J.; Meyer, M.M.; Tham, F.S. Dewar benzene as a protecting group? Demonstration of photolithographic crystallization. *Org. Lett.* **2001**, *V3*, 3847–3849.
12. Gaussian; Frisch, M.J.; Trucks, G.W.; Schlegel, H.B.; Scuseria, G.E.; Robb, M.A.; Cheeseman, J.R.; Montgomery, J.A., Jr.; Vreven, T.; Kudin, K.N.; Burant, J.C.; Millam, J.M.; Iyengar, S.S.; Tomasi, J.; Barone, V.; Mennucci, B.; Cossi, M.; Scalmani, G.; Rega, N.; Petersson, G.A.; Nakatsuji, H.; Hada, M.; Ehara, M.; Toyota, K.; Fukuda, R.; Hasegawa, J.; Ishida, M.; Nakajima, T.; Honda, Y.; Kitao, O.; Nakai, H.; Klene, M.; Li, X.; Knox, J.E.; Hratchian, H.P.; Cross, J.B.; Adamo, C.; Jaramillo, J.; Gomperts, R.; Stratmann, R.E.; Yazyev, O.; Austin, A.J.; Cammi, R.; Pomelli, C.; Ochterski, J.W.; Ayala, P.Y.; Morokuma, K.; Voth, G.A.; Salvador, P.; Dannenberg, J.J.; Zakrzewski, V.G.; Dapprich, S.; Daniels, A.D.; Strain, M.C.; Farkas, O.; Malick, D.K.; Rabuck, A.D.; Raghavachari, K.; Foresman, J.B.; Ortiz, J.V.; Cui, Q.; Baboul, A.G.; Clifford, S.; Cioslowski, J.; Stefanov, B.B.; Liu, G.; Liashenko, A.; Piskorz, P.; Komaromi, I.; Martin, R.L.; Fox, D.J.; Keith, T.; Al-Laham, M.A.; Peng, C.Y.; Nanayakkara, A.; Challacombe, M.; Gill, P.M.W.; Johnson, B.; Chen, W.; Wong, M.W.; Gonzalez, C.; Pople, J.A. Gaussian, Inc.: Pittsburgh, PA, 2003.
13. Schleyer, P.V.; Maerker, C.; Dransfeld, A.; Jiao, H.J.; Hommes, N. Nucleus-independent chemical shifts—A simple and efficient aromaticity probe. *J. Am. Chem. Soc.* **1996**, *V118*, 6317–6318.
14. Herges, R.; Geuenich, D. Delocalization of electrons in molecules. *J. Phys. Chem.* **2001**, *105*, 3214–3220.
15. Herges, R.; Papafilippopoulos, A. Homoaromaticity in *tris*(ethylene)nickel(0) and *tris*(ethyne)nickel(0). *Angew. Chem., Int. Ed.* **2001**, *40*, 4671.
16. Kimball, D.B.; Herges, R.; Haley, M.M. Two unusual, competitive mechanisms for (2-ethynylphenyl)triazene cyclization: Pseudocoarctate versus pericyclic reactivity. *J. Am. Chem. Soc.* **2002**, *124*, 1572–1573.
17. Stahl, F.; Schleyer, P.V.; Jiao, H.J.; Schaefer, H.F.; Chen, K.H.; Allinger, N.L. Resurrection of neutral *tris*-homoaromaticity [Review]. *J. Org. Chem.* **2002**, *67*, 6599–6611.
18. Paquette, L.A. Cyclooctatetraenes: Conformational and  $\pi$ -electronic dynamics within polyolefinic [8]annulene frameworks. *Adv. Theor. Interest. Mol.* **1992**, *2*, 1–77.
19. Strauss, H.L.; Katz, T.J.; Fraenkel, G.K. Electron spin resonance studies of the cyclooctatetraenyl anions. *J. Am. Chem. Soc.* **1963**, *85*, 2360–2364.
20. Heinz, W.; Räder, H.-J.; Müllen, K. Changing the size of a cavity via an electron-transfer: Synthesis and reduction of 1, 5, 22, 26-tetraoxa-[5,5]-(2,8)-dibenzo[*a,e*]-cyclooctatetraeneophane. *Tetrahedron Lett.* **1989**, *30*, 159–162.
21. Marsella, M.J.; Piao, G.Z.; Tham, F.S. Expanding

- tetra[2,3-thienylene]-based molecular muscles to larger [4*n*]annulenes. *Synthesis* **2002**, 1133–1135.
22. Marsella, M.J.; Reid, R.J. Toward molecular muscles: Design and synthesis of an electrically conducting poly[cyclooctatetrathiophene]. *Macromolecules* **1999**, *32*, 5982–5984.
23. Marsella, M.J.; Reid, R.J.; Estassi, S.; Wang, L.S. Tetra[2,3-thienylene]: A building block for single-molecule electromechanical actuators. *J. Am. Chem. Soc.* **2002**, *124*, 12507–12510.
24. Rathore, R.; Le Magueres, P.; Lindeman, S.V.; Kochi, J.K. A redox-controlled molecular switch based on the reversible C–C bond formation in octamethoxytetraphenylene. *Angew. Chem., Int. Ed.* **2000**, *39*, 809–812. 663.
25. Marsella, M.J.; Kim, I.T.; Tham, F. Toward double helical ladder polymers: Cyclooctatetrathiophene as a highly versatile double helical scaffold. *J. Am. Chem. Soc.* **2000**, *122*, 974–975.
26. Rajca, A.; Safronov, A.; Rajca, S.; Shoemaker, R. Double helical octaphenylene. *Angew. Chem., Int. Ed. Engl.* **1997**, *36*, 489–491.
27. Heilbronner, E. Hückel molecular orbitals of Möbius-type conformations of annulenes. *Tetrahedron Lett.* **1964**, 1923.
28. Castro, C.; Isborn, C.M.; Karney, W.L.; Mauksch, M.; Schleyer, P.V. Aromaticity with a twist: Möbius [4*n*]annulenes. *Org. Lett.* **2002**, *4*, 3431–3434.
29. Mitchell, R.H. The metacyclophanediene-dihydropyrene photochromic  $\pi$  switch. *Eur. J. Org. Chem.* **1999**, 2695–2703.
30. Mitchell, R.H.; Ward, T.R.; Wang, Y.X.; Dibble, P.W.  $\pi$ -Switches: Synthesis of three-way molecular switches based on the dimethyldihydropyrene-metacyclophanediene valence isomerization. *J. Am. Chem. Soc.* **1999**, *121*, 2601–2602.
31. Marsella, M.J.; Wang, Z.Q.; Mitchell, R.H. Backbone photochromic polymers containing the dimethyldihydropyrene moiety: Toward optoelectronic switches. *Org. Lett.* **2000**, *2*, 2979.
32. Stevenson, C.D.; Kurth, T.L. Isotopic perturbations in aromatic character and new closely related conformers found in [16]- and [18]annulene. *J. Am. Chem. Soc.* **2000**, *122*, 722–723.

# Anticrowns

Vladimir B. Shur

Irina A. Tikhonova

Russian Academy of Sciences, Moscow, Russia

## INTRODUCTION

Anticrowns are peculiar antipodes of crown ethers and their thia and aza analogues. They contain several Lewis acidic centers in the macrocyclic chain and so are able to efficiently bind various anions and neutral Lewis bases with the formation of unusual complexes, wherein the Lewis basic species is simultaneously bonded to all Lewis acidic atoms of the macrocycle. This remarkable property of anticrowns, being reminiscent of the behavior of conventional crown compounds in metal cation binding, makes them prospective aids in the areas of molecular recognition, ion transport, as well as organic synthesis and catalysis.

The first reports on the anion-binding capacity of anticrowns emerged in the late 1980s–early 1990s. Subsequently, a considerable amount of information on different aspects of the chemistry of these novel reagents was accumulated. Nowadays, data on complexing properties of macrocycles containing two, three, four, and five Lewis acidic centers in the chain were published. Especially impressive results were obtained for polymer-curamacrocycles, which proved to be efficient hosts for binding various anionic and neutral Lewis basic species. Polytin- and polysilicon-containing macrocycles were also studied as anticrowns.

In the present article, host–guest chemistry of anticrowns as well as available data on their applications in catalysis and as ionophores will be briefly reviewed. Strictly speaking, only macrocycles with three and more Lewis acidic centers in the chain can be considered as genuine anticrowns. Nevertheless, the binding properties of some macrocycles containing only two Lewis acidic atoms in the ring will also be discussed.

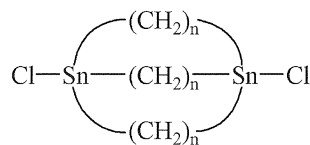
## HOST-GUEST CHEMISTRY OF ANTICROWNS

### Polytin- and Polysilicon-Containing Macrocycles

In 1987, Newcomb et al.<sup>[1]</sup> reported the synthesis of the macrocycles  $[\text{Cl}_2\text{Sn}(\text{CH}_2)_n]_2$  ( $n=8, 10, 12$ ) containing two tin atoms in the macrocyclic chain, and they showed by  $^{119}\text{Sn}$ -NMR method that these macrocycles form com-

plexes with chloride anion in an acetonitrile solution. It was suggested that the anionic species in the resulting complexes is bonded to both tin atoms of the cycle. The most stable adduct was formed from the macrocycle with  $n=8$ .

The interaction of halide anions with a series of macrobicyclic compounds (**1–4**) containing two tin atoms in bridgehead positions was also studied by  $^{119}\text{Sn}$ -NMR.<sup>[2]</sup> It turned out that bicyclic host **1** is able to bind fluoride anion, but it does not react with bulkier chloride, bromide, and iodide ions. By contrast, compounds **2–4** readily coordinate chloride ion but they are unable to bind fluoride anion. According to x-ray diffraction data, the fluoride ion in the complex with **1** is bonded to both tin centers of the Lewis acidic host, whereas the chloride ion in its adduct with **2** is coordinated only to a single tin atom.



**1** ( $n = 6$ ), **2** ( $n = 8$ ), **3** ( $n = 10$ ), **4** ( $n = 12$ )

In 1989, Jurkschat et al.<sup>[3]</sup> described the synthesis of the 12-membered macrocycles  $[\text{R}^1\text{R}^2\text{Sn}(\text{CH}_2)_3]_3$  [ $\text{R}^1=\text{R}^2=\text{Cl}$  (**5**);  $\text{R}^1=\text{Me}$ ,  $\text{R}^2=\text{Cl}$  (**6**)] containing three tin atoms in the macrocyclic chain. According to  $^{119}\text{Sn}$ -NMR spectra, both macrocycles are able to bind successively at first one and then the second chloride ions. The complex of **5** with one chloride ion was isolated from the reaction solution. An x-ray diffraction study of this complex revealed that the anionic species is coordinated here with two Lewis acidic centers of the cycle. For the analogous 1:1 complex of macrocycle **6**, the structure including the simultaneous coordination of  $\text{Cl}^-$  with all three tin atoms of the cycle was proposed.

In a subsequent study, the ability of the 15-membered polytin-containing macrocycle  $[\text{Me}_2\text{Sn}(\text{CH}_2)_4]_3$  to bind chloride and bromide anions as well as to transport them through liquid membrane was demonstrated.<sup>[4]</sup> Similar capacity to transport halide anions ( $\text{Cl}^-$ ,  $\text{Br}^-$ ) through

liquid membranes was previously established for the macrocycle  $[\text{Me}_2\text{Si}(\text{CH}_2)_3]_3$  containing three silicon atoms.<sup>[15]</sup> Recently, the synthesis of the eight-membered macrocycle  $[\text{cyclo-CH}_2\{\text{Sn}(\text{Cl}_2)\text{CH}_2\text{Si}(\text{Me}_2)\}_2\text{O}]$  with two tin and two silicon atoms in the ring was described.<sup>[16]</sup> This macrocycle reacts with chloride, fluoride, and hydroxide ions to form 1:1 complexes, wherein only tin atoms of the cycle are involved in the coordination with the anionic guest.

### Perfluorinated Polymercuramacrocycles

The possibility of using polymercuramacrocycles as anion receptors was demonstrated for the first time in 1989, when it was reported that cyclic trimeric *o*-phenylene-mercury (*o*- $\text{C}_6\text{H}_4\text{Hg}$ )<sub>3</sub> (**7**)<sup>[17]</sup> containing three Hg atoms in a planar nine-membered cycle is capable of binding halide anions ( $\text{Cl}^-$ ,  $\text{Br}^-$ ,  $\text{I}^-$ ) in halomethane solutions.<sup>[18]</sup> However, the resulting complexes could not be isolated here due to, apparently, their insufficient stability. Further progress in mercury anticrown chemistry was achieved when the perfluorinated analogue of **7**, viz. cyclic trimeric perfluoro-*o*-phenylenemercury (*o*- $\text{C}_6\text{F}_4\text{Hg}$ )<sub>3</sub> (**8**)<sup>[9]</sup> was employed as a macrocyclic host.<sup>[10,11]</sup> The presence of fluorine atoms in the aromatic rings of **8** sharply increases the Lewis acidity of the Hg centers and, as a consequence, quite stable and isolable complexes of unusual structures are formed in the interaction of this macrocycle with anions and neutral Lewis bases. Subsequently, one other perfluorinated polymercuramacrocycle,  $[(\text{CF}_3)_2\text{CHg}]_5$  (**9**),<sup>[12]</sup> with five Hg atoms in a planar 10-membered ring was also successfully used as an anticrown.

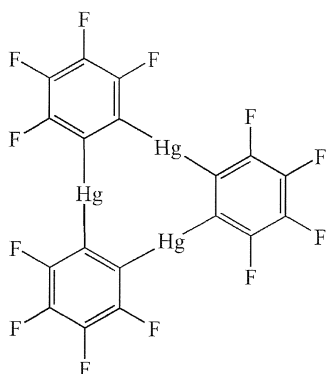
Macrocycle **8** exhibits a high affinity toward various anionic species ( $\text{Cl}^-$ ,  $\text{Br}^-$ ,  $\text{I}^-$ ,  $\text{SCN}^-$ ,  $\text{BH}_4^-$ , *closo*- $[\text{B}_{10}\text{H}_{10}]^{2-}$ , *closo*- $[\text{B}_{12}\text{H}_{12}]^{2-}$ , etc.), forming complexes with compositions and structures that are strongly dependent on the nature of the anion and the reagent ratio. In the

case of bromide, iodide, and thiocyanate ions, the isolated compounds  $[(\text{o-C}_6\text{F}_4\text{Hg})_3\text{X}]^-$  ( $\text{X}=\text{Br}, \text{I}, \text{SCN}$ ) contain one anionic guest per one molecule of the macrocycle.<sup>[10,11,13]</sup> The reaction of **8** with chloride ions gives the complex  $\{[(\text{o-C}_6\text{F}_4\text{Hg})_3\text{Cl}_2]^{2-}\}$ , containing two anionic species per three macrocycle molecules.<sup>[10]</sup>

An x-ray diffraction study of the complexes of **8** with bromide and iodide anions showed<sup>[10,11]</sup> that they are polymeric in the solid state and have unprecedented structures of polydecker bent sandwiches  $[(\cdots\mathbf{8}\cdots\text{X}\cdots)]_n^-$  ( $\text{X}=\text{Br}, \text{I}$ ), wherein every halide anion is simultaneously coordinated to six Hg atoms of two neighboring molecules of **8**. A unique feature of the complexes is that the role of the coordinating centers in their molecules is played not by the metal atoms or cations, as in the case of normal sandwich complexes, but by the anions of the halogen. An analogous polydecker sandwich structure was established for a 1:1 complex of **8** with thiocyanate anion.<sup>[13]</sup> The anionic species in this complex is bonded to the Hg centers of **8** through the sulfur atom. However, the coordination of the anionic guest with Lewis acidic host is here less symmetrical: every  $\text{SCN}^-$  ion forms with each of the macrocycles two relatively short and one considerably longer Hg–S bonds. One may suggest that the above-mentioned complex of **8** with chloride anions,  $\{[(\text{o-C}_6\text{F}_4\text{Hg})_3\text{Cl}_2]^{2-}\}$ , has a structure of triple-decker sandwich.<sup>[10]</sup> Quantum-chemical calculations also predict the possibility of the existence of double-decker sandwich complexes of macrocycle **8** with halide and sulfide anions.<sup>[14]</sup>

In the interaction of **8** with borohydride anions in THF, the complexes of three different compositions, viz.  $\{[(\text{o-C}_6\text{F}_4\text{Hg})_3]_2(\text{BH}_4)^-\}$ ,  $\{[(\text{o-C}_6\text{F}_4\text{Hg})_3](\text{BH}_4)^-\}$ , and  $\{[(\text{o-C}_6\text{F}_4\text{Hg})_3](\text{BH}_4)_2\}^{2-}$  are formed depending on the reagent ratio.<sup>[15]</sup> According to IR spectra, the bonding of the  $\text{BH}_4^-$  ions to the Hg atoms is accomplished here through B–H–Hg bridges. Quantum-chemical calculations of the complexes suggest that they should have unusual double-decker sandwich, half-sandwich (pyramidal), and bipyramidal structures, respectively. The complexes are quite stable. For example, the stability constant of  $\{[(\text{o-C}_6\text{F}_4\text{Hg})_3]_2(\text{BH}_4)^-\}$  in THF at 20°C reaches a value of  $10^7 \text{ l}^2 \text{ mol}^{-2}$ .

The first structurally characterized double-decker sandwich complexes of perfluorinated polymercuramacrocycles with anions were obtained from the reactions of polyhedral *closo*- $[\text{B}_{10}\text{H}_{10}]^{2-}$  and *closo*- $[\text{B}_{12}\text{H}_{12}]^{2-}$  dianions with the excess of **8**.<sup>[16]</sup> The anionic guest in these remarkable complexes  $\{[(\text{o-C}_6\text{F}_4\text{Hg})_3]_2(\text{B}_n\text{H}_n)^{2-}\}$  ( $n=10, 12$ ) is located between the planes of two macrocycles and is bonded to each through B–H–Hg bridges of two types. One type is the simultaneous coordination of the B–H group to all Hg centers of the neighboring molecule of the macrocycle. The other type is the coordination of the B–H



moiety only to a single Hg atom of the cycle. When the interaction of **8** with the above polyhedral dianions is conducted at an equimolar ratio of the reagents, the corresponding half-sandwiches  $\{[(o\text{-C}_6\text{F}_4\text{Hg})_3(\text{B}_n\text{H}_n)]\}^{2-}$  are produced.<sup>[16]</sup>

For macrocycle **9**, complexes with halide, acetate, trifluoroacetate, and sulfate anions were obtained. In the case of halide ions, the isolated compounds,  $\{[(\text{CF}_3)_2\text{CHg}]_5\text{X}_2\}^{2-}$  ( $\text{X}=\text{Cl}, \text{Br}, \text{I}$ ), contain two anionic species per one macrocycle molecule and have bipyramidal structures.<sup>[14,17,18]</sup> The halide anions in these adducts are arranged above and below the metallacycle plane, and each is symmetrically bonded to all Lewis acidic centers of the cycle, so that the coordination number of the halogen atoms here becomes equal to five. In the *bis*-acetate and *bis*-trifluoroacetate complexes of **9**, the anionic guests are also disposed on different sides of the metallacycle plane and are bonded to **9** in the same manner.<sup>[19]</sup> In each of the carboxylate ligands, one of the oxygen atoms is coordinated with three metallic centers of the cycle, whereas the other is bonded to two remaining metal atoms. Different coordinated geometry is observed in the complex of **9** with sulfate anion.<sup>[19]</sup> In this 1:1 complex  $\{[(\text{CF}_3)_2\text{CHg}]_5(\text{SO}_4)\}^{2-}$ , the anionic guest behaves as a tetradentate ligand and forms three types of the Hg–O bonds with the macrocycle. One type is the cooperative binding of one of the oxygen atoms of the  $\text{SO}_4^{2-}$  ion by all Lewis acidic sites of the host. This oxygen atom is located nearly in the plane of a 10-membered mercuracarborane ring. Two other oxygen atoms are coordinated each to a single Hg atom of **9**, while the fourth oxygen atom is bonded to two Hg centers.

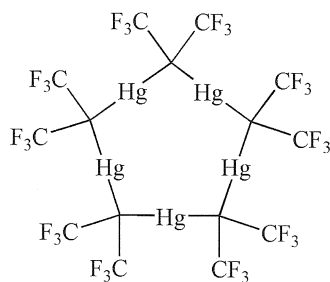
Macrocycle **8** is able to bind effectively not only anions but also various neutral Lewis bases, such as nitriles,<sup>[20]</sup> carbonyl compounds,<sup>[21,22]</sup> aromatic hydrocarbons,<sup>[23]</sup> and some others.<sup>[21]</sup> As a result of the reactions, complexes containing one, two, or three Lewis basic species per one macrocycle molecule are produced, depending on the nature of a Lewis base. For example, the interaction of

**8** with acrylonitrile,<sup>[20]</sup> acetone,<sup>[22]</sup> acetaldehyde,<sup>[22]</sup> and benzophenone<sup>[22]</sup> gives 1:1 complexes having pyramidal structures in which the Lewis basic species is coordinated with all mercury centers of **8**. The reactions of **8** with acetonitrile,<sup>[20]</sup> *N,N*-dimethylformamide,<sup>[21]</sup> and acetophenone<sup>[22]</sup> afford complexes containing two Lewis bases per molecule of **8**, and these complexes have the corresponding bipyramidal structures, with the Lewis basic moieties being located on different sides of the metallacycle plane. And, at last, from the interaction of **8** with benzonitrile,<sup>[20]</sup> ethyl acetate,<sup>[21]</sup> and acetone,<sup>[22]</sup> complexes containing three molecules of a Lewis base were isolated. Interestingly, in the case of the benzonitrile complex  $[(o\text{-C}_6\text{F}_4\text{Hg})_3(\text{PhCN})_3]$ , all the nitrile ligands are disposed on one side of the metallacycle plane and, in addition, differ from each other in the geometry of coordination with the macrocycle. By contrast, in the 1:3 complexes of **8** with ethyl acetate and acetone, two of three molecules of a Lewis base are located above and below the metallacycle plane. It should be stressed that independent of their structure, all the 1:3 complexes contain at least one fragment wherein the Lewis basic guest is simultaneously bonded to all Lewis acidic sites of the macrocycle. Note also that according to IR spectra, the complexation of the above carbonyl compounds with **8** leads to a significant weakening of their C=O bonds, which is of interest for organic synthesis and catalysis.

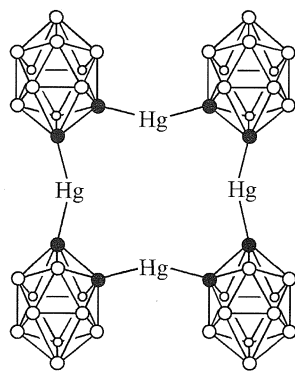
The reactions of macrocycle **8** with benzene, biphenyl, naphthalene, and triphenylene result in the formation of 1:1 complexes with polydecker sandwich structures in the solid state.<sup>[23]</sup> The bonding of the aromatic molecules to **8** in these unusual complexes is due to secondary  $\pi$ -interactions between the C=C bonds of the arenes and the Lewis acidic Hg centers. Thus, even weak Lewis bases such as aromatic hydrocarbons are able to form host–guest complexes with **8**.

### ***o*-Carboranylmercury Macrocycles (Mercuracarborands)**

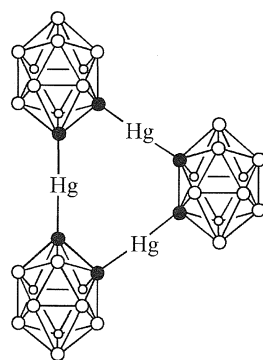
*o*-Carboranylmercury macrocycles or mercuracarborands<sup>[24,25]</sup> also exhibit a high efficiency in the binding of anions and neutral Lewis bases, which is due to the electron-withdrawing character of the carborane cages increasing the Lewis acidity of the mercury centers. This class of anticrowns was developed by Hawthorne et al.<sup>[24,25]</sup> At present, data on the synthesis and complexing properties of mercuracarborands (*o*-C<sub>2</sub>B<sub>10</sub>H<sub>10</sub>Hg)<sub>4</sub> (**10**), (*o*-C<sub>2</sub>B<sub>10</sub>H<sub>10</sub>Hg)<sub>3</sub> (**11**), and their substituted derivatives, containing four and three Hg atoms in 12- and 9-membered cycles, respectively, are available.



**9**



10



11

In 1991, Hawthorne et al. reported that the reaction of 1,2-dilithio-*o*-carborane  $o\text{-C}_2\text{B}_{10}\text{H}_{10}\text{Li}_2$  with  $\text{HgCl}_2$  results in the formation of a 1:1 complex of mercuracarborand **10** with chloride ion.<sup>[24,25]</sup> The anionic guest in this unique complex  $[(o\text{-C}_2\text{B}_{10}\text{H}_{10}\text{Hg})_4\text{Cl}]^-$  (**12**) resides nearly in the center of the mercuracarborand ring and is symmetrically coordinated to the four Hg atoms of the cycle. It was proposed that the chloride ion plays a role of a template in this macrocyclization reaction. Similarly, a treatment of  $o\text{-C}_2\text{B}_{10}\text{H}_{10}\text{Li}_2$  with  $\text{HgI}_2$  afforded the corresponding mono- or diiodide complexes,  $[(o\text{-C}_2\text{B}_{10}\text{H}_{10}\text{Hg})_4\text{I}]^-$  and  $[(o\text{-C}_2\text{B}_{10}\text{H}_{10}\text{Hg})_4\text{I}_2]^{2-}$  (**13**), depending on the reaction conditions.<sup>[24,25]</sup> As in the above-mentioned diiodide complex  $\{[(\text{CF}_3)_2\text{CHg}]_5\text{I}_2\}^{2-}$ , the anionic species in **13** are arranged above and below the metalla-cycle plane, but their coordination with the mercury atoms is less symmetrical here, which can be explained by the electrostatic repulsion of the iodide anions. The same indirect procedure was utilized successfully for the synthesis of halide complexes with a number of substituted derivatives of **10**.<sup>[24,25]</sup> In particular, a 1:1 complex of the tetraphenyl derivative of **10** with iodide ion,  $[(3\text{-Ph-}$

$o\text{-C}_2\text{B}_{10}\text{H}_9\text{Hg})_4\text{I}]^-$ , having a symmetrical pyramidal structure, was synthesized in this way.<sup>[25]</sup>

The free macrocyclic host **10** was prepared by the reaction of its diiodide **13** with silver acetate.<sup>[24,25]</sup> In a similar fashion, a series of substituted derivatives of **10** was obtained from the corresponding dihalide complexes and silver acetate. The structure of **10** in a form of the  $\text{10} \cdot (\text{THF})_4 \cdot (\text{H}_2\text{O})_2$  adduct was established by an x-ray diffraction study. A treatment of **10** with  $\text{I}^-$  regenerates the initial **13**.

Macrocycle **10** reacts with two equivalents of  $\text{KNO}_3$  in acetone in the presence of 18-crown-6 to give the bis-nitrate complex  $[(o\text{-C}_2\text{B}_{10}\text{H}_{10}\text{Hg})_4(\text{NO}_3)_2(\text{H}_2\text{O})]^{2-}$  (**14**) containing one coordinated water molecule.<sup>[26]</sup> Both nitrate ions in **14** behave as monodentate ligands but differ strongly from each other in the mode of coordination with the host. One of the  $\text{NO}_3^-$  ions in **14** is bonded through the oxygen atom to all four Hg centers of **10**, while the second nitrate is bonded to only two Hg atoms. The remaining coordination site between two other Hg centers is occupied by a molecule of water. Interestingly, when the reaction of **10** with potassium nitrate is conducted at a  $\text{NO}_3^-:\text{10}$  molar ratio of 3:1 the bis-nitrate complex  $[(o\text{-C}_2\text{B}_{10}\text{H}_{10}\text{Hg})_4(\text{NO}_3)_2]^{2-}$  (**15**) containing no water is formed, and this complex has a different structure.<sup>[26]</sup> A remarkable feature of **15** is that each of the nitrate ions here is coordinated to **10** in an unprecedented tridentate, face-on fashion, and, in addition, all four Hg atoms of the macrocycle are involved in the bonding to the anionic guests.

The interaction of **10** and its octaethyl derivative (9,12- $\text{Et}_2\text{-}o\text{-C}_2\text{B}_{10}\text{H}_8\text{Hg})_4$  (**16**) with  $\text{closo-}[\text{B}_{10}\text{H}_{10}]^{2-}$  anions in acetone solution affords 1:1 adducts even in the presence of an excess of the anionic guest, which is indicated by NMR spectra. However, the crystal product isolated from the reaction of **16** with  $\text{closo-}[\text{B}_{10}\text{H}_{10}]^{2-}$  contained two polyhedral dianions per one macrocycle molecule. This unusual supramolecular aggregate has a bipyramidal structure wherein each of the  $[\text{B}_{10}\text{H}_{10}]^{2-}$  species is bonded to all Hg atoms of the cycle through B–H–Hg bridges.<sup>[24,25]</sup> In the case of the bulkier  $\text{closo-}[\text{B}_{12}\text{H}_{12}]^{2-}$  ion, no complexation with **10** and **16** occurs. The bipyramidal complexes of **16** with neutral  $\text{closo-9,12-I}_2\text{-}o\text{-C}_2\text{B}_{10}\text{H}_{10}$  and  $\text{closo-9-I-12-Et-}o\text{-C}_2\text{B}_{10}\text{H}_{10}$  species were also described.<sup>[25]</sup> In these 1:2 complexes, an iodine atom of each of the boron-containing guests is bound to four Hg centers of the macrocyclic host.

Mercuracarborand **11** is structurally similar to the above-mentioned perfluorinated polymercuramacrocyclic **8**. It was synthesized by the interaction of 1,2-dilithio-*o*-carborane with  $\text{Hg}(\text{OAc})_2$ .<sup>[24,25]</sup> The same method was applied for the synthesis of hexamethyl derivative of **11**, (9,12- $\text{Me}_2\text{-}o\text{-C}_2\text{B}_{10}\text{H}_8\text{Hg})_3$  (**17**). The formation of **11**

A

rather than acetate complex of **10** or free **10** in the above reaction can be explained by the greater strength of a mercuracarbon ring in **11** than in **10**, as well as by the inability of noncoordinating acetate ion (in contrast to halide ions) to act as a template and thereby to direct the process of the cyclization toward **10**.

Both mercuracarborands **11** and **17** are able to bind halide anions and acetonitrile molecules. In the case of **17**, the resulting complexes with halide anions ( $\text{Cl}^-$ ,  $\text{Br}^-$ ,  $\text{I}^-$ ) contain two molecules of the macrocycle per one anionic guest and have unique structures of double-decker sandwiches.<sup>[27]</sup> The halide ion is situated here between two parallel mercuracarbon rings and is symmetrically bonded to six Hg centers. Thus, the coordination number of the halogen atom in these sandwiches as in the above-discussed polydecker bent sandwich complexes of **8** with bromide and iodide anions is equal to six. Structures of the halide adducts formed by macrocycle **11** are not yet determined.

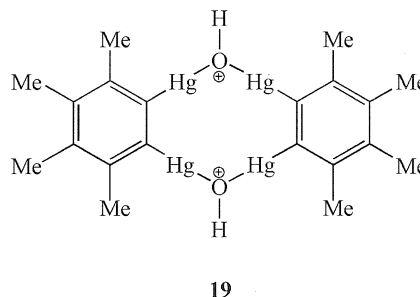
From the interaction of **11** with acetonitrile, two cocrystallized complexes,  $[(o\text{-C}_2\text{B}_{10}\text{H}_{10}\text{Hg})_3(\text{MeCN})_3]$  and  $[(o\text{-C}_2\text{B}_{10}\text{H}_{10}\text{Hg})_3(\text{MeCN})_5]$ , containing three and five nitrile molecules, were isolated.<sup>[24,25]</sup> In each of these complexes, two acetonitrile ligands are coordinated through the nitrogen atoms with all Hg atoms of the cycle. In contrast to **11**, macrocycle **17** gives with acetonitrile the sole complex  $[(o\text{-C}_2\text{B}_{10}\text{H}_8\text{Me}_2\text{Hg})_3(\text{MeCN})_3]$ , wherein only one MeCN ligand is simultaneously bonded to all Hg centers of the mercuracarbon ring.

The reaction of **17** with acetone/water (50:1) mixture yields the complex containing one water and three acetone species per one macrocyclic host.<sup>[28]</sup> The water molecule in this complex is coordinated by its oxygen atom to three mercury atoms, while the carbonyl oxygen atom of each of the acetone ligands is bound only to a single Hg center. Interestingly, all four guest species in this adduct are arranged on one side of the metallacycle plane. An even more unusual host-guest complex  $\{[(o\text{-C}_2\text{B}_{10}\text{H}_8\text{Me}_2\text{Hg})_3(\text{H}_2\text{O})]_2(\text{C}_6\text{H}_6)\}$  was obtained from the interaction of **17** with benzene and water in dichloromethane.<sup>[28]</sup> In this complex, every  $\text{H}_2\text{O}$  molecule is  $\eta^3$ -coordinated at the center of **17**, and the benzene ligand is disposed between two  $[(o\text{-C}_2\text{B}_{10}\text{H}_8\text{Me}_2\text{Hg})_3(\text{H}_2\text{O})]$  fragments, forming  $\pi$ -hydrogen bonds with both hydrogen atoms of each water molecule. The driving force for the formation of such multiple  $\pi$ -hydrogen bonds with benzene seems to be an increase in the acidity of the hydrogen atoms of water due to its  $\eta^3$ -coordination with the Lewis acidic centers of **17**.

### Other Polymercuramacrocycles

In 1987, Wuest et al. published data on the synthesis of a 2:1 complex of THF with the 22-membered macrocycle

$[o\text{-C}_6\text{H}_4\text{HgOC(O)(CF}_2)_3\text{C(O)OHg}]_2$  (**18**) containing four mercury atoms in the ring.<sup>[29,30]</sup> In this adduct, each of the THF ligands is coordinated with two Hg centers of the corresponding *o*-phenylenedimercury unit. Subsequently, a complex of the octamethyl derivative of **18**,  $[o\text{-C}_6\text{Me}_4\text{HgOC(O)(CF}_2)_3\text{C(O)OHg}]_2$ , with four 1,2-dimethoxyethane (DME) ligands was prepared and structurally characterized.<sup>[30,31]</sup> In this complex, one oxygen atom of each molecule of DME is bound with two Hg atoms of a *o*-phenylenedimercury moiety, while the other oxygen atom is bonded to a single mercury center. Evidently, the sizes of both macrocycles are too large, and the distance between *o*-phenylenedimercury fragments is too long for cooperative binding of a Lewis base by all Lewis acidic sites of these macrocyclic compounds. Wuest et al. also described a 2:1 complex of diethylformamide with dicationic macrocycle  $[(o\text{-C}_6\text{Me}_4\text{HgO(H)Hg})_2]^{2+}$  (**19**) containing four Hg atoms in a planar 10-membered ring.<sup>[30,32]</sup> The complex has a bipyramidal structure. The amide molecules in **19** are located above and below the metallacycle plane, and each is symmetrically coordinated through the oxygen atom with all four metal centers of the host. A high Lewis acidity of this macrocycle is due to its dicationic character.



### APPLICATIONS OF ANTICROWNS IN CATALYSIS AND AS IONOPHORES

There are at least two types of reactions wherein anticrowns could be successfully used as catalysts. The first type is reactions catalyzed or promoted by conventional monodentate Lewis acids. An application of anticrowns in such reactions could result in an additional increase in the reaction rate due to cooperative effects of several Lewis acidic centers. The ability of anticrowns to form lipophilic anionic species as a result of the complexation with anions suggests that these compounds will be capable of effectively transferring various organic and inorganic cations from an aqueous phase to an organic phase. Therefore, another field of synthetic organic chemistry in which anticrowns could be useful is phase-transfer catalysis of electrophilic reactions.



The first example of the successful application of anticrowns in phase-transfer catalysis was reported in 1989, when it was shown that nonfluorinated polymercuramacrocyclic **7** is able to catalyze the azo-coupling reaction between benzenediazonium halides  $\text{PhN}_2^+\text{X}^-$  ( $\text{X}=\text{Cl}, \text{Br}$ ) and  $\beta$ -naphthol in the two-phase  $\text{H}_2\text{O}-\text{CH}_2\text{Br}_2$  system.<sup>[8]</sup> Diphenylmercury proved to be totally inactive in this reaction.

Subsequently, it turned out that perfluorinated polymercuramacrocyclic **8** displays high efficiency in the phase-transfer nitration of acenaphthene with 21% nitric acid in the presence of sodium nitrite as an initiator and  $\text{NaCl}$  as a promoter.<sup>[33]</sup> The process proceeds at room temperature and gives a quantitative yield of 5-nitro- and 3-nitroacenaphthenes (in a 90–93:10–7 ratio) after 40 min ( $[\text{acenaphthene}]_0=0.5 \text{ M}$ , a 100:15  $\text{PhH}-\text{PhNO}_2$  mixture as an organic phase). In the absence of **8**, the yield of the nitro compounds does not exceed 1%, even in 3 h. Noteworthy is that macrocycle **8** is stable under the nitration conditions for at least 1 h and can be recovered from the reaction mixture in a 95% yield. Even greater activity in the nitration of acenaphthene with 21%  $\text{HNO}_3$  is exhibited by macrocycle **9**, in the presence of which a practically full conversion of the starting aromatic substrate into its nitro products is reached after 10 min.<sup>[34]</sup> According to the kinetic data, the introduction of **9** in the system increases the initial nitration rate by more than three orders of magnitude. Mercury dichloride and *bis*(perfluorophenyl)-mercury show no catalytic activity.

Macrocycles **8** and **9** also catalyze the phase-transfer nitration of pyrene, acenaphthene and 1,3-dimethylnaphthalene with a mixture of sodium nitrite and 25.6%  $\text{H}_2\text{SO}_4$  (i.e., with nitrous acid) in the presence of sodium chloride.<sup>[35]</sup> The reaction proceeds according to the following stoichiometric equation:



The highest nitration rates are observed for pyrene, which in the presence of **8** is quantitatively transformed into 1-nitropyrene within 9 min in a dinitrogen atmosphere ( $[\text{ArH}]_0=0.092 \text{ M}$ , a  $\text{NaNO}_2:\text{ArH}$  molar ratio is 4:1). When the catalyst is absent, no nitration occurs for at least 4 h. The ability of **8** and **9** to transfer protons from an aqueous phase to benzene was also reported.<sup>[33,34]</sup> This result opens prospects for using macrocycles of such a type in the phase-transfer catalysis of acid-catalyzed reactions.

Mercuracarborand **17** and octamethyl derivative of **10**, (9,12- $\text{Me}_2$ -*o*- $\text{C}_2\text{B}_{10}\text{H}_8\text{Hg}$ )<sub>4</sub> (**20**) were applied as catalysts for the Diels–Alder reaction of a thionoester *trans*- $\text{MeCH}=\text{CHC}(\text{S})\text{OMe}$  with cyclopentadiene.<sup>[36]</sup> It was found that on carrying out the reaction in  $\text{CH}_2\text{Cl}_2$  at 0°C in the presence of **20** (diene:**20**=7.5:1,  $[\text{thioester}]_0=1 \text{ M}$ )

racemic mixtures of *endo* and *exo* adducts (in a 60:40 ratio) are formed with an 89% total  $^1\text{H}$ -NMR yield (75% isolated yield) after 2.5 days. When **17** is used as a catalyst, almost exclusively, the *endo* isomer in a 94%  $^1\text{H}$ -NMR yield (83% recovered yield) is produced after 7.5 days under similar conditions. The replacement of **17** or **20** by monodentate *bis*(*closo*-9,12-dimethyl-1,2-carboranyl)-mercury (**21**) leads to a further decrease in the rate of the process (65% isolated yield of the *endo* isomer after 11 days). In the absence of a catalyst or when  $\text{HgI}_2$  or  $\text{Hg}(\text{OAc})_2$  were employed instead of **17** or **20**, no reaction was observed. For an explanation of the greater activity level of macrocycle **20** as compared to **17** and **21** in this reaction, it was assumed that among the carboranyl-mercury compounds tested, only **20** is capable of co-operatively binding the  $\text{C}=\text{S}$  group of the thionoester by all Lewis acidic centers. Methyl crotonate does not form Diels–Alder adducts with cyclopentadiene in the presence of **17**, **20**, or **21**, which is due to its inability to coordinate with the mercury atoms, as indicated by  $^{199}\text{Hg}$ -NMR spectra.

Anticrowns are also promising reagents for the development of a new type of anion-selective electrodes. The first success in this important area was achieved by Hawthorne et al.,<sup>[37]</sup> who described highly sensitive and selective chloride liquid/polymeric membrane electrodes based on mercuracarborand **11** as an ionophore and tridodecylmethylammonium chloride as a cationic additive. Optimized electrodes show a near-Nernstian behavior toward chloride anions over a wide concentration range and are characterized by a fast response time, short recovery time, long lifetime, insensitivity to pH changes over the pH range of 2.5–7.0 as well as by micromolar detection limits. Subsequently, highly selective optical sensors for chloride ions based on the same mercuracarborand **11** as an ionophore were developed.<sup>[38]</sup> In their selectivity coefficients toward chloride, both types of sensors meet the requirements for clinical applications.

## CONCLUSION

Investigations of latter years led to the discovery of a novel class of highly efficient anion receptors—anticrowns that can be considered as charge-reversed analogues of crown ethers. The host–guest chemistry of anticrowns toward various anionic species was explored; the first promising results were also obtained on the use of anticrowns as catalysts and ionophores. The efficacy of the anion binding by anticrowns depends strongly on the Lewis acidity of metal centers incorporated in their macrocyclic chain, the number of these electron-deficient centers, and size of the macrocycle. The most effective anticrowns were found among perfluorinated polymercu-

ramacrocycles and mercuracarborands containing three, four, and five Lewis acidic Hg atoms in 9-, 10-, and 12-membered mercuracarbon rings. Various neutral Lewis bases such as nitriles, carbonyl compounds, aromatic hydrocarbons, and some others can also be bound by anticrowns. A unique feature of anticrowns is their capacity to bind Lewis basic species simultaneously by all Lewis acidic centers of the macrocycle. Such cooperative binding sharply increases the strength of the host-guest interaction and leads to the formation of complexes of unprecedented structures.

One of the serious problems of anticrown chemistry is a poor assortment of synthetic routes to these remarkable reagents. As a result, the range of the presently known anticrowns is narrow, being limited only by a number of polymcury-, polytin-, and polysilicon-containing macrocycles. One may expect that a successful solution of this important synthetic problem will lead to the wide application of anticrowns in various branches of chemistry.

## ACKNOWLEDGMENTS

The authors wish to thank the Russian Foundation for Basic Research (Project code 02-03-33304) for financial support and Mr. Kirill I. Tugashov for his assistance in the preparation of the manuscript of this article.

## ARTICLES OF FURTHER INTEREST

*Anion-Directed Assembly*, p. 51

*Cryptands*, p. 334

*Ionophores*, p. 760

*Organometallic Anion Receptors*, p. 1006

*Protonated Aza-Macrocycles for Anion Complexation*, p. 1170

*Secondary Bonding*, p. 1215

## REFERENCES

1. Newcomb, M.; Madonik, A.M.; Blanda, M.T.; Judice, J.K. Macrocycles containing tin.  $^{119}\text{Sn}$  NMR studies of chloride binding by Lewis acidic tin compounds. *Organometallics* **1987**, *6*, 145–150.
2. Newcomb, M.; Horner, J.H.; Blanda, M.T.; Squattrito, P.J. Macrocycles containing tin. Solid complexes of anions encrypted in macrobicyclic Lewis acidic hosts. *J. Am. Chem. Soc.* **1989**, *111*, 6294–6301.
3. Jurkschat, K.; Kuivila, H.G.; Liu, S.; Zubieta, J.A. 1,5,9-Tristannacyclododecanes as Lewis acids. Novel structure of a chloride complex. *Organometallics* **1989**, *8*, 2755–2759.
4. Jurkschat, K.; Rühlemann, A.; Tzschach, A. Synthese und transporteigenschaften von 1,1,6,6,11,11-hexamethyl-1,6,11-tristannacyclopentadecan. *J. Organomet. Chem.* **1990**, *381*, C53–C56.
5. Jung, M.E.; Xia, H. Synthesis and transport properties of 12-silacrown-3, a new type of anion complexing agent. *Tetrahedron Lett.* **1988**, *29*, 297–300.
6. Schulte, M.; Schürmann, M.; Jurkschat, K. [*cyclo*-CH<sub>2</sub>{Sn(Cl<sub>2</sub>)CH<sub>2</sub>Si(Me<sub>2</sub>)<sub>2</sub>O}]<sub>2</sub>: Synthesis and complexation behavior of a novel, cyclic, bidentate Lewis acid and its conversion into a tin-containing fluorosilane with intermolecular Si-F...Sn bridges. *Chem. Eur. J.* **2001**, *7*, 347–355.
7. Brown, D.S.; Massey, A.G.; Wickens, D.A. A re-investigation of *o*-phenylenemercurials (V) [1]: The crystal and molecular structure of monoclinic tribenzo[*b,e,h*][1,4,7]trimercuronin. *Inorg. Chim. Acta* **1980**, *44*, L193–L194.
8. Shur, V.B.; Tikhonova, I.A.; Petrovskii, P.V.; Vol'pin, M.E. Complex formation between trimeric *o*-phenylene-mercury and halide anions and the phase transfer catalysis of the azo-coupling reaction. *Metalloorg. Khim.* **1989**, *2*, 1431–1432. [*Organomet. Chem. USSR* **1989**, *2*, 759–760 (Engl. Transl.)].
9. Ball, M.C.; Brown, D.S.; Massey, A.G.; Wickens, D.A. A reinvestigation of *o*-phenylenemercurials. IV. Adducts of perfluorotribenzo[*b,e,h*][1,4,7]trimercuronin and the crystal and molecular structure of its 1:1 4-phenylpyridine solvate. *J. Organomet. Chem.* **1981**, *206*, 265–277.
10. Shur, V.B.; Tikhonova, I.A.; Yanovsky, A.I.; Struchkov, Yu.T.; Petrovskii, P.V.; Panov, S.Yu.; Furin, G.G.; Vol'pin, M.E. Crown compounds for anions. Unusual complex of trimeric perfluoro-*o*-phenylene-mercury with the bromide anion having a polydecker sandwich structure. *J. Organomet. Chem.* **1991**, *418*, C29–C32.
11. Shur, V.B.; Tikhonova, I.A.; Yanovsky, A.I.; Struchkov, Yu.T.; Petrovskii, P.V.; Panov, S.Yu.; Furin, G.G.; Vol'pin, M.E. Polydecker sandwich complex of trimeric perfluoro-*o*-phenylene-mercury with iodide anion. *Dokl. Akad. Nauk SSSR* **1991**, *321*, 1002–1004. [*Dokl. Chem.* **1991**, *321*, 391–393 (Engl. Transl.)].
12. Antipin, M.Yu.; Struchkov, Yu.T.; Volkousky, A.Yu.; Rokhlin, E.M. X-ray study of 2,2,4,4,6,6,8,8,10,10-deca-kis(trifluoromethyl)-1,3,5,7,9-pentamercuracyclodecane [(CF<sub>3</sub>)<sub>2</sub>CHg]<sub>5</sub>·2C<sub>5</sub>H<sub>5</sub>N·2H<sub>2</sub>O. *Izv. Akad. Nauk SSSR, Ser. Khim.* **1983**, 452–455.
13. Tikhonova, I.A.; Dolgushin, F.M.; Yanovsky, A.I.; Struchkov, Yu.T.; Gavrilova, A.N.; Saitkulova, L.N.; Shubina, E.S.; Epstein, L.M.; Furin, G.G.; Shur, V.B. Crown compounds for anions. A polymeric complex of cyclic trimeric perfluoro-*o*-phenylene-mercury with thiocyanate anion containing an infinite helical chain of alternating molecules of mercury-containing macrocycle and SCN<sup>−</sup> ions. *J. Organomet. Chem.* **1996**, *508*, 271–273.
14. Chistyakov, A.L.; Stankevich, I.V.; Gambaryan, N.P.; Struchkov, Yu.T.; Yanovsky, A.I.; Tikhonova, I.A.; Shur, V.B. Crown compounds for anions. A new approach to the description of chemical bonds in the complexes of halide anions with polymcury-containing macrocycles. *J. Organomet. Chem.* **1997**, *536–537*, 413–424.
15. Saitkulova, L.N.; Bakhmutova, E.V.; Shubina, E.S.;

- Tikhonova, I.A.; Furin, G.G.; Bakhmutov, V.I.; Gambaryan, N.P.; Chistyakov, A.L.; Stankevich, I.V.; Shur, V.B.; Epstein, L.M. Crown compounds for anions. Spectroscopic and theoretical studies of complexation of borohydride anions with cyclic trimeric perfluoro-*o*-phenylenemercury. *J. Organomet. Chem.* **1999**, *585*, 201–210.
16. Shubina, E.S.; Tikhonova, I.A.; Bakhmutova, E.V.; Dolgushin, F.M.; Antipin, M.Yu.; Bakhmutov, V.I.; Sivaev, I.B.; Teplitskaya, L.N.; Chizhevsky, I.T.; Pisareva, I.V.; Bregadze, V.I.; Epstein, L.M.; Shur, V.B. Crown compounds for anions: Sandwich and half-sandwich complexes of cyclic trimeric perfluoro-*o*-phenylenemercury with polyhedral *closo*-[B<sub>10</sub>H<sub>10</sub>]<sup>2-</sup> and *closo*-[B<sub>12</sub>H<sub>12</sub>]<sup>2-</sup> anions. *Chem. Eur. J.* **2001**, *7*, 3783–3790.
17. Shur, V.B.; Tikhonova, I.A.; Dolgushin, F.M.; Yanovsky, A.I.; Struchkov, Yu.T.; Volkonsky, A.Yu.; Solodova, E.V.; Panov, S.Yu.; Petrovskii, P.V.; Vol'pin, M.E. Crown compounds for anions. A spinning top-shaped complex of cyclic pentameric perfluoroisopropylidenemercury with two chloride anions. *J. Organomet. Chem.* **1993**, *443*, C19–C20.
18. Shur, V.B.; Tikhonova, I.A.; Dolgushin, F.M.; Yanovsky, A.I.; Struchkov, Yu.T.; Volkonsky, A.Yu.; Petrovskii, P.V.; Solodova, E.V.; Panov, S.Yu.; Vol'pin, M.E. Crown compounds for anions. A spinning top-shaped complex of cyclic pentameric perfluoroisopropylidenemercury with two bromide anions. *Dokl. Akad. Nauk* **1993**, *328*, 339–341.
19. Tugashov, K.I.; Tikhonova, I.A.; Dolgushin, F.M.; Petrovskii, P.V.; Volkonsky, A.Yu.; Shur, V.B. Crown Compounds for Anions. Unusual Complexes of Cyclic Pentameric Perfluoroisopropylidenemercury with Sulphate, Acetate and Trifluoroacetate Anions. In *Book of Abstracts*, Mark Vol'pin (1923-1996) Memorial International Symposium "Modern Trends in Organometallic and Catalytic Chemistry", Moscow, Russia, May 18–23, **2003**, 151.
20. Tikhonova, I.A.; Dolgushin, F.M.; Yanovsky, A.I.; Starikova, Z.A.; Petrovskii, P.V.; Furin, G.G.; Shur, V.B. Complexation of cyclic trimeric perfluoro-*o*-phenylenemercury with nitriles. A remarkable sensitivity of the composition and structure of the resulting complexes to the nature of a nitrile. *J. Organomet. Chem.* **2000**, *613*, 60–67.
21. Tikhonova, I.A.; Dolgushin, F.M.; Tugashov, K.I.; Petrovskii, P.V.; Furin, G.G.; Shur, V.B. Coordination chemistry of polymercuramacrocycles. Complexation of cyclic trimeric perfluoro-*o*-phenylenemercury with neutral oxygeneous Lewis bases. *J. Organomet. Chem.* **2002**, *654*, 123–131.
22. King, J.B.; Tsunoda, M.; Gabbai, F.P. Complexation of aldehydes and ketones by trimeric perfluoro-*ortho*-phenylene mercury, a tridentate Lewis acid. *Organometallics* **2002**, *21*, 4201–4205.
23. Haneline, M.R.; Tsunoda, M.; Gabbai, F.P.  $\pi$ -Complexation of biphenyl, naphthalene, and triphenylene to trimeric perfluoro-*ortho*-phenylene mercury. Formation of extended binary stacks with unusual luminescent properties. *J. Am. Chem. Soc.* **2002**, *124*, 3737–3742.
24. Hawthorne, M.F.; Yang, X.; Zheng, Z. Host-guest chemistry of anion-complexation by macrocyclic multidentate Lewis acids. *Pure Appl. Chem.* **1994**, *66*, 245–254.
25. Hawthorne, M.F.; Zheng, Z. Recognition of electron-donating guests by carborane-supported multidentate macrocyclic Lewis acid hosts: Mercuracarborand chemistry. *Acc. Chem. Res.* **1997**, *30*, 267–276.
26. Zinn, A.A.; Knobler, C.B.; Harwell, D.E.; Hawthorne, M.F. Molecular aggregates of nitrate ion with the tetravalent Lewis acid host 12-mercuracarborand-4: Novel trihapto coordination of NO<sub>3</sub><sup>-</sup>. *Inorg. Chem.* **1999**, *38*, 2227–2230.
27. Lee, H.; Knobler, C.B.; Hawthorne, M.F. Octahedral coordination of halide ions (I<sup>-</sup>, Br<sup>-</sup>, Cl<sup>-</sup>) sandwich bonded with tridentate mercuracarborand-3 receptors. *J. Am. Chem. Soc.* **2001**, *123*, 8543–8549.
28. Lee, H.; Knobler, C.B.; Hawthorne, M.F. A hydrogen-bonded [(mercuracarborand-water)<sub>2</sub>-benzene]  $\pi$ -sandwich complex. *Angew. Chem. Int. Ed.* **2001**, *40*, 3058–3060.
29. Wuest, J.D.; Zacharie, B. Multidentate Lewis acids. Complex of macrocyclic tetradentate organomercuric perfluoroglutarate. *J. Am. Chem. Soc.* **1987**, *109*, 4714–4715.
30. Wuest, J.D. Multiple coordination and activation of Lewis bases by multidentate Lewis acids. *Acc. Chem. Res.* **1999**, *32*, 81–89.
31. Nadeau, F.; Simard, M.; Wuest, J.D. Multidentate Lewis acids. Complex of a macrocyclic host with a bidentate guest. *Organometallics* **1990**, *9*, 1311–1314.
32. Vaugois, J.; Simard, M.; Wuest, J.D. Quadruple coordination of the carbonyl oxygen atom of an amide by a cyclic tetradentate Lewis acid. *Organometallics* **1998**, *17*, 1215–1219.
33. Zarausky, A.P.; Kachurin, O.I.; Velichko, L.I.; Tikhonova, I.A.; Furin, G.G.; Shur, V.B.; Vol'pin, M.E. Cyclic trimeric perfluoro-*o*-phenylenemercury as the phase transfer catalyst for nitration with dilute nitric acid. *Izv. Akad. Nauk, Ser. Khim.* **1994**, 547–548. [*Russ. Chem. Bull.* **1994**, *43*, 507–508. (Engl. Transl.)].
34. Zarausky, A.P.; Kachurin, O.I.; Velichko, L.I.; Tikhonova, I.A.; Volkonsky, A.Yu.; Shur, V.B. New highly efficient phase transfer catalyst for nitration with dilute nitric acid. *Izv. Akad. Nauk, Ser. Khim.* **1994**, 2047–2048. [*Russ. Chem. Bull.* **1994**, *43*, 1936–1937. (Engl. Transl.)].
35. Zarausky, A.P.; Kachurin, O.I.; Velichko, L.I.; Shur, V.B.; Tikhonova, I.A.; Furin, G.G. Phase transfer catalysis in reactions of electrophilic substitution. VIII. Phase transfer catalytic nitration of arenes with sodium nitrite in an acidic medium. *Zh. Org. Khim.* **1999**, *35*, 1063–1067.
36. Lee, H.; Diaz, M.; Hawthorne, M.F. Mercuracarborand-catalyzed Diels–Alder reactions of a thionoester with cyclopentadiene. *Tetrahedron Lett.* **1999**, *40*, 7651–7655.
37. Badr, I.H.A.; Diaz, M.; Hawthorne, M.F.; Bachas, L.G. Mercuracarborand "anti-crown ether"-based chloride-sensitive liquid/polymeric membrane electrodes. *Anal. Chem.* **1999**, *71*, 1371–1377.
38. Badr, I.H.A.; Johnson, R.D.; Diaz, M.; Hawthorne, M.F.; Bachas, L.G. A selective optical sensor based on [9]mercuracarborand-3, a new type of ionophore with a chloride complexing cavity. *Anal. Chem.* **2000**, *72*, 4249–4254.

# Artificial Enzymes

**Jun-ichi Kikuchi**

*Nara Institute of Science and Technology, Nara, Japan*

**Hiroki Kondo**

*Kyushu Institute of Technology, Fukuoka, Japan*

## INTRODUCTION

Study of artificial enzymes began as early as in the mid-twentieth century in pioneering work on enzyme model reactions.<sup>[1–4]</sup> On the basis of a vast amount of findings on structures and catalytic mechanisms of naturally occurring enzymes from the physical, chemical, and biological viewpoints, we can now discuss the properties and reactions of enzymes in great detail at the molecular level. In general, enzymes are ingeniously designed biocatalysts, exhibiting marked rate enhancement, high substrate specificity, and distinct reaction selectivity under mild reaction conditions. Such characteristic features of enzymes are generated essentially through the formation of specific enzyme–substrate complexes as key intermediates. On these grounds, various artificial enzymes capable of performing substrate-binding behavior were developed up to the present time. In addition, while well-known hydrolases such as  $\alpha$ -chymotrypsin, lysozyme, and ribonuclease do not require cofactors, many enzymes exhibit catalytic activity in collaboration with coenzymes and metal ions. For simulation of the latter class of enzymatic reactions, molecular design of artificial holoenzymes comprising an apoenzyme model and a cofactor is important.<sup>[5–8]</sup> Artificial enzymes can be classified mainly into the following three categories: macrocyclic compounds, molecular assemblies, and macromolecules.

## MACROCYCLIC COMPOUNDS AS ARTIFICIAL ENZYMES

In general, the active site of an enzyme is regarded as a hydrophobic cavity or cleft created by folding of the polypeptide chain. Such a substrate-binding site is provided by macrocyclic compounds such as cyclodextrins<sup>[9]</sup> (Fig. 1), crown ethers,<sup>[10–12]</sup> cyclophanes,<sup>[13–15]</sup> and calixarenes,<sup>[16–18]</sup> each having an inclusion cavity as a basic skeleton of potent artificial enzymes.

Cyclodextrins (**1**) are cyclic glucose oligomers of cylindrical shape having primary hydroxyl groups at the

more restricted rim of the cylinder. The three most common cyclodextrins are  $\alpha$ -,  $\beta$ -,  $\gamma$ -species, which are composed of six, seven, and eight glucopyranose units, respectively. In early work in the 1950s and 1960s, it was shown that the oxyanion of cyclodextrin could react with pyrophosphates and carboxylate esters bound in the cyclodextrin cavity in aqueous media, and that acyl-group transfer from the esters could be accelerated with moderate substrate selectivity. Since then, many kinds of modified cyclodextrins were developed by introducing a catalytic group selectively into the primary or the secondary hydroxyl moieties. By employing the functional groups similar to those in the side chain of amino acids, such as imidazolyl and thiol groups, the resulting cyclodextrin derivatives were expected to serve as mimics of hydrolases. In fact, cyclodextrins bearing a metal-binding site worked as hydrolytic metalloenzyme models. Various functionalized cyclodextrins bearing a cofactor, such as vitamin B<sub>1</sub>, B<sub>2</sub>, B<sub>6</sub>, B<sub>12</sub>, nicotinamide, or porphyrin, were prepared as holoenzyme models. The introduction of multiple functional groups into cyclodextrins is essential to design more sophisticated artificial enzymes. For example, a  $\beta$ -cyclodextrin bearing two imidazolyl groups (**2**) acts as an excellent artificial ribonuclease, showing turnover behavior possibly through bifunctional catalytic assistance of the imidazolyl groups. A compound (**3**) carrying a pyridoxamine and an ethylenediamine unit attached to  $\beta$ -cyclodextrin on the neighboring primary methylene groups behaved as a potent artificial aminotransferase. Aromatic L- $\alpha$ -amino acids such as phenylalanine, tryptophan, and phenylglycine were generated with high (90–96% ee) enantiomeric excess by the catalysis of **3**. In addition, the prototropy rate observed with **3** was drastically enhanced relative to simple pyridoxamine. However, the true catalytic cycle, exhibiting amino group transfer from an  $\alpha$ -amino acid to an  $\alpha$ -keto acid, was not successful with this modified cyclodextrin.

While cyclodextrins are used as enzyme mimics in aqueous media, crown ethers can act as a key component of artificial enzymes in organic solutions (Fig. 2). Crown ether was discovered by Pedersen in 1967,<sup>[10]</sup> which

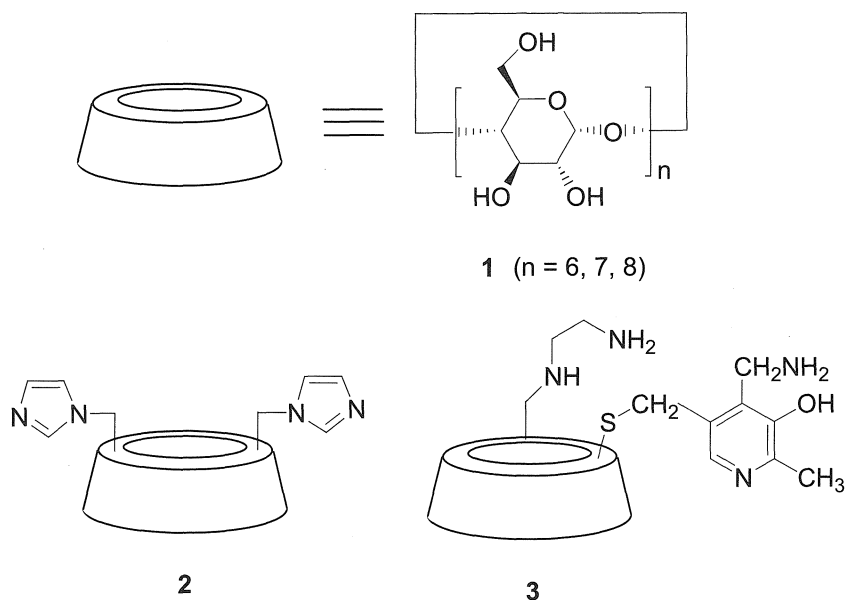


Fig. 1 Cyclodextrin (1) and its derivatives (2 and 3) as artificial enzymes.

eventually won him, together with Cram and Lehn, the Nobel prize in 1987. This discovery triggered the research on host-guest chemistry and artificial enzymes at large, including practical applications. For example, binding of a pyridinium substrate to a crown ether bearing dihydronicotinamide moieties (4) led to enhancement of the hydrogen-transfer rate from the dihydropyridine moiety to

the pyridinium within the intermediate complex in acetonitrile. In addition, the potentiality in enantioselective reductions was examined with a series of chirally bridged macrocyclic 1,4-dihydropyridines of crown ether type. In the reduction of ethyl benzoylformate by 5 having L-valine residues in the macrocyclic skeleton, (*S*)-mandelate was obtained with an enantiomeric excess of 90% in

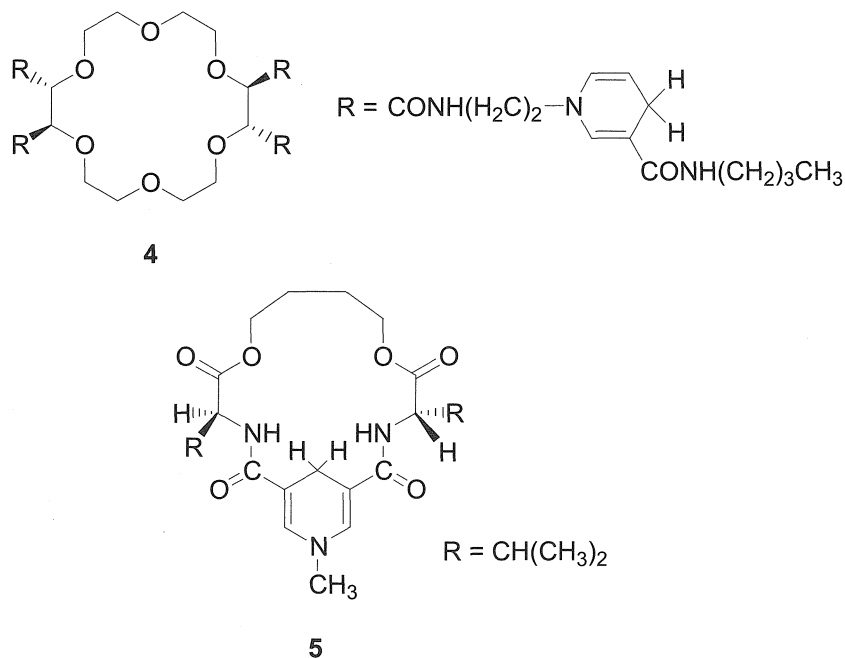


Fig. 2 Examples of crown ether derivatives (4 and 5) as artificial enzymes.

acetonitrile-chloroform at room temperature in the presence of Mg(II) ions.

Cyclophanes with a sizable internal cavity also proved to be useful as supramolecular elements of artificial enzymes. While a relatively limited range of structural modifications is possible with cyclodextrins, a wide synthetic variation of cyclophanes can be achieved so that an appropriate recognition site with regard to size, shape, and microenvironment is provided for a target substrate molecule. In an early study in the 1970s, [20]paracyclophanes and [10.10]paracyclophanes were employed to demonstrate that cyclophanes are effective as macrocyclic enzyme models. Since then, various cyclophane derivatives were developed as artificial enzymes. While binding constants of simple cyclodextrins with typical substrates in aqueous media are ca.  $10^4 \text{ M}^{-1}$  or less in general, the substrate-binding ability can be enhanced by various types of molecular design of the cyclophane skeleton, especially by creating three-dimensionally extended hydrophobic cavities. Enzyme mimetic

reactions catalyzed by the artificial enzymes of cyclodextrin type would be duplicated and improvable by employing functionalized cyclophanes. For example, the octopus cyclophane (**6**) bearing eight hydrocarbon chains on a macrocyclic tetraazacyclophane ring provides a large and flexible hydrophobic cavity in which to incorporate as large as a hydrophobic vitamin B<sub>12</sub> derivative (**7**) through the induced-fit mechanism (Fig. 3). The resulting host-guest complex acted as an efficient vitamin B<sub>12</sub>-dependent artificial holoenzyme, showing turnover behavior for carbon-skeleton rearrangement reactions specifically catalyzed by methylmalonyl-CoA mutase and glutamate mutase. In addition, this artificial enzyme also catalyzed unique ring-expansion reactions for which naturally occurring vitamin B<sub>12</sub>-dependent enzymes are not known.

Calixarenes developed by Gutsche<sup>[16]</sup> belong to a family of cyclophanes by definition, and much attention has focused on their catalytic functions as artificial enzymes based on their versatile molecular recognition

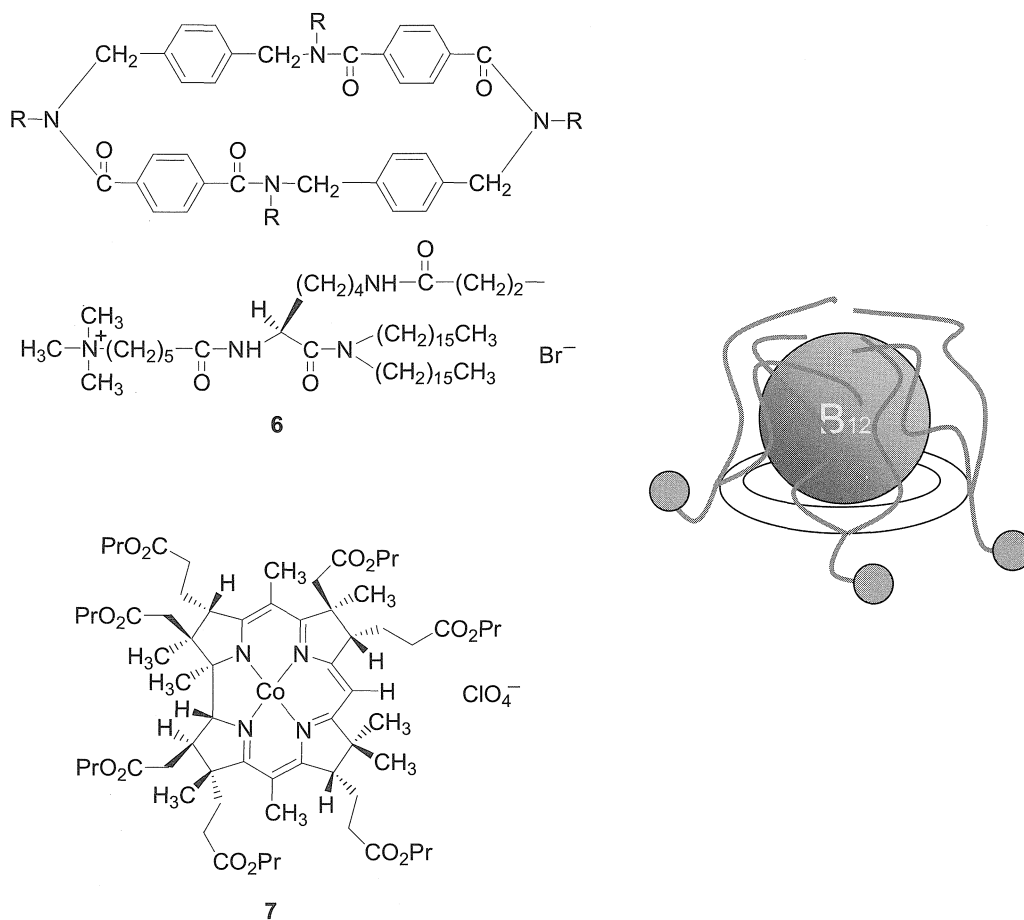


**Fig. 3** An example of artificial holoenzyme formed with the octopus cyclophane (**6**) and the hydrophobic vitamin B<sub>12</sub> derivative (**7**). (View this art in color at [www.dekker.com](http://www.dekker.com).)

abilities. Other macrocyclic compounds such as cryptands, spherands, and cucurbiturils seem to be feasible as equally promising enzyme mimics.

## MOLECULAR ASSEMBLIES AS ARTIFICIAL ENZYMES

There is another type of enzyme mimics that provide a substrate-binding site as a result of self-aggregation of functional elements through noncovalent intermolecular interactions in solution: reversed micelles in organic solutions, and micelles and lipid bilayer membranes in aqueous media.<sup>[4,18–21]</sup>

Reversed micelles formed with various surfactants in apolar solvents in the presence of small amounts of water were extensively studied on their characteristic features of cores in enzyme-mimetic reactions. In the spatially restricted microenvironment of reversed micelles, a unique catalytic behavior analogous to enzymatic reactions was observed.

Aqueous micelles are typical and simple aggregates of surfactants, and numerous applications as enzyme models were accumulated up to 1980 (Fig. 4). In general, molecular structures characteristic of micelle-forming amphiphiles are composed of a polar head moiety, a long hydrophobic chain, and in some cases, an additional functional group for effective catalysis. Cationic amphiphiles having an imidazolyl (**8**) or a thiol moiety (**9**) in the polar head are typical examples. While micelles provide hydrophobic reaction sites effective for the acceleration of various enzyme-mimetic reactions, those aggregates are generally soft, and it is difficult to fix the disposition of substrates in space for regio- and stereospecificity of reactions to appear.

Another type of well-known molecular aggregate in an aqueous media is a bilayer membrane. In general, the bilayer membrane is superior to aqueous micelles with respect to aggregate rigidity and spacial orientation of component molecules, so that substrate specificity, catalytic activity, and reaction selectivity are more readily exhibited. In addition, phase states, gel and liquid crystalline, and phase-separation behavior among the component species can be utilized to control catalytic pathways.

Preparation and characterization of liposomes formed with natural phospholipids were well established. However, in using liposomes for simulation of enzymatic functions, especially in acid–base catalysis, difficulties would be encountered due to their chemical and morphological instabilities. Thus, bilayer membranes composed of synthetic amphiphiles are more favorable candidates for enzyme mimics. For example, artificial vitamin B<sub>6</sub>-dependent enzymes were constructed from catalytic bilayer membranes in combination with a bilayer-forming peptide lipid (**10**), a hydrophobic vitamin B<sub>6</sub> derivative (**11**), and metal ions (Fig. 5). The catalyst acts as an artificial aminotransferase, showing marked substrate specificity, high enantioselectivity, and turnover behavior for the transamination of  $\alpha$ -amino acid with  $\alpha$ -keto acids. In addition, the reaction fields provided by the catalytic bilayer membranes are suitable to establish multienzyme systems through functional alignments of artificial enzymes and natural ones in a sequential manner.

## MACROMOLECULES AS ARTIFICIAL ENZYMES

On the basis of structural resemblance to enzymes, various kinds of macromolecules were developed as artificial enzymes. These macromolecules are classified mainly into two categories: modification of biopolymers and totally synthetic functional polymers.

The design of artificial enzymes through site-directed mutagenesis is well established.<sup>[22]</sup> By single or multiple replacement of an amino acid residue placed in the enzyme protein, enzymatic functions such as reactivity, substrate specificity, and reaction selectivity, can be altered. Although the site-directed mutagenesis gives rise to only a small change in the amino acid sequence of a target protein, such modification can induce a drastic change in the catalytic behavior. Incorporation of unnatural amino acids and nonamino acids into proteins is also possible.

Development of catalytic antibodies or abzymes is another fascinating approach to artificial enzymes.<sup>[5]</sup> The concept of catalytic antibodies is that if a putative transition state analogue of a reaction for which a selective and efficient catalyst is desired is used to elicit antibodies,

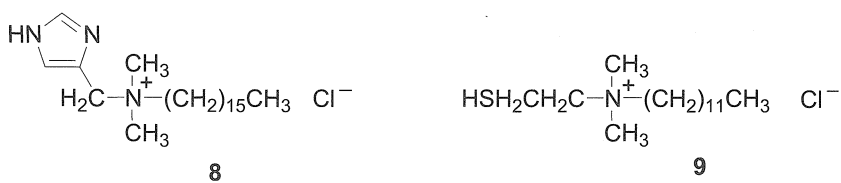
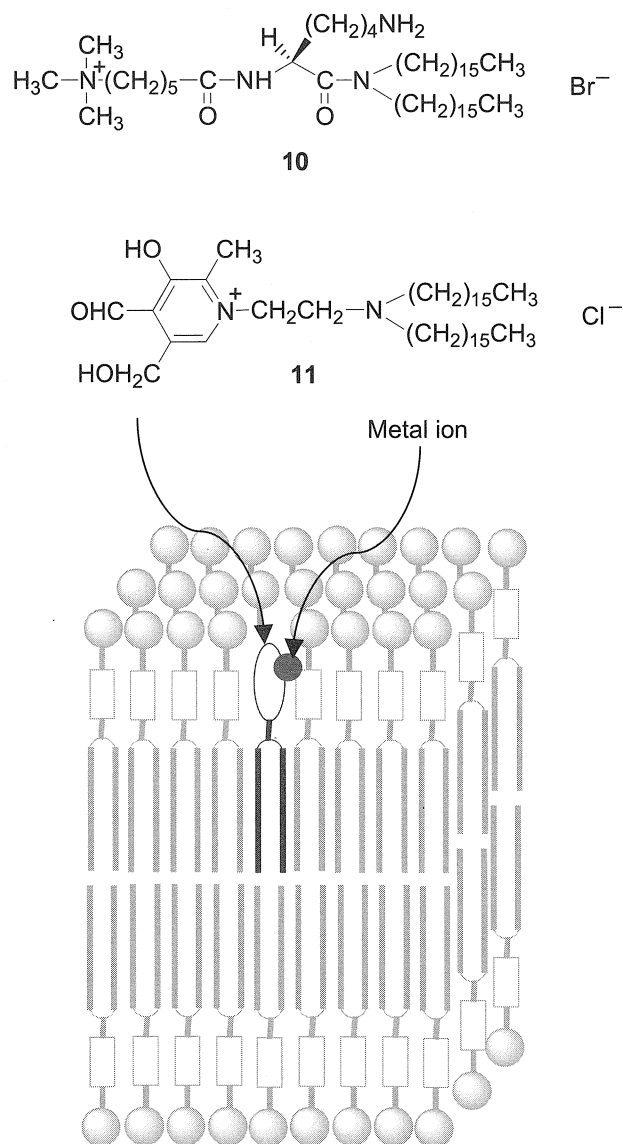


Fig. 4 Examples of micelle-forming amphiphiles (**8** and **9**) as a component of artificial enzyme.





**Fig. 5** An example of an artificial holoenzyme formed with the bilayer-forming peptide lipid (**10**), the hydrophobic vitamin B<sub>6</sub> derivative (**11**), and metal ions. (View this art in color at [www.dekker.com](http://www.dekker.com).)

they are likely to catalyze the reaction of a parent compound. Because antibodies are specialized only for binding of ligands called antigens or haptens, semisynthetic strategies for introducing catalytic functionalities into the active site of an antibody is additionally necessary in some cases. Catalytic antibodies were elicited for reactions for which no enzyme exists, such as the Diels–Alder reaction, Claisen rearrangement, and oxy-Cope rearrangement.

Although the site-directed mutagenesis and catalytic antibody technique are useful genetic methods, chemical modification of enzymes remains a valuable tool for protein engineering. The latter approaches are divided into

direct modification of an enzyme protein and modification of a cofactor bound to the enzyme.<sup>[23–26]</sup> These chemical methods led to modification of existing enzyme activity or introduction of new enzyme functions into proteins and enzymes.

As regard to enzyme mimics formed with totally synthetic polymers, relatively simple water-soluble polymers with catalytic functionalities were employed in the early work before 1980.<sup>[4]</sup> Although simulation of enzymatic behavior was successful to a certain extent by employing such prototype models, recent interests focused on more intelligent synthetic polymers, such as imprinted polymers<sup>[5]</sup> and dendrimers.<sup>[27]</sup>

When a polymer is prepared in the presence of “print molecules” as the transition state or intermediate analogues, which are extracted after polymerization, the remaining polymer may contain catalytic cavities capable of recognizing the print molecules. By analogy to the catalytic antibodies, where a function complementary to that of the hapten can be induced in a specific place, polymers can be imprinted with print molecules containing suitable catalytic functionalities. Because dendrimers are structurally regulated polymers with an inner core like an enzyme active site, their characteristics as enzyme mimics also attract attention.

## CONCLUSION

In recent years, the traditional definition of biocatalysts with enzymes that are proteins having catalytic functions in biological systems was expanded to a point where a series of ribonucleic acids, called ribozymes, also acts as a biocatalyst. Much effort was devoted to developing artificial ribozymes as well.<sup>[28]</sup> In such approaches, a combination of strategies to mimic ribonucleases and to simulate complementary molecular recognition of nucleic acids is essential.

As mentioned above, studies on artificial enzymes were extensively developed to date. Although the catalytic performance of artificial enzymes rarely surpasses that of the corresponding naturally occurring enzymes from every point of view, some of them close in on catalytic performance of the natural counterparts. In addition, advantages of artificial enzymes relative to those of natural ones are flexibility in molecular design, structural stability, and possible applications to substrates and reactions for which natural enzymes are not available.

One of the targets in the study of artificial enzymes would be creation of integrated reaction systems on the nanometer scale inspired by the reaction network in cells, from the viewpoint of nanoscience and nanotechnology. For such a purpose, construction of artificial multienzyme systems, collaboration between enzymes and receptors,

and synchronization of individual supramolecules seem to be essential.<sup>[7,21,25,29]</sup>

## ARTICLES OF FURTHER INTEREST

*Biological Models and Their Characteristics*, p. 101  
*Carbonic Anhydrase Models*, p. 178  
*Enzyme Mimics*, p. 546  
*Enzymes: Characteristics and Mechanisms*, p. 554  
*Ion Channels and Their Models*, p. 742  
*Molecular-Level Machines*, p. 931  
*O<sub>2</sub> Uptake and Transport, Models of*, p. 1023  
*Selectivity: Thermodynamic and Kinetic*, p. 1225  
*Vitamin B<sub>12</sub> and Heme Models*, p. 1569  
*Zinc-Containing Enzymes and Their Models*, p. 1631

## REFERENCES

1. Bruice, T.C.; Benkovic, S.J. *Bioorganic Mechanisms*; W.A. Benjamin Inc.: New York, 1966.
2. Jencks, W.P. *Catalysis in Chemistry and Enzymology*; McGraw-Hill: New York, 1969.
3. Bender, M.L. *Mechanisms of Homogeneous Catalysis from Protons to Proteins*; Wiley Interscience: New York, 1971.
4. Fendler, J.H.; Fendler, E.J. *Catalysis in Micellar and Macromolecular Systems*; Academic Press: New York, 1975.
5. Feiters, M.C. Supramolecular Catalysis. In *Comprehensive Supramolecular Chemistry*; Atwood, J.L., Davies, J.E.D., MacNicol, D.D., Vígtle, F., Lehn, J.-M., Reinhoudt, D.N., Eds.; Pergamon: Oxford, 1996; Vol. 10, 268–360.
6. Ogoshi, H.; Mizutani, T. Biomimetic Reactions Catalyzed by Metalloporphyrins. In *Comprehensive Supramolecular Chemistry*; Atwood, J.L., Davies, J.E.D., MacNicol, D.D., Vígtle, F., Lehn, J.-M., Murakami, Y., Eds.; Pergamon: Oxford, 1996; Vol. 4, 337–385.
7. Murakami, Y.; Kikuchi, J.; Hisaeda, Y.; Hayashida, O. Artificial enzymes. *Chem. Rev.* **1996**, 96 (2), 721–758.
8. Ridder, A.M.; Kellogg, R.M. Models for Zinc-Containing Enzymes. In *Comprehensive Supramolecular Chemistry*; Atwood, J.L., Davies, J.E.D., MacNicol, D.D., Vígtle, F., Lehn, J.-M., Murakami, Y., Eds.; Pergamon: Oxford, 1996; Vol. 4, 387–413.
9. Breslow, R.; Dong, S.D. Biomimetic reactions catalyzed by cyclodextrins and their derivatives. *Chem. Rev.* **1998**, 98 (5), 1997–2011.
10. Pedersen, C.J. The discovery of crown ether. *Angew. Chem., Int. Ed. Engl.* **1988**, 27 (8), 1021–1027.
11. Cram, D.J. The design of molecular hosts, guests, and their complexes. *Angew. Chem., Int. Ed. Engl.* **1988**, 27 (8), 1009–1020.
12. Lehn, J.-M. Supramolecular chemistry—Scope and perspectives. Molecules, supramolecules, and molecular devices. *Angew. Chem., Int. Ed. Engl.* **1988**, 27 (1), 89–112.
13. Murakami, Y. Functionalized cyclophanes as catalysts and enzyme models. *Top. Curr. Chem.* **1983**, 115, 107–155.
14. Murakami, Y.; Kikuchi, J.; Hisaeda, Y. Catalytic Applications of Cyclophanes. In *Inclusion Compounds*; Atwood, J.L., Davies, J.E.D., MacNicol, D.D., Eds.; Oxford Univ. Press: Oxford, 1991; Vol. 4, 448–478.
15. Seel, C.; Vígtle, F. Molecules with large cavities in supramolecular chemistry. *Angew. Chem., Int. Ed. Engl.* **1992**, 31, 528–549.
16. Gutsche, C.D. Calixarenes. In *Monographs in Supramolecular Chemistry*; Stoddart, J.F., Ed.; The Royal Society of Chemistry: Cambridge, England, 1989; Vol. 1.
17. *Calixarenes: A Versatile Class of Macrocyclic Compounds*; Vecens, J., Böhmer, V., Eds.; Kluwer Academic Publishers: Dordrecht, 1991.
18. Fendler, J.H. *Membrane Mimetic Chemistry*; John Wiley & Sons: New York, 1982.
19. Kunitake, T. Synthetic bilayer membranes: Molecular design, self-organization, and application. *Angew. Chem., Int. Ed. Engl.* **1992**, 31, 709–726.
20. Murakami, Y.; Kikuchi, J. Supramolecular Assemblies Formed with Synthetic Peptide Lipids. Functional Models of Biomembranes and Enzymes. In *Bioorganic Chemistry Frontiers*; Dugas, H., Ed.; Springer-Verlag: Berlin, 1991; Vol. 2, 73–113.
21. Murakami, Y.; Kikuchi, J.; Hisaeda, Y.; Ohno, T. Artificial Enzymes with Vitamin B<sub>6</sub> and B<sub>12</sub> Activity. In *Comprehensive Supramolecular Chemistry*; Atwood, J.L., Davies, J.E.D., MacNicol, D.D., Vígtle, F., Lehn, J.-M., Murakami, Y., Eds.; Pergamon: Oxford, 1996; Vol. 4, 415–472.
22. Kondo, H. Towards Design of Artificial Enzymes and Receptors Through Site-Directed Mutagenesis of Proteins. In *Comprehensive Supramolecular Chemistry*; Atwood, J.L., Davies, J.E.D., MacNicol, D.D., Vígtle, F., Lehn, J.-M., Murakami, Y., Eds.; Pergamon: Oxford, 1996; Vol. 4, 528–547.
23. Kaiser, E.T.; Lawrence, D.S. Chemical mutation of enzyme active sites. *Science* **1984**, 226, 505–511.
24. Qi, D.; Tann, C.-M.; Haring, D.; Distefano, M.D. Generation of new enzymes via covalent modification of existing proteins. *Chem. Rev.* **2001**, 101 (10), 3081–3111.
25. Hayashi, T.; Hisaeda, Y. New functionalization of myoglobin by chemical modification of heme-propionates. *Acc. Chem. Res.* **2002**, 35 (1), 35–43.
26. Hamachi, I.; Watanabe, J.; Eboshi, R.; Hiraoka, T.; Shinkai, S. Incorporation of artificial receptors into a protein/peptide surface: A strategy for on/off type of switching of semisynthetic enzymes. *Biopolymers* **2000**, 55 (6), 459–468.
27. Astruc, D.; Chardac, F. Dendritic catalysts and dendrimers in catalysis. *Chem. Rev.* **2001**, 101 (9), 2991–3023.
28. Trawick, B.N.; Daniher, A.T.; Bachkin, J.K. Inorganic mimics of ribonucleases and ribozymes: From random cleavage to sequence-specific chemistry to catalytic antisense drugs. *Chem. Rev.* **1998**, 98 (3), 939–960.
29. Kikuchi, J.; Ariga, K.; Sasaki, Y. Molecular Recognition and Functional Connection in Lipid Membranes. In *Advances in Supramolecular Chemistry*; Gokel, G.W., Ed.; Cerberus Press: Miami, 2001; 131–173.

# Aurophilic Interactions

Antonio Laguna

Universidad de Zaragoza—CSIC, Zaragoza, Spain

Eduardo J. Fernández

José M. López-de-Luzuriaga

Universidad de La Rioja, UA—CSIC, Logroño, Spain

## INTRODUCTION

The word “aurophilic,” derived from the Latin word “Aurum” (gold) and the Greek word “Philos” (with an affinity for), was coined in the late 1980s<sup>[1–3]</sup> to describe the tendency of gold(I) compounds to form dimers, oligomers, chains, or even layers via gold(I)–gold(I) interactions. In these interactions, the distances between the adjacent gold atoms range from 2.7–3.6 Å, and are shorter than the sum of their van der Waals radii (3.6 Å). These interactions have a strength between 20–50 kJ/mol, close to that found in hydrogen bonds. This result is surprising, as two gold(I) centers with an external  $d^{10}$  configuration would normally be expected to repel each other. In addition, gold attractions are already present in metallic gold, where the gold–gold distances are shorter than the corresponding silver–silver distances. This phenomenon, although it can be considered a general feature when comparing the metallic radii of the second- and third-row elements, cannot be considered as the result of a lanthanoid contraction, because the rest of the “anomalies” of gold, such as its high electroaffinity and electronegativity or the presence of highly stable  $\text{Au}_2$  molecules in the gas phase, cannot be explained in these terms. Of course, with these properties, it is considered to be the “king of the metals.”

## THEORETICAL CONSIDERATIONS

The latest contributions of physicists and the theoretical chemists to the explanation of this phenomenon stem from the results of *ab initio* and density functional theory calculations, which refute the previous *s-d* hybridization proposed by the extended Hückel theory. They suggest that the metallophilic attraction can be considered a correlation effect strengthened by the relativistic effect, which is important in the case of gold.<sup>[4,5]</sup>

Postlanthanide elements have a large number of protons in their atomic nuclei (79 protons for gold). Moreover, the electrons move in a field with a high

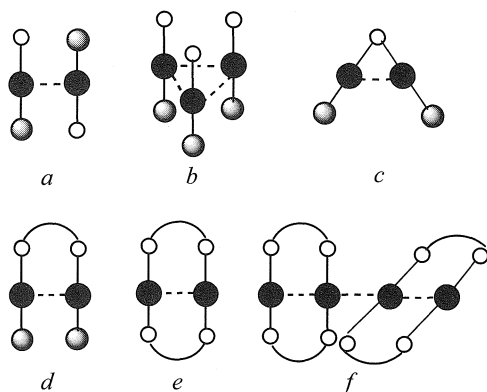
nuclear charge, and therefore, their speed is similar to that of light. Electrons moving at such a speed cannot be treated in terms of classical physics, rather they have to be treated on the basis of Einstein’s Theory of Relativity:  $m_r = m_o(1 - v^2/c^2)^{-1/2}$ . According to this equation, the relativistic mass ( $m_r$ ) of these electrons is larger than the conventional nonrelativistic mass ( $m_o$ ), resulting in a contraction of orbital radius. This effect, known as relativistic contraction, is particularly important for the orbitals with radial functions that have local maxima in the neighborhood of the nucleus, particularly in the *s*-orbitals. Thus, the expected marked effect on the 1*s* electrons of postlanthanide elements also has continuity in the 2*s*, 3*s*, 4*s*, 5*s*, and 6*s* orbitals, as they are orthogonal to one another. The ratio of the relativistic radius of the valence electrons to their nonrelativistic radius as a function of the atomic number strongly deviates from unity and reaches a local minimum for gold. Therefore, gold occupies a unique position among all the elements.

The main consequences for gold are that the energy gap between the 5*d*, 6*s*, and 6*p* orbitals diminishes, the closed-shell configuration  $5d^{10}$  is no longer chemically inert, and the interaction between two gold(I) centers can be explained. Furthermore, the formation of linear two-coordinate gold(I) complexes is also favored.

Let us analyze some examples where this interaction is present. These examples establish a great affinity between gold atoms, which are as close as possible to each other and, generally, at distances even shorter than the ones found in metallic gold (2.88 Å). We excluded gold clusters with formal metal–metal bonds and oxidation states between 0 and +1 from the description. We will refer only to the interactions among atoms with closed-shell configurations.

## GOLD(I)–GOLD(I) INTERACTIONS

The term “aurophilic interactions” was first coined in connection with the chemistry of gold(I). Gold(I)



**Scheme 1** Some attractive interactions in gold(I) complexes.

complexes are of general formula  $X\text{-Au-L}$ , where the ligands  $X$  and  $L$  may be neutral or anionic and have a linear geometry. After the advent of crystal structure analysis in the 1960s, it became apparent that virtually all such complexes are packed or arranged in such a way that the gold(I) atoms are as close as possible to each other. This attractive interaction gathers the gold atoms in pairs, rings, chains, or even layers (Scheme 1).

As can be seen in the scheme, the presence of ligands acting as bridges between the gold centers favors the appearance of such interactions (*c, d, e, f*) and, sometimes, ligands have even been considered responsible for their presence. In the *e* case, inter- and intramolecular interactions are present in the same molecule. Nevertheless, the existence of these interactions is undoubtedly evident in hundreds of examples of nonbridged complexes (types *a* and *b*), where the distances between the adjacent gold atoms depend on the electronic nature of the ligands and their steric requirements.<sup>[6–10]</sup> A particularly sophisticated structural arrangement appears in the complex  $[\text{Au}(\text{C}_5\text{H}_5\text{NS})_2]\text{ClO}_4$ , where five of the six cations in the unit cell are linked to one another by short  $\text{Au}\cdots\text{Au}$  contacts leading to a linear chain. The sixth cation is monomeric and does not show interaction with other cations.<sup>[10]</sup> In the *c* case, dinuclear complexes with two gold centers bonded by a monoatomic bridge ligand are limited to elements of the 16 and 17 groups. Therefore, the structure proves the existence of metal–metal interactions in the cationic complex  $[\text{Au}_2(\mu\text{-Cl})(\text{PPh}_3)_2]\text{ClO}_4$ <sup>[11]</sup> or the neutral derivatives  $[\text{Au}_2(\mu\text{-X})(\text{PPh}_3)_2]$  ( $\text{X}=\text{S}$ ,<sup>[12]</sup>  $\text{Se}$ <sup>[13]</sup>). In these examples, the environment surrounding gold is almost linear and, interestingly, the  $\text{Au-X-Au}$  angle is shorter than expected from the involvement of  $p$  orbitals of the heteroatom.

An aryl group can also act as a bridging ligand, bonding the two metal atoms with a carbon center. This is

the case of the complex  $[\text{Au}_2(\mu\text{-C}_6\text{F}_5\text{H}_2)(\text{PPh}_3)_2]\text{ClO}_4$  obtained by substituting the chloro atom of the chloro-bridged complex by its reaction with  $[\text{Ag}(2,4,6\text{-C}_6\text{F}_3\text{H}_2)]$ . In this case, due to the narrow  $\text{Au-C-Au}$  angle ( $79.3^\circ$ ), a three-center two-electron bond was suggested.<sup>[14]</sup>

Other amazing cases of a single atom bridging more than two gold(I) metal centers are the complexes with  $\text{O}$ ,<sup>[15]</sup>  $\text{S}$ ,<sup>[16]</sup>  $\text{Se}$ ,<sup>[17]</sup>  $\text{N}$ ,<sup>[18,19]</sup>  $\text{P}$ ,<sup>[20]</sup> or  $\text{C}$ ,<sup>[21,22]</sup> which include striking cases of hypervalence at these atoms, a situation unknown to typical  $p$ -block chemistry or postulated as an unstable intermediate. In these examples, the aurophilic interactions seem to be the driving force that stabilizes these complexes and determines their geometry. For example, the complex  $[\text{S}(\text{AuPPh}_3)_4]^{2+}$  adopts a pyramidal structure instead of the expected tetrahedral one (Fig. 1).

On the other hand, some complexes that attracted considerable attention for the study of aurophilicity are the homo- or heterobridged diauracycles. In these complexes, the two metallic centers are bonded by two bidentate ligands such as diphosphines, *bis*(ylide) or dithiocarbamates, and intra- or intermolecular interactions appear. In most of the examples described, it is possible to observe a deviation from linearity around the gold centers caused by gold–gold interactions. Besides, the nature of the bridging ligands also has an impact on their strength. Thus, while  $[\text{Au}_2(\mu\text{-S}_2\text{CNEt}_2)_2]$  has gold–gold distances of 2.782 (intramolecular) and 3.004 Å (intermolecular), the heterobridged complex  $[\text{Au}_2(\mu\text{-(CH}_2)_2\text{PPh}_2)(\mu\text{-S}_2\text{CNEt}_2)]$  shows distances of 2.865 (intramolecular) and 2.9839 Å (intermolecular), and the complex  $[\text{Au}_2(\mu\text{-(CH}_2)_2\text{PPh}_2)_2]$  only has an intramolecular distance of 2.977 Å.<sup>[23]</sup>

A hexanuclear complex with three pairs of gold atoms displaying short contacts can be obtained by using *bis*-(diphenylphosphino)methanediide as ligand, which can act as an eight-electron donor bonded to four gold atoms. The reaction of  $[\text{Au}_2(\mu\text{-(PPh}_2)_2\text{CH}_2)_2]$  with  $[\text{Au}(\text{PPh}_3)(\text{tht})]\text{ClO}_4$  leads to a tetranuclear derivative that can be further deprotonated by reaction with  $[\text{Au}(\text{acac})(\text{PPh}_3)]$  to give the hexanuclear complex<sup>[24]</sup> (Scheme 2).

On the other hand, and as we already mentioned, gold(I) usually has a linear two-coordinate geometry. Nevertheless, three- and four-coordination, although much less abundant, is also well established.<sup>[25]</sup> Unlike linear coordination, where the gold(I) molecules are often

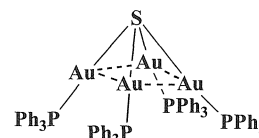
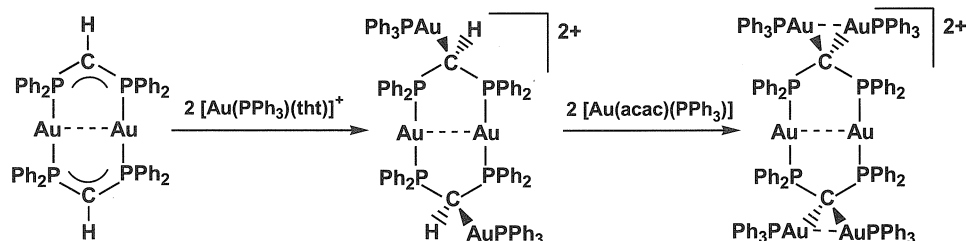


**Fig. 1** Structural arrangement of the cation  $[\text{S}(\text{AuPPh}_3)_4]^{2+}$ .



Scheme 2 Reactions from  $[\text{Au}_2(\mu\text{-(PPh}_2)_2\text{CH}_2)_2]$ .

associated to form dimers, trimers, chains, or even layers through gold–gold interactions, in the rest of geometries, the presence of these interactions is almost an anecdote. Thus, there are a few cases reported, and most are examples of gold diauracycles, where solvent molecules or anions, with a coordinating capacity, interact with one or more gold centers. For instance, this is the case of the complex  $[\text{Au}_2\text{Cl}_2(\text{dppm})_2]$ <sup>[26]</sup> with a gold–gold distance of 3.028 Å, visibly longer than that of the homologous  $[\text{Au}_2(\text{dppm})_2](\text{BF}_4)_2$  complex<sup>[27]</sup> with a distance of 2.931 Å, and with anions that do not interact with the gold atoms. In addition, the ligand coordination causes a small deviation from the original linearity in the L–Au–L angles.

An outstanding example of mixed coordination numbers and geometries of gold(I) is the complex  $[\text{Au}_2(\text{PPh}_3)_3(\text{SCH}_2\text{CH}(\text{OH})\text{CH}_2\text{OH})](\text{BF}_4)$ , where the coordination spheres of the two gold atoms are completely different. One of the atoms has a conventional linear two-coordination, whereas the other has a slightly distorted trigonal planar coordination with one sulfur and two phosphorus atoms. The gold centers exhibit a short gold–gold contact of 3.0162 Å, which is not forced by the presence of bidentate bridging ligands<sup>[28]</sup> (Fig. 2).

Che's laboratory studied the strength of the three-coordinate gold–gold interaction by Raman spectroscopy in the complex  $[\text{Au}_2(\text{dmpm})_3](\text{ClO}_4)_2$  [*dmpm* = *bis*(dime-methylphosphine)methane], with atoms that exhibit an interaction of 3.050 Å. They obtained a wave number of 79  $\text{cm}^{-1}$  for the gold–gold stretching mode. Significantly, the wave number increased to 165  $\text{cm}^{-1}$ , and the gold–gold distances decreased when the sample was irradiated

with 256 nm ultraviolet radiation, suggesting that the gold–gold interaction was strengthened in the excited state.<sup>[29]</sup> This result opens a new research field.

## GOLD(I)–GOLD(III) INTERACTIONS

In addition to gold(I), gold(III) with a  $d^8$  configuration and a square-planar geometry can be considered a closed-shell cation. Thus, interactions with other closed-shell centers such as gold(I) can be covered by the general term *auropilicity*. Nevertheless, in spite of the huge number of examples of gold(I)–gold(I) contacts, interactions involving gold(III) centers are less represented, and many times, the oxidation states of the gold atoms are not completely clear. This is the case of the complexes obtained in the reaction of double-bridge ylide derivatives with gold(I) or gold(III) precursor complexes, such as  $[\text{Au}_2(\mu\text{-(CH}_2)_2\text{PPh}_2)_2\text{Au}(\text{C}_6\text{F}_5)_3]$  obtained by reaction of the dimer  $[\text{Au}_2(\mu\text{-(CH}_2)_2\text{PPh}_2)_2]$  with the gold(III) complex  $[\text{Au}(\text{C}_6\text{F}_5)_3(\text{OEt}_2)]$ . Nevertheless, the shorter distance between the two gold(I) centers of the dimer compared with the starting product, as well as the gold(I)–gold(III) distance of just 2.572 Å, are indicative of a more convincing Au(I)–Au(II)–Au(II) sequence than the expected Au(I)–Au(I)–Au(III) one.<sup>[30]</sup>

On the other hand, the reaction between the gold(II) dimer  $[\text{Au}_2(\mu\text{-(CH}_2)_2\text{PPh}_2)_2(\text{C}_6\text{F}_5)(\text{tht})]\text{ClO}_4$  and  $\text{NBu}_4\text{[Au}(\text{C}_6\text{F}_5)_2]$  leads, after the displacement of the weakly coordinated *tht*, to a pentanuclear complex, where a formal gold(I) unit acts as a bridge between two adjacent gold(II) dimers. But, in this case, the theoretical calculations provide a sequence of Au(III)–Au(I)–Au(I)–Au(I)–Au(III) oxidation states based on the charges identified in the gold atoms.<sup>[31]</sup> Interactions in mixed-valence double-bridged ylide systems are often proposed due to the geometry of the ligands.<sup>[32–35]</sup>

Apart from these cases where the double-bridged ylide systems force the gold atoms to be in close proximity, there are some other examples where the gold(I)–gold(III)

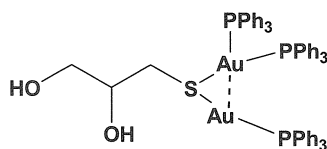


Fig. 2 Structural arrangement of the cation  $[\text{Au}_2(\text{PPh}_3)_3(\text{SCH}_2\text{CH}(\text{OH})\text{CH}_2\text{OH})]^+$ .

interaction seems not to be influenced by the ligand architecture. This is, for instance, the case of the poly nuclear sulfur-centered complex  $[\{S(Au_2^I dppf)\}\{Au^{III}(C_6F_5)_3\}]OTf$  [ $dppf=1,1'$ -bis(diphenylphosphino)ferrocene;  $OTf$ =trifluoromethylsulfonate],<sup>[36]</sup> the derivative  $[Au^IAu^{III}Me_2(C_4F_6(PMe_3)_2)]$ <sup>[37]</sup> or the novel  $[Au^{III}(C_6F_5)_2\{PPh_2C_6H_4N(Au^IPPh_3)_2\}]ClO_4$ ,<sup>[38]</sup> which have Au(I)–Au(III) distances close to 3.3 Å.

Finally, the case of interacting gold(III) centers with a  $d^8$  configuration is unknown. Even with the most appropriate structural arrangement, i.e., a single atom bridging two gold(III) metal centers, this type of interaction does not appear. Examples of this are, among others,  $[S(AuPPh_3)_2(Au(C_6F_5)_3)_2]$ <sup>[39]</sup> or  $[Se(AuPPh_3)_2(Au(C_6F_5)_3)_2]$ .<sup>[40]</sup> In all these cases, the Au(III)–Au(III) distances are longer than the sum of their van der Waals radii.

## FUTURE PERSPECTIVES

The great development of structural analyses in the last few years allowed us to realize that the interactions among metal centers at distances shorter than the sum of their van der Waals radii are not exclusive to homometallic gold systems. In fact, they also appear in molecules containing gold and other closed-shell metal centers. Therefore, words such as auophilicity or auophilic interactions are being replaced with more general terms such as metallophilicity or metallophilic interactions. Apart from the unquestionable interest of these molecules from a theoretical point of view, recent studies on their synthesis are being performed due to their fascinating and unique physicochemical properties, properties such as luminescence or conductivity, for instance, which might be exploited by industry in the near future.<sup>[41]</sup>

There are many examples of heterometallic molecules with gold-closed-shell interactions, including ions such as Rh(I), Ir(I), Pd(II), or Pt(II) with a  $d^8$ -square planar configuration, or Cu(I), Ag(I), or Hg(II) and Tl(I) and Pb(II) with  $d^{10}$  and  $s^2$  configurations, respectively.<sup>[4,5]</sup> A recent ab initio study on bridged dinuclear Au–Ag and Au–Cu molecules concludes that the presence of just one gold atom is enough to induce metallophilic attractions in their group congeners and that this effect can be modulated depending on the gold ligand<sup>[42]</sup> involved. In this case, the relativistic effects of gold force a numismophilicity. On the other hand, theoretical studies on an Au–Pd interaction show that the dispersion is the key contribution to the Pd(II)–Au(I) attraction, whereas the charge-transfer type contributions are about half as important, considering that the two contributions  $Pd \rightarrow Au$  and  $Au \rightarrow Pd$  are energetically comparable.<sup>[43]</sup>

In short, it is clear that gold makes an essential contribution to metallophilic interactions. Thus, the design of synthetic strategies to prepare systems with these bonds of unique versatility and flexibility must include gold as an essential building block.

## ACKNOWLEDGMENT

We thank the Dirección General de Investigación (M.C.T.)(BQU2001-2409) for financial support.

## ARTICLES OF FURTHER INTEREST

*Cation– $\pi$  Interactions*, p. 214

*Hydrogen Bonding*, p. 658

*Hydrogen Bonds to Metals and Metal Hydrides*, p. 666

*Second-Sphere Coordination*, p. 1209

*Secondary Bonding*, p. 1215

*X-Ray Crystallography*, p. 1586

## REFERENCES

- Schmidbaur, H. The fascinating implications of new results in gold chemistry. *Gold Bull.* **1990**, 23, 11.
- Schmidbaur, H. High-carat gold compounds. *Chem. Soc. Rev.* **1995**, 24, 391.
- Schmidbaur, H. The auophilicity phenomenon: A decade of experimental finding, theoretical concepts and emerging applications. *Gold Bull.* **2000**, 33, 3.
- Pyykkö, P. Strong closed-shell interactions in inorganic chemistry. *Chem. Rev.* **1997**, 97, 597.
- Kaltsoyannis, N. Relativistic effects in inorganic and organometallic chemistry. *J. Chem. Soc. Dalton Trans.* **1997**, 1.
- Pyykkö, P.; Runeberg, N. Predicted ligand dependence of the Au(I)···Au(I) attraction in  $(XauPh_3)_2$ . *Chem. Phys. Lett.* **1994**, 218, 133.
- Assefa, Z.; McBurnett, B.G.; Staples, R.J.; Fackler, J.P., Jr. Structures and spectroscopic properties of gold(I) complexes of 1,3,5-Triaza-7-phosphaadamantane (TPA). 2. Multiple-state emission from  $(TPA)AuX$  ( $X = Cl, Br, I$ ) complexes. *Inorg. Chem.* **1995**, 34, 4965.
- Assefa, Z.; McBurnett, B.G.; Staples, R.J.; Fackler, J.P., Jr.; Assmann, B.; Angermaier, K.; Schmidbaur, H. Synthesis, structures, and spectroscopic properties of gold(I) complexes of 1,3,5-Triaza-7-phosphaadamantane (TPA). Correlation of the supramolecular Au···Au interaction and photoluminescence for the species  $(TPA)AuCl$  and  $[(TPA-HCl)AuCl]$ . *Inorg. Chem.* **1995**, 34, 3475.

9. Pyykkö, P.; Runeberg, N.; Mendizábal, F. Theory of the  $d^{10}$ - $d^{10}$  closed-shell attraction: 1. Dimers near equilibrium. *Chem. Eur. J.* **1997**, *3*, 1451.
10. Usón, R.; Laguna, A.; Laguna, M.; Jiménez, J.; Gómez, M.P.; Jones, P.G. Gold complexes with heterocyclic thiones as ligands. X-ray structure determination of  $[\text{AuC}_5\text{H}_5\text{NS}]_2(\text{ClO}_4)$ . *J. Chem. Soc. Dalton Trans.* **1990**, 3457.
11. Jones, P.G.; Sheldrick, G.M.; Usón, R.; Laguna, A.  $\mu$ -Cl-bis(triphenylphosphine)digold(I) perchlorate, dichloromethane solvate. *Acta Crystallogr.* **1980**, *B36*, 1486.
12. Lensch, C.; Jones, P.G.; Sheldrick, G.M. Crystal structures of the selenide- and sulfide-bridged gold(I) complexes  $[\text{Se}(\text{AuPPh}_3)_3]\text{PF}_6$  and  $[\text{S}(\text{AuPPh}_3)_2\cdot\text{CH}_2\text{Cl}_2]$ . *Z. Naturforsch* **1982**, *37b*, 944.
13. Li, J.; Pyykkö, P. Relativistic pseudo-potential analysis of the weak gold(+1)-gold(+1) attraction. *Chem. Phys. Lett.* **1992**, *197*, 586.
14. Usón, R.; Laguna, A.; Fernández, E.J.; Mendía, A.; Jones, P.G. (Polyhalophenyl)silver(I) complexes as arylating agents: Crystal structure of  $[(\mu\text{-}2,4,6\text{-C}_6\text{F}_3\text{H}_2(\text{AuPPh}_3)_2)\text{ClO}_4]$ . *J. Organomet. Chem.* **1988**, *350*, 129.
15. Schmidbaur, H.; Hofreiter, S.; Paul, M. Synthesis of the gold analog of the elusive doubly protonated water molecule. *Nature* **1995**, *377*, 503.
16. Canales, F.; Gimeno, M.C.; Jones, P.G.; Laguna, A. Auropphilicity at sulfur centers: Synthesis and structure of the tetragold species  $[(\text{PPh}_3\text{PAu})_4\text{S}](\text{CF}_3\text{SO}_3)_2\cdot 2\text{CH}_2\text{Cl}_2$ . *Angew. Chem., Int. Ed. Engl.* **1994**, *33*, 769.
17. Canales, S.; Crespo, O.; Gimeno, M.C.; Jones, P.G.; Laguna, A. Synthesis of the first gold complex with a central  $\mu^4$ -seleninido ligand. *J. Chem. Commun.* **1999**, 679.
18. Grohmann, A.; Riede, J.; Schmidbaur, H. Electron-deficient bonding at pentacoordinate nitrogen. *Nature* **1990**, *345*, 140.
19. Schier, A.; Grohmann, A.; López-de-Luzuriaga, J.M.; Schmidbaur, H. The elusive structures of pentakis(triphenylphosphine)gold[jammonium(2+) bis[tetrafluoroborate(1-)]]. *Inorg. Chem.* **2000**, *39*, 547.
20. Bachman, R.E.; Schmidbaur, H. Isolation and structural characterization of  $[\text{P}(\text{AuPPh}_3)_5](\text{BF}_4)_2$  via cleavage of a P-P bond by cationic gold fragments. Direct evidence of the structure of the elusive tetrakis[phosphineaurio(I)]phosphonium(+) cation. *Inorg. Chem.* **1996**, *35*, 1399.
21. Scherbaum, F.; Grohmann, A.; Huber, B.; Krüger, C.; Schmidbaur, H. "Auropphilicity" as a consequence of relativistic effects: The hexakis(triphenylphosphineaurio)methane dication  $[(\text{Ph}_3\text{PAu})_6\text{C}]^{2+}$ . *Angew. Chem., Int. Ed. Engl.* **1988**, *27*, 1544.
22. Scherbaum, F.; Grohmann, A.; Müller, G.; Schmidbaur, H. Synthesis, structure and bonding of the cation  $[(\text{C}_6\text{F}_5)_3\text{PAu}]_5\text{C}^{+}$ . *Angew. Chem., Int. Ed. Engl.* **1989**, *28*, 463.
23. Bardají, M.; Connelly, N.G.; Gimeno, M.C.; Jiménez, J.; Jones, P.G.; Laguna, A.; Laguna, M. Synthesis of dinuclear gold(I) ring complexes containing two different bridging ligands. Crystal structure of  $[\text{Au}_2\{\mu\text{-(CH}_2)_2\text{PPh}_2\}(\mu\text{-S}_2\text{CNEt}_2)]$ . *J. Chem. Soc. Dalton Trans.* **1994**, 1163.
24. Fernández, E.J.; Gimeno, M.C.; Jones, P.G.; Laguna, A.; Laguna, M.; López-de-Luzuriaga, J.M. A hexanuclear gold(I) complex:  $[\{(\text{Ph}_3\text{PAu})_2\text{C}(\text{PPh}_2\text{AuPPh}_2)_2\}(\text{ClO}_4)_2]$ . *Angew. Chem., Int. Ed. Engl.* **1994**, *33*, 87.
25. Gimeno, M.C.; Laguna, A. Three- and four-coordinate gold(I) complexes. *Chem. Rev.* **1997**, *97*, 511.
26. Schmidbaur, H.; Wohleben, A.; Schubert, U.; Frank, A.; Huttner, G. Synthese und Kristallstruktur achtgliedriger Ringverbindungen von gold(I) mit Au-Au-Wechselwirkung. *Chem. Ber.* **1977**, *110*, 2751.
27. Porter, L.C.; Khan, N.I., Md.; King, C.; Fackler, J.P., Jr. Structure of the bis[bis(diphenylphosphino)methane]digold(I) cation in  $[\text{Au}_2(\text{dppm})_2](\text{BF}_4)_2$ . *Acta Crystallogr., C* **1989**, *45*, 947.
28. López-de-Luzuriaga, J.M.; Sladek, A.; Schmidbaur, H. Mixed coordination numbers and geometries of gold(I) in a dinuclear complex of thioglycerol. *J. Chem. Soc. Dalton Trans.* **1996**, 4511.
29. Leung, K.H.; Phillips, D.L.; Mao, Z.; Che, C.M.; Miskowski, V.M.; Chan, C.K. Electronic excited states of  $[\text{Au}_2(\text{dmpm})_3](\text{ClO}_4)_2$  (dmpm = bis(dimethylphosphine)-methane). *Inorg. Chem.* **2002**, *41*, 2054.
30. Usón, R.; Laguna, A.; Laguna, M.; Tartón, M.T.; Jones, P.G. The first example of a direct formal gold(I)-gold(III) bond. Synthesis and structure of  $[\{\text{Au}(\text{CH}_2)_2\text{PPh}_2\}_2\text{Au}(\text{C}_6\text{F}_5)_3]$ . *J. Chem. Soc., Chem. Commun.* **1988**, 740.
31. Usón, R.; Laguna, A.; Laguna, M.; Jiménez, J.; Jones, P.G. A mixed-valent pentanuclear gold complex containing a linear  $\text{Au}_5$  chain. *Angew. Chem., Int. Ed. Engl.* **1991**, *30*, 198.
32. Mazany, A.M.; Fackler, J.P., Jr. Isomeric species of  $[\text{AuCH}_2\text{P}(\text{S})(\text{C}_6\text{H}_5)_2\text{I}]_2$ . Mixed-valent Au(I)/Au(III) and isovalent Au(II)/Au(II) complexes with the same methylenethiophosphinate ligand. *J. Am. Chem. Soc.* **1984**, *106*, 801.
33. Fackler, J.P., Jr.; Trzcinska-Bancroft, B. Isomerization of a symmetrical metal-metal bonded gold(II) ylide dimer to a mixed-valence gold(III)/gold(I) species. *Organometallics* **1985**, *4*, 1891.
34. Raptis, R.G.; Porter, L.C.; Emrich, R.J.; Murray, H.H.; Fackler, J.P., Jr. Synthesis of a mixed-valence  $\text{Au}^{\text{I}}/\text{Au}^{\text{III}}$  complex,  $\{\text{Au}(\text{CH}_2)_2\text{PPh}_2\}_2\text{Br}_2$ , and its characterization by x-ray crystallography and x-ray photoelectron-spectroscopy. *Inorg. Chem.* **1990**, *29*, 4408.
35. Schmidbaur, H.; Hartmann, C.; Reber, G.; Müller, G. Isovalent and mixed-valent ylide complexes of gold: The synthesis of trinuclear compounds having double paddle-wheel structure. *Angew. Chem., Int. Ed. Engl.* **1987**, *26*, 1146.
36. Calhorda, M.J.; Canales, F.; Gimeno, M.C.; Jiménez, J.; Jones, P.G.; Laguna, A.; Veirós, L.F. Gold(I)-gold(III) interactions in polynuclear sulfur-centered complexes. Synthesis and structural characterization of  $[\text{S}(\text{Au}_2\text{dppf})\{\text{Au}(\text{C}_6\text{F}_5)_3\}]$  and  $[\{\text{S}(\text{Au}_2\text{dppf})\}_2\{\text{Au}(\text{C}_6\text{F}_5)_2\}]\text{OTf}$  (dppf = 1,1'-bis(diphenylphosphino)ferrocene). *Organometallics* **1997**, *16*, 3837.



37. Jarvis, J.A.; Johnson, A.; Puddephatt, R.J. The mechanism of insertion of an acetylene into the methylgold bond: Structure of a reaction intermediate. *J. Chem. Soc., Chem. Commun.* **1973**, 373.
38. Fernández, E.J.; Gil, M.; Olmos, M.E.; Crespo, O.; Laguna, A.; Jones, P.G. The ability of a Au<sub>3</sub>-N unit to bond two aurophilically interacting gold(I) centers. *Inorg. Chem.* **2001**, *40*, 3018.
39. Canales, F.; Gimeno, M.C.; Laguna, A.; Jones, P.G. Synthesis and structural characterization of tetranuclear sulfur-centered complexes with mixed-valent gold atoms: [S(Au<sub>2</sub>dppf){Au(C<sub>6</sub>F<sub>5</sub>)<sub>3</sub>}<sub>2</sub>] (dppf = 1,1'-bis(diphenylphosphino)ferrocene) and [S(AuPPh<sub>3</sub>)<sub>2</sub>{Au(C<sub>6</sub>F<sub>5</sub>)<sub>3</sub>}<sub>2</sub>]. *Organometallics* **1996**, *15*, 3412.
40. Canales, O.; Crespo, O.; Gimeno, M.C.; Jones, P.G.; Laguna, A.; Mendizábal, F. Mixed gold(I)-gold(III) complexes with bridging selenido ligands. Theoretical studies of the gold(I)-gold(III) Interactions. *Organometallics* **2001**, *20*, 4985.
41. Fernández, E.J.; Laguna, A.; López-de-Luzuriaga, J.M. Luminescence in gold-heterometal complexes. *Gold Bull.* **2001**, *34*, 14.
42. Fernández, E.J.; López-de-Luzuriaga, J.M.; Monge, M.; Rodríguez, M.A.; Crespo, O.; Gimeno, M.C.; Laguna, A.; Jones, P.G. Heteropolynuclear complexes with the ligand PPh<sub>2</sub>CH<sub>2</sub>SPh. Theoretical evidence of relativistic Au-M interactions. *Chem. Eur. J.* **2000**, *6*, 636.
43. Crespo, O.; Laguna, A.; Fernández, E.J.; López-de-Luzuriaga, J.M.; Jones, P.G.; Teichert, M.; Monge, M.; Pyykkö, P.; Runeberg, N.; Schütz, M.; Werner, H. Experimental and theoretical studies of the d<sup>8</sup>-d<sup>10</sup> interactions between Pd(II) and Au(I): bis(chlorophenylthiomethyldiphenylphosphinegold(I))dichloropalladium (II) and related systems. *J. Inorg. Chem.* **2000**, *39*, 4786.

# Biological Ligands

Andrew Hinton

Paul Taylor

Malcolm D. Walkinshaw

University of Edinburgh, Edinburgh, United Kingdom

## INTRODUCTION

The binding of a small-molecule ligand to a protein enzyme or receptor is governed by a host of weak non-bonding electrostatic effects like hydrogen bonds and van der Waals interactions. Entropic changes caused by displacement of water and by changes in ligand flexibility are also important in determining binding strength. An understanding of these processes is crucial for the design of novel enzyme inhibitors and other protein ligands. This is an area of great importance in the pharmaceutical industry, where more protein targets are becoming available. We now have high-resolution structures of over 1700 protein–ligand complexes as determined by protein x-ray crystallography.<sup>[1]</sup> This information coupled with the measured binding data of many protein–ligand systems is now providing insight into what factors are important for ligand binding. We provide a broad overview of the field, with examples of structures from a variety of ligand classes (Table 1). Current computational approaches for discovering new ligands and estimating the strength of ligand binding are also described.

## ENERGETICS OF PROTEIN–LIGAND INTERACTIONS

The simple picture of protein–ligand binding is given by a bimolecular equilibrium (Eq. 1) in which a ligand in solution binds to the receptor protein to form a complex. In the context of this article, we define a ligand to be a mainly organic molecule with a molecular weight of up to 1500 Dalton, which may be reasonably expected to form a complex with a protein. We restrict our discussion to noncovalent complexes, though as in the case of enzymatic reactions or the binding of suicide inhibitors, covalent bonds can frequently be formed. The binding constant (or equilibrium constant) relates the concentrations of free and bound components.



where  $K_d = [P][L]/[P \cdot L]$  or (the reverse reaction)  $K_b = [P \cdot L]/[P][L]$ ,  $K_d$  = dissociation constant,  $K_b$  = binding constant,  $[P \cdot L]$  = concentration of protein–ligand complex,  $[P]$  = concentration of unbound protein, and  $[L]$  = concentration of unbound ligand.

Drug–protein interactions tend to have dissociation constants ( $K_d$ ) in the nanomolar to picomolar range. In the field of drug discovery, so-called lead ligands with potentials for being developed into drug candidates bind to their target proteins with  $K_d$  values in the micromolar range. The dissociation constants<sup>[2]</sup> can be converted (Eq. 2) to binding energies from the following:

$$\begin{aligned} \Delta G^\circ &= -RT \ln K_d \\ &= -5.6 \log_{10} K \\ &\times (\text{at room temperature } 20^\circ\text{C or } 293^\circ\text{K}) \end{aligned} \quad (2)$$

where  $K_d$  = dissociation constant (Mol),  $\Delta G^\circ$  = Gibbs free energy change of the reaction ( $\text{kJ mol}^{-1}$ ),  $R = 8.31$  ( $\text{J}^\circ \text{mol}$ ), and  $T$  = temperature ( $^\circ\text{K}$ ).

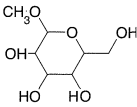
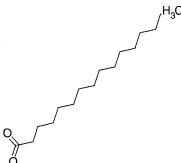
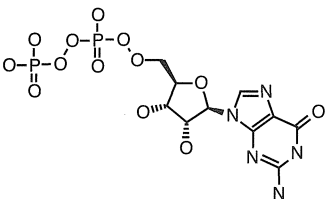
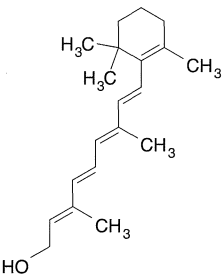
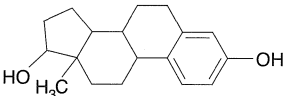
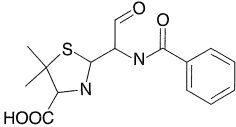
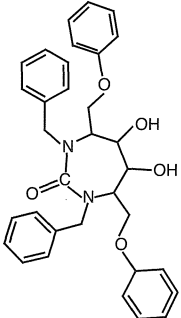
Thus, a change in the binding constant by an order of magnitude only corresponds to a difference in binding energy of about 5.6 kJ/mol. A  $K_d$  of  $10^{-9}$  M gives a calculated dissociation energy of +50.4 kJ/mol (which equals a free energy of binding of  $-50.4$  kJ/mol), while a ligand that binds with a micromolar  $K_d$  has a dissociation energy of +33.6 kJ/mol (see also Table 5).

This overall binding energy can be regarded as consisting of a number of components including hydrogen bonding, van der Waals interactions, and other thermodynamic terms. Approximate energies for these components (Table 2) were calculated by correlating structural data with measured thermodynamic binding data.<sup>[3,4]</sup> A number of empirical energy terms were published, and one such example is shown in Eq. 3.<sup>[3,4]</sup>

$$\begin{aligned} \Delta G_{\text{binding}} &= \Delta G_0 + \Delta G_{\text{polar}} + \Delta G_{\text{apolar}} + \Delta G_{\text{solv}} \\ &\quad + \Delta G_{\text{flexi}} \end{aligned} \quad (3)$$

As shown in Table 2,  $\Delta G_0$ ,  $\Delta G_{\text{hb}}$ ,  $\Delta G_{\text{ion}}$ ,  $\Delta G_{\text{rot}}$ ,  $\Delta G_{\text{aro}}$ , and  $\Delta G_{\text{esrep}}$  are enthalpic terms that describe contributions made by H-bond, ionic, rotational, aromatic, and nonspecific interaction energies. The  $\Delta G_{\text{lipo}}$  includes lipophilic

**Table 1** Selected PDB entries of protein–ligand complexes indicating structural diversity and biological function

Biological class	Protein–ligand complex		Ligand structure	PDB ID
Saccharide	Porcine pancreatic amylase	Pseudo-octasaccharide		1PIG
	Human lysozyme	V-1532 (trestatin A)		1LZS
	Strep. <i>Pneumonia</i>	Hexa- <i>N</i> -acetyl-chitohexose		1C82
	hyaluronate Lysase	Hyaluronic acid		
Lipid	<b>Concanavalin-A</b>	<b>Alpha-methyl-D-mannopyranoside<sup>a</sup></b>		<b>5CNA</b>
	Human serum albumin	Decanoic acid		1E7F
	<b>Bovine β-lactoglobulin</b>	<b>Palmitate<sup>a</sup></b>		<b>1BO0</b>
	Mycobacterium tuberculosis enoyl-ACP reductase	Hexadecenoyl-thioester		1BVR
	RAt P-450:nadph-p450 reductase	Butenoic acid		1LFO
Signal molecule	Rat phosphatidylinositol transfer protein (Pitp)	Phosphatidylcholine		1FVZ
	<b>Catalytic domain of human c-H-ras p21.</b>	<b>Guanosine diphosphate<sup>a</sup></b>		<b>4Q21</b>
	Growth factor receptor-bound protein 2	Phosphatytrosyl heptapeptide		1TZE
Retinol related	<b>Rat cellular retinol binding Protein c-RBP</b>	<b>Trans-retinol</b>		<b>1CRB</b>
	Bovine plasma retinol-binding protein (bRBP)	Fenretinide		1FEL
Steroid	Rat α-hydroxysteroid dehydrogenases (3 α-HSDs)	Testosterone		1AFS
	Human sex hormone-binding globulin (SHBG)	Dihydrotestosterone, (androgen)		1D2S
	<b>17-β-hydroxysteroid dehydrogenase</b>	<b>17-β-estradiol (estradiol)<sup>a</sup></b>		<b>1FDT</b>
Antibiotic	<b>β-Lactamase mutant</b>	<b>Penicillin-G (open)<sup>a</sup></b>		<b>1GHP</b>
		<b>Cephaloridine</b>		<b>1GHM</b>
Drug molecule	<b>HIV-1, protease</b>	<b>C33-cyclic urea inhibitor Aha001<sup>a</sup></b>		<b>1AJX</b>
Drug molecule	Human rhinovirus, 16 coat protein	Vp63843 (Pleconaril)		1C8M
Drug molecule	Influenza virus, neuraminidase	Carboxamide inhibitor		2QWK
Thyroxine	Human transthyretin (TTR)	Thyroxine		2ROX

<sup>a</sup>Denotes structure shown.

Source: From Ref. [1].

**Table 2** The relationship and approximate value of individual energy terms to the change in Gibbs free energy of binding ( $\Delta G$ )

Energy component	Value (kJ/mol)	Interaction type	Example
$\Delta G_0$	-2.8	$\Delta G_0$	Nonspecific
$\Delta G_{hb}$	-3.2	$\Delta G_{polar}$	$=O:---H---O$
$\Delta G_{ionic}$	-5.7	$\Delta G_{polar}$	$NH_4^+---COO^-$
$\Delta G_{lipo}$	-0.09	$\Delta G_{solv}$	$C_n---H_2O$
$\Delta G_{rot}$	+1.0	$\Delta G_{flexi}$	$C---CH_3$ Rotation about single bond
$\Delta G_{aro}$	-2.6	$\Delta G_{apolar}$	$C---C$
$\Delta G_{lipo\ water}$	-1.3	$\Delta G_{solv}$	$C_n---H_2O$
$\Delta G_{esrep}$	+0.5	$\Delta G_{polar}$	$NH_4^+---COO^-$

interaction energy as a function of all pair-wise atom–atom interaction energies. The  $\Delta G_{lipo\ water}$  describes energy change through desolvation effects. These energy terms contribute to a simple representation of the components that make up  $\Delta G_{binding}$ , including polar ( $\Delta G_{polar}$ ), apolar

( $\Delta G_{apolar}$ ), solvation ( $\Delta G_{solv}$ ), and flexibility ( $\Delta G_{flexi}$ ) interactions as given in Eq. 3. Approximate energies for these terms were calculated by correlating structural data with measured thermodynamic binding data.<sup>[3,4]</sup>

## MEASUREMENT OF LIGAND BINDING STRENGTH

A number of spectroscopic and thermodynamic measurements can be used to measure the strength of protein–ligand interactions, including fluorescence spectroscopy, surface plasmon resonance, calorimetry, and enzyme inhibition. The change in property (for example, fluorescence signal,<sup>[5]</sup> heat of reaction,<sup>[6]</sup> crystallographic occupancy,<sup>[7]</sup> and NMR chemical shift<sup>[8]</sup>) is measured as a function of increasing concentration of added ligand until a maximum signal is obtained. For a simple protein–ligand binding experiment (with no substrate or other inhibitory ligand present), the  $K_d$  value can be simply determined by titrating a ligand solution into a protein solution of known concentration. The  $K_d$  is the slope of

**Table 3** Techniques for measuring binding constants

Technique	Description	Example	Ref.
NMR ( $^{15}N$ -HSQC)	Observation of change in two-dimensional $^1H$ - or $^{15}N$ -heteronuclear single quantum correlation (HSQC) backbone chemical shift spectra upon ligand binding; described as $\Delta\delta(^1H, ^{15}N) = [L]/([L] + K_d)$	FKBP	[9]
Fluorescence spectrophotometry	Measurement of fluorescence signal quenching of an active-site tryptophan as a function of ligand binding; described as $\Delta F = \Delta F_{max} - K_d(\Delta F/[L])$	FKBP	[5]
X-ray crystallography	Crystallographic refinement of ligand occupancy from a range of ligand soaking concentrations	Cyclophilin	[7]
Isothermal calorimetry (ITC)	Isothermal titration calorimetry (ITC) measures the enthalpy change caused by a binding event; the gradient of the generated ITC curve can be used to determine the binding constant $K_b$	OppA	[10]
Surface plasmon resonance (SPR)	SPR-biosensors measure the change in refractive index units (RU) of a solvent near the surface that occurs during complex formation with an immobilized protein target	HIV1-protease	[6]
Enzyme inhibition	The measurement of the rate (v) of products/reactants formation can be measured by spectrophotometry; the dissociation constant $K_d$ corresponds to the concentration of inhibitor at which the observed constant ( $k_{obs}$ ) is half its maximum value	Bovine cyclophilin	[9]

the straight-line plot of  $[PL]$  against  $[PL]/[L]$  used to fit Eq. 4.

$$[PL] = P_o - K_d([PL]/[L]) \quad (4)$$

where  $[PL]$  = concentration of the ligated protein,  $[L]$  = concentration of the ligand, and  $[P_o]$  = total protein concentration.

The  $IC_{50}$  value is the ligand concentration that produces 50% reduction (or increase) in the measured effect (i.e., the concentration of unbound protein  $[P]$  equals the concentration of ligand-bound protein  $[PL]$ ). For a simple binary protein–ligand mixture, the dissociation constant  $K_d$  is identical to the  $IC_{50}$  value.

In Table 3, a description of different techniques employed in the measurement of binding constants is presented, where  $\Delta\delta(^1H, ^{15}N)$  is the average weighted change in  $^{15}N$ - or  $^1H$ -amide chemical shift in two-dimensional  $^1H$ - or  $^{15}N$ -heteronuclear single quantum correlation (HSQC) spectra, where  $[L]$  and  $K_d$  are ligand concentration and dissociation constants, respectively. The  $\Delta F$  and  $\Delta F_{max}$  is the change in fluorescence measured at 340 nm.

The relationship between  $IC_{50}$  and  $K_d$  (Eq. 5) for competitive enzyme inhibition or competitive receptor ligand studies is complicated by the additional presence of substrate (S). Note that in such experiments,  $K_d$  the dissociation constant and  $K_i$  the inhibition constant can be used synonymously:

$$K_i = IC_{50} * K_m / ([S] + K_m) \quad (5)$$

where  $K_i$  = equilibrium dissociation constant of the inhibitor ligand,  $IC_{50}$  = inhibitor concentration that produces 50% change in the measured effect,  $[S]$  = substrate concentration used in the assay, and  $K_m$  = substrate concentration (in the absence of inhibitor) at which the velocity of the reaction is half-maximal.

The  $K_i$  is an equilibrium dissociation constant corresponding to the concentration of the inhibitor ligand  $[I]$  that would bind to half of the binding sites at equilibrium (in the absence of other substrates). If  $[S]$  is small (usually in the nanomolar range) and the  $IC_{50}$  is in the micromolar range, then measured  $IC_{50}$  still closely approximates the  $K_i$ .

## FINDING NEW LIGANDS

Over the last 10 years, the pharmaceutical industry invested in automating high-throughput screening (HTS) methods that enable libraries of ligands consisting of over 250,000 compounds to be screened in biological assays. A typical threshold for a hit is binding to or inhibiting a ligand with a  $K_i$  of less than about  $10^{-6}$  M. It was es-

timated that it takes over 2 million trials to discover one lead compound (roughly defined as a ligand that proceeds to preclinical trials). A complementary approach to high-throughput screening is a structure-based computer-aided approach. A prerequisite is the availability of an accurate three-dimensional structure of the protein target. The protein data bank PDB<sup>[11]</sup> now contains nearly 20,000 entries mainly determined by protein x-ray crystallography. Of these, over 650 are different domain folds,<sup>[11]</sup> and 1700 are protein–ligand complexes.<sup>[11]</sup>

The structure of a protein's ligand-binding pocket provides a template into which novel (mainly inhibitory) ligands can be designed and visualized with the aid of computer graphics. The traditional method is to make use of a known inhibitor complex and make small changes to the ligand to modify the binding properties. This is exemplified in the development of influenza neuraminidase antivirals.<sup>[12]</sup> Prior to the elucidation of the crystal structure of influenza neuraminidase, *N*-acetylneuraminic (Neu5Ac) inhibitors had  $K_i$  values of above 1  $\mu$ M. Knowledge of the enzyme structure allowed the addition of the bulky basic substituents at the 4-position to produce the 4-guanidino-Neu5Ac2en. Known as Zanamivir, this compound has a  $K_i$  of 0.1 nM. An ester prodrug of a cyclohexene–carboxylic derivative of Zanamivir called GS4071 was resolved to 1.8 Å (2QWK) complexed with wild-type neuraminidase. GS4071 has subnanomolar potency against Types A and B influenza neuraminidase.<sup>[12]</sup> An overlay of the crystal forms of wild-type neuraminidase complexed with GS4071 and a carboxy-amide analogue (G2800) can be seen in Fig. 1.

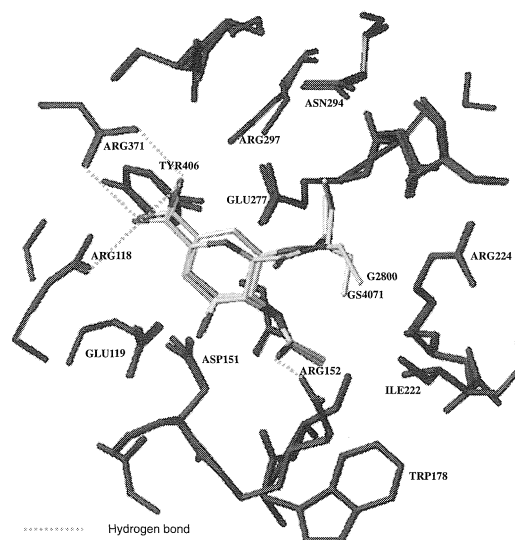


**Fig. 1** A superimposition of two neuraminidase–inhibitor complexes. (View this art in color at [www.dekker.com](http://www.dekker.com).)

Shown in Fig. 1 is a superimposition of the inhibitor GS4071 and a carboxyamide analogue crystallized with wild-type influenza neuraminidase. The clinical inhibitor GS4071 (2QWK) and the carboxyamide analogue G2800 (2QWG) can be seen to be making a range of electrostatic and hydrophobic interactions with the residues of the sialic acid-binding pocket of wild-type influenza neuraminidase (blue).<sup>[12]</sup>

## COMPUTATIONAL TECHNIQUES IN LIGAND DISCOVERY

### De novo Design, Database Mining, and Filtering

A more radical approach is to attempt the design of completely novel entities in the binding pocket with the required complementarity of shape and charge properties. Computer programs such as LUDI<sup>[13]</sup> and SMOG<sup>[14]</sup> use libraries of small chemical building blocks to generate such theoretical inhibitors.

Another related computational approach to ligand discovery is the method of database mining. Here, the HTS approach is essentially carried out in-silico. Libraries of small molecules are converted to three-dimensional structures using molecular mechanics methods incorporated into programs such as CONCORD<sup>[15]</sup> and CORINA.<sup>[16]</sup> These three-dimensional libraries of small molecules can, in theory, contain almost infinite numbers of potential ligands. In practice, it is convenient to consider compounds that are already (commercially) available. The Available Chemicals Database (ACD),<sup>[17]</sup> for example, contains some 260,000 compounds and is frequently used as the basis for database mining trials.

Further prescreening steps in the search for potential drug ligands can be made by excluding molecules with properties that make them unlikely to be biologically ac-

cessible. These properties are summarized in Lipinski's Rules,<sup>[18]</sup> which are based on the fact that 2245 known small molecular drugs (as cataloged in the USAN<sup>[19]</sup>) show poor absorption or permeation when the following occur:

1. There are more than five H-bond donors (expressed as the sum of OHs and NHs).
2. The molecular weight is over 500.
3. The LogP is over 5.
4. There are more than 10 H-bond acceptors (expressed as the sum of Ns and Os).

LogP is a partition coefficient defined as the ratio of concentrations of a compound in aqueous phase to the concentration in an immiscible solvent (e.g., octanol). According to Ghose et al.,<sup>[20]</sup> 80% of all drugs fall in the range of 160–480 Da, with an average of 357 Da, and have calculated log P values in the range of –0.4–5.6, with an average value of 2.3. Theoretically, there are at least  $10^{12}$  compounds that would fit these Lipinski criteria. (The estimate is based on molecules derived from consideration of a tetrahedral lattice of 20 points, each of which can be occupied by four possible substituents.) Current HTS approaches, even using libraries of 1 million compounds, are therefore sampling less than one millionth of potential ligands.

### Automated Docking

A number of computer programs are now available to carry out the automated docking of molecules selected from databases into the protein-binding pocket.

Shown in Fig. 2 is a schematic representation of the stages of automated docking of ligands into a protein-binding pocket. The stages include the generation of a description of a binding pocket using spheres or grid points (1), matching the ligand to the points or spheres (2). Finally, the fitted ligand is given an energy score (3).

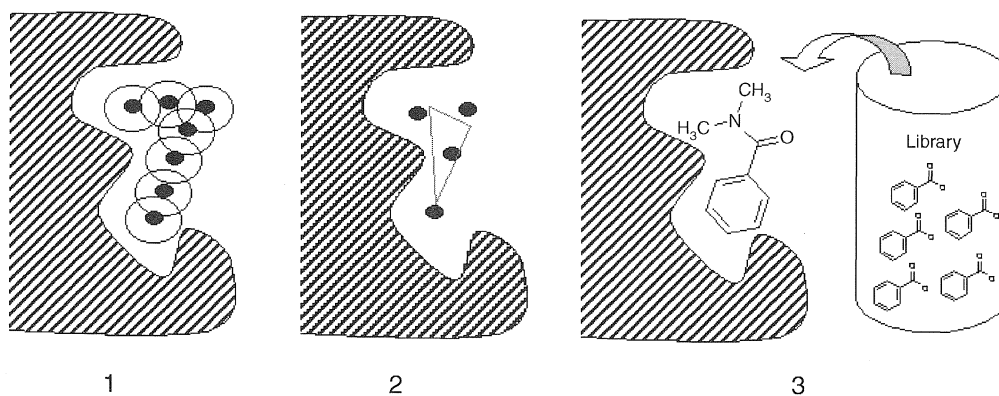


Fig. 2 Stages of automated docking.

**Table 4** Scoring functions employed in docking algorithms

Docking algorithm	Scoring functions	Attributes	Ref.
GLIDE	$\Delta G_{\text{binding}} = \Delta G_0 + \Delta G_{\text{hbond}} \sum_{il} g_1(\Delta r) g_2(\Delta \alpha)$ $+ \Delta G_{\text{metal}} \sum_{aM} f(r_{aM}) + \Delta G_{\text{lipo}} \sum_{IL} f(r_{IL})$ $+ \Delta G_{\text{rot}} H_{\text{rot}}$ <p><math>\Delta G_0</math> is a nonspecific energy term. <math>\Delta G_{\text{hbond}} \sum_{il} g_1(\Delta r) g_2(\Delta \alpha)</math> is an H-bond term between ligand and receptor atoms with an ideal bond length and angle deviation penalty. <math>\Delta G_{\text{metal}} \sum_{aM} f(r_{aM})</math> is a term accounting for metal atoms. <math>\Delta G_{\text{lipo}} \sum_{IL} f(r_{IL})</math> accounts for lipophilic atoms. <math>\Delta G_{\text{rot}} H_{\text{rot}}</math> is a flexibility penalty for frozen bonds.</p>	<ul style="list-style-type: none"> <li>Screens at 6 min per ligand</li> <li>Includes entropic flexibility penalty</li> <li>Lipophilic terms account for long-range terms</li> <li>Incorporates metal ligand binding</li> </ul>	[24]
GOLD	$\text{Score} = \sum (-E_{\text{pair}} - (E_{ij} + (E_{ijkl} + E_{ij})))$ $= -\text{H-bond energy} - (\text{Internal energy} + \text{Complex energy})$ <p><math>E_{\text{pair}}</math> is a weighted H-bond interaction energy term between donor–acceptor atom pairs, accounting for water displacement. <math>E_{ij}</math> is a ligand steric energy using 6–12 Leonard–Jones factors accounting for dispersion of atom pairs caused by ionization and polarization. <math>E_{ijkl}</math> is a ligand torsion angle value calculated with a Tripos forcefield for four connected atoms. <math>E_{ij}</math> is an energy distance constraint with a 4–8 Leonard–Jones potential, accounting for close contacts with a covalent bond energy term.</p>	<ul style="list-style-type: none"> <li>Screens 12 min per ligand</li> <li>The genetic algorithm (GA) explores full ligand and partial receptor flexibility</li> <li><math>\Delta G</math> difficult to calculate, as only enthalpic consideration is considered</li> <li>Surface-accessible area term is not included</li> </ul>	[25]
FlexX	$\Delta G = \Delta G_0 + \Delta G_{\text{rot}} \times N_{\text{rot}} + \Delta G_{\text{hb}} \sum_{\text{natural hbonds}} f(\Delta R, \Delta \alpha)$ $+ \Delta G_{\text{io}} \sum_{\text{ionic int.}} f(\Delta R, \Delta \alpha) + \Delta G_{\text{aro}} \sum_{\text{aro int.}} f(\Delta R, \Delta \alpha)$ $+ \Delta G_{\text{lipo}} \sum_{\text{lipo cont.}} f^*(\Delta R)$ <p><math>\Delta G_0</math>, <math>\Delta G_{\text{hb}}</math>, <math>\Delta G_{\text{io}}</math>, <math>\Delta G_{\text{rot}}</math>, <math>\Delta G_{\text{aro}}</math> are entropic terms that describe contributions made by nonspecific, H-bond, ionic, rotational, and aromatic interaction energies offset by an idealized penalty function <math>f(\Delta R, \Delta \alpha)</math>. <math>\Delta G_{\text{lipo}}</math> includes lipophilic interaction energy as a function of all pair-wise atom–atom interaction energies.</p>	<ul style="list-style-type: none"> <li>Screens at 3 min per ligand</li> <li>Large number of ligand conformations are generated</li> <li>Lipophilic interactions are accounted for</li> <li>Limited to ligands with less than 17–20 rotatable bonds</li> </ul>	[23]
DOCKv4 GB/SA	$G_{\text{binding}} = \sigma_1 \Delta(\text{SA}_{\text{hp}}) + \beta \cdot \text{VDW} - \sigma_2 \Delta(\text{SA}) + G_{\text{pol}}$ <p><math>\Delta(\text{SA}_{\text{hp}})</math> and <math>\Delta(\text{SA})</math> are a measure of change in hydrophobic and total accessible surface areas. <math>\sigma_1</math>, <math>\sigma_2</math> are solvation parameters for nonpolar atoms and a linear coefficient for the scaling of van der Waals interactions <math>\beta \cdot \text{VDW}</math>. <math>G_{\text{pol}}</math> includes ligand–receptor electrostatic energy and partial desolvation energy terms for receptor and ligand atoms.</p>	<ul style="list-style-type: none"> <li>Screens at 7 min per ligand</li> <li>The desolvation states of ligand and receptor are included in term accounts for hydrophobic interactions</li> <li>Effects of translational, rotational, and conformational entropy loss upon binding not included in function</li> </ul>	[22]



**Table 5** Structural and thermodynamic data for a selection of different classes of protein–ligand complexes

Protein–ligand	Number of H-bonds contacts	Number of non-H-bond contacts	Solvent accessible surface area (Å <sup>2</sup> ) of the ligand			K <sub>i</sub> M <sup>-1</sup>	ΔG° kJ mol <sup>-1</sup>  (ΔG° = - RT lnK <sub>i</sub> )
			Uncomplexed Å <sup>2</sup>	Complexed Å <sup>2</sup>	Buried Å <sup>2</sup>	%Buried	
OppA (1B1H.pdb)	12	103	201.151	5.687	195.464	97.17	9.3 × 10 <sup>-8</sup> +40.1
Cyclophilin-A (1CW.A.pdb)	5	15	342.429	193.203	149.226	43.57	5–200 × 10 <sup>-9</sup> +45.6 to + 51.5
FKBP (1FKF.pdb)	3	110	261.332	126.936	134.396	51.42	4.0 × 10 <sup>-10</sup> +52.6
FABP (2IFB.pdb)	1	109	154.195	9.744	144.451	93.68	7 × 10 <sup>-9</sup> +46.4
ConA (1I3H.pdb)	8	58	121.752	51.562	70.19	57.64	4.2 × 10 <sup>-3</sup> +13.5
HIV-1-protease (1HVR.pdb)	6	153	230.994	17.829	213.165	92.28	3.1 × 10 <sup>-10</sup> +54.2
Estrogen receptor (1ERR.pdb)aps	3	137	196.285	16.911	179.374	91.38	IC <sub>50</sub> = 0.2 nm +55.3

The process allows for whole libraries of ligands to be screened against a single binding pocket.

The steps in the process are as follows:

1. Generate a description of the binding pocket. This is usually in the form of a set of grid points or spheres.
2. Match the ligand to the grid points by fitting atoms of the ligand onto grid points that have appropriate electrostatic properties.
3. Calculate an energy score showing how well the ligand fits into the binding pocket.
4. Rank and order the hits.

The well-established DOCK algorithm<sup>[21]</sup> generates a sphere-filled inverse representation of the binding pocket, subsequently matching thousands of ligand orientations to the spheres. DOCK version 5<sup>[22]</sup> includes a desolvation term in its scoring system to account for the shedding of water upon ligand binding. The incremental construction algorithm FlexX<sup>[23]</sup> considers ligands as totally flexible; fragment placing allows subsequent reconstruction of the ligand within the receptor. The scoring function (Table 4) is relatively computationally efficient and includes entropic terms covering lipophilic, aromatic, and ionic interactions. The GOLD (genetic optimization for the ligand docking) program<sup>[25]</sup> developed at the Cambridge Crystallographic Data Centre (CCDC) employs a genetic algorithm to fully explore ligand flexibility within a partially flexible receptor. The scoring system uses observations of nonbonded contacts from crystal structures to rank ligand orientations.

## A BROAD SURVEY OF LIGAND CLASSES

For structural and thermodynamic data for a selection of different classes of protein–ligand complexes, see Table 5.

### Peptides: OppA Complexed with 8-Peptides

The structures of eight OppA–peptide complexes were determined by protein x-ray crystallography<sup>[10]</sup> (Fig. 3a). OppA is a peptide transport receptor in gram-negative bacteria that binds a wide range of peptides between two to five amino acids in length. In a study by Davies et al.,<sup>[10]</sup> eight complexes of tripeptides K–X–K (X = abnormal side chain) were prepared, and the enthalpy, entropy, and binding affinity were measured when bound to OppA. The resultant  $K_d$  values ranged from 15 nM–29  $\mu$ M. The complexes revealed a rigid binding pocket with well-ordered water molecules. The OppA system shows preferential binding for hydrophobic groups over positively charged groups. Small differences in ligand side

chains cause a disproportionately large effect on ligand binding, resulting in an inability to rank or predict binding affinities within classes of ligands. Predictions of binding affinities are complicated due to favorable enthalpy changes being offset by a compensating cost in entropy change, making it difficult to correlate structure with binding affinity. The observed water displacement upon ligand binding associated with the Opp–A system and the resultant enthalpy–entropy compensation makes predicting binding affinities using scoring functions that do not account for unreliable solvent interactions.

### Peptides: Cyclophilin A Complexed with Cyclosporin A

Cyclosporin A (CsA) is a cyclic undecapeptide that has seven of the 11 amides in the *N*-methylated form and is used as an immunosuppressant to prevent the rejection of organs after transplant surgery. CsA's immunosuppressive qualities arise from the formation of a tightly bound complex of CsA with Cyclophilin A (CypA); a ubiquitous 165 amino long cytosolic protein. The CsA/CypA composite surface binds and inhibits the serine/threonine phosphatase calcineurin, preventing further signal transduction. The CsA/CypA complex was solved to 1.8 Å resolution. Analysis of 11 CypA/CsA derivative crystal complexes by Kallen et al.<sup>[27]</sup> provides a useful database of protein–ligand interactions, revealing the effect of small chemical differences on hydrogen bond, van der Waals, and water interactions. Only six of the CsA residues form van der Waals or hydrogen-bonded contacts with the binding pocket of cyclophilin. There is an excellent complementarity of fit between the MeVal side chain and the hydrophobic active site pocket of cyclophilin, which is designed to accommodate proline. There are five direct hydrogen bonds between CsA and CypA and a solvent-excluded area of 150 Å<sup>2</sup>. Despite only half the residues being involved in the interaction with the protein, there is a strong interaction with a  $K_d$  of 15 nM. The conformation of the ligand undergoes a dramatic conformational change from its uncomplexed state in organic solvents.

### Macrolides: FKBP Complexed with FK506 and Rapamycin

FKBP is the soluble receptor for the immunosuppressant drug FK506 (see Fig. 3b). The native crystal structure of FKBP as well as with FK506 and rapamycin-bound forms were determined to a resolution of better than 2.0 Å.<sup>[5]</sup> A range of bound ligands describes the enthalpic and entropic contributions caused by differing electrostatic, chiral, and solvation properties of the ligand. X-ray

structures of a series of ligand molecules related to dimethylsulfoxide were complexed with FKBP. The structures allow for the correlation of physiochemical properties with experimentally observed binding affinities.<sup>[5]</sup> Analysis of macrolide and small-ligand FKBP complexes reveals an active site cavity able to flex in relation to the size of the bound ligand. Comparison of

FKBP complexed with DMSO and methyl sulfinyl-methylsulfoxide (DSS) shows similar protein and solvent structures. The observed threefold increase in  $K_d$  in the FKBP/DSS complex compared to DMSO can be contributed to increase in enthalpic (van der Waals) interactions energy due to the presence of the methyl sulfide group. The correlation of three-dimensional structure with

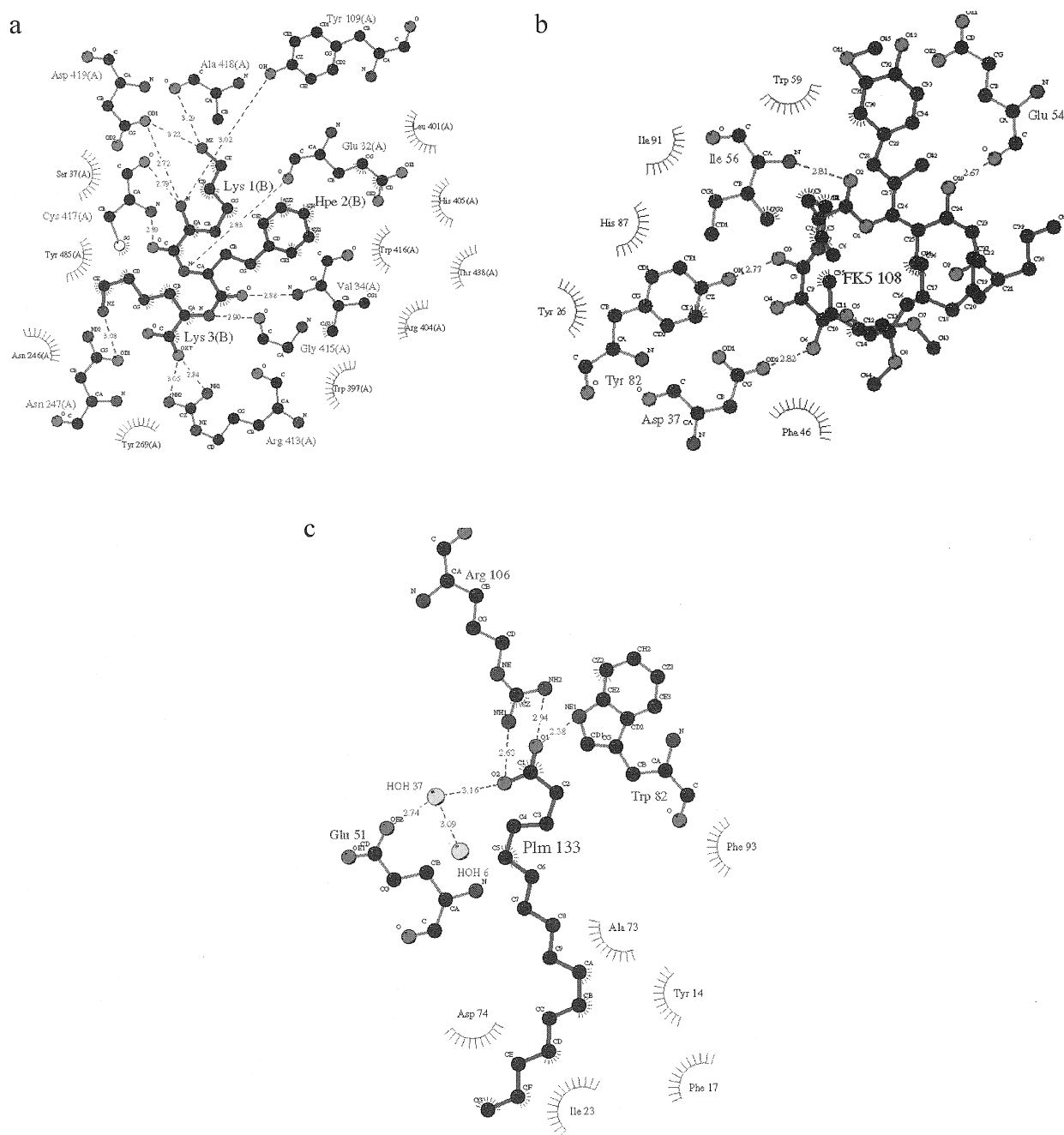


**Fig. 3** (a) OppA K-HpH-K complex (1B1H.pdb); (b) FKBP-FK506 complex (1FKF.pdb); (c) FABP-palmitate complex (2IFB.pdb); (d) ConA-dimannose complex (1I3H.pdb); (e) HIV-I protease-cyclic urea inhibitor (1HVR.pdb). Pictures generated using LigPlotv4.0. Source: From Ref. [26]. (View this art in color at [www.dekker.com](http://www.dekker.com).)

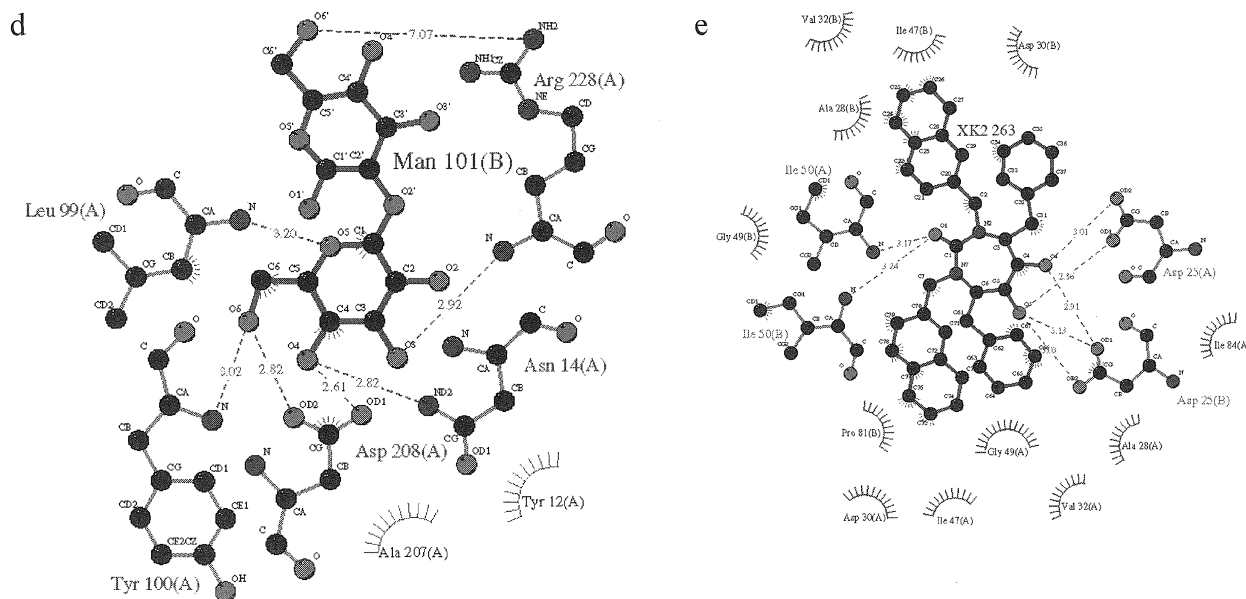


Fig. 3 (Continued).

ligand-binding data suggests that for each  $\text{\AA}^2$  contact between ligand and protein contributes between  $-0.1$  kJ/mol<sup>[4]</sup> up to an estimated  $-0.5$  kJ/mol binding energy.<sup>[5]</sup> FK506 binds to human FKBP with a  $K_d$  of  $0.4$  nM. With an estimated  $134$   $\text{\AA}^2$  buried contact area, each  $\text{\AA}^2$  contact contributes  $-0.4$  kJ/mol binding energy.

### Lipids and Fatty Acids: FABP–Palmitate Complex

Fatty acid binding protein (FABP) is involved in fatty acid transport (Fig. 3c). High-resolution crystal- and NMR-derived structures of apo and holo forms of rat intestinal FABP complexed with palmitate allowed Bakowies et al.<sup>[28]</sup> to derive a 5 nsec molecular dynamics (MD) simulation.<sup>[28]</sup> The FABP family shares a common  $\beta$ -barrel motif with a large internal binding cavity, which when uncomplexed, contains 20 to 25 well-ordered water molecules. Thermodynamic studies conclude that binding is enthalpically driven but cannot distinguish between entropic compensations between the ligand and water effects. Side-chain H-bond interactions are consistent between MD simulations and crystal structures, however, crystal and NMR representations show poor agreement in the apo-FABP form. The holo-FABP complex MD simulation shows that palmitate ligand moves  $3$ – $4$   $\text{\AA}$  back toward the cavity entrance. Crystal structures overestimated the electrostatic contribution; while the MD simulation shows that palmitate is able to sustain

substantial flexibility and motion while bound in the protein cavity. The apo-FABP shows a high-density droplet of water in the cavity center. The holo-FABP complex reveals that water molecules are displaced from the cavity by palmitate, with one water molecule being replaced by three methylene fragments. The observed high mobility of water molecules within the interior and exterior of FABP when palmitate binds is due to a combination of water droplet dispersion and a more favorable exchange pathway via the portal region of FABP. Displacement of several  $\beta$ -strands around the exit channel observed in the NMR and MD representations but absent from the crystal form of apo-FABP show the importance of solvation on the overall protein structure.

### Saccharides: Concanavalin-A Complexed with Dimannose

The interaction of plant lectin concanavalin-A (Con A) with different saccharides was studied in great depth and provides a unique insight into protein–oligosaccharide interactions. Sanders et al.<sup>[29]</sup> crystallized the structure of Jack Bean Con A in complex with dimannose (Man-( $\alpha$ 1-2)Man) to a resolution of  $1.2$   $\text{\AA}$ .<sup>[29]</sup> Comparison with the complexed and uncomplexed forms shows that the water displacement that occurs upon ligand binding forms a network of well-defined H-bonds that helps to stabilize the Con A–dimannose complex. The H-bonding network provides an explanation for the observed preferences in

binding  $\alpha$ 1-2 linked disaccharides. The formation of eight direct hydrogen bonds (and seven indirect interactions, with well-observed waters) between dimannose and Con A combined with a buried contact area of  $70.2 \text{ \AA}^2$  gives a  $K_d$  of 4.2 mM. The high resolution of the structure revealed the protonation of an Asp208 OD1, a feature that was unaccounted for in previous modeling studies (Fig. 3d).

### Steroids: Estrogen Receptor Complexed with $17\beta$ -Estradiol and Raloxifene

Estrogens play an important role in tissue growth, development, and homeostasis. These steroids mediate their effects through direct interactions with a ligand-inducible nuclear transcription factor termed the estrogen receptor (ER), resulting in the activation or repression of target genes. How estrogens mediated their biological effects at the molecular level has been a source of continuous debate. The cocrystallization of the endogenous estrogen agonist  $17\beta$ -estradiol ( $3.1 \text{ \AA}$ ) and the clinically used selective antagonist Raloxifene ( $2.6 \text{ \AA}$ ) with the  $\alpha$ -estrogen receptor, respectively, by Brzozowski et al. provided insight into the molecular basis of agonism and antagonism of the ER.<sup>[30]</sup> Comparison between these structures reveals that the large side chain of Raloxifene protrudes from the cavity and causes a  $10 \text{ \AA}$  rigid body displacement of one of the receptor helices (Helix 12). The formation of three hydrogen-bond interactions and a  $179 \text{ \AA}^2$  buried contact area between Raloxifene and the ER results in Raloxifene having an  $IC_{50}$  of 0.2 nM. It is proposed that the failure of Helix 12 to fully cap the entrance of the binding cavity prevents the formation of a competent transcriptional activation function (AF-2) site that is able to effectively recruit coactivators. It is thought

that this observed helical rearrangement of Helix 12 leads Raloxifene to behave as an antagonist in certain tissues.

Related in Table 5 are protein–ligand complexes described with the number of intermolecular contacts made and solvent-accessible surface area to thermodynamic binding data. The number of H-bonds, inhibition concentration ( $K_i$ ), and change in Gibbs free energy ( $\Delta G$ ), respectively, were taken from original sources. The number of non-H-bonded contacts was generated using the Ligand–Protein Contact software.<sup>[31]</sup> The solvent-accessible surface was generated using the Connolly<sup>[32]</sup> accessible surface of the ligand in isolation and when bound in the protein (without water). The buried surface is taken as the difference between these values. A probe radius of  $1.5 \text{ \AA}$  was used with the implementation of the Connolly algorithm within the modeling program WITNOTP.<sup>[33]</sup>

### Synthetic Drugs: HIV-1 Protease Inhibitors

In the fight against HIV, the National Cancer Institute developed a database of HIV protease–ligand complexes. The HIV-PR database<sup>[34]</sup> holds the coordinates for 142 different crystal structures of HIV protease–ligand complexes (Table 6). In conjunction with the Autodock3 docking package, a modified combined energy weighted grid system was used to predict the correct ligand-binding conformation for 21 of these complexes. The results showed that the energy grid could allow structural flexibility of the binding site and distinguish between ligands that required water for binding. The cyclic urea inhibitor that was tested, which does not require the presence of water for binding to HIV protease, was accommodated within the energy grid system, returning a predicted conformation close to that of the crystal structure.<sup>[35]</sup>

**Table 6** Online ligand–protein databases

Database	Description	Web address
LIGAND	Contains compound, metabolic, and enzymatic information	<a href="http://www.genome.ad.jp/ligand/">http://www.genome.ad.jp/ligand/</a>
RELIBASE	Easy searching of protein–ligand complexes	<a href="http://relibase.ccdc.cam.ac.uk/">http://relibase.ccdc.cam.ac.uk/</a>
PLD	Binding data for 150 protein–ligand complex's	<a href="http://www-mitchell.ch.cam.ac.uk/pld/pld2.html">http://www-mitchell.ch.cam.ac.uk/pld/pld2.html</a>
BindingDB	Database of measured binding affinities	<a href="http://www.bindingdb.org">http://www.bindingdb.org</a>
LPC	Automated analysis of interatomic contacts in protein–ligand complexes	<a href="http://bioinfo.weizmann.ac.il:8500/oca-bin/lpccsu/">http://bioinfo.weizmann.ac.il:8500/oca-bin/lpccsu/</a>
HIV Protease Database	Structure database of HIV proteases complexed with their inhibitors	<a href="http://srdata.nist.gov/hivdb/">http://srdata.nist.gov/hivdb/</a>

Described in Table 6 is a list of online databases that hold thermodynamic data on protein–ligand complexes.

## CONCLUSION

The event of ligand binding is thermodynamically complex and is composed from a range of enthalpic and entropic factors. Recent technological developments allowed for improved experimental measurement of ligand binding. Linking binding data to the type of intermolecular forces observed within protein–ligand complexes (Table 5 and Fig. 3) provides a route to improving energy terms used in structure-based drug design. Listed in Table 6 are online databases that give thermodynamic and enzymatic information about selected protein–ligand complexes. However, current techniques can still only sample a small percentage of the total available ligands. Increasingly, computational techniques such as de novo design, database mining, and automated docking are being employed to predict new sources of protein–ligand interactions.

The future prospects for this in-silico technology depends on incorporating improved parameters for describing the dynamic effects of water and protein flexibility in the system. The ability to achieve these computational advances will be helped by the increasing number of high-resolution crystal structures of protein–ligand complexes becoming available in publicly accessible databases. Such structures provide an opportunity for the detailed analysis of the poorly defined factors that influence the strength of protein–ligand interactions.

## ACKNOWLEDGMENTS

We are grateful to Prof. J.W. Keillor at the Université de Montreal, Department of Chimie, for his many useful discussions.

The authors would like to thank the BBSRC for their financial support.

## ARTICLES OF FURTHER INTEREST

*The Cambridge Structural Database*, p. 161

*Drug Delivery*, p. 484

*Hydrogen Bonding*, p. 658

*The Hydrophobic Effect*, p. 673

*Kinetics of Complexation*, p. 776

*Molecular Modeling and Related Computational Techniques*, p. 901

*Nuclear Magnetic Resonance Spectroscopy*, p. 981

*van der Waals Forces*, p. 1550

*Weak Hydrogen Bonds*, p. 1576

*X-Ray Crystallography*, p. 1586

## REFERENCES

1. Berman, H.M.; Westbrook, J.; Feng, Z.; Gilliland, G.; Bhat, T.N.; Weissig, H.; Shindyalov, I.N.; Bourne, P.E. The protein data bank. *Nucleic Acids Res.* **2000**, *28*, 235–242.
2. Knegtel, R.M.A.; Grootenhuys, P.D.J. Binding affinities and non-bonded interaction energies. *Pers. Drug Dis. Des.* **1998**, *9–11*, 99–114.
3. Klebe, G.; Bohm, H.J. Energetic and entropic factors determining binding affinity in protein–ligand complexes. *J. Recep. Signal Transduc. Res.* **1997**, *17*, 459–473.
4. Bohm, H.J. Prediction of binding constants of protein ligands: A fast method for the prioritisation of hits obtained from de-novo design or 3D-database search programs. *J. Comput. Aided Mol. Des.* **1998**, *12*, 309–323.
5. Burkhard, P.; Taylor, P.; Walkinshaw, M.D. X-ray structures of small ligand FKBP complexes provide an estimate for hydrophobic interaction energies. *J. Mol. Biol.* **2000**, *295*, 953–962.
6. Rich, R.L.; Myszka, D.G. Advances in surface plasmon resonance biosensor analysis. *Curr. Opin. Biotechnol.* **2000**, *11*, 54–61.
7. Wu, S.Y.; Dornan, J.; Kontopidis, G.; Taylor, P.; Walkinshaw, M.D. The first direct determination of a ligand binding constant in protein crystals. *Angewandte Chemie—International Edition* **2001**, *40*, 582–586.
8. Shuker, S.B.; Hajduk, P.J.; Meadows, R.P.; Fesik, S.W. Discovering high affinity ligands for proteins: SAR by NMR. *Science* **1996**, *274*, 1531–1534.
9. Kofron, J.L.; Kuzmic, P.; Kishore, V.; Colonbonilla, E.; Rich, D.H. Determination of kinetic constants for peptidyl prolyl *cis trans* isomerases by an improved spectrophotometric assay. *Biochemistry* **1991**, *30*, 6127–6134.
10. Davies, T.G.; Hubbard, R.E.; Tame, J.R.H. Relating structure to thermodynamics: The crystal structures and binding affinity of eight OppA–peptide complexes. *Protein Science* **1999**, *8*, 1432–1444.
11. Murzin, A.G.; Brenner, S.E.; Hubbard, T.; Chothia, C. SCOP—A structural classification of proteins database for the investigation of sequences and structures. *J. Mol. Biol.* **1995**, *247*, 536–540.
12. Varghese, J.N.; Smith, P.W.; Sollis, S.L.; Blick, T.J.; Sahasrabudhe, A.; McKimm-Breschin, J.L.; Colman, P.M. Drug design against a shifting target: A structural basis for resistance to inhibitors in a variant of influenza virus neuraminidase. *Structure* **1998**, *6*, 735–746.
13. Bohm, H.J. The computer-program ludi—A new method for the de novo design of enzyme-inhibitors. *J. Comput. Aided Mol. Des.* **1992**, *6*, 61–78.
14. DeWitte, R.S.; Ishchenko, A.V.; Shakhnovich, E.I. SMOG. de Novo—Design method based on simple fast and accurate free energy estimates 2. Case studies in molecular design. *J. Am. Chem. Soc.* **1997**, *119*, 4608–4617.

15. Ricketts, E.M.; Bradshaw, J.; Hann, M.; Hayes, F.; Tanna, N.; Ricketts, D.M. Comparison of conformations of small-molecule structures from the Protein Data-Bank with those generated by concord, cobra, chemdb3D, and converter and those extracted from the Cambridge Structural Database. *J. Chem. Inf. Comput. Sci.* **1993**, *33*, 905–925.
16. Sadowski, J.; Gasteiger, J.; Klede, G. Comparison of automatic 3-dimensional model builders using 639 x-ray structures. *J. Chem. Inf. Comput. Sci.* **1994**, *34*, 1000–1008.
17. *ACD Available Chemicals Directory*; <http://www.mdli.com> (accessed July 2002).
18. Lipinski, C.A.; Lombardo, F.; Dominy, B.W.; Feeney, P.J. Experimental and computational approaches to estimate solubility and permeability in drug discovery and development settings. *Advances in Drug Delivery Review* **1997**, *23*, 3–25.
19. *USP Dictionary of USAN and International Drug Names*; <http://www.usp.org> (accessed July 2002).
20. Ghose, A.K.; Viswanadhan, V.N.; Wendoloski, J.J. A knowledge-based approach in designing combinatorial or medicinal chemistry libraries for drug discovery. I. A qualitative and quantitative characterisation of known drug databases. *Journal of Combinatorial Chemistry* **1999**, *1*, 55–68.
21. Ewing, T.J.A.; Makino, S.; Skillman, A.G.; Kuntz, I.D. DOCK 4.0: Search strategies for automated molecular docking of flexible molecule databases. *J. Comput. Aided Mol. Des.* **2001**, *15*, 411–428.
22. Zou, X.Q.; Sun, Y.X.; Kuntz, I.D. Inclusion of solvation in ligand binding free energy calculations using the generalized-Born model. *Journal of the American Chemical Society* **1999**, *121*, 8033–8043.
23. Rarey, M.; Kramer, B.; Lengauer, T.; Klebe, G. A fast flexible docking method using an incremental construction algorithm. *J. Mol. Biol.* **1996**, *261*, 470–489.
24. Eldridge, M.D.; Murray, C.W.; Auton, T.R.; Paolini, G.V.; Mee, R.P. Empirical scoring functions: I. The development of a fast empirical scoring function to estimate the binding affinity of ligands in receptor complexes. *J. Comput. Aided Mol. Des.* **1997**, *11*, 425–445.
25. Jones, G.; Willett, P.; Glen, R.C.; Leach, A.R.; Taylor, R. Development and validation of a genetic algorithm for flexible docking. *J. Mol. Biol.* **1997**, *267*, 727–748.
26. Wallace, A.C.; Laskowski, R.A.; Thornton, J.M. LIGPLOT: A program to generate schematic diagrams of protein–ligand interactions. *Prot. Eng.* **1995**, *8*, 127–134.
27. Kallen, J.; Mikol, V.; Taylor, P.; Walkinshaw, M.D. X-ray structures and analysis of 11 cyclosporin derivatives complexed with Cyclophilin A. *J. Mol. Biol.* **1998**, *283*, 435–449.
28. Bakowies, D.; Van Gunsteren, W.F. Simulations of apo and holo-fatty acid binding protein. Structure and dynamics of protein, ligand and internal water. *J. Mol. Biol.* **2002**, *315*, 713–736.
29. Sanders, D.A.R.; Moothoo, D.N.; Raftery, J.; Howard, A.J.; Helliwell, J.R.; Naismith, J.H. The 1.2 Å resolution structure of the Con A–dimannose complex. *J. Mol. Biol.* **2001**, *310*, 875–884.
30. Brzozowski, A.M.; Pike, A.C.W.; Dauter, Z.; Hubbard, R.E.; Bonn, T.; Engstrom, O.; Ohman, L.; Greene, G.L.; Gustafsson, J.A.; Carlquist, M. Molecular basis of agonism and antagonism in the oestrogen receptor. *Nature* **1997**, *389*, 753–758.
31. Sobolev, V.; Sorokine, A.; Prilusky, J.; Abola, E.E.; Edelman, M. Automated analysis of interatomic contacts in proteins. *Bioinformatics* **1999**, *15*, 327–332.
32. Connolly, M.L. Solvent-accessible surfaces of proteins and nucleic-acids. *Science* **1983**, *221*, 709–713.
33. Widmer, A. *WITNOTP: A Computer Program for Molecular Modelling*; Novartis AG: Basel, 1997.
34. *The HIV Protease Databank*; <http://mcII.ncicrf.gov/hivdb> (accessed July 2002).
35. Osterberg, F.; Morris, G.M.; Sanner, M.F.; Olson, A.J.; Goodsell, D.S. Automated docking to multiple target structures: Incorporation of protein mobility and structural water heterogeneity. *Proteins* **2002**, *46*, 34–40.

# Biological Models and Their Characteristics

**Paolo Scrimin**

*University of Padova, Padova, Italy*

**Paolo Tecilla**

*University of Trieste, Trieste, Italy*

## INTRODUCTION

The ability to mimic and take advantage of the complexity of living matter as a way to store and transfer information, accelerate chemical reactions, selectively recognize chemical species, self-replicate, and so on is at the basis of supramolecular chemistry in the biological field. The concepts that spurred the growth of supramolecular chemistry came from the biological world, as scientists started to comprehend the extreme difficulty (if not the impossibility) of obtaining complex systems with specific function just by connecting building blocks via covalent synthesis. It is apparent that in the biological world, the most challenging and intriguing systems express their functions as collections of simpler elements held together not by covalent bonds but by reversible, singularly weak, interactions. Supramolecular chemistry was the response of scientists to this clear evidence: complex structures able to perform spectacular achievements can be obtained minimizing chemical synthesis and relying on weak interactions, i.e., the way molecules reciprocally communicate without the formation of covalent bonds.<sup>[1]</sup> In order to do this, they had to master the way these weak interactions (like hydrogen bonds, hydrophobic forces, for instance) operate.

In order to address the characteristics of biological models, we have to first define the basic principles of biological systems that a supramolecular model may mimic. Among the most important are selective molecular recognition of a molecular entity; selective and highly accelerated modification of a substrate (typical role of enzymes); compartmentalization and selective translocation of chemical species across boundaries (typical role of biomembranes); harvesting and transformation of energy; and self-replication.

## SELECTIVE MOLECULAR RECOGNITION

Molecular recognition relies on weak to moderate forces,<sup>[2]</sup> and the process depends critically on the struc-

ture of the molecular partners involved as well as on the nature of the surrounding solvent. Typical interactions involved in molecular recognition are ion-ion, ion-dipole, dipole-dipole, cation- $\pi$ ,  $\pi$ - $\pi$  stacking, dispersion (London), and solvent effects. The classical recognition process requires two entities: the molecular receptor (host) and the recognized molecule (guest). However, self-recognition should not be overlooked, as it is one of the most important processes in the biological world. Self-recognition, for instance, is what dictates the folding of a protein into its secondary and tertiary structures. Those synthetic oligomers showing the property to fold into a specific conformation following the information encoded in their synthesis were dubbed Foldamers.<sup>[3]</sup> Interesting examples are those constituted by  $\beta$ -peptides<sup>[4,5]</sup> (unnatural oligomers composed of  $\beta$ -amino acids) that fold into a  $3_{14}$  helix already at the level of a dodecamer. Even more striking are short oligomers (six to eight units) composed of  $\alpha$ -tetrasubstituted unnatural amino acids<sup>[6]</sup> that fold into  $3_{10}$  helices. Probably the system most studied as a model for molecular recognition is that constituted by cyclodextrins (CDs), cyclic oligomers (six to eight units) composed of glucose units with a doughnut shape and an hydrophobic interior.<sup>[7]</sup> This property led to the use of functional cyclodextrins as enzyme models (see below). However, as an example to illustrate molecular recognition, we will show a cage receptor for glucose able to extract the sugar from an aqueous solution into an organic one.<sup>[8,9]</sup> This is a challenging endeavor, because water is obviously an excellent solvent for a saccharide. The molecule (Fig. 1) comprises a rigid cavity (a tricycle), with amide groups pointing inward into the cavity and suitable for hydrogen bonding the sugar molecule. The design resembles key structural motifs present in carbohydrate-binding proteins that, as stated by the authors, “commonly place aromatic surfaces against patches of carbohydrate CH groups while accepting the hydroxyl groups into networks of hydrogen bonds.” This receptor has an affinity for D-glucose, which is five times larger than that for D-galactose and >10 times that for D-mannose.



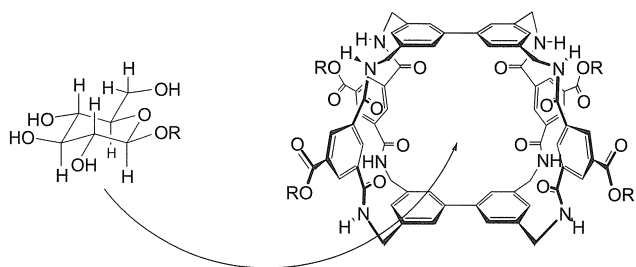


**Fig. 1** Structure of the macrotricyclic receptor for the selective extraction of glucose from aqueous solutions: the sugar binds inside the cavity, taking advantage of the formation of a hydrogen bonds network.

## CATALYSIS

An essential prerequisite for enzymatic catalysis is the binding of the substrate to the protein before its transformation into products. The two processes (binding and modification) may occur on different sites of the protein. The binding site should not change during the catalytic process, while, in the reactive site, bonds are broken and new ones are formed, charge is developed or

disappears.<sup>[10]</sup> Accordingly, the mimicry of a recognition site, compared with a catalytic site that is dynamic in nature, is much easier in a supramolecular system. Supramolecular (enzyme-like) catalysts typically provide the recognition site for a substrate, while they are much less effective as far as the catalytic site is concerned. Apart from the dynamic aspect mentioned above, a catalytic site requires the refinement of the pKa of acids or bases eventually involved in the process and accurate control of the solvation of all species. Nevertheless, effective supramolecular catalysts were reported, because just the proximity of reactant and catalyst achieved upon binding is enough to guarantee (sometimes) impressive rate accelerations. A typical example is that provided by cyclodextrins.<sup>[11]</sup> The hydrophobic cavity of these natural molecules was used to recognize substrates, while the hydroxyl rim was used as a source of a nucleophile for a transacylation process. By optimizing the substrate, Breslow and collaborators<sup>[12]</sup> were able to achieve 6-million-fold rate accelerations compared with the uncatalyzed hydrolysis reaction. The critical aspect stressed by these systems is that a substrate, rather rigid and complementary to the cavity, may be designed with the ester group sitting precisely over the CD secondary side

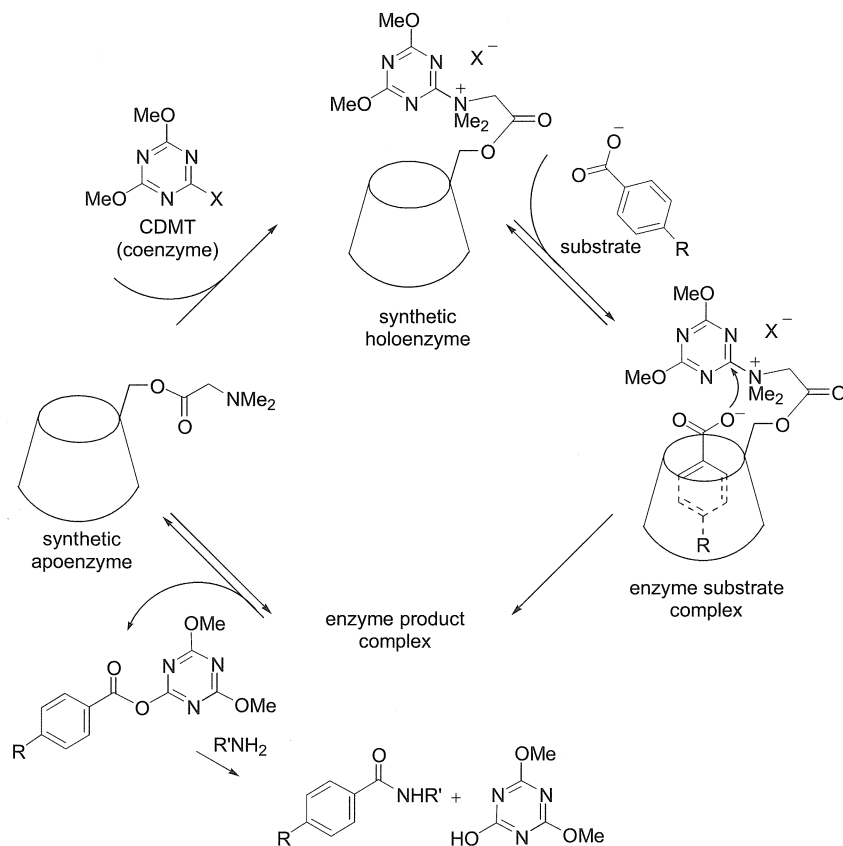


**Fig. 2** Catalytic cycle for a CD-based artificial acyltransferase.

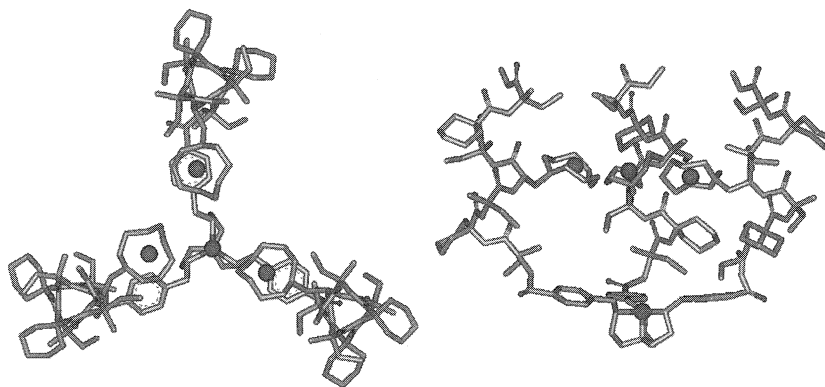


**Fig. 3** Tripodal polypeptide used as a biomimetic supramolecular catalyst for the cleavage of phosphate esters. The tren platform is an allosteric control site. (View this art in color at [www.dekker.com](http://www.dekker.com).)

hydroxyl group. Thus, the proximity is the source of the rate acceleration. More sophisticated systems require the modification of the cyclodextrin so that a catalytic site can be designed by placing suitable functional groups. An example<sup>[13]</sup> illustrating this point was recently reported by Kunishima et al. They simply esterified one of the primary hydroxyls of  $\beta$ -CD with *N,N*-dimethylglycine (see Fig. 2), transforming it into a catalyst (holoenzyme) for the amidation of carboxylic acids in aqueous solution. The process requires 2-chloro-4,6-dimethoxy-1,3,5-triazine (CDMT) as a coenzyme consumed during the reaction. The results indicate that, in the catalyst, the substrate-binding site (the CD cavity) and the catalytic site (the dimethylamino group at the rim) must be linked to each other in order to achieve substrate-specific amidation. Other molecular receptors can be used as supramolecular, biomimetic catalysts. For instance, Diederich<sup>[14]</sup> functionalized a cationic cyclophane with flavin and thiazolium groups and obtained a pyruvate oxidase mimic. Pyruvate oxidase is an enzyme that employs two cofactors: flavin and thiamine-diphosphate to catalyze the transformation of pyruvate to acetyl phosphate. The coexistence of the two cofactors on the same molecular receptor makes this molecule one of the most active artificial enzymes known to date. In an attempt to mimic the catalytic site of a nuclease we synthesized<sup>[15]</sup> the molecule shown in Fig. 3 by attaching three copies of an helical heptapeptide to a derivative of tren (*tris*-aminoethylamine). The sequence of each single peptide is designed in such a way that by folding into an helical conformation, two ammonium groups are placed on one side of the helix, and a triazacyclononane ligand of synthetic amino acid ATANP is placed on the other. The tripodal derivative can bind up to four metal ions: one on the tren platform and three on the triazacyclononane moieties. The tren site is used to control the conformation of the molecule (like an allosteric site in proteins), while the remaining triazacy-

clononane complexes define a catalytic site for the metal-catalyzed hydrolysis of a phosphate. The metal complex is active in the cleavage of a phosphate model of RNA, with clear evidence of cooperativity between the metal centers. Surprisingly, however, it is active as the free amine in the cleavage of linear RNA. It appears that the allosteric site is responsible for this behavior of striking selectivity in the interaction with the substrate. By using natural sequences the group of Baltzer<sup>[16–19]</sup> recently described a series of fully synthetic polypeptides that are good catalysts of the cleavage of esters. The molecules contain 42 amino acids and were designed to fold into a helix-loop-helix conformation. The monomers dimerize into a four-helix bundle that provides a shallow reactive site for the substrate (Fig. 4). Here, the emphasis is on the careful control of the properties of the catalytic units placed on

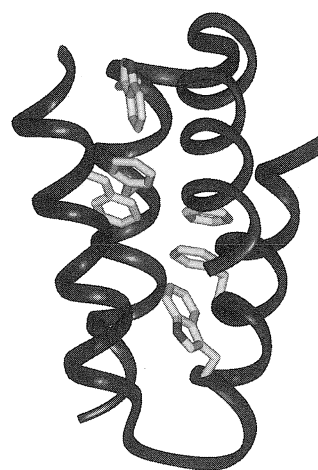


**Fig. 4** Four-helix bundle formed by two helix-loop-helix peptides. The self-assembly of the two monomers provides a shallow reactive site for the substrate. (View this art in color at [www.dekker.com](http://www.dekker.com).)

the reactive site. Thus, by introducing flanking amino acids with charged side chains, the authors were able to finely tune the pKa of the imidazole of the histidines so as to maximize their cooperative role at the optimum pH for the occurrence of the catalytic process. As stated above, this is a major challenge for everybody trying to prepare an artificial (supramolecular) catalyst. To conclude this section, we will mention two extremes in the design of supramolecular enzyme models. The first takes advantage of putting together, in a polymer, several functional groups and hydrophobic units. These successful molecules were called synzimes.<sup>[20–22]</sup> The second is that represented by catalytic antibodies,<sup>[23]</sup> where the catalyst is a protein generated by the immune system against a model of the transition state of the reaction under investigation. The first is rude and devoid of any specific geometrical design of the catalytic site, while the second is highly sophisticated, although the recognition of the model of a transition state does not necessarily imply acceleration of the related reaction. Nevertheless, both provided promising results.

## COMPARTMENTALIZATION AND TRANSLOCATION

Biological membranes play a fundamental role in compartmentalizing and insulating the living cell from the external medium. However, an organized trafficking of molecules and ions across the membrane is needed to sustain life. In nature, this traffic is regulated by a variety of systems able to form ion channels or to act as molecular carriers and to selectively affect the membrane permeability.<sup>[24]</sup> In particular, ion channels are formed following two general approaches: the first rely on molecules that, due to their peculiar structures, form a discrete pore in the membrane as exemplified by the  $\beta$ -helix of the gramicidin A dimer. The second is based on the hydrophobically driven self-assembling of amphipatic units in the membrane that form a cluster where the hydrophilic face of each unit points inward, defining a channel with a polar inner surface (barrel-stave model).<sup>[25]</sup> Examples of this include the ion channel proteins of the nervous system in which the channel is formed by four or five homologous  $\alpha$ -helices containing several serine residues lining the pore.<sup>[26]</sup> Several other shorter peptides like peptaibols<sup>[27]</sup> or nonpeptidic systems like amphotericin B<sup>[28]</sup> are thought to affect membrane permeability with this mechanism. Supramolecular chemists undertook the ambitious challenge of preparing systems able to rival the natural ones. Example of models inspired to both types of ion channels described above are present in the literature. Recently, the group of Ghadiri<sup>[29–32]</sup> reported channel obtained from self-assembled cyclic peptides. The key feature of these

cyclopeptides is the presence of alternating L, D amino acids, so that hydrogen bonding assembles them in a stack of rings. This strategy resembles that adopted by gramicidin A. When the assembling of the tubes (diameter  $> 7 \text{ \AA}$ , depending on the size of the cycle) occurs in a membrane, this leads to the alteration of its permeability (Fig. 5, left). The group of Voyer<sup>[33]</sup> synthesized a 21 amino acid peptide composed of 15 L-leucines and six 21-crown-7-L-phenylalanines: the sequence is such to allow the partial alignment of the macrocycles, one over the other, when the peptide adopts an  $\alpha$ -helical conformation (Fig. 5, right), forming a pore in the membrane. A similar design was used by Matile in realizing a rigid oligo(*p*-phenylene) rod functionalized with several monoaza-18-crown-6 subunits.<sup>[34]</sup> Models based on the self-assembling of amphipatic subunits were also developed. They are based on peptides,<sup>[26]</sup> polyhydroxylated *p*-biphenyl oligomers,<sup>[35]</sup> cholic acid,<sup>[36]</sup> or polyhydroxylated steroid<sup>[37]</sup> derivatives. Often, the design of these systems is inspired by the naturally occurring ionophores, amphotericin B (AmB) and squalamine,<sup>[38]</sup> which are thought to form pores in lipid bilayers. The analysis of these two ionophores made by Regen is interesting in understanding how a biological model may be constructed.<sup>[39]</sup> AmB and squalamine have different structures but share some common elements: a long and rigid hydrophobic unit; a hydrophilic chain that is linked to the hydrophobic unit and can extend across its “face”; and a polar head group. On these bases, the author designed the sterol derivative shown in Fig. 6, which mixes elements taken from squalamine, like the sterol-based hydrophobic unit and the polar head group, with the polyoxygenated chain, taken from AmB. This derivative is able to affect the membrane permeability of model liposomes with an activity and a mechanism of action comparable with that of AmB.<sup>[40]</sup> In particular, it is suggested that the ionophore assumes a folded conformation, like the one shown in Fig. 6, and is inserted in the membrane with the sulfate and the protonated amino group anchored to the surface of the liposome. Eventually, clusters are formed where the oxygenated chain points inward, toward a water-filled pore. Furthermore, because the system is too short, the alignment of two of these clusters is needed to span the membrane across and alter its permeability.

## HARVESTING AND TRANSFORMING ENERGY

Photoinduced electron and energy transfer are fundamental processes in nature.<sup>[41]</sup> In photosynthetic organisms, photoinduced electron transfer that induces conversion of light into chemical energy begins when photonic excitation reaches the so-called reaction center (RC). Usually,

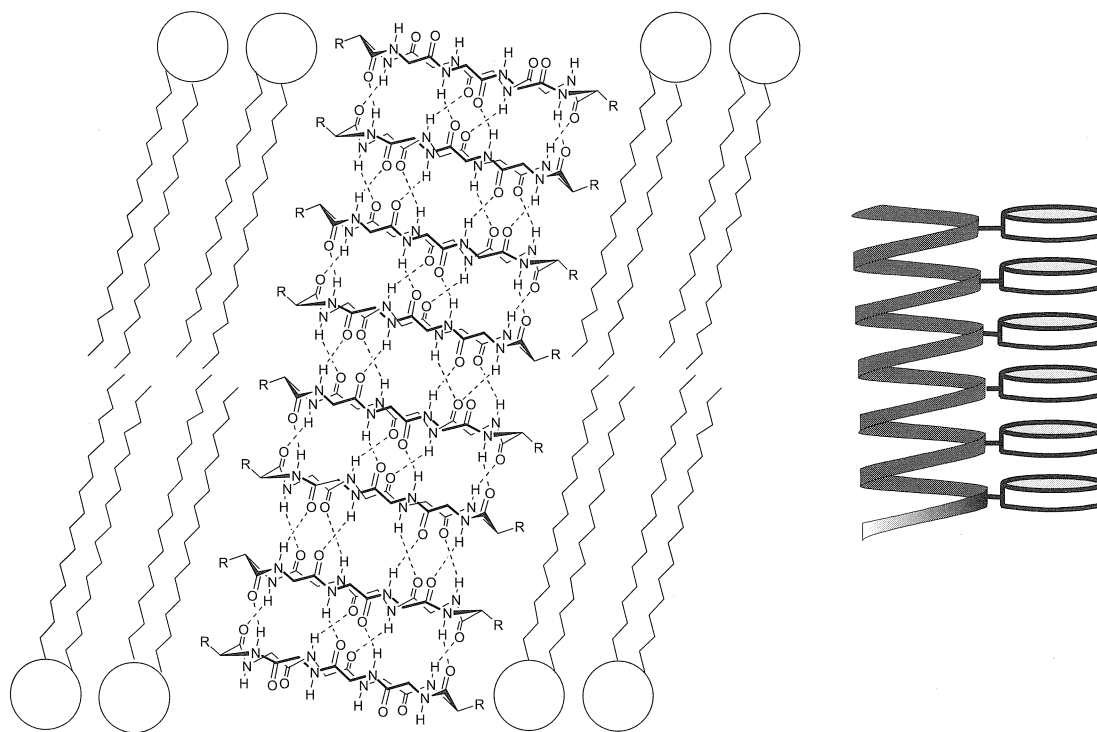


**Fig. 5** Examples of systems able to form channels in membranes. Left: the Ghadiri's self-assembled nanotube formed by cyclopeptides. Right: The Voyer's 21 amino acid peptide containing six 21-crown-7 L-phenylalanines. In a membrane, the peptide adopts an  $\alpha$ -helical conformation that allows the partial alignment of the macrocycles, one over the other.

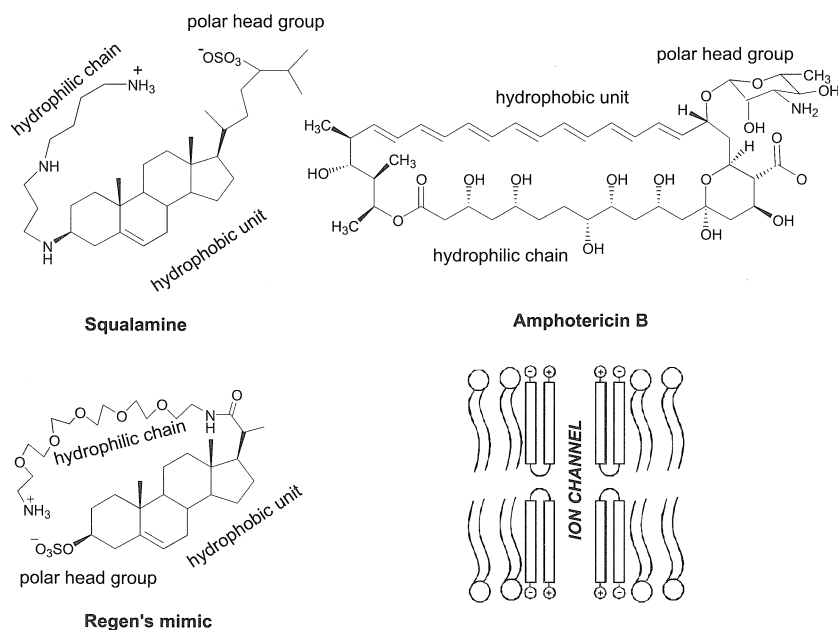


**Fig. 6** Regen's mimic of amphotericin B and squalamine. In the bottom left corner, the cartoon illustrates the proposed mode of action of this ionophore.

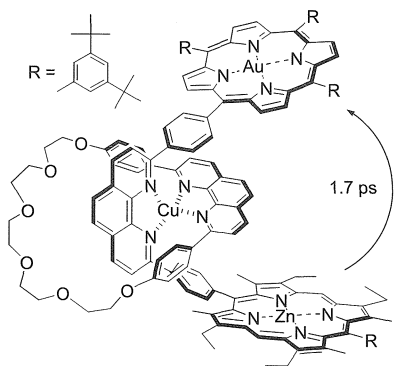


**Fig. 7** A rotaxane that mimics the special pair/bacteriopheophytin (BPh) arrangement and electron-transfer properties of the bacterial photosynthetic reaction center.

light is trapped and transferred through a pool of well-organized chromophores included in the light-harvesting antenna protein. For example, in the bacteria *Rhodospseudomonas acidophila*, the light-harvesting system is formed by two rings of noncovalently linked bacteriochlorophyll chromophores (BCh), one consisting of nine pigments and the other of 18 chromophores. This highly organized structure enhances the spectral width of the light trapped and the efficiency of energy transfer toward the RC, where electron transfer to a quinone group generates a long-lived charge separation state.<sup>[42]</sup>

Energy-transfer and electron-transfer processes inspired many research groups, and a variety of systems employing different chromophores were exploited.<sup>[43]</sup> Popular are tetrapyrrolic systems, the naturally occurring chromophores in the photosynthetic reaction center. In particular, supramolecular chemists are trying to reproduce the naturally occurring electron- and energy-transfer processes occurring through noncovalently linked proteins, using self-assembled systems. Sophisticated and efficient models of the photosynthetic RC and antenna systems were obtained.<sup>[44]</sup> For instance, Sauvage designed the rotaxane shown in Fig. 7 that mimics the special pair (SP, a closely associated dimer of BCh)/bacteriopheophytin (BPh) arrangement and electron-transfer properties of the bacterial photosynthetic RC.<sup>[45]</sup> In the natural system, the electron transfer from the excited state of SP to BPh occurs at a rate of  $3 \text{ ps}^{-1}$ . In the synthetic model, the electron donor is a zinc porphyrin in its excited state, and the electron acceptor is an Au(III) porphyrin. Light irradiation of the zinc porphyrin chromophore is followed by electron transfer to the gold porphyrin acceptor, which occurs at a rate similar to the natural system ( $1.7 \text{ ps}^{-1}$ ). The rotaxane structure is important, and in the absence of the Cu(I) ion that positions the second phenanthroline ligand in between the two porphyrin rings, the electron transfer process is substantially slower ( $36 \text{ ps}^{-1}$ ).

Self-assembling of multiporphyrin arrays was also exploited to model the properties of the antenna system. For instance, using a cooperative self-assembly process based on hydrogen bonding and metal–ligand interaction, Hunter was able to assemble five porphyrin rings in a well-defined structure in which a central free-base porphyrin is encapsulated in a spherical array of four zinc porphyrins.<sup>[46]</sup> Light excitation of these peripheral chromophores results in an efficient energy transfer to the central one, mimicking the funneling effect of the antenna system. A step forward is constituted by a self-assembled array of 16 zinc-porphyrins delivering energy to a central free-base porphyrin.<sup>[47]</sup>

## SELF-REPLICATION

One of the peculiar characteristics of the living world is the ability to self-replicate. Undoubtedly, reproducing such a characteristic in the abiotic world is a demanding challenge. Supramolecular chemists have done it. Historically, the first example is that provided by von Kiedrowski,<sup>[48]</sup> who reported evidence of self-replication in a nonenzymatic nucleotide-based system. More exciting examples were subsequently reported.<sup>[49–51]</sup> These systems rely on the fact that the product of a reaction recognizes the reactants and catalyzes their transformations into the product. A typical problem of these systems is product inhibition, circumvented by von Kiedrowski by using solid-phase cycling. Examples of self-replicating peptides<sup>[52]</sup> were also reported by Ghadiri<sup>[53,54]</sup> and Chmielewski.<sup>[55–57]</sup> These systems take advantage of Kent's chemical ligation strategy for the formation of a peptide bond.<sup>[58]</sup> Recent advances comprise the mimicry of many fundamental properties of living systems, like sensitivity to the environment,<sup>[59]</sup> sensitivity to chirality,<sup>[60]</sup> and ability to correct errors.<sup>[61]</sup> A recent example from the work of Chmielewski<sup>[62]</sup> provides an illustration of the principle. Two halves of the peptide **I**, namely, **Ia** and **Ib** (Fig. 8), are subject to ligation under Kent's conditions in the presence and absence of **I**. Peptide **I** provides a remarkable rate acceleration to the process due

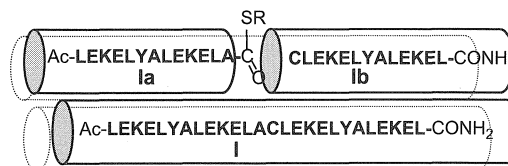


**Fig. 8** A self-replicating system. Peptide **I** binds the two halves of **I** (actually a coiled-coil trimer, **I**<sub>3</sub>), acting as a template, and placing **Ia** and **Ib** in the correct position for the occurrence of the ligation reaction.

to the binding of the two halves to **I** (actually a coiled-coil trimer, **I**<sub>3</sub>) that acts as a template, thus placing **Ia** and **Ib** in the correct positions for the occurrence of the ligation reaction. The relative stability of the coiled-coil complexes appears to be the basis of the enhanced catalytic efficiency and low product inhibition of this system. A step forward into complexity in self-replication is provided by many of the systems described by Luisi and his group.<sup>[63–65]</sup> The basic idea behind this chemistry is that the lipid aggregates that are the constituents of a liposome (or vesicle) provide the elements for the minimal reaction vessel, a protocell, where reactions pertinent to living systems may occur.<sup>[66]</sup> They were able to show that under appropriate conditions, these lipids can be continuously generated from a precursor, thus providing new constituents for new vesicle formation. If the vesicles catalyze the process of the generation of the constituent lipids from the precursor, the system becomes self-replicating. This proved to be the case, and self-replicating vesicles were reported. Now the system can be even more complex, in that self-replication may be controlled via a competing reaction that consumes the lipids. Depending on the conditions, the relative rates of lipid formation ( $v_f$ ) and consumption ( $v_c$ ) may be such as to produce the growth of the vesicles ( $v_f > v_c$ ), their death ( $v_f < v_c$ ), or homeostasis ( $v_c = v_f$ ). A chemical model for such a system was reported.<sup>[67]</sup> The basic component of this chemical model is a vesicular solution composed of an oleic acid/oleate lipid mixture charged with dihydroquinidine and OsO<sub>4</sub>. These vesicles are continuously fed with oleic anhydride that is hydrolyzed in the oleic acid/oleate bilayer thus providing the source of new lipids (and, hence, new vesicles) and an oxidizing agent [K<sub>3</sub>Fe(CN)<sub>6</sub>]. This latter oxidizes the *cis* double bond of the lipid in a process that is OsO<sub>4</sub> catalyzed. If the hydrolysis reaction induces the growth of the vesicles, the oxidation one brings about their destruction, because the dihydroxystearic acid derivatives produced do not form vesicles. The careful control of the conditions leads to  $v_f = v_c$  and to homeostasis of the system. As pointed out by the authors, the model is primitive, but it sets the basis for the obtainment of more complex and biologically relevant systems and, perhaps, to a metabolic model of a cell.

## CONCLUSION

The mimicry of biological systems and, even more interesting, the synthesis of molecules working on the basis of the same principles that govern the natural ones but with unprecedented properties, are the challenges that supramolecular chemistry faces in this new century. The overview provided above gives readers an idea of some of

the avenues chemists working in this field are undertaking. More exciting results are expected in the future.

## ARTICLES OF FURTHER INTEREST

*The Allosteric Effect*, p. 20  
*Artificial Enzymes*, p. 76  
*Catalytic Antibodies*, p. 193  
*Crown Ethers*, p. 326  
*Cyclodextrins*, p. 398  
*DNA Nanotechnology*, p. 475  
*Enzyme Mimics*, p. 546  
*Enzymes: Characteristics and Mechanisms*, p. 554  
*Hydrogen Bonding*, p. 658  
*Hydrophobic Effects*, p. 673  
*Ion Channels and Their Models*, p. 742  
*Ionophores*, p. 760  
*Molecular-Level Machines*, p. 931  
*Rotaxanes and Pseudorotaxanes*, p. 1194  
*Self-Assembly in Biochemistry*, p. 1257  
*The Template Effect*, p. 1493  
*Vitamin B<sub>12</sub> and Heme Models*, p. 1569

## REFERENCES

1. Lehn, J.-M. Toward complex matter: Supramolecular chemistry and self-organization. *Proc. Natl. Acad. Sci. U. S. A.* **2002**, *99*, 4763–4768.
2. Goshe, A.J.; Steele, I.M.; Ceccarelli, C.; Rheingold, A.; Bosnich, B. Supramolecular recognition: On the kinetic lability of thermodynamically stable host-guest association complexes. *Proc. Natl. Acad. Sci. U. S. A.* **2002**, *99*, 4823–4829.
3. Gellman, S.H. Foldamers: A manifesto. *Acc. Chem. Res.* **1998**, *31*, 173–180.
4. Etezady-Esfarjani, T.; Hilty, C.; Wütrich, K.; Rueping, M.; Schreiber, J.; Seebach, D. NMR-structural investigations of a  $\beta^3$ -dodecapeptide with proteinogenic side chains in methanol and in aqueous solutions. *Helv. Chim. Acta* **2002**, *85*, 1197–1209.
5. Raguse, T.L.; Porter, E.A.; Weisblum, B.; Gellman, S.H. J. Structure-activity studies of 14-helical antimicrobial  $\beta$ -peptides: Probing the relationship between conformational stability and antimicrobial potency. *Am. Chem. Soc.* **2002**, *124*, 12774–12785.
6. Toniolo, C.; Crisma, M.; Formaggio, F.; Valle, G.; Cavicchioni, G.; Précigoux, G.; Aubry, A.; Kamphuis, J. Linear oligopeptide. 279. Structures of peptides from  $\alpha$ -amino-acids methylated at the  $\alpha$ -carbon. *Biopolymers* **1993**, *33*, 1061–1073.
7. Connors, K.A. The stability of cyclodextrin complexes in solution. *Chem. Rev.* **1997**, *97*, 1325–1357.
8. Davis, A.P.; Wareham, R.S. A tricyclic polyamide receptor

- for carbohydrates in organic media. *Angew. Chem., Int. Ed.* **1998**, *37*, 2270–2273.
9. Ryan, T.J.; Lecollinet, G.; Velasco, T.; Davis, A.P. Phase transfer of Monosaccharides through noncovalent interactions: Selective extraction of glucose by a lipophilic cage receptor. *Proc. Natl. Acad. Sci. U. S. A.* **2002**, *99*, 4863–4866.
  10. Kirby, A.J. Enzyme mechanisms, models, and mimics. *Angew. Chem., Int. Ed.* **1996**, *35*, 707–724.
  11. Breslow, R.; Dong, S.D. Biomimetic reactions catalyzed by cyclodextrins and their derivatives. *Chem. Rev.* **1998**, *98*, 1997–2011.
  12. Breslow, R.; Trainor, G.; Ueno, J. Optimization of metallocene substrates for  $\beta$ -cyclodextrin in reactions. *Am. Chem. Soc.* **1983**, *105*, 2739–2740.
  13. Kunishima, M.; Yoshimura, K.; Morigaki, H.; Kawamata, R.; Terao, K.; Tani, S. Cyclodextrin-based artificial acyl-transferase: Substrate-specific catalytic amidation of carboxylic acids in aqueous solvent. *J. Am. Chem. Soc.* **2001**, *123*, 10760–10761.
  14. Mattei, P.; Diederich, F. Catalytic cyclophanes. 11. A flavo-thiazolio-cyclophane as a biomimetic catalyst for the preparative-scale electro-oxidation of aromatic aldehydes to methyl esters. *Helv. Chim. Acta* **1997**, *80*, 1555–1588.
  15. Scarso, A.; Scheffer, U.; Göbel, M.; Broxterman, Q.B.; Kaptein, B.; Formaggio, F.; Toniolo, C.; Scrimin, P. A peptide template as an allosteric supramolecular catalyst for the cleavage of phosphate esters. *Proc. Natl. Acad. Sci. U. S. A.* **2002**, *99*, 5144–5149.
  16. Baltzer, L. Functionalization of designed folded polypeptides. *Curr. Opin. Struct. Biol.* **1998**, *8*, 466–470.
  17. Nilsson, J.; Baltzer, L. Reactive-site design in folded-polypeptide catalyst—The leaving group  $pK_a$  of reactive esters sets the stage for cooperativity in nucleophilic and general-acid catalysis. *Chem. Eur. J.* **2000**, *6*, 2214–2220.
  18. Baltzer, L.; Nilsson, H.; Nilsson, J. De Novo design of proteins. What are the rules? *Chem. Rev.* **2001**, *101*, 3153–3163.
  19. Anderson, L.K.; Caspersson, M.; Baltzer, L. Control of lysine reactivity in four-helix bundle proteins by site-selective  $pK_a$  depression: Expanding the versatility of proteins by postsynthetic functionalisation. *Chem. Eur. J.* **2002**, *8*, 3687–3697.
  20. Klotz, I. *Enzyme Models-Synthetic Polymers*; Williams, A., Page, M., Eds.; The Royal Society of Chemistry: London, 1987; 14–34.
  21. Hollfelder, F.; Kirby, A.J.; Tawfik, D.S. Efficient catalysis of proton transfer by synzymes. *J. Am. Chem. Soc.* **1997**, *119*, 9578–9579.
  22. Lie, L.; Breslow, R. A potent polymer/pyridoxamine enzyme mimic. *J. Am. Chem. Soc.* **2002**, *124*, 4978–4979.
  23. Wentworth, P. Antibody design by man and nature. *Science* **2002**, *296*, 2247–2249.
  24. Jain, M. *Introduction to Biological Membranes*, 2nd Ed.; Wiley: New York, 1992.
  25. Urry, D.W. Chemical basis of ion transport specificity in biological membranes. *Top. Curr. Chem.* **1985**, *128*, 175–191.
  26. Åkerfeldt, K.S.; Lear, J.D.; Wasserman, Z.R.; Chung, L.A.; DeGrado, W.F. Synthetic peptides as models for ion channel protein. *Acc. Chem. Res.* **1993**, *26*, 191–197.
  27. Benedetti, E.; Bavoso, A.; Di Blasio, B.; Pavone, V.; Pedone, C.; Toniolo, C.; Bonora, G.M. Peptaibol antibiotics: A study on the helical structure of the 2-9 sequence of emerimicins III and IV. *Proc. Natl. Acad. Sci. U. S. A.* **1982**, *79*, 7951–7955.
  28. Gennis, R.B. *Biomembranes: Molecular Structure and Function*; Springer-Verlag: New York, 1989.
  29. Ghadiri, R.M.; Granja, J.R.; Buehler, L.K. Artificial transmembrane ion channels from self-assembling peptide nanotubes. *Nature* **1994**, *369*, 301–305.
  30. Khazanovich, N.; Granja, J.R.; McRee, D.E.; Milligan, R.A.; Ghadiri, M.R. Nanoscale tubular ensembles with specified internal diameters. Design of a self-assembled nanotube with a 13-Å pore. *J. Am. Chem. Soc.* **1994**, *116*, 6011–6012.
  31. Ghadiri, M.R.; Granja, J.R.; Milligan, R.A.; McRee, D.E.; Khazanovich, N. Self-assembling organic nanotubes based on a cyclic peptide architecture. *Nature* **1993**, *366*, 324–328.
  32. Kim, H.S.; Hartgerink, J.D.; Ghadiri, M.R. Oriented self-assembly of cyclic peptide nanotubes in lipid membranes. *J. Am. Chem. Soc.* **1998**, *120*, 4417–4418.
  33. Voyer, N.; Robitaille, M. Novel functional artificial ion channel. *J. Am. Chem. Soc.* **1995**, *117*, 6599–6600.
  34. Winum, J.-Y.; Matile, S. J. Rigid push-pull oligo(p-Phenylene) rods: Depolarization of bilayer membranes with negative membrane potential. *Am. Chem. Soc.* **1999**, *121*, 7961–7962.
  35. Sakai, N.; Brennan, K.C.; Weiss, L.A.; Matile, S. Toward biomimetic ion channels formed by rigid-rod molecules: Length-dependent ion-transport activity of substituted oligo(p-phenylene)s. *J. Am. Chem. Soc.* **1997**, *119*, 8726–8727.
  36. Goto, C.; Yamamura, M.; Satake, A.; Kobuke, Y. J. Artificial ion channels showing rectified current behavior. *Am. Chem. Soc.* **2001**, *123*, 12152–12153.
  37. De Riccardis, F.; Di Filippo, M.; Garrisi, D.; Izzo, I.; Mancin, F.; Pasquato, L.; Scrimin, P.; Tecilla, P. An artificial ionophore based on a polyhydroxylated steroid dimer. *Chem. Commun.* **2002**, 3066–3067.
  38. Moore, K.S.; Wehrli, S.; Roder, H.; Rogers, M.; Forrest, J.N., Jr.; McCrimmon, D.; Zasloff, M. Squalamine: An aminosterol antibiotic from the shark. *Proc. Natl. Acad. Sci. U. S. A.* **1993**, *90*, 1354–1357.
  39. Sadownik, A.; Deng, G.; Janout, V.; Regen, S.L. Rapid construction of squalamine mimic. *J. Am. Chem. Soc.* **1995**, *117*, 6138–6139.
  40. Otto, S.; Osifchin, M.; Regen, S.L. Squeezing a synthetic ionophore and mechanistic insight out of a lipid bilayer. *J. Am. Chem. Soc.* **1999**, *121*, 10440–10441.
  41. Balzani, V.; Scandola, F. Photochemical and PhotoPhysical Devices. In *Comprehensive Supramolecular Chemistry*; Atwood, J.L., Davies, J.E.D., MacNicol, D.D., Vögtle, F., Lehn, J.-M., Reinhoudt, D.N., Eds.; Pergamon: Oxford, 1996; Vol. 10.

42. Chambron, J.-C.; Heitz, V.; Sauvage, J.-P. Noncovalent Multiporphyrin Assemblies. In *The Porphyrin Handbook*; Kadish, K.M., Smith, K.M., Guillard, R., Eds.; Academic Press: New York, 2000; Vol. 6, 1–42.
43. *Supramolecular Photochemistry*; Balzani, V., Scandola, F., Eds.; Ellis Horwood Ltd.: New York, 1991.
44. Ward, M.D. Photo-induced electron and energy transfer in non-covalently bonded supramolecular assemblies. *Chem. Soc. Rev.* **1997**, *26*, 365–375.
45. Blanco, M.-J.; Jimenez, M.C.; Chambron, J.-C.; Heitz, V.; Linke, M.; Sauvage, J.-P. Rotaxanes as new architectures for photoinduced electron transfer and molecular motions. *Chem. Soc. Rev.* **1999**, *28*, 293–305.
46. Haycock, R.A.; Yartsev, A.; Michelsen, U.; Sundstrom, V.; Hunter, C.A. Self-assembly of pentameric porphyrin light-harvesting antennae complexes. *Angew. Chem., Int. Ed.* **2000**, *39*, 3616–3619.
47. Sugou, K.; Sasaki, K.; Kitajima, K.; Iwaki, T.; Kuroda, Y. J. Light-harvesting heptadecameric porphyrin assemblies. *Am. Chem. Soc.* **2002**, *124*, 1182–1183.
48. von Kiedrowski, G. A self-replicating hexadeoxynucleotide. *Angew. Chem., Int. Ed. Engl.* **1986**, *25*, 932–934.
49. Li, T.; Nicolaou, K.C. Chemical self-replication of palindromic duplex DNA. *Nature* **1994**, *369*, 218–221.
50. Sievers, D.; von Kiedrowski, G. Self-replication of complementary nucleotide-based oligomers. *Nature* **1994**, *369*, 221–224.
51. Luther, A.; Brandsch, R.; von Kiedrowski, G. Surface-promoted replication and exponential amplification of DNA analogues. *Nature* **1998**, *396*, 245–248.
52. Issac, R.; Ham, Y.-W.; Chmielewski, J. The design of self-replicating helical peptides. *Curr. Opin. Struct. Biol.* **2001**, *11*, 458–463.
53. Lee, D.H.; Granja, J.R.; Martinez, J.A.; Severin, K.; Ghadiri, M.R. A self-replicating peptide. *Nature* **1996**, *382*, 525–529.
54. Severin, K.; Lee, D.B.; Martinez, J.A.; Ghadiri, M.R. Peptide self-replication via template-directed ligation. *Chem. Eur. J.* **1997**, *3*, 1017–1023.
55. Yao, S.; Ghosh, I.G.; Zutshi, R.; Chmielewski, J. A pH-modulated, self-replicating peptide. *J. Am. Chem. Soc.* **1997**, *119*, 10559–10560.
56. Yao, S.; Ghosh, I.G.; Zutshi, R.; Chmielewski, J. Selective amplification by auto- and cross-catalysis in a replicating peptide system. *Nature* **1998**, *396*, 447–450.
57. Yao, S.; Ghosh, I.G.; Zutshi, R.; Chmielewski, J. A self-replicating peptide under ionic control. *Angew. Chem., Int. Ed.* **1998**, *37*, 478–481.
58. Dawson, P.E.; Muir, T.W.; Clark-Lewis, L.; Kent, S.B.H. Synthesis of proteins by native chemical ligation. *Science* **1994**, *266*, 776–778.
59. Yao, S.; Chmielewski, J. A pH-tunable peptide ligase. *Biopolymers* **1999**, *51*, 370–375.
60. Saghtelian, A.; Yobobayeshi, Y.; Soltani, K.; Ghadiri, M.R. A chiroselective peptide replicator. *Nature* **2001**, *409*, 797–801.
61. Severin, K.; Lee, D.H.; Martinez, J.A.; Vieth, M.; Ghadiri, M.R. Dynamic error correction in autocatalytic peptide networks. *Angew. Chem., Int. Ed.* **1998**, *37*, 126–128.
62. Issac, R.; Chmielewski, J. Approaching exponential growth with a self-replicating peptide. *J. Am. Chem. Soc.* **2002**, *124*, 6808–6809.
63. Bachmann, P.A.; Luisi, P.L.; Lang, J. Autocatalytic self-replicating micelles as models for prebiotic structures. *Nature* **1992**, *357*, 57–59.
64. Walde, P.; Wick, R.; Fresta, M.; Mangone, A.; Luisi, P.L. Autopoietic self-reproduction of fatty acid vesicles. *J. Am. Chem. Soc.* **1994**, *116*, 11649–11654.
65. Morigaki, K.; Dallavalle, S.; Walde, P.; Colonna, S.; Luisi, P.L. Autopoietic self-reproduction of chiral fatty acid vesicles 301. *J. Am. Chem. Soc.* **1997**, *119*, 292–301.
66. Szostak, J.W.; Barteld, P.; Luisi, P.L. Synthesizing life. *Nature* **2001**, *409*, 387–390.
67. Zepik, H.H.; Blöchliger, E.; Luisi, P.L. A chemical model of homeostasis. *Angew. Chem., Int. Ed.* **2001**, *40*, 199–202.



# Biomaterials

Judith R. Meakin

*University of Aberdeen, Foresterhill, Aberdeen, United Kingdom*

## INTRODUCTION

A biomaterial is any natural or synthetic material that is employed as, or part of, a medical device. Typical materials include metals, ceramics, glasses, polymers, and tissue-engineered materials. The requirements of a biomaterial are that it should have the correct properties to allow it to achieve its intended function and be biocompatible. Over recent decades, there have been many developments in biomaterials research. Some of these developments have involved a movement from the use of inert materials to more sophisticated ones, which actively invoke a beneficial response from the body.

## WHAT ARE BIOMATERIALS AND WHY DO WE NEED THEM?

Biomaterials are natural or synthetic materials that can be used as, or part of, a medical device to augment, repair, or replace a natural tissue within the body. They include tissue from the recipient's body (autograft), from another human being (allograft), from an animal of another species (xenograft), or a synthetic substitute. In this article, emphasis will be given to synthetic materials (metals, glasses, ceramics, polymers, and tissue-engineered materials) and some of the recent developments in this field.

The types of medical devices that require biomaterials are wide ranging across most medical disciplines.<sup>[1]</sup> Artificial heart valves, contact lenses, drug delivery implants, urinary catheters, and replacement hip joints are just a few examples that demonstrate where biomaterials can be employed in the body.

Medical devices, and hence biomaterials, are becoming increasingly important in developed countries due to changes in society. With increasing life expectancy and better health care, people expect to remain active into their seventies and eighties. An increase in leisure time has led to an increase in injuries from sports, e.g., skiing. Furthermore, diseases such as heart disease and diabetes, which have become more prevalent in recent decades, require biomaterials to provide long-term solutions rather than the palliative treatments currently available.<sup>[2]</sup>

In the U.K., there is a demand for medical devices that are quick and easy to implant, that minimize postsurgical complications, and that last the intended duration.<sup>[1]</sup> The importance given to this demand is demonstrated by the "Building up Biomaterials" program, which was recently launched by the Department of Trade and Industry. This program aims to promote the growth and competitiveness of the Biomaterials industry in the U.K. by bringing together clinicians, researchers, and the medical device industry.

## GENERAL REQUIREMENTS OF A BIOMATERIAL

The two principal requirements of any biomaterial used in a medical device are that it should have the correct physical properties in order for it to perform its intended function, and it should be biocompatible. Other requirements are that it can be easily manufactured and can be suitably sterilized. There are various sterilization methods; the use depends mainly on the material being sterilized. Gamma-ray or high-temperature sterilization methods, for example, are unsuitable for polyurethanes, as they produce toxic and carcinogenic compounds.<sup>[3]</sup>

The physical properties of a biomaterial include mechanical properties, such as stiffness, strength, and durability, together with other properties, such as oxygen permeability. The properties need to be suitable for the intended lifetime of the implant, which can range from the few weeks required for resorbable sutures to the lifetime of the patient receiving a hip replacement.

Biocompatibility essentially means that the material produces no adverse response from the body; this may be toxic, allergenic, carcinogenic, or mechanical. However, the body can tolerate even nonbiocompatible materials if the quantity of the material is small enough. Adverse responses can arise in response to chemical or particulate products that are released from a biomaterial. Metals, for example, are particularly susceptible to corrosion by body fluids, and the products of corrosion, such as metallic ions, salts, and oxides, can induce an immune response.<sup>[4]</sup> Particles, resulting from mechanical wear of an implant, may also invoke an immune response, even if this would

not be induced by the bulk material.<sup>[5]</sup> Not only can loss of material from an implant lead to an adverse reaction, but it can also compromise the integrity, and hence function, of the device.

As well as physiological effects, implants can have adverse mechanical effects. Ideally, the mechanical properties of an implant should be compatible with those of the surrounding tissues. Large differences in stiffness though, can result in high interfacial shear stresses. The resulting micromovement may then lead to loosening and eventual failure of the implant. A difference in stiffness also changes the distribution of mechanical stress on the surrounding tissues. This can cause the tissue to degenerate or remodel. In hip replacements, for example, the high stiffness of the implants compared to the bone of the femur can reduce the stress in the bone.<sup>[6]</sup> This “stress shielding” results in the bone being resorbed by the body. It is also hypothesized that modified stress distributions may result in continuing pain for the patient.<sup>[7]</sup>

## TYPICAL BIOMATERIALS

### Metals

The metals commonly used in medical devices are stainless steel (Types 316 and 316 L), cobalt-chromium-based alloys, titanium, and titanium-based alloys. Metals are used extensively in orthopedic surgery for load-bearing devices, such as artificial joints and fixation devices (wires, pins, screws, fracture plates, etc.). Other metals include tantalum, gold, and mercury alloys; the latter two are used predominantly in dentistry.

One of the main problems of metallic orthopedic implants is that they are much stiffer than the natural tissues they replace (see Table 1). As described above, a difference in stiffness between adjacent materials can lead to a number of problems, including loosening as a result of micromovement and bone resorption due to stress shielding. Adequate fixation of an orthopedic implant to the

surrounding bone is therefore of paramount importance. It can be achieved using a number of methods, such as interference fitting, screws, poly(methyl methacrylate) bone cement, and coatings to achieve a chemical bond or porous ingrowth.<sup>[5]</sup>

Titanium may appear to be the ideal metal, as its stiffness is the closest to bone (Table 1). It has the lowest density (nearly half that of the other two metals), and it has the highest resistance to corrosion due to the formation of a nonreactive layer of titanium oxide on the surface of the metal. However, its shear strength is low, making it unsuitable for use in screws and bone plates. It also has a high coefficient of friction when in contact with itself or another metal, making it unsuitable as a load-bearing surface.

Stainless steel, which is typically used for bone plates, screws, and nails, is particularly susceptible to corrosion, although its chromium and molybdenum content (about 17% and 3%, respectively) helps to make it more resistant. Cobalt-chromium-molybdenum alloys exhibit excellent durability and strength, making them apposite for artificial joints, although their coefficients of friction make them unsuitable for load-bearing surfaces.

One interesting alloy of titanium and nickel, called Nitinol, exhibits shape-memory properties. Below a particular temperature (the transformation temperature), the crystal structure of the alloy is such that it can be plastically deformed (martensitic). As the alloy is heated, the crystal structure alters to one that is more ordered and rigid (austenitic), and the deformed metal reverts to its original shape.<sup>[8]</sup> This effect has been exploited in a number of devices, including a stent (a device used to hold open passageways such as arteries). The stent is placed inside a small-diameter catheter for insertion into the body, where it expands on being warmed to body temperature.<sup>[8]</sup>

Tantalum, which is used for a number of applications,<sup>[9]</sup> was recently made into a porous material that could be used for bone reconstruction. The porous structure is made by depositing the metal onto a vitreous carbon scaffold using chemical vapor deposition/infiltration techniques. Its low structural density means that its stiffness (2.5–4 GPa) is closer to that of natural bone than the solid metal, and the porosity means that bone can fully integrate into the structure, forming an excellent bond.<sup>[9]</sup>

### Ceramics and Glasses

Ceramics, such as the commonly used Alumina ( $\text{Al}_2\text{O}_3$ ) and Zirconia ( $\text{ZrO}_2$ ), tend to have a very high elastic modulus (around 400 GPa), have a low coefficient of friction, and are resistant to wear. These properties make them useful as the load-bearing surfaces in orthopedic implants,

**Table 1** Typical material properties of metals and bone

Material	Elastic modulus (GPa)
Stainless steel	200
Co-Cr-Mb alloy	230
Titanium	110
Cortical bone	12–17
Cancellous bone	0.1

Cortical bone is a dense structure located at the surfaces of bones; cancellous bone is an open pore structure located internally. (From Ref. [5].)

such as hip prostheses.<sup>[6]</sup> Another of their properties, which leads to them being popular for dental applications, is their inertness, which makes them very biocompatible. However, more interesting ceramics exist that, rather than being inert, provoke a beneficial response from the body.

Calcium phosphate is a mineral found in several different forms, including hydroxyapatite,  $\beta$ -whitlockite, and tricalcium phosphate. The crystal structure of hydroxyapatite  $[\text{Ca}_{10}(\text{PO}_4)_6(\text{OH})_2]$ , is similar to that of the calcium and phosphate apatites that are present in the mineral phase of bone. It was found that if a metallic implant is coated with a calcium-phosphate-based material, the formation of bone around the implant is accelerated, and surface contact in the early stages of healing is improved.<sup>[10,11]</sup> This is because, in addition to providing a porous surface with which the bone can integrate, the coatings are able to form a direct chemical bond with the bone.

Bioactive glasses are another type of material that actively promote a useful response from the tissue into which they are implanted. Bioactive glasses are a family of glass materials made from  $\text{Na}_2\text{O}-\text{CaO}-\text{P}_2\text{O}_5-\text{SiO}_2$ . Certain formulations of these glasses are able to form very strong bonds with bone. When the glass is exposed to fluids in the body, a 12-stage reaction occurs<sup>[12]</sup> that involves formation of a hydroxyl carbonate apatite (HCA) layer on the outer surface of the glass. It is this outer layer that is thought to be crucial for bonding to bone to occur.

A smaller subset of the bioactive glasses can also form bonds with collagen.<sup>[12]</sup> In vitro tests showed that the collagen fibrils integrate into the outer HCA layer. This is similar to the way that collagen fibrils in natural tissues such as cartilage, ligament, etc., bond to the underlying bone. Hence, bioactive glasses have the potential to provide a solution to the problem of how to attach replacement soft tissues such as ligaments or the menisci of the knee.

The main drawback of bioactive glasses is their brittle properties and insufficient strength, making them unsuitable for load-bearing applications. However, combining them with polymers was shown to improve the mechanical properties while retaining the bioactivity.<sup>[13]</sup>

## Polymers

Many different polymers are used in a variety of medical devices.<sup>[3]</sup> These range from ultrahigh-density polyethylene, which is used as the load-bearing surface of artificial joints,<sup>[6]</sup> to much softer elastomers, such as silicones, which are employed, among other uses, as finger joint replacements and maxillofacial prostheses.

One particular class of polymers that absorb and retain significant amounts of water are called hydrogels. The

water in a hydrogel is retained in the gel by hydrogen bonding to hydroxyl groups along the polymer backbone. Over the years, there has been considerable controversy on the exact state of the water.<sup>[14]</sup> However, some of the most recent research, using thermal analysis, suggests that the water is present as three different phases in dynamic equilibrium.<sup>[15]</sup>

Hydrogels have many actual or potential uses—most notably as contact lenses, wound dressings, coatings, and drug delivery systems.<sup>[16]</sup> The hydrophilic nature of hydrogels, plus their high water content, makes them extremely biocompatible. As a coating on a device such as a catheter, particularly in combination with antimicrobial agents, they can help prevent the buildup of bacteria that may otherwise lead to blockage and infection.

As a contact lens, their soft rubbery properties make them comfortable to wear. However, one of their limitations is the high water content and thin cross section required to achieve sufficient oxygen transport to the cornea. This is extremely important, as the cornea does not have its own vascular supply and relies on obtaining oxygen in this way.

The more recently developed silicone hydrogels have the potential to solve this problem because although they have relatively low water contents (about 30%), in comparison to the conventionally used hydrogels, their oxygen permeability is far higher.<sup>[17]</sup> This characteristic, combined with their good biocompatibility, has allowed them to be manufactured into lenses that can be worn continuously for up to a month.

Another exciting development for hydrogels is self-assembly.<sup>[18]</sup> Self-assembly means that the constituent molecules of a material organize themselves, under thermodynamic equilibrium, into a well-defined and stable configuration, held together by noncovalent bonds. The structural form of the molecules determines the way they fit together, and this can be influenced by environmental factors including temperature and pH value.<sup>[18]</sup>

Biodegradable polymers, as their name suggests, slowly degrade once they are implanted into the body. Several biodegradable polymers have been approved for implantation [poly(glycolide), poly(lactide), poly( $\epsilon$ -caprolactone), poly(dioxanone), and their copolymers] and have been manufactured into a number of medical devices, such as sutures, screws, and tissue repair barbs.<sup>[19]</sup> One advantage of using a biodegradable material is that additional surgery to remove a temporary device is unnecessary. Also, in applications such as fixation of a broken bone, the gradual degradation of the device means that load is transferred to the bone as it heals; this can help the bone regain its complete strength.

Degradation occurs due to hydrolysis of the polymer backbone or by enzymatic attack, which breaks the polymer into increasingly smaller units. The resulting

compounds may then dissolve into the surrounding body fluids or may be metabolized and excreted by the body [e.g., lactic acid removed as a product of poly(lactide)].

### Tissue-Engineered Materials

Tissue engineering is perhaps most memorable to many people as an image of an ear growing on the back of a mouse.<sup>[20]</sup> Currently, the only commercially available product is skin grown from human fibroblasts on a biodegradable mesh. However, research continues toward achieving the ultimate aim of growing a fully functioning tissue or organ using cells from the patient's own body (e.g., Ref. [21]).

One of the potential benefits of tissue engineering is that it could eliminate the need for donor tissue and organs, which are in short supply. Additionally, there is less likely to be the problems of rejection or disease transfer that occur when using allografts or xenografts.

Essentially, the technique involves seeding cells onto a scaffold and providing them with the appropriate nutrients, growth factors, and environmental conditions.<sup>[22]</sup> When they sufficiently proliferated, the structure can be implanted into the patient, where it becomes integrated into its surroundings with the formation of blood vessels, etc. The scaffold not only determines the shape of the tissue but can also provide mechanical support as it develops. Once the tissue forms, the scaffold becomes redundant. Hence, materials for scaffolds are ideally made from synthetic biodegradable polymers, as described in the previous section, or from natural polymers such as collagen.

Fabrication of a three-dimensional scaffold can be achieved using a number of methods. One technique that was recently explored is fused deposition modeling (FDM). This is a rapid prototyping method, where the material [poly( $\epsilon$ -caprolactone)] is heated to just above its melting temperature and extruded as a thin thread that is laid down in layers.<sup>[23]</sup> Effectively, any three-dimensional structure can be made providing there is a computer file describing its geometry; this has useful applications for defining scaffolds from medical images.

The future success of tissue engineering is heavily dependent on understanding what external factors influence cell behavior (e.g., cell attachment, proliferation, migration, and expression of extracellular matrix). The laying down of extracellular matrix components such as collagen, for example, is important for growing tissues like ligaments, which require the collagen to be aligned in a specific direction.<sup>[24]</sup> So far, various external stimuli have been shown to influence cell behavior. These include surface topography in the form of grooves or surface texture and mechanical deformation.<sup>[22]</sup>

### CONCLUSION

Since the first metal implants used in the early part of the twentieth century, biomaterials for use in medical devices have developed significantly. In the last few decades, materials technology has become more sophisticated, and there has been a move from the use of passive, inert materials toward ones that interact with the body to elicit a beneficial response or more closely mimic the natural tissues. However, there is still a need for further developments, and a recent report highlighted the desperate need for new biomaterials in all clinical disciplines.<sup>[2]</sup>

In the shorter term, improvements in existing materials are required. For example, 10% of hip replacement operations are revision surgeries. These are more technically difficult than the primary surgeries, are considerably more expensive, and tend to be less successful.<sup>[2]</sup> Hence, improvements can still be made in the materials used for hip prostheses and the methods used to fix them in place.

Over the longer term, a demand exists for materials that can provide permanent solutions. Tissue engineering may provide solutions to some of these needs in the future. However, despite recent success in this area, the development of functional tissue may still be a long way off. For example, it was estimated that it may take another 10–15 years to develop tissue-engineered kidneys.<sup>[2]</sup> Furthermore, for load-bearing tissues such as ligaments, the mere development of a material with suitable mechanical properties is only one concern. A major problem that requires resolution, is how to attach the ligament to the bones. However, as previously described, bioactive glasses may provide a solution.

In this article, the various biomaterials described have, in general, been considered separately. However, the use of biodegradable polymers in tissue engineering<sup>[23]</sup> and the fabrication of hydrogels by self-assembly<sup>[25]</sup> suggest that future developments in biomaterials research may benefit from an increasingly integrated approach.

### ACKNOWLEDGMENTS

I would like to thank the Wellcome Trust for funding my current research. I would also like to thank Dr. Simon Lee for his helpful comments concerning this manuscript.

### ARTICLES OF FURTHER INTEREST

*Crystal Growth Mechanisms*, p. 364

*Drug Delivery*, p. 484

*Gels*, p. 586

*Mesoporous Silicas and Silica-Organic Hybrids*, p. 852  
*Nanocasting Strategies and Porous Materials*, p. 950  
*Self-Assembly: Definition and Kinetic and Thermodynamic Considerations*, p. 1248  
*Self-Assembly: Terminology*, p. 1263

## REFERENCES

1. Bromhead, J. *Biomaterials State of the Art Report 2002*; 2002. LGC/GEN/2002/002, LGC (Teddington) Limited.
2. Bromhead, J. *Directory of Clinical Need*; 2002. LGC/GEN/2002/004, LGC (Teddington) Limited.
3. Yoda, R. Elastomers for biomedical applications. *J. Biomater. Sci., Polym. Ed.* **1998**, *9* (6), 561–626.
4. Hallab, N.; Merritt, K.; Jacobs, J.J. Metal sensitivity in patients with orthopaedic implants. *J. Bone Jt. Surg., Am.* **2001**, *83A* (3), 428–436.
5. Park, J.B.; Lakes, R.S. *Biomaterials: An Introduction*, 2nd Ed.; Plenum Press: New York, 1992.
6. Huo, M.H. What's new in hip arthroplasty. *J. Bone Jt. Surg., Am.* **2002**, *84A* (10), 1894–1905.
7. Mulholland, R.C.; Sengupta, D.K. Rationale, principles and experimental evaluation of the concept of soft stabilization. *Eur. Spine J. Suppl.* **2002**, *11*, S198–S205.
8. Barras, C.D.J.; Myers, K.A. Nitinol—Its use in vascular surgery and other applications. *Eur. J. Vasc. Endovasc. Surg.* **2000**, *19*, 564–569.
9. Bobyn, J.D.; Stackpool, G.J.; Hacking, S.A.; Tanzer, M.; Krygier, J.J. Characteristics of bone ingrowth and interface mechanics of a new porous tantalum biomaterial. *J. Bone Jt. Surg., Br.* **1999**, *81B* (5), 907–914.
10. Barrere, F.; van der Valk, C.M.; Dalmeijer, R.A.J.; van Blitterswijk, C.A.; de Groot, K.; Layrolle, P. In vitro and in vivo degradation of biomimetic octacalcium phosphate and carbonate apatite coatings on titanium implants. *J. Biomed. Mater. Res., A* **2003**, *64A* (2), 378–387.
11. Schliephake, H.; Scharnweber, D.; Dard, M.; Rossler, S.; Sewing, A.; Hutmacher, C. Biological performance of biomimetic calcium phosphate coating of titanium implants in the dog mandible. *J. Biomed. Mater. Res., A* **2003**, *64A* (2), 225–234.
12. Hench, L.L. Bioceramics. *J. Am. Chem. Soc.* **1998**, *81* (7), 1705–1728.
13. Thompson, I.D.; Hench, L.L. Mechanical properties of bioactive glasses, glass-ceramics and composites. *J. Eng. Med.* **1998**, *212*, 127–137.
14. McBrierty, V.J.; Martin, S.J.; Karasz, F.E. Understanding hydrated polymers: The perspective of NMR. *J. Mol. Liq.* **1999**, *80* (2–3), 179–205.
15. Meakin, J.R.; Imrie, C.T.; Hukins, D.W.L.; Aspden, R.M. Thermal analysis of poly(2-hydroxyethyl methacrylate) (pHEMA) hydrogels. *J. Mater. Sci., Mater. Med.* **2003**, *14* (1), 9–15.
16. Rosiak, J.M.; Yoshii, F. Hydrogels and their medical applications. *Nucl. Instrum. Methods, B* **1999**, *151*, 56–64.
17. Tighe, B. Silicone hydrogels—What are they and how should they be used in everyday practice? *Optician* **1999**, *281* (5726), 31–32.
18. Zhang, S. Emerging biological materials through molecular self-assembly. *Biotechnol. Adv.* **2002**, *20*, 321–339.
19. Middleton, J.C.; Tipton, A.J. Synthetic biodegradable polymers as orthopedic devices. *Biomaterials* **2000**, *21*, 2335–2346.
20. Cao, Y.L.; Vacanti, J.P.; Paige, K.T.; Upton, J.; Vacanti, C.A. Transplantation of chondrocytes utilizing a polymer-cell construct to produce tissue-engineered cartilage in the shape of a human ear. *Plast. Reconstr. Surg.* **1997**, *100* (2), 297–302.
21. Kim, T.H.; Vacanti, J.P. Tissue Engineering of the Liver. In *The Biomedical Engineering Handbook, Volume II*, 2nd Ed.; Bronzino, J.D., Ed.; CRC Press LLC: Boca Raton, FL, 2000; 121,1–121,9.
22. Berthiaume, F.; Yarmush, M.L. Tissue Engineering. In *The Biomedical Engineering Handbook, Volume II*, 2nd Ed.; Bronzino, J.D., Ed.; CRC Press LLC: Boca Raton, FL, 2000; 109,1–109,12.
23. Hutmacher, D.W. Scaffolds in tissue engineering bone and cartilage. *Biomaterials* **2000**, *21*, 2529–2543.
24. Hukins, D.W.L.; Aspden, R.M. Composition and properties of connective tissues. *Trends Biochem. Sci.* **1985**, *10* (7), 260–264.
25. Otsuka, H.; Nagasaki, Y.; Kataoka, K. Self-assembly of poly(ethylene glycol)based block copolymers for biomedical applications. *Curr. Opin. Colloid Interface* **2001**, *6*, 3–10.

# Biosensors

Jun-ichi Anzai

Tohoku University, Sendai, Japan

## INTRODUCTION

Enzyme–substrate, antibody–antigen, and other protein–ligand interactions are representative constituents of biological supramolecular systems. The structure and function of some of these biological supramolecular systems were mimicked by chemists in order to construct synthetic counterparts such as host–guest compounds, self-assembled monolayers and ordered multilayers, and related molecular assemblies. On the other hand, little was reported on the development of artificial supramolecular systems that use proteins as building blocks. Described in this article is the fabrication of biosensors using protein-based supramolecules based on avidin–biotin and lectin–sugar interactions.

## BIOSENSORS

Biosensors comprise a class of analytical devices that are fabricated by combining transducers, such as electrodes and optodes, with biological materials, including enzyme, antibody, and other proteins, for medical, environmental, or industrial applications. The biological materials are usually immobilized on the surface of the sensing part of the transducers in order to fabricate biosensors. Therefore, the technique of protein immobilization is crucial for developing high-performance biosensors. Numerous procedures for protein immobilization, including physical adsorption, entrapment into a polymer matrix, covalent bonding to a reactive surface, self-assembling on the surface, and others were reported. Physical adsorption is a convenient and simple way to immobilize proteins on the surface of the transducer, because proteins tend to be adsorbed more or less to any type of solid surfaces. Thus, the surface of the transducer can be modified irreversibly by immersing the transducer in an aqueous solution of dissolved proteins, which are then adsorbed into the transducer. However, this protocol suffers from the drawback that proteins often lose their biological activity due to denaturing on the surface (i.e., surface-induced conformational changes), resulting in a short life of the sensor. This drawback can be overcome by entrapping proteins into a polymer matrix on the surface of transducer, because the proteins are entrapped in organic

materials without direct contact with the surface of transducer. On the other hand, covalent bonding and self-assembly of proteins on the surface are sophisticated techniques that enable one to design structures and functions of sensors, although training to learn certain skills is often required. Recently, attention was devoted to the molecular-level modification of the surface of an electrode with proteins, in which the electrode surface is covered with a nanometer-sized thin film. One of the advantages of the molecular-level modification is that rapid-response sensors can be fabricated by removing the conventional type of thick membrane from the surface of the electrode. Another merit is that this method makes it possible to arbitrarily tune the performance of the sensors on the basis of the molecular-level design of the protein film.

## AVIDIN–BIOTIN SYSTEMS

Avidin is a tetramer protein (molecular mass: 67,000) found in egg white, and each subunit of avidin contains a binding site to biotin and forms a highly stable complex noncovalently (the binding constant;  $10^{15} \text{ M}^{-1}$ ) (Fig. 1).<sup>[1]</sup> Therefore, a single avidin molecule can accommodate up to four biotin molecules simultaneously. This strong and specific binding led to its widespread use in diagnostic and biochemical assays in which the formation of practically irreversible complexes is required. This is because avidin binds not only biotin but also its derivatives, with a carboxyl side chain that is modified covalently with protein and other macromolecules. Many kinds of activated biotins for labeling and biotin- or avidin-labeled reagents were developed for this purpose and are now commercially available.

A crystallographic study of avidin shows that the interactions include a hydrogen-bond network between the biotin ureide group and amino acid residues in the binding site, an interaction between the biotin sulfur atom and hydroxyl group of threonine in avidin, and a hydrogen bond between carboxylate in the biotin side chain and protein backbone.<sup>[2,3]</sup> Among these, the first interaction plays a dominant role in biotin binding. In the binding pocket, several polar residues are available, including asparagine, tyrosine, serine, and threonine, which participate in the network of hydrogen bonds with biotin

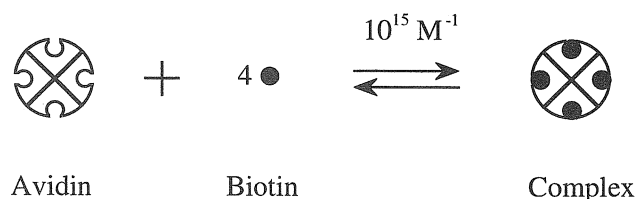


Fig. 1 Avidin-biotin complexation.

ureide groups. In addition, the contributions of hydrophobic and van der Waals' interactions between biotin and aromatic residues in the binding pocket were also suggested. Avidin is a tetrameric protein with 222 molecular symmetry, and each subunit is organized in an eight-stranded antiparallel orthogonal  $\beta$ -barrel.<sup>[4]</sup> An avidin molecule (tetramer) is in a cubic-like shape (ca.  $5.5 \times 6 \times 4$  nm). The binding sites to biotin are arranged in two pairs on opposed faces of the molecule. The two binding sites on the same faces ( $6 \times 5.5$  nm) are separated 2–2.5 nm from each other.<sup>[5]</sup> The shape and size of avidin makes its use promising as a building block for constructing supramolecular protein architectures.

## BIOSENSORS MODIFIED WITH AVIDIN-BIOTIN ARCHITECTURES

Electrochemical biosensors are usually fabricated by immobilizing enzymes or other functional proteins on the surface of electrodes. Illustrated in Fig. 2 is a typical structure and reactions involved in a glucose sensor fabricated by immobilizing glucose oxidase (GOx) on the surface of a metal electrode. The chemical events on the electrode surface induced by GOx can be transferred into the output signals (i.e., electric current). Thus, the immobilization technique of enzyme is crucial to the development of high-performance biosensors. Therefore, many techniques were developed for immobilizing proteins. Early studies of enzyme biosensors often employed thick polymer membranes (thickness: 0.01–1 mm) in which enzymes are physically or chemically anchored. They sometimes suffer from such drawbacks as insufficient reusability and slow response due to the suppressed diffusion of analytes in the thick polymer membrane. To overcome these problems, attention was recently devoted to the molecular-level modification of electrode surfaces (thickness: 10–100 nm) with enzymes or other proteins. An avidin-biotin system was employed for this purpose. For another example, in 1989, Walt and coworkers immobilized biotin-modified enzymes (urease, esterase, and penicillinase) on the surface of biotin-modified optical fibers using avidin as a binder.<sup>[6]</sup> They demon-

strated the general use of this procedure in immobilizing any kind of enzyme. Gunaratna and Wilson also used an enzyme column in which enzymes were immobilized through avidin-biotin complexation.<sup>[7]</sup>

It may be possible to build up a two- or three-dimensional architecture composed of proteins, using avidin and biotin-labeled enzymes as building blocks. An enzyme multilayer (illustrated in Fig. 3) would be constructed using enzymes tagged with more than two biotin residues, because avidin contains four biotin-binding sites per molecule. The biotin-binding sites are fortunately located in two pairs on the opposing faces of an avidin molecule. In order to check the possibility of multilayer formation, we immobilized fluorescein-5-isothiocyanate (FITC)-conjugated avidin and biotin-labeled GOx alternately on a quartz slide and monitored the absorption spectra of the modified slide.<sup>[8]</sup> A silylated quartz slide was immersed in FITC-avidin and biotin-labeled GOx solutions alternately and repeatedly, which provided both sides of the slide with the protein multilayer. FITC-avidin is immobilized in each layer as a roughly monomolecular layer.

An electrochemical technique, cyclic voltammetry (CV), was employed for further characterization of the GOx multilayer film.<sup>[9]</sup> In the GOx-catalyzed oxidation reaction of glucose, a cofactor flavine adenine dinucleotide (FAD), which is contained at the active center of GOx, oxidizes glucose to gluconolactone. The resultant  $\text{FADH}_2$  is converted back to the active FAD form by  $\text{O}_2$ . In the conventional type of enzyme sensor, the  $\text{H}_2\text{O}_2$  generated from  $\text{O}_2$  is oxidized at the electrode surface. It was reported that a GOx-catalyzed reaction can be mediated by synthetic redox compounds such as hydroquinone and ferrocene.<sup>[10–13]</sup> These redox compounds mediate electron relay from  $\text{FADH}_2$  in GOx to electrode (i.e., electron mediator). In this situation, the magnitude of oxidation current in CV of the electron mediator would be a function of the loading of the enzyme on the electrode surface. Therefore, the CV measurements in the solution of a constant amount of dissolved mediator and glucose

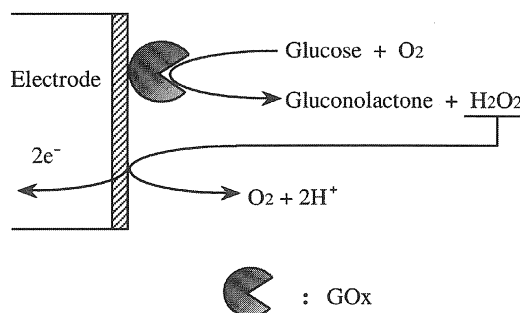
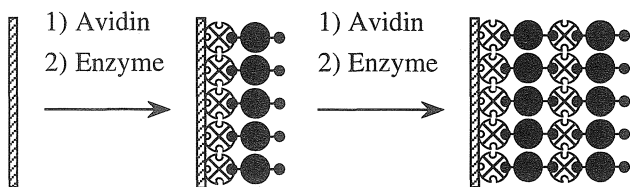


Fig. 2 Chemical reactions of a glucose sensor.





**Fig. 3** Enzyme multilayer films composed of avidin and biotin-labeled enzymes.

reveal the loading of GOx immobilized on the electrode. Thus, the oxidation current in CV was measured in the presence of ferrocenemethanol as mediator. The oxidation current depended linearly on the number of GOx layers, confirming that the present procedure can afford an enzyme multilayer composed of layers containing a constant amount of GOx.

A merit of enzyme multilayer films is that two or more different kinds of enzymes can be assembled simultaneously in the film, resulting in multienzyme biosensors. As an example, we prepared interference-free glucose sensors by assembling ascorbate oxidase (AOx) together with GOx on the Pt electrode.<sup>[14]</sup> Glucose sensors often suffer from interference arising from the direct oxidation of oxidizable substances such as ascorbic acid (vitamin C) and uric acid in biological fluids.<sup>[15]</sup> For the elimination of ascorbate interference, the enzyme multilayers composed of 10 GOx layers and an additional 10 AOx layers were assembled by depositing avidin and biotin-labeled GOx and AOx in a stepwise formation. In this glucose sensor, ascorbic acid is oxidized to an electrochemically inactive dehydroascorbic acid in the outer AOx layer, and the interference can be eliminated. Another example of the bienzyme multilayer-modified sensor includes acetylcholine sensors prepared using choline oxidase (ChOx) and choline esterase (ChE).<sup>[16]</sup>

It should be noted here that the avidin–biotin system can be applicable to the construction of many different types of protein architectures containing enzymes<sup>[17–19]</sup> and antibodies.<sup>[20,21]</sup> The biggest advantage of an avidin–biotin system is that the proteins can be strongly immobilized through biological affinity without cross-linking or chemical bonding, resulting in acceptable long-term stability.

## LECTIN–SUGAR SYSTEMS

Lectins are made up of a group of sugar-binding proteins widely found in plants and animals. Concanavalin A (Con A) is isolated from jack bean (*Canavalia ensiformis*) and is studied extensively among lectins. Con A (molecular mass: 104,000) is known to contain four identical binding

sites to  $\alpha$ -D-mannose and  $\alpha$ -D-glucose (binding constant:  $10^5$ – $10^6$  M<sup>-1</sup>).<sup>[22,23]</sup> Therefore, if an enzyme molecule is labeled with several residues of mannose or glucose units, one can expect that an alternate deposition of Con A and the sugar-labeled enzyme gives multilayer structures, as in the case of an avidin–biotin system. Glycoproteins can be used directly as materials for this purpose, because they inherently contain sugar chains on the surface. In case proteins do not contain a sugar chain, the surface of the protein may be labeled with sugar by using phenylisothiocyanate derivatives of sugar (Fig. 4), which react to an amino group in the protein. We used Con A and GOx and horseradish peroxidase (HRP), which contain sugar chains on the surface, for constructing supramolecular protein architectures, and they are employed as a sensitive layer of enzyme biosensors.

## BIOSENSORS MODIFIED WITH CON A–SUGAR ARCHITECTURES

Con A–GOx multilayer films were constructed using a native GOx, which inherently contains mannose residues on the surface of the polypeptide chains.<sup>[23,24]</sup> A layer-by-layer deposition of Con A and native GOx afforded a multilayer thin film composed of Con A and GOx layers. The multilayer film was coated on the surface of a Pt electrode to prepare glucose biosensors. The output current of the Con A/GOx multilayer film-modified electrode increased with an increasing number of layers, confirming that GOx is catalytically active in the film. Also, a constant amount of GOx was immobilized upon each deposition. The Con A–GOx multilayer-modified glucose sensors showed rapid responses to glucose, the response times being 10–15 sec for the sensors modified with 10 Con A–Gox layers. The rapid responses of the sensors can be ascribed to the thin nature of the multilayer films (the thickness of the unit layer: 10–15 nm). The sensors exhibited a linear calibration over the concentration range of  $1 \times 10^{-5}$  to  $2 \times 10^{-2}$  M glucose, which covers the normal and diabetic blood levels of glucose.

We also used HRP, because this enzyme is reported to contain ca. 18% sugar chains on the surface.<sup>[25,26]</sup> A layer-by-layer deposition of Con A and HRP afforded a multilayer film as expected, and HRP exhibited catalytic

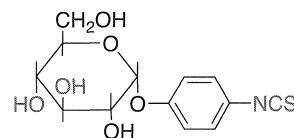


**Fig. 4** Phenylisothiocyanate derivative of sugar.



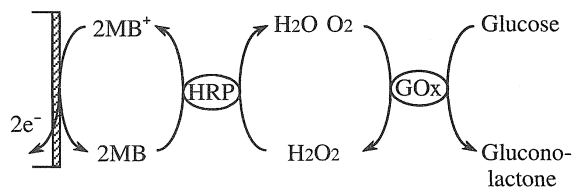


Fig. 5 Successive reactions of GOx and HRP.

activity to  $H_2O_2$  in the presence of methylene blue (MB) as the electron mediator. The HRP–GOx bienzyme multilayer films were prepared on the surface of a Pt electrode so as to develop glucose sensors, which detect glucose through successive reactions depicted in Fig. 5. In these bienzyme sensors, the response current depended on the geometry of the enzymes in the film. In practice, we prepared four different types of multilayer films:  $(HRP)_5 + (GOx)_5$ ,  $(GOx)_5 + (HRP)_5$ ,  $(HRP + GOx)_5$ , and  $(GOx + HRP)_5$ . These films contained an identical number of enzyme layers, but the sequence of enzyme layers differed. Among the films, the highest response was observed for the  $(HRP)_5 + (GOx)_5$  film, which is composed of inner  $(HRP)_5$  and outer  $(GOx)_5$  layers. Thus, the present technique is useful for designing the molecular geometry of the film.

We emphasize here that the Con A system can be used for immobilizing glycoproteins directly, without chemical modifications, which often induce deactivation of the biological activity of the protein.

## CONCLUSION

Supramolecular protein assemblies prepared by a layer-by-layer deposition technique are useful in the development of high-performance biosensors. Avidin–biotin and lectin–sugar systems are employed for this purpose. Many kinds of enzymes can be used as building blocks for the protein assemblies by modifying them with biotin and sugar residues. Glycoenzymes can be used to prepare Con A and enzyme multilayer assemblies without pretreatment. The advantages of this technique include rapid response of the biosensors due to the thinness of the multilayer film and versatile design of the geometries of bienzyme films.

## ARTICLES OF FURTHER INTEREST

*Biological Ligands*, p. 88

*Electrochemical Sensors*, p. 505

*Protein Supramolecular Chemistry*, p. 1161  
*Supramolecular Electrochemistry*, p. 1412

## REFERENCES

1. Wilchek, M.; Bayer, E.A. The avidin–biotin complex in bioanalytical applications. *Anal. Biochem.* **1988**, *171*, 117.
2. Pugliese, L.; Coda, A.; Malcovati, M.; Bolognesi, M. Three-dimensional structure of the tetragonal crystal form of egg-white avidin in its functional complex with biotin at 2.7 Å resolution. *J. Mol. Biol.* **1993**, *231*, 698.
3. Weber, P.C.; Ohlendorf, D.H.; Wendoloski, J.J.; Salemme, F.R. Structural origin of high-affinity binding to streptavidin. *Science* **1989**, *243*, 85.
4. Chilkoti, A.; Stayton, P.S. Molecular origin of the slow streptavidin–biotin dissociation kinetics. *J. Am. Chem. Soc.* **1995**, *117*, 10622.
5. Green, N.M.; Konievzny, L.; Toms, E.J.; Valentine, R.C. The use of bifunctional biotinyl compounds to determine the arrangement of subunits in avidin. *Biochem. J.* **1971**, *125*, 781.
6. Luo, S.; Walt, D.R. Avidin–biotin coupling as a general method for preparing enzyme-based fiber-optic sensors. *Anal. Chem.* **1989**, *61*, 1069.
7. Gunaratna, P.C.; Wilson, G.S. Optimization of multienzyme flow reactors for determination of acetylcholine. *Anal. Chem.* **1990**, *62*, 402.
8. Hoshi, T.; Anzai, J.; Osa, T. Controlled deposition of glucose oxidase on platinum electrode based on an avidin/biotin system for the regulation of output current of glucose sensors. *Anal. Chem.* **1995**, *67*, 770.
9. Anzai, J.; Kobayashi, Y.; Suzuki, Y.; Takeshita, H.; Chen, Q.; Osa, T.; Hoshi, T.; Du, X.-Y. Enzyme sensors prepared by layer-by-layer deposition of enzymes on a platinum electrode through avidin–biotin interaction. *Sens. Actuators, B* **1998**, *52*, 3.
10. Cass, A.E.G.; Davis, G.; Francis, G.D.; Hill, H.A.O.; Aston, W.J.; Higgins, I.J.; Plotkin, E.V.; Scott, L.D.L.; Turner, A.P.F. Ferrocene-mediated enzyme electrode for amperometric determination of glucose. *Anal. Chem.* **1984**, *56*, 667.
11. Frew, J.E.; Hill, H.A.O. Direct and indirect electron transfer between electrodes and redox proteins. *Eur. J. Biochem.* **1988**, *172*, 261.
12. Heller, A. Electrical connection of enzyme redox centers to electrodes. *J. Phys. Chem.* **1992**, *96*, 3579.
13. Yang, L.; Janle, E.; Huang, T.; Gitzen, J.; Kissinger, P.; Vreeke, M.; Heller, A. Applications of “wired” peroxidase electrodes for peroxide determination in liquid chromatography coupled to oxidase immobilized enzyme reactions. *Anal. Chem.* **1995**, *67*, 1326.
14. Anzai, J.; Takeshita, H.; Kobayashi, Y.; Osa, T.; Hoshi, T. Layer-by-layer construction of enzyme multilayers on an electrode for the preparation of glucose and lactate sensors: Elimination of ascorbate interference by means of an ascorbate oxidase multilayer. *Anal. Chem.* **1998**, *70*, 811.

15. Sasso, S.V.; Pierce, R.J.; Walla, R.; Yacynych, A.M. Electropolymerized 1,2-diaminobenzene as a means to prevent interferences and fouling and to stabilize immobilized enzyme in electrochemical biosensors. *Anal. Chem.* **1990**, *62*, 1111.
16. Chen, Q.; Kobayashi, Y.; Takeshita, H.; Hoshi, T.; Anzai, J. Avidin-biotin system-based enzyme multilayer membranes for biosensor applications: Optimization of loading of choline esterase and choline oxidase in the bienzyme membrane for acetylcholine biosensors. *Electroanalysis* **1998**, *10*, 94.
17. Anzai, J.; Takeshita, H.; Hoshi, T.; Osa, T. Regulation of output current of L-lactate sensors based on alternate deposition of avidin and biotinylated lactate oxidase on electrode surface through avidin-biotin complexation. *Chem. Pharm. Bull.* **1995**, *43*, 520.
18. Du, X.-Y.; Anzai, J.; Osa, T.; Motohashi, R. Amperometric alcohol sensors based on protein multilayers composed of avidin and biotin-labeled alcohol oxidase. *Electroanalysis* **1996**, *8*, 813.
19. Hoshi, T.; Saiki, H.; Takeuchi, K.; Anzai, J. Enzyme coupled lactose sensors based on bienzyme membrane prepared by an avidin/biotin method. *Trans. IEE Jpn.* **1999**, *119E*, 576.
20. Hoshi, T.; Saiki, H.; Anzai, J. Layer-by-layer deposition of avidin and biotin-labeled antibody on a solid surface to prepare a multilayer array of antibody. *J. Chem. Soc., Perkin Trans. 2* **1999**, 1293.
21. Hoshi, T.; Saiki, H.; Anzai, J. Preparation of spatially ordered multilayer thin films of antibody and their binding properties. *Biosens. Bioelectron.* **2000**, *15*, 623.
22. Becker, J.W.; Reeke, G.N., Jr.; Cunningham, B.A.; Edelman, G.M. New evidence on the location of the saccharide-binding site of concanavalin A. *Nature* **1976**, *259*, 406.
23. Anzai, J.; Kobayashi, Y. Construction of multilayer thin films of enzymes by means of sugar-lectin interactions. *Langmuir* **2000**, *16*, 2851.
24. Anzai, J.; Kobayashi, Y.; Nakamura, N. Alternate deposition of concanavalin A and mannose-labeled enzymes on a solid surface to prepare catalytically active enzyme thin films. *J. Chem. Soc., Perkin Trans. 2* **1998**, 461.
25. Kobayashi, Y.; Hoshi, T.; Anzai, J. Glucose and lactate biosensors prepared by a layer-by-layer deposition of concanavalin A and mannose-labeled enzymes: electrochemical response in the presence of electron mediators. *Chem. Pharm. Bull.* **2001**, *49*, 755.
26. Kobayashi, Y.; Anzai, J. Preparation and optimization of bienzyme multilayer films using lectin and glyco-enzymes for biosensor applications. *J. Electroanal. Chem.* **2001**, *507*, 250.

# Bond-Stretch Isomerism

Gerard Parkin

Columbia University, New York, New York, U.S.A.

## INTRODUCTION

Bond-stretch isomerism may be defined as the phenomenon whereby molecules of the same spin state, on the same potential energy surface, differ only in the length of one or several bonds.<sup>[1–4]</sup> In contrast to exhibiting a single-minimum on the potential energy surface for the stretching of a bond, the existence of bond-stretch isomers requires the presence of a double-minimum, with a significant barrier between the two minima (Fig. 1). The theoretical concept of bond-stretch isomerism, with the existence of a double-minimum on a potential energy surface, was first discussed by Hoffmann in a 1972 study on a series of hypothetical organic molecules, of the types illustrated in Fig. 2.<sup>[5–7]</sup> Interestingly, experimental evidence in support of bond-stretch isomerism was actually reported shortly prior to Hoffmann's proposal. Specifically, Chatt reported in 1970 that the molybdenum oxo complex *mer*-MoOCl<sub>2</sub>(PMe<sub>2</sub>Ph)<sub>3</sub> could be isolated in blue and green isomeric forms.<sup>[6]</sup> Originally, these complexes were considered to be geometric isomers, namely *cis-mer*-MoOCl<sub>2</sub>(PMe<sub>2</sub>Ph)<sub>3</sub> and *trans-mer*-MoOCl<sub>2</sub>(PMe<sub>2</sub>Ph)<sub>3</sub>, differing only in whether the two chloride ligands were *cis* or *trans*. X-ray diffraction studies on the blue isomer established a *cis* configuration, from which it was assumed that the green isomer possessed a *trans* configuration (Fig. 3).<sup>[6,8]</sup> However, X-ray diffraction studies on the green analogue *mer*-MoOCl<sub>2</sub>(PEt<sub>2</sub>Ph)<sub>3</sub> revealed that the chloride ligands were also *cis* and not *trans*.<sup>[8]</sup> Thus, the structures of blue *cis-mer*-MoOCl<sub>2</sub>(PMe<sub>2</sub>Ph)<sub>3</sub> and green *cis-mer*-MoOCl<sub>2</sub>(PEt<sub>2</sub>Ph)<sub>3</sub> were similar, with the exception that the Mo=O bond length in green *cis-mer*-MoOCl<sub>2</sub>(PEt<sub>2</sub>Ph)<sub>3</sub> [1.803(11) Å] was significantly longer than that observed in blue *cis-mer*-MoOCl<sub>2</sub>(PMe<sub>2</sub>Ph)<sub>3</sub> [1.676(7) Å]. As a result, Chatt suggested that the principal difference in the blue and green isomers of *cis-mer*-MoOCl<sub>2</sub>(PMe<sub>2</sub>Ph)<sub>3</sub> centered on their Mo=O bond lengths, and he termed these complexes "distortional isomers" (Fig. 3).<sup>[7a]</sup> In accord with his proposal, the actual green isomer of *cis-mer*-MoOCl<sub>2</sub>(PMe<sub>2</sub>Ph)<sub>3</sub> was structurally characterized and also found to possess a long Mo=O bond length of 1.80(2) Å.<sup>[10]</sup> Consistent with the different Mo=O bond lengths, the blue and green isomers exhibited slightly different  $\nu_{\text{Mo=O}}$  stretching frequencies (blue, 954 cm<sup>-1</sup>; green 943 cm<sup>-1</sup>), and different

stabilities, with solutions of the green isomer irreversibly converting to the blue isomer upon gentle heating.

Following Chatt's report, experimental evidence for bond-stretch (or distortional) isomerism was reported for a variety of systems, as illustrated in Fig. 4.<sup>[3]</sup> The blue and green tungsten oxo derivatives [(Me<sub>3</sub>tacn)W(O)Cl<sub>2</sub>]<sup>+</sup> represented particularly important examples, since these were reported to be the first set of bond-stretch isomers that were stable in solution for several days and also did not interconvert at temperatures up to ca. 180°C. The blue and green isomers also exhibited different  $\nu_{\text{W=O}}$  stretching frequencies of 980 cm<sup>-1</sup> and 960 cm<sup>-1</sup>, respectively, with the higher energy vibration corresponding to the shorter W=O bond. With a series of transition metal complexes that exhibit bond-stretch isomerism now in existence, Jean, Lledos, Burdett, and Hoffmann extended the earlier calculations on hypothetical species to rationalize the presence of double-minima in the potential energy surfaces of the complexes actually reported to exhibit the phenomenon.<sup>[11]</sup>

## A REINVESTIGATION OF BOND-STRETCH ISOMERISM IN *cis-mer*-MoOCl<sub>2</sub>(PMe<sub>2</sub>Ph)<sub>3</sub>

In 1991, a series of detailed crystallographic studies resulted in the discovery that the original example of bond-stretch isomerism in transition metal complexes was an artifact due to crystallographic disorder.<sup>[12,13]</sup> Specifically, the green "isomer" of *cis-mer*-MoOCl<sub>2</sub>(PMe<sub>2</sub>Ph)<sub>3</sub> was identified as a mixture of blue *cis-mer*-MoOCl<sub>2</sub>(PMe<sub>2</sub>Ph)<sub>3</sub> and yellow *mer*-MoCl<sub>3</sub>(PMe<sub>2</sub>Ph)<sub>3</sub>. Evidence for the presence of *mer*-MoCl<sub>3</sub>(PMe<sub>2</sub>Ph)<sub>3</sub> was provided by <sup>1</sup>H-NMR spectroscopy. Thus, although the <sup>1</sup>H-NMR spectrum of *mer*-MoCl<sub>3</sub>(PMe<sub>2</sub>Ph)<sub>3</sub> is characterized by broad paramagnetically shifted signals, careful examination provided evidence that the green "isomer" of *cis-mer*-MoOCl<sub>2</sub>(PMe<sub>2</sub>Ph)<sub>3</sub> was contaminated by *mer*-MoCl<sub>3</sub>(PMe<sub>2</sub>Ph)<sub>3</sub>. It is important to emphasize that the green "isomer" of *cis-mer*-MoOCl<sub>2</sub>(PMe<sub>2</sub>Ph)<sub>3</sub> was not a heterogeneous mixture of crystals of *cis-mer*-MoOCl<sub>2</sub>(PMe<sub>2</sub>Ph)<sub>3</sub> and *mer*-MoCl<sub>3</sub>(PMe<sub>2</sub>Ph)<sub>3</sub> but was actually a homogeneous mixture such that each single crystal was a solid solution of the two compounds. The formation of

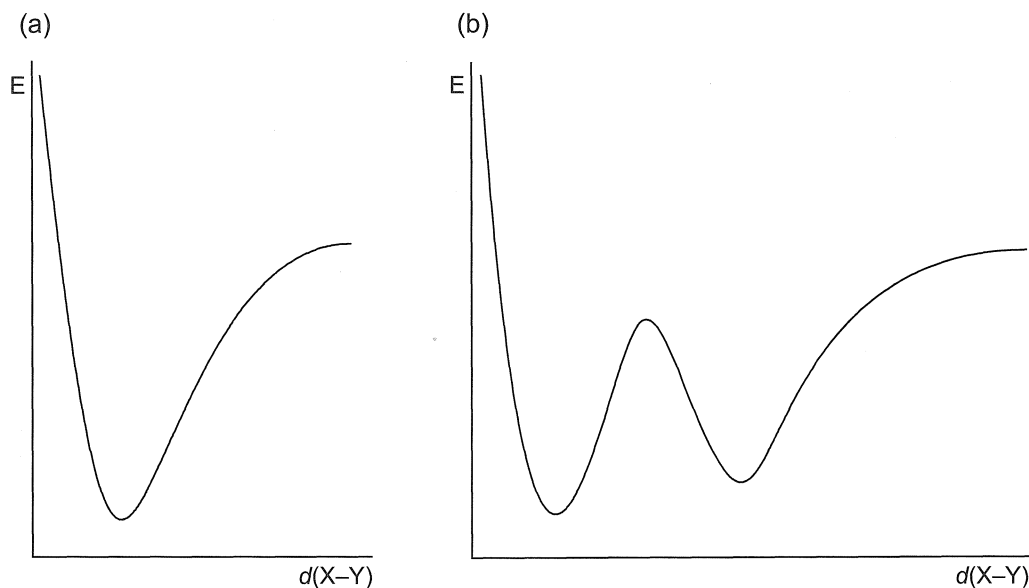


**Fig. 1** Potential energy surfaces for (a) a normal X-Y bond and (b) a pair of X-Y bond-stretch isomers.

such a solid solution is made possible by the fact that *cis-mer*- $\text{MoOCl}_2(\text{PMe}_2\text{Ph})_3$  and *mer*- $\text{MoCl}_3(\text{PMe}_2\text{Ph})_3$  are isostructural and only differ by the exchange of oxygen for chlorine.

The impact of small amounts of the impurity *mer*- $\text{MoCl}_3(\text{PMe}_2\text{Ph})_3$  on the structure determination is profound and strongly influences the *apparent* Mo=O bond length. The apparent lengthening is a result of the fact that the location of an “atom” at the disordered site is a weighted average of oxygen and chlorine positions (Fig. 5). Since the Mo-Cl bond is longer than the Mo=O bond, the presence of a chloride contaminant has the

effect of apparently lengthening the Mo=O bond. Examination of Fig. 5 indicates that only very small amounts of the *mer*- $\text{MoCl}_3(\text{PMe}_2\text{Ph})_3$  impurity are required to have a significant effect on the apparent Mo=O

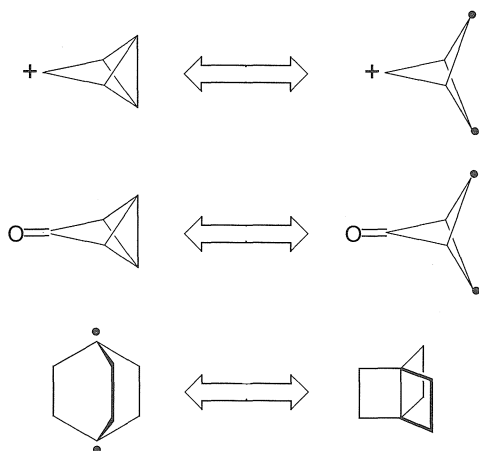
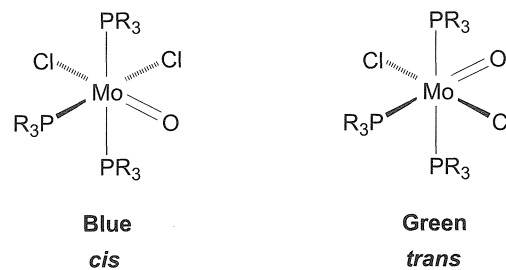


**Fig. 2** Some hypothetical isomers that were studied theoretically.

**(a) First proposal: *cis* and *trans* isomers**



**(b) Second proposal: distortional (bond-stretch) isomers**

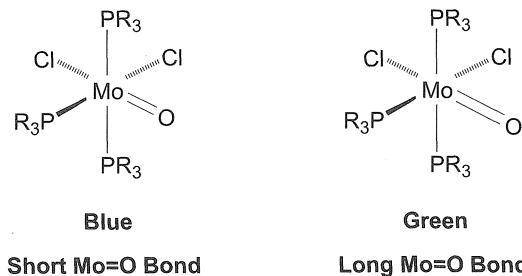


**Fig. 3** Original, incorrect proposals for the structures of blue and green isomers of  $\text{MoOCl}_2(\text{PMe}_2\text{Ph})_3$ . (a) *cis* and *trans* isomers; (b) distortional (bond-stretch) isomers with short and long Mo=O bonds.

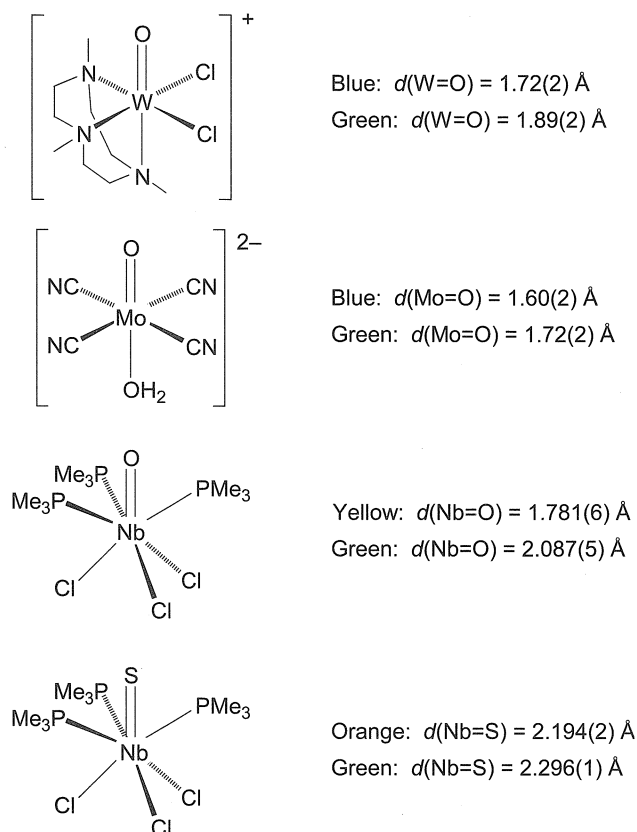


Fig. 4 Other examples of originally proposed bond-stretch isomers.

bond length. The reasons for this are twofold: (i) the Mo–Cl bond (ca.  $2.45 \text{ \AA}$ ) is considerably longer than the Mo=O bond (ca.  $1.68 \text{ \AA}$ ), and (ii) the scattering power (which is a function of the number of electrons) of chlorine is much greater than that of oxygen. Despite the contamination by chlorine being sufficient to apparently lengthen the Mo=O bond, the thermal parameter was not abnormal, and so the x-ray structure provided no evidence for contamination.

The reevaluation of the structures of *cis-mer*- $\text{MoOCl}_2(\text{PMe}_2\text{Ph})_3$  demonstrated that there was no structural evidence for bond-stretch isomerism for the complexes that were originally proposed to exhibit the phenomenon. Furthermore, the origin of the two different  $\nu_{\text{Mo}=\text{O}}$  stretching frequencies for *cis-mer*- $\text{MoOCl}_2(\text{PMe}_2\text{Ph})_3$  in the solid state was attributed to the existence of two different modifications, with only one value being observed in solution.<sup>[14]</sup> This reevaluation of bond-stretch isomerism in *cis-mer*- $\text{MoOCl}_2(\text{PMe}_2\text{Ph})_3$  also cast doubt on the other proposed examples of bond-stretch isomerism. Indeed, subsequent studies on  $[(\text{Me}_3\text{tacn})\text{W}(\text{O})\text{Cl}_2]^+$  demonstrated that the system was considerably more complex than that for *cis-mer*- $\text{MoOCl}_2(\text{PMe}_2\text{Ph})_3$  and was composed of three components with different oxidation states:  $[(\text{Me}_3\text{tacn})\text{W}(\text{O})\text{Cl}_2]^+$ ,  $[(\text{Me}_3\text{tacn})\text{W}(\text{O})_2\text{Cl}]^+$ , and  $[(\text{Me}_3\text{tacn})\text{W}(\text{O})\text{Cl}(\text{solv})]^+$ .<sup>[15]</sup> Likewise,  $\text{NbCl}_4(\text{PMe}_3)_3$  has been recognized as an impurity for influencing the apparent Nb=O and Nb=S bond lengths in  $\text{Nb}(\text{O})\text{Cl}_3(\text{PMe}_3)_3$  and  $\text{Nb}(\text{O})\text{Cl}_3(\text{PMe}_3)_3$ , respectively.<sup>[16]</sup>

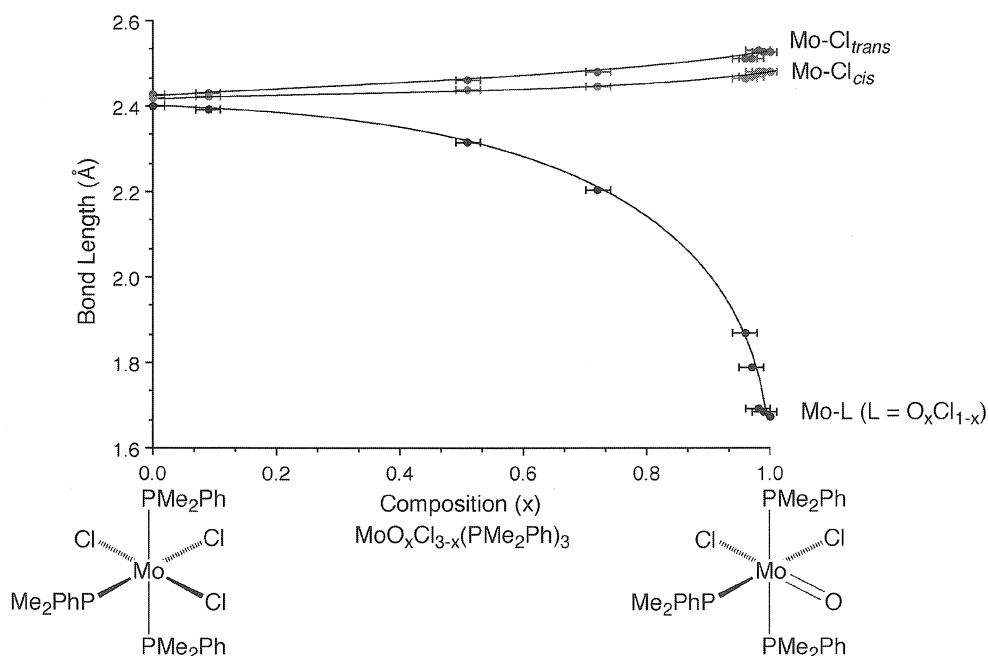


Fig. 5 Variation of apparent Mo=O bond length as a function of composition.

## SPIN-STATE ISOMERISM AND RELATED PHENOMENA

Blue and green *cis-mer*-Mo(O)Cl<sub>2</sub>(PMe<sub>2</sub>Ph)<sub>3</sub> were originally classified as bond-stretch (distortional) isomers because there was no simple explanation for the existence of a pair of complexes in which the only significant difference resided in the length of one of the bonds. In this regard, it is important to note that there are several other examples of isomerism in which a bond between a pair of atoms differs in length, but the situation is fundamentally different than that proposed for *cis-mer*-Mo(O)Cl<sub>2</sub>(PMe<sub>2</sub>Ph)<sub>3</sub>, because the change in bond length is accompanied by other significant geometric and/or spin-state changes.<sup>[17]</sup> For example, there are many transition-metal complexes that exhibit different spin states (high-spin/low-spin equilibria) for which significant structural changes are also observed.<sup>[18,19]</sup> Likewise, [Cp\*RuCl<sub>2</sub>]<sub>2</sub> exists as singlet and triplet isomers that differ substantially in their Ru—Ru separations (2.93 Å versus 3.75 Å), Ru—Cl—Ru bond angles (76.5° versus 100.2°), and Ru—Cl bond lengths (Fig. 6).<sup>[20]</sup> In addition, [(MesP\*)<sub>2</sub>CHCSiMe<sub>3</sub>] exists in monocyclic and bicyclic structures (Fig. 6) with planar and puckered geometries, respectively, with the latter having a shorter C—C bond length (1.52 Å versus 2.47 Å).<sup>[21]</sup> The trinuclear dipyriddyamide cobalt complex Co<sub>3</sub>(dpa)<sub>4</sub>Cl<sub>2</sub> [dpaH = di(2-pyridyl)amine] exhibits a particularly interesting structural variability (Fig. 6).<sup>[22]</sup> Specifically, depending on the crystalline form, the Co<sub>3</sub>

chain may be symmetrical (*s*-), with Co—Co distances of ca. 2.3 Å, or unsymmetrical (*u*-) with Co—Co distances of ca. 2.29 Å and 2.47 Å; however, only the symmetrical species exists in solution. It should also be noted that while the *s*-Co<sub>3</sub>(dpa)<sub>4</sub>Cl<sub>2</sub> and *u*-Co<sub>3</sub>(dpa)<sub>4</sub>Cl<sub>2</sub> species are isomeric, the compositions of the crystals are different by virtue of the solvents of crystallization, and thus the crystalline materials are not isomeric. Related chromium complexes Cr<sub>3</sub>(dpa)<sub>4</sub>X<sub>2</sub> are also known, and depending upon the nature of the axial ligands and the solvent of crystallization, the Cr<sub>3</sub> chain is likewise either symmetrical or unsymmetrical.<sup>[23]</sup> The complexes (Cp\*RuCl<sub>2</sub>)<sub>2</sub>, [(MesP\*)<sub>2</sub>CHCSiMe<sub>3</sub>], and Co<sub>3</sub>(dpa)<sub>4</sub>Cl<sub>2</sub> represent extremely interesting examples of isomerism but are distinct from the bond-stretch isomerism proposed for *cis-mer*-Mo(O)Cl<sub>2</sub>(PMe<sub>2</sub>Ph)<sub>3</sub> by virtue of the fact that the lengthening of one bond is compensated for by other significant geometrical changes.

## OTHER EXAMPLES OF CRYSTALLOGRAPHIC DISORDER RESULTING IN ANOMALOUS BOND LENGTHS AND THE INCORRECT FORMULATION OF COMPOUNDS

The interpretation of x-ray diffraction data in providing experimental evidence for bond-stretch isomerism in *cis-mer*-Mo(O)Cl<sub>2</sub>(PMe<sub>2</sub>Ph)<sub>3</sub> provides an extreme illustration

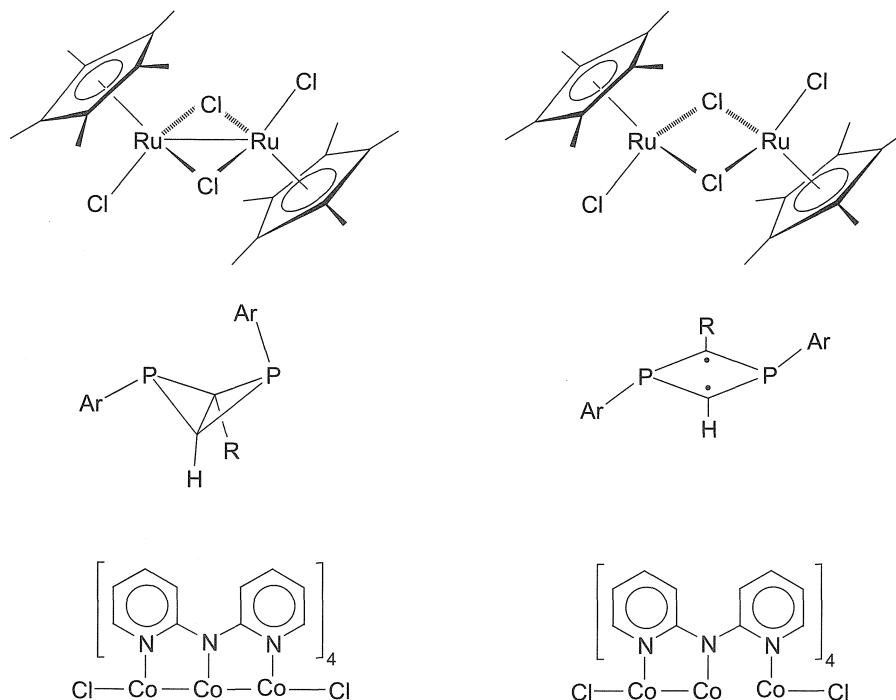


Fig. 6 Structurally characterized examples of isomers with different X—X bond lengths and other structural modifications.

of how crystallographic disorder may be deceptive. In this regard, although crystallographic disorder is well known, the presence of a disorder is normally only discerned at the stage of refinement when an anomaly is detected. It is likely that there are many other circumstances where disorder has gone undetected but has, nevertheless, had an impact on the derived structure. Indeed, this notion was reinforced by a series of studies on *tris*(pyrazolyl)hydroborato zinc complexes  $[\text{Tp}^{\text{Bu}^t}]\text{ZnX}$  to quantify the sensitivity of the apparent bond length to the composition of a disordered site.<sup>[24]</sup> Significantly, it was noted that for the series  $[\text{Tp}^{\text{Bu}^t}]\text{ZnCl}_{1-n}\text{I}_n$ , reasonable thermal parameters could still be obtained at impurity levels that were sufficient to result in a significant apparent change in the true bond length. Furthermore, the disordered site of the crystal of composition  $[\text{Tp}^{\text{Bu}^t}]\text{ZnCl}_{0.5}\text{I}_{0.5}$  could be refined very well as bromine, with none of the unusual lengthening of the thermal ellipsoid along the bond vector that would have been anticipated given the true locations of Cl and I. Representative examples of how initially unrecognized disorder resulted in incorrect bond-length determinations include the following:

1. The complex *mer*- $\text{WCl}_3(\text{PMe}_2\text{Ph})_3$  was reported to possess three different W–Cl bond lengths [2.295(2) Å, 2.437(1) Å, and 2.441(1) Å], with one exceptionally short W–Cl bond.<sup>[25]</sup> Further studies demonstrated that the origin of the short W–Cl bond was due to disorder with the isostructural oxo complex *cis-mer*- $\text{WOCl}_2(\text{PMe}_2\text{Ph})_3$ .<sup>[26]</sup>
2. The molecular structure of  $\text{Cp}_2\text{Hf}(\text{CH}_3)_2$  was originally reported to exhibit two significantly distinct Hf–CH<sub>3</sub> bond lengths [2.318(8) Å and 2.382(7) Å].<sup>[27]</sup> The origin of this inequivalence was subsequently reinterpreted as arising from cocrystallization with the chloride derivative  $\text{Cp}_2\text{Hf}(\text{CH}_3)\text{Cl}$ .<sup>[28]</sup>

Crystallographic disorder is not restricted to pairs of structurally similar groups, and controlled disorder between structurally inequivalent groups was investigated by determining the effect that partial occupancy of a halide ligand ( $X = \text{Cl}, \text{Br}, \text{I}$ ) may exert upon the apparent structure of the cyanide derivative  $[\text{Tp}^{\text{Bu}^t}]\text{ZnCN}$ .<sup>[29]</sup> For chloride- and bromide-doped crystals of composition  $[\text{Tp}^{\text{Bu}^t}]\text{Zn}(\text{CN})_{0.8}\text{Cl}_{0.2}$  and  $[\text{Tp}^{\text{Bu}^t}]\text{Zn}(\text{CN})_{0.95}\text{Br}_{0.05}$ , the disorder between the halide and the carbon of the cyanide ligand was not resolved. Although  $[\text{Tp}^{\text{Bu}^t}]\text{Zn}(\text{CN})_{0.8}\text{Cl}_{0.2}$  did not refine well in the absence of a disorder model, the bromide-doped crystal of composition  $[\text{Tp}^{\text{Bu}^t}]\text{Zn}(\text{CN})_{0.95}\text{Br}_{0.05}$  refined well; however, the bond lengths associated with the CN ligand were observed to be incorrect, with a long Zn–C bond length and a short  $\text{C}\equiv\text{N}$  bond length. More extreme examples of disorder may also occur. For example, the complex  $[\text{Tp}^{\text{Ant}}]\text{Ti}$  cocrystallizes with  $[\text{Tp}^{\text{Ant}}]\text{CoNCS}$ , so that in effect, a site that is disordered

between a vacancy and a chain of *three* atoms results.<sup>[30]</sup> A representative example of how initially unrecognized disorder between pairs of structurally dissimilar groups resulted in incorrect bond length determinations is provided by the observation that the dinitrogen complex *trans*- $\text{Cr}(\text{dmpe})_2(\text{N}_2)_2$  was reported to have an unusually short N–N bond length of 0.985(4) Å,<sup>[31]</sup> however, subsequent studies suggested that the origin of the exceptionally short N–N bond length in this molecule is compositional disorder with the chloride impurity, *trans*- $\text{Cr}(\text{dmpe})_2\text{Cl}_2$ .<sup>[32]</sup>

It is important to note that crystallographic disorder is not restricted to the positions of ligands, and the metal centers may also be disordered. As an illustration, the entire  $\text{Zr}(\eta^2\text{-Te}_2)(\text{CO})$  moiety of the tetragonal modification of  $\text{Cp}^*_2\text{Zr}(\eta^2\text{-Te}_2)(\text{CO})$  is disordered.<sup>[33]</sup> The nature of the disorder is such that the  $\text{Cp}^*_2\text{Zr}(\eta^2\text{-Te}_2)(\text{CO})$  molecules pack so that the carbonyl ligands are statistically distributed about the crystallographic twofold axis, which bisects the two Zr–Te bond vectors. In the absence of modeling disorder of the zirconium atom, the derived Zr–CO bond was observed to be anomalously long. However, after deliberately displacing the Zr from the twofold axis and refining with half-occupancy, a more reasonable value for Zr–C bond length is obtained.

In addition to affecting observed bond lengths, crystallographic disorder may also result in the incorrect formulation of a compound. Furthermore, the incorrect determination of bond lengths, or misformulation of a compound, do not require a crystal to be impure, because disorder between inequivalent groups can also be achieved as a result of packing identical molecules in different orientations in the crystal. As an illustration, a molecule originally believed to be a dicarbonyl derivative of a ruthenium porphyrin complex,  $\text{Ru}(\text{TPP})(\text{CO})_2$  (TPP = *meso*-tetraphenylporphyrin dianion) was reported to possess *bent* carbonyl ligands, with a Ru–C–O bond angle of 153.3(9)°.<sup>[34]</sup> The structure was reinvestigated and determined to be, in fact, a monocarbonyl–ethanol complex  $\text{Ru}(\text{TPP})(\text{CO})(\text{EtOH})$ .<sup>[35]</sup> However, the CO and EtOH ligands were statistically disordered so that a superposition was observed, resulting in the appearance of an apparently bent carbonyl ligand.

A related example of undetected disorder between the methyl ( $\text{CH}_3$ ) and ethylidyne ( $\text{CCH}_3$ ) ligands of  $\text{W}(\text{PMe}_3)_4(\text{CH}_3)(\text{CCH}_3)$  resulted in the terminal carbon atom of the disordered ethylidyne ligand not being located, so that the molecule was originally formulated as the dimethyl derivative  $\text{W}(\text{PMe}_3)_4(\text{CH}_3)_2$ .<sup>[36]</sup> However, x-ray diffraction studies on a better-quality crystal successfully revealed the presence of the disordered methyl group of the ethylidyne ligand, thereby reformulating  $\text{W}(\text{PMe}_3)_4(\text{CH}_3)_2$  as  $\text{W}(\text{PMe}_3)_4(\text{CH}_3)(\text{CCH}_3)$ .<sup>[37]</sup>

Other examples of disorder resulting in misformulation, include: (1) the structure of the unusual technetium

oxo polymer  $[\text{Cp}^*\text{Tc}(\mu\text{-O})_3\text{Tc}]_n$  has been reinterpreted as that of the monomeric rhenium complex,  $\text{Cp}^*\text{Re}(\text{O})_3$ , with the original misassignment having been due to a combination of disorder and twinning,<sup>[38]</sup> and (2) dinitrogen molecules of crystallization have been reinterpreted as disordered dichloromethane solvent.<sup>[39]</sup>

### ANOMALOUS BOND LENGTHS AND INCORRECT FORMULATION OF COMPOUNDS IN THE ABSENCE OF CRYSTALLOGRAPHIC DISORDER

Structural errors in interpretation of x-ray diffraction data are by no means limited to problems resulting from disorder. Thus, it is well known that errors in atom assignment, space group assignment, and the refinement into a false minimum may each have a dramatic impact upon the accuracy of a structure determination.<sup>[3]</sup> In terms of atom assignment, atoms of similar atomic number have similar x-ray scattering powers, and so it is often difficult to distinguish definitively between such pairs by using x-ray diffraction techniques. As such, the incorrect formulation of a compound can occur even when the crystal is pure and there is no crystallographic disorder. For example, the structures of the bridging chloride complexes  $\text{Nb}_2(\mu\text{-Cl})_2\text{Cl}_4(\text{SMe}_2)_4$ ,  $\text{Ta}_2(\mu\text{-Cl})_2\text{Cl}_4(\text{SMe}_2)_4$ , and  $\text{Nb}_2(\mu\text{-Cl})_2\text{Cl}_4(\text{EtSCH}_2\text{CH}_2\text{SEt})_2$  were reformulated as having two  $\mu\text{-S}$  groups, rather than two  $\mu\text{-Cl}$  groups;<sup>[40]</sup> the structures of the cobalt complex  $\text{Co}(\eta^2\text{-S}_2\text{CSEt})_3$  were reformulated as that of the chromium derivative  $\text{Cr}(\eta^2\text{-S}_2\text{CSEt})_3$ ;<sup>[41]</sup> the structure of the nickel(III) 1,4,7-triazacyclononane-*N,N,N'*-triacetate was shown to be that of the cobalt(III) derivative;<sup>[42]</sup> the structure of the unusual compound  $[\text{ClF}_6]^+[\text{CuF}_4]^-$  was proposed to be that of  $[\text{SiF}_6]^-[\text{Cu}(\text{OH}_2)_4]^+$ ;<sup>[43]</sup> the structures of both the copper and silver complexes  $[1,3,5\text{-C}_6\text{Ph}_3\text{H}_2]\text{Cu}$  and  $[1,3,5\text{-C}_6\text{Ph}_3\text{H}_2]\text{Ag}$  were reformulated as that of the bromine compound  $[1,3,5\text{-C}_6\text{Ph}_3\text{H}_2]\text{Br}$ <sup>[44]</sup> and the structure of  $\text{Mo}(\text{PMe}_3)_2\text{Cl}_2$  was reformulated as  $\text{Zn}(\text{PMe}_3)_2\text{Cl}_2$ .<sup>[45]</sup> The latter is a particularly striking example, because the scattering powers of Zn ( $Z = 30$ ) and Mo ( $Z = 42$ ) are very different.<sup>[46]</sup>

Knowledge of the correct space group is essential for obtaining the correct structure of a molecule. Frequently, however, the space group is incorrectly assigned,<sup>[47]</sup> with the result that derived bond lengths are in error. In many such examples, the noncentrosymmetric space group is erroneously selected in preference to the true centrosymmetric space group. Noncentrosymmetric space groups present an additional problem in that it is important to establish that the correct absolute structure was determined. For a molecule that crystallizes in a polar space group, two minima exist in a least-squares refinement

procedure, corresponding to chemically identical structures related by a reflection perpendicular to the polar axis. The structures corresponding to the two polar configurations typically differ slightly in bond lengths as a consequence of the “polar dispersion error,”<sup>[48]</sup> so that it is essential to establish that the correct polarity was determined by refining both configurations. As an illustration, the alternating C–C bond lengths in *s-cis*-1,3-butadiene transition metal complexes, and specifically  $(\eta^4\text{-C}_4\text{H}_6)_2\text{Mn}(\text{CO})$ , is an artifact due to the incorrect absolute structure being refined.<sup>[49]</sup> The redetermined nonalternation of bond lengths is more in line with calculations, which predict that donation from the butadiene HOMO and back-donation into the butadiene LUMO should lengthen the terminal C–C bond.

A more extreme problem associated with polar space group results when the derived structure is a hybrid of the two possible polar configurations. Such a situation becomes feasible when the x-ray scattering is dominated by a heavy atom. As an illustration, the structures of  $\text{W}(\text{PMe}_3)_4\text{H}_2\text{Cl}_2$ <sup>[50]</sup> corresponding to false minima in the refinements are compared to its true structure in Fig. 7. A similar effect was observed for  $[\eta^4\text{-Me}_8\text{taa}]\text{Pb}$ .<sup>[51]</sup> Since the incorrect structures are related to the true structure by a reflection perpendicular to the polar axis of only a *selection* of the atoms, the effect is described as a “partial polar ambiguity” to distinguish it from the well-known “polar dispersion error,” an effect concerned with two structures related by a reflection perpendicular to the polar axis of *all* atoms. The severity of the pseudosymmetry problem is such that truly noncentrosymmetric structures were incorrectly refined as disordered centrosymmetric structures. For example, the *tris*(pyrazolyl)hydroborato indium complex  $[\text{Tp}^{\text{Bu}}]\text{In}$  was originally reported to possess an unusual twofold disorder in such a manner that a nitrogen atom of one molecule was coincident with the boron atom of its disordered configuration, as illustrated in Fig. 8. Thus, the disordered configurations are related by a twofold rotation about the  $\text{In}\cdots\text{B}$  axis, coupled with a canting of the molecules. Further studies, however, demonstrated that refinement of the correct model in the noncentrosymmetric space

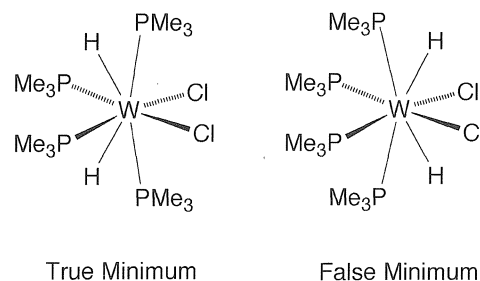
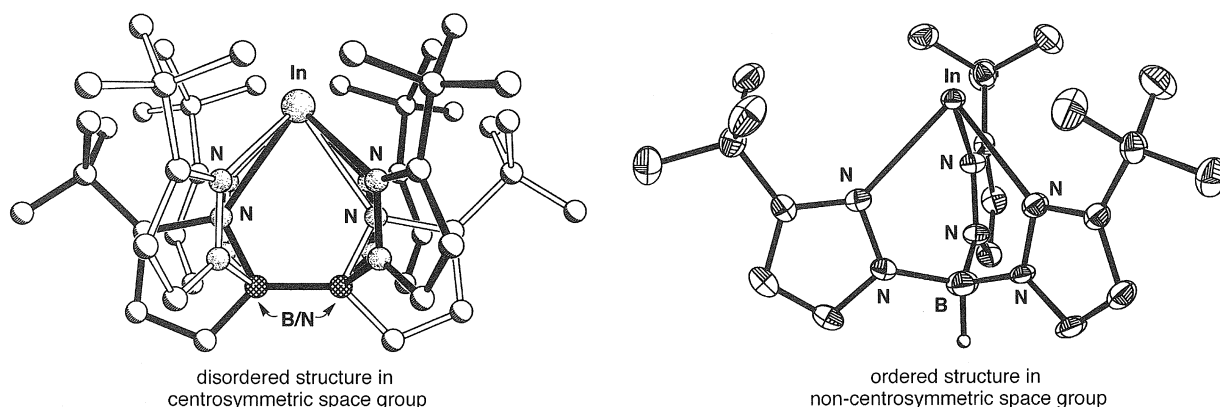


Fig. 7 True and false minima for  $\text{W}(\text{PMe}_3)_4\text{H}_2\text{Cl}_2$ .





**Fig. 8** Incorrect, disordered structure of  $[\text{Tp}^{\text{Bu}^{\text{I}}}\text{In}]$  refined in the centrosymmetric space group (left). The true structure refined in the noncentrosymmetric space group (right).

group resulted in a well-behaved, ordered structure.<sup>[52]</sup> Thus,  $[\text{Tp}^{\text{Bu}^{\text{I}}}\text{In}]$  provides an interesting counter example, where the structure is much better described as ordered in the noncentrosymmetric space group, rather than disordered in the centrosymmetric alternative.

## CONCLUSION

Reinvestigation of *cis-mer*- $\text{MoOCl}_2(\text{PMe}_2\text{Ph})_3$  demonstrated that the original proposal for bond-stretch isomerism is erroneous due to a crystallographic artifact resulting from disorder. The fact that the original x-ray diffraction study was not questioned at the time it was reported, and was considered sufficiently reliable to prove the existence of such isomers, is a consequence of two facts: first, the widespread notion that x-ray diffraction is the ultimate arbiter of a chemical structure; and second, the disorder was not detected, even though it had a significant effect on the apparent bond length. The apparent experimental verification of bond-stretch isomerism represents the tip of the iceberg and indicates that other unrecognized problems exist, as illustrated by the examples described above. These problems range from incorrect atom assignments to incorrect molecular geometries.

A variety of molecules, such as  $[\text{Cp}^*\text{RuCl}_2]_2$ ,  $[(\text{MesP}^*)_2\text{CHCSiMe}_3]$ , and  $\text{Co}_3(\text{dpa})_4\text{Cl}_2$ , exhibit isomerism in which there is a variation in bond lengths. However, to date there has been no convincing evidence presented to support the existence of isomers analogous to the bond-stretch isomerism proposed for *cis-mer*- $\text{Mo}(\text{O})\text{Cl}_2(\text{PMe}_2\text{Ph})_3$ , in which the difference is principally associated with the mere lengthening of a bond between a single pair of atoms.

## REFERENCES

1. Parkin, G.; Hoffmann, R. Bond-stretch isomers and spin-state isomers: A comment on the article 'Bond-Stretch Isomers: Fact not Fiction'. *Angew. Chem., Int. Ed. Engl.* **1994**, 33, 1462.
2. Parkin, G. Do bond-stretch isomers really exist? *Acc. Chem. Res.* **1992**, 25, 455–460.
3. Parkin, G. Bond-stretch isomerism in transition metal complexes: A reevaluation of crystallographic data. *Chem. Rev.* **1993**, 93, 887–911.
4. Labinger, J.A. Bond-stretch isomerism: A case study of a quiet controversy. *C. R. Chim.* **2002**, 5, 235–244.
- 5a. Stohrer, W.-D.; Hoffmann, R. Electronic-structure and reactivity of strained tricyclic hydrocarbons. *J. Am. Chem. Soc.* **1972**, 94, 779–786.
- 5b. Stohrer, W.-D.; Hoffmann, R. Bond-stretch isomerism and polytopal rearrangements in  $(\text{CH})_5^+$ ,  $(\text{CH})_5^-$ , and  $(\text{CH})_4\text{CO}$ . *J. Am. Chem. Soc.* **1972**, 94, 1661–1668.
6. Nagase, S. Polyhedral compounds of the heavier group-14 elements—Silicon, germanium, tin, and lead. *Acc. Chem. Res.* **1995**, 28, 469–476.
7. Butcher, A.V.; Chatt, J. Complexes of tertiary phosphines and tertiary arsines with molybdenum(IV). *J. Chem. Soc., A* **1970**, 2652–2656.
- 8a. Manojlovic-Muir, L. X-ray crystal structure of oxodichlorotris(dimethylphenylphosphine)molybdenum(IV)  $[\text{MoOCl}_2(\text{PMe}_2\text{Ph})_3]$ . *Chem. Commun.* **1971**, 147.
- 8b. Manojlovic-Muir, L. Molybdenum(IV) oxo-complexes. 1. Crystal and molecular structure of the blue isomer of oxodichlorotris(dimethylphenylphosphine)molybdenum(IV), *cis-mer*- $[\text{MoOCl}_2(\text{PMe}_2\text{Ph})_3]$ . *J. Chem. Soc., A* **1971**, 2796–2800.
- 9a. Chatt, J.; Manojlovic-Muir, L.; Muir, K.W. X-ray determination of molecular structures of molybdenum(IV) oxo-complexes—Possibility of a new type of isomerism. *Chem. Commun.* **1971**, 655–656.
- 9b. Manojlovic-Muir, L.; Muir, K.W. Molybdenum(IV) oxo-complexes. 2. Crystal and molecular structure of dichlo-

- rottris(diethylphenylphosphine)oxomolybdenum(IV), *cis-mer*-[MoOCl<sub>2</sub>(PEt<sub>2</sub>Ph)<sub>3</sub>]. J. Chem. Soc., Dalton Trans. **1972**, 686–690.
10. Haymore, B.L.; Goddard, W.A., III; Allison, J.N. Proc. Int. Conf. Coord. Chem., 23rd **1984**, 535.
  - 11a. Jean, Y.; Lledos, A.; Burdett, J.K.; Hoffmann, R. Bond-stretch isomerism in transition-metal complexes. J. Am. Chem. Soc. **1988**, *110*, 4506–4516.
  - 11b. Jean, Y.; Lledos, A.; Burdett, J.K.; Hoffmann, R. Electronic mechanisms associated with bond-stretch isomerism in transition-metal complexes. J. Chem. Soc., Chem. Commun. **1988**, 140–142.
  - 12a. Yoon, K.; Parkin, G.; Rheingold, A.L. A re-investigation of the molecular structures of *cis-mer*-MoOCl<sub>2</sub>(PR<sub>3</sub>)<sub>3</sub>: Do bond-stretch isomers really exist? J. Am. Chem. Soc. **1991**, *113*, 1437–1438.
  - 12b. Yoon, K.; Parkin, G.; Rheingold, A.L. Bond-stretch isomerism in the complexes *cis-mer*-MoOCl<sub>2</sub>(PR<sub>3</sub>)<sub>3</sub>: A re-investigation. J. Am. Chem. Soc. **1992**, *114*, 2210–2218.
  13. Desrochers, P.J.; Nebesny, K.W.; LaBarre, M.J.; Lincoln, S.E.; Loehr, T.M.; Enemark, J.H. Studies of distortional isomers—Spectroscopic evidence that green *cis,mer*-dichlorotris(dimethylphenylphosphine)-oxomolybdenum(IV) is a mixture. J. Am. Chem. Soc. **1991**, *113*, 9193–9200.
  14. Bashall, A.P.; Bligh, S.W.A.; Edwards, A.J.; Gibson, V.C.; McPartlin, M.; Robinson, O.B. Distortional isomerism in oxomolybdenum systems—The evidence reevaluated. Angew. Chem., Int. Ed. Engl. **1992**, *31*, 1607–1609.
  15. Desrochers, P.J.; Nebesny, K.W.; Labarre, M.J.; Bruck, M.A.; Neilson, G.F.; Sperline, R.P.; Enemark, J.H.; Backes, G.; Wieghardt, K. Studies of distortional isomers. 2. Evidence that green [LWOCl<sub>2</sub>]PF<sub>6</sub> is a ternary mixture. Inorg. Chem. **1994**, *33*, 15–24.
  16. Gibson, V.C.; McPartlin, M. Bond stretch isomerism—Fact or artifact. J. Chem. Soc., Dalton Trans. **1992**, 947–956.
  17. Rohmer, M.-M.; Bénard, M. Bond-stretch isomerism in strained inorganic molecules and in transition metal complexes: A revival? Chem. Soc. Rev. **2001**, *30*, 340–354.
  18. König, E. Structural-changes accompanying continuous and discontinuous spin-state transitions. Prog. Inorg. Chem. **1987**, *35*, 527–622.
  19. Gütllich, P.; Goodwin, H.A.; Hendrickson, D.N. Bond-stretch isomers—Fact not fiction. Angew. Chem., Int. Ed. Engl. **1994**, *33*, 425–427.
  20. Kölle, U.; Kossakowski, J.; Klaff, N.; Wesemann, L.; Englert, U.; Heberich, G.E. Dichloro(pentamethylcyclopentadienyl)ruthenium—Novel dichotomy in a molecular-structure. Angew. Chem., Int. Ed. Engl. **1991**, *30*, 690–691.
  21. Niecke, E.; Fuchs, A.; Nieger, M.; Schmidt, O.; Schoeller, W.W. Valence Isomerization of a 1,3-diphosphacyclobutane-2,4-diyl: Photochemical ring closure to 2,4-diphosphabicyclo[1.1.0]butane and its thermal ring opening to gauche-1,4-diphosphabutadiene. Angew. Chem., Int. Ed. Engl. **1999**, *38*, 3028–3031.
  - 22a. Clérac, R.; Cotton, F.A.; Daniels, L.M.; Dunbar, K.R.; Murillo, C.A.; Wang, X. Tuning the metal–metal bonds in the linear tricobalt compound Co<sub>3</sub>(dpa)<sub>4</sub>Cl<sub>2</sub>: Bond-stretch and spin-state isomers. Inorg. Chem. **2001**, *40*, 1256–1264.
  - 22b. Clérac, R.; Cotton, F.A.; Daniels, L.M.; Dunbar, K.R.; Kirschbaum, K.; Murillo, C.A.; Pinkerton, A.A.; Schultz, A.J.; Wang, X. Linear tricobalt compounds with di(2-pyridyl)amide (dpa) ligands: Temperature dependence of the structural and magnetic properties of symmetrical and unsymmetrical forms of Co<sub>3</sub>(dpa)<sub>4</sub>Cl<sub>2</sub> in the solid state. J. Am. Chem. Soc. **2000**, *122*, 6226–6236.
  23. Clérac, R.; Cotton, F.A.; Daniels, L.M.; Dunbar, K.R.; Murillo, C.A.; Pascual, I. Linear trichromium complexes with direct Cr to Cr contacts. 1. Compounds with Cr<sub>3</sub> (di-pyridylamide)<sub>4</sub><sup>2+</sup> cores. Inorg. Chem. **2000**, *39*, 748–751.
  24. Yoon, K.; Parkin, G. Artificial manipulation of apparent bond lengths as determined by single crystal x-ray diffraction. J. Am. Chem. Soc. **1991**, *113*, 8414–8418.
  25. Hills, A.; Hughes, D.L.; Leigh, G.J.; Prieto-Alc n, R. Preparation and structure of trichlorotris(dimethylphenylphosphine)tungsten(III), the 1<sup>st</sup> structurally characterized neutral mononuclear complex of tungsten(III). J. Chem. Soc., Dalton Trans. **1991**, 1515–1517.
  26. Yoon, K.; Parkin, G.; Hughes, D.L.; Leigh, G.J. Origin of the two significantly different W–Cl bond lengths for chemically equivalent bonds in *mer*-WCl<sub>3</sub>(PMe<sub>2</sub>Ph)<sub>3</sub>. J. Chem. Soc., Dalton Trans. **1992**, 769–773.
  27. Fronczek, F.R.; Baker, E.C.; Sharp, P.R.; Raymond, K.N.; Alt, H.G.; Rausch, M.D. Structures of dimethylhafnocene and its hydrolysis product,  $\mu$ -oxo-bis(methylhafnocene). Inorg. Chem. **1976**, *15*, 2284–2289.
  28. Hunter, W.E.; Hrcir, D.C.; Bynum, R.V.; Penttil , R.A.; Atwood, J.L. The search for dimethylzirconocene—Crystal-structures of dimethylzirconocene, dimethylhafnocene, chloromethylzirconocene, and ( $\mu$ -oxo)bis(methylzirconocene). Organometallics **1983**, *2*, 750–755.
  29. Yoon, K.; Parkin, G. Resolved and unresolved crystallographic disorder between { $\eta^3$ -HB(3-Bu<sup>t</sup>p<sub>z</sub>)<sub>3</sub>}ZnCN and { $\eta^3$ -HB(3-Bu<sup>t</sup>p<sub>z</sub>)<sub>3</sub>}ZnX (X = Cl, Br, I). Inorg. Chem. **1992**, *31*, 1656–1662.
  30. Han, R.; Parkin, G.; Trofimenko, S. The *tris*[3-(9-anthryl)pyrazol-1-yl]hydroborato Ligand, [Tp<sup>Ant</sup>]: Compositional disorder between a vacancy and a chain of three atoms. Polyhedron **1995**, *14*, 387–391.
  31. Girolami, G.S.; Salt, J.E.; Wilkinson, G.; Thornton-Pett, M.; Hursthouse, M.B. Alkyl, hydride, and dinitrogen 1,2-bis(dimethylphosphino)ethane complexes of chromium—Crystal-structures of Cr(CH<sub>3</sub>)<sub>2</sub>(dmpe)<sub>2</sub>, CrH<sub>4</sub>(dmpe)<sub>2</sub>, and Cr(N<sub>2</sub>)<sub>2</sub>(dmpe)<sub>2</sub>. J. Am. Chem. Soc. **1983**, *105*, 5954–5956.
  32. Salt, J.E.; Girolami, G.S.; Wilkinson, G.; Motevalli, M.; Thornton-Pett, M.; Hursthouse, M.B. Synthesis and characterization of 1,2-bis(dimethylphosphino)ethane (dmpe) complexes of chromium(0) and chromium(IV)—X-ray crystal-structures of *trans*-Cr(N<sub>2</sub>)<sub>2</sub>(dmpe)<sub>2</sub>, *cis*-Cr(CO)<sub>2</sub>(dmpe)<sub>2</sub>, Cr(C<sub>2</sub>Ph)<sub>2</sub>(dmpe), and CrH<sub>4</sub>(dmpe)<sub>2</sub>. J. Chem. Soc., Dalton Trans. **1985**, 685–692.
  33. Howard, W.A.; Parkin, G.; Rheingold, A.L. Non-classical carbonyl complexes of zirconium: The syntheses,

- characterization, and reactivities of  $(\eta^5\text{-C}_5\text{Me}_5)_2\text{Zr}(\eta^2\text{-E}_2)(\text{CO})$  ( $\text{E} = \text{S}, \text{Se}, \text{Te}$ ). *Polyhedron* **1995**, *14*, 25–44.
34. Cullen, D.; Meyer, E., Jr.; Srivastava, T.S.; Tsutsui, M. Unusual metallocporphyrins—Structure of product from reaction of dodecacarbonylruthenium with meso-tetraphenylporphine—Dicarbonyltetraphenylporphinatoruthenium (II). *J. Chem. Soc., Chem. Commun.* **1972**, 584–585.
  35. Bonnet, J.J.; Eaton, S.S.; Eaton, G.R.; Holm, R.H.; Ibers, J.A. Spectroscopic and structural characterization of ruthenium(II) carbonyl-porphine complexes. *J. Am. Chem. Soc.* **1973**, *95*, 2141–2149.
  36. Jones, R.A.; Wilkinson, G.; Galas, A.M.R.; Hursthouse, M.B. Interaction of hexamethyltungsten(VI) with trimethylphosphine—X-ray crystal-structure of dimethyltetraakis(trimethylphosphine)tungsten(II). *J. Chem. Soc., Chem. Commun.* **1979**, 926–927.
  37. Chiu, K.W.; Jones, R.A.; Wilkinson, G.; Galas, A.M.R.; Hursthouse, M.B.; Malik, K.M.A. Reactions of hexamethyltungsten(VI) in the presence of trimethylphosphine—Synthesis of methyl, ethylidyne, hydrido-tungsten, alkoxo-tungsten, and other tungsten compounds—X-ray crystal-structures of *trans*-ethylidyne-(methyl)tetrakis(trimethylphosphine)tungsten(IV) and trihydrido-(phenoxo)-tetrakis(trimethylphosphine)tungsten(IV). *J. Chem. Soc., Dalton Trans.* **1981**, 1204–1211.
  38. Burrell, A.K.; Cotton, F.A.; Daniels, L.M.; Petricek, V. Structure of crystalline  $(\text{C}_5\text{Me}_5)\text{ReO}_3$  and implied nonexistence of  $(\text{C}_5\text{Me}_5)\text{Tc}_2\text{O}_3$ . *Inorg. Chem.* **1995**, *34*, 4253–4255.
  39. Marsh, R.E.; Olmstead, M.M.; Schaefer, W.P.; Schomaker, V. Dinitrogen or dichloromethane? *Inorg. Chem.* **1993**, *32*, 4658–4659.
  40. Babaian-Kibala, E.; Cotton, F.A.; Kibala, P.A. A new bis( $\mu$ -sulfido)ditantalum(IV) edge-sharing bioctahedral molecule and a reassessment of some earlier bis( $\mu$ -chloro) molecules. *Inorg. Chem.* **1990**, *29*, 4002–4005.
  41. Li, T.-I.; Lippard, S.J. Crystal and molecular-structure of tris(ethylthioxanthato)cobalt(III)—Reinvestigation. *Inorg. Chem.* **1974**, *13*, 1791–1792.
  42. Boeyens, J.C.A.; van der Merwe, M.J. The nonexistent crystals of macrocyclic nickel(III). Structure of the cobalt(III) complex of 1,4,7-triazacyclononane- $\text{N}, \text{N}', \text{N}''$ -triacetate. *Inorg. Chem.* **1997**, *36*, 3779–3780.
  43. von Schnering, H.G.; Vu, D. Are the previously described  $[\text{ClF}_6][\text{CuF}_4]$  and  $[\text{Cu}(\text{H}_2\text{O})_4][\text{SiF}_6]$  identical? *Angew. Chem., Int. Ed. Engl.* **1983**, *22*, 408.
  44. Haaland, A.; Rypdal, K.; Verne, H.P.; Scherer, W.; Thiel, W.R. The crystal-structures of base-free, monomeric arylcopper(I) and arylsilver(I) compounds—2 cases of mistaken identity. *Angew. Chem., Int. Ed. Engl.* **1995**, *33*, 2443–2445.
  45. Cotton, F.A.; Schmid, G. Proposed reformulation of recently reported “tetrahedral molybdenum(II)” complexes: Trimethylphosphine complexes of zinc chloride. *Polyhedron* **1996**, *15*, 4053–4059.
  - 46a. Marsh, R.E. Is there any Zr in  $\text{Na}_2\text{NiZr}(\text{P}_2\text{O}_7)_2$  or  $\text{Na}_2\text{CoZr}(\text{P}_2\text{O}_7)_2$ ? *Acta Crystallogr.* **1990**, *C46*, 2497–2499.
  - 46b. Marsh, R.E. On the structure of  $\text{Zn}(\text{C}_4\text{H}_8\text{N}_2\text{O}_6)$ . *Acta Crystallogr.* **1986**, *C42*, 1327–1328.
  47. Marsh, R.E. Some thoughts on choosing the correct space group. *Acta Crystallogr.* **1995**, *B51*, 897–907.
  48. Templeton, L.K.; Templeton, D.H.; Zalkin, A.; Ruben, H.W. Anomalous scattering by praseodymium, samarium and gadolinium and structures of their ethylenediamine-tetraacetate (edta) salts. *Acta Crystallogr.* **1982**, *B38*, 2155–2159.
  49. Reiß, G.J.; Konietzny, S. How realistic are alternating C–C-bond lengths in *s-cis*-1,3-butadiene transition metal complexes? *J. Chem. Soc., Dalton Trans.* **2002**, 862–864.
  - 50a. Murphy, V.J.; Rabinovich, D.; Parkin, G. False minima and the perils of a polar axis in x-ray structure solutions: The molecular structures of  $\text{W}(\text{PMe}_3)_4\text{H}_2\text{X}_2$  ( $\text{X} = \text{F}, \text{Cl}, \text{Br}$ ) and  $\text{W}(\text{PMe}_3)_4\text{H}_2\text{F}_2(\text{H}_2\text{O})$ . *J. Am. Chem. Soc.* **1995**, *117*, 9762–9763.
  - 50b. Murphy, V.J.; Rabinovich, D.; Hascall, T.; Klooster, W.T.; Koetzle, T.F.; Parkin, G. False minima in x-ray structure solutions associated with a ‘partial polar ambiguity’: Single crystal x-ray and neutron diffraction studies on the eight-coordinate tungsten hydride complexes,  $\text{W}(\text{PMe}_3)_4\text{H}_2\text{X}_2$  ( $\text{X} = \text{F}, \text{Cl}, \text{Br}, \text{I}$ ) and  $\text{W}(\text{PMe}_3)_4\text{H}_2\text{F}(\text{FHF})$ . *J. Am. Chem. Soc.* **1998**, *120*, 4372–4387.
  51. Kuchta, M.C.; Parkin, G. Incorrect atom connectivity in x-ray structures associated with a ‘partial polar ambiguity’: A non-macrocyclic structure for the macrocyclic lead complex,  $[\eta^4\text{-Me}_8\text{taa}]\text{Pb}$ . *New J. Chem.* **1998**, *22*, 523–530.
  52. Kuchta, M.C.; Dias, H.V.R.; Bott, S.G.; Parkin, G. The synthesis and structure of  $[\text{Tp}^{\text{Bu}_2}]\text{In}$ , a highly twisted *tris*(3,5-di-*t*-butylpyrazolyl)hydroborato indium(I) complex: Comparison with the re-evaluated ordered structure of  $[\text{Tp}^{\text{Bu}_2}]\text{In}$ . *Inorg. Chem.* **1996**, *35*, 943–948.

# Brillouin Scattering

Claude Ecolivet

Université de Rennes, Rennes, France

## INTRODUCTION

Brillouin scattering is a technique in which, through an inelastic scattering process of photons by acoustic waves (also called acoustic phonons),<sup>[1,2]</sup> the investigation of the elastic properties of materials can take place. Although transparent materials make experiments easier and more fruitful, some measurements can be successfully performed on opaque semiconductors and even metals.<sup>[3,4]</sup> One of the interests of this noncontact technique is that it does not require large samples. Some experimental setups even use microscopes to collect the scattered light, allowing measurements on microscopic or heterogeneous samples.<sup>[5]</sup> This is an advantage on ultrasonics or inelastic neutron scattering that can also measure sound velocities but usually necessitate larger samples. The essential microscopic physical information provided by Brillouin scattering is the magnitude of the interatomic or intermolecular elastic interactions revealing what actually occurs inside the material. In supramolecular crystals consisting in host and guest molecules, it can then be possible to identify and evaluate the interactions between the different constituents.

Moreover, the technical progress in Brillouin scattering spectroscopy, mainly due to the use of tandems of Fabry Perot interferometers,<sup>[6]</sup> allows us to investigate, in the same experiment, the acoustic phonons and the low-lying Raman lines and the Rayleigh wings often generated by instabilities and relaxations.<sup>[7]</sup> Often, these modes are coupled to the acoustic waves, and their scattering geometries and polarizations facilitate their assignment and give a deeper insight to their dynamics. Brillouin spectra, like the Raman spectra, appear as doublets, where their intensity, frequency, and line width are the main characteristics that can be used to produce quantitative data about elastic, photoelastic,<sup>[8]</sup> and anharmonic properties of the materials.

In this article, we briefly recall the principles of the technique and the state of the art of the technique as it is currently used in laboratories. Then we present some results obtained on supramolecular compounds: charge-transfer crystals and inclusion compounds (clathrates and channel-like composites). These results were chosen to give a broad scope of what the interest of Brillouin scattering is for supramolecular scientists. More details on

the technique or its application to other materials can be found in other review papers.<sup>[9,10]</sup>

## PRINCIPLE

It is well known since the beginning of the last century that acoustic waves (longitudinal and transverse) are generated by thermal agitation even at very low temperatures. The Debye  $T^3$  law of specific heat is but one of the numerous consequences. These waves of frequency  $\nu$  and wave vector  $q = 2\pi/\lambda$  have a linear dispersion:

$$2\pi\nu = Vq$$

where  $V$  is the phase velocity (longitudinal or transverse). They carry a (pseudo) momentum  $\hbar q$  that can combine with the one of an incident photon  $\hbar k_i$  to satisfy a conservation law defining the wave vector of scattered photons  $k_s$ :

$$\hbar k_s = \hbar(k_i \pm q)$$

This process can also be considered a Bragg diffraction of incident photons by an index grating resulting from the refractive index modulation by the density variations of the longitudinal acoustic mode or the shearing strains for the transverse modes. Because the energy of the incident photon ( $\approx 2$  eV) is much larger than that of the acoustic phonon ( $\approx 0.1$  meV), the magnitude of  $k_s$  is similar to the one of  $k_i$ , yielding:

$$\|k_s - k_i\| \approx 2\|k_i\| \sin(\theta/2)$$

like in a Bragg reflection, where  $\theta$  is the scattering angle, which will define the magnitude of the phonon wavevector. Because the scattering grating moves at the sound of velocity in opposite directions  $\pm q$ , the scattered intensity is Doppler shifted and appears as a doublet centered on the incident photon frequency:

$$\nu_s = \nu_i \pm \nu_{\text{phonon}} = \nu_i \pm 2(nV/\lambda) \sin(\theta/2)$$

This relation is obtained through the linear dispersion relation of acoustic phonons and photons in the simple case

of an optically isotropic material of index  $n$ . The last term of the right-hand side (rhs) of the above equation is called the Brillouin shift, which is equal to the frequency of the detected phonon. In the case of an optically anisotropic material, the scattered and incident wave vectors can be very different, and the  $2n \sin(\theta/2)$  term in the above formula is replaced by:  $(n_i^2 + n_s^2 - 2n_i n_s \cos\theta)^{1/2}$ , where  $n_i$  and  $n_s$  are the refractive indices for the incident and scattered beams.

Thus, the choice of an incident radiation  $\lambda_i$  defines  $\mathbf{k}_i$ , whereas the choice of a scattering angle (usually  $90^\circ$  or  $180^\circ$ ) unambiguously determines  $\mathbf{k}_s$  and, henceforth, the Brillouin shift related to each of the three acoustic modes with their own velocities. Typically, for an incident visible radiation, and a material characterized by an index of refraction about 1.5 and sound velocities of a few km/s, the Brillouin shift lies in the range of 10–30 GHz ( $0.33\text{--}1\text{ cm}^{-1}$ ) in backscattering geometry. Obviously, the study of Brillouin lines requires a more consequent resolution than the one of a conventional Raman spectrometer.

In the absence of any perturbation by other modes, the Brillouin lines can be described by a damped oscillator profile derived from the imaginary part  $\chi''(\omega)$  of the oscillator susceptibility:

$$I(\omega) = I_0[n(\omega, T) + 1/2 \pm 1/2]\chi''(\omega) \\ \approx I_0 kT\gamma / \{[\omega^2 - (\omega_i \mp Vq)^2]^2 + \gamma^2 \omega^2\}$$

where  $n(\omega, T)$  is the Bose factor defining the phonon population at a given temperature  $T$ ;  $\gamma$  is the half-width at half height; and  $\omega_i$  is the pulsation of the incident light. The upper sign is related to what is called the Stokes

process, where an acoustic phonon is created by a photon inside the sample, and the associated frequency is then:

$$\nu_s(\text{Stokes}) = \nu_i - \nu_{\text{phonon}}$$

whereas the lower sign is related to the opposite case, called Antistokes, where an acoustic phonon is destroyed in the scattering process corresponding to a line located at a frequency higher than the incident one:

$$\nu_s(\text{antiStokes}) = \nu_i + \nu_{\text{phonon}}$$

The probability of this process being strictly proportional to the phonon population by the Bose factor decreases at low temperatures. Except at very low temperatures, there is no detectable intensity difference between the Stokes and anti-Stokes contributions at variance to Raman scattering.

The intensity  $I_0$  depends on geometric factors characteristic of the setup and also on the photoelastic constants, which relate the refractive index variations to the elastic strains and some internal rotations. Brillouin scattering, by comparison with a substance where the photoelastic constants are well known (usually benzene, quartz, ...), is a method for determining these coefficients.<sup>[8]</sup> In some scattering geometries, the calculated intensity of some well-polarized modes can be zero, but at variance to Raman scattering where optic modes are not always active, acoustic modes can always be seen, at least theoretically, in some other scattering geometry, usually labeled in the Porto notation  $\mathbf{k}_i(\mathbf{E}_i, \mathbf{E}_s)\mathbf{k}_s$ , where  $\mathbf{E}$  is the radiation electric field (Fig. 1).

The line width  $\gamma$  is related to the damping of elastic waves, which results from anharmonic interactions of the acoustic phonons with other phonons, relaxation

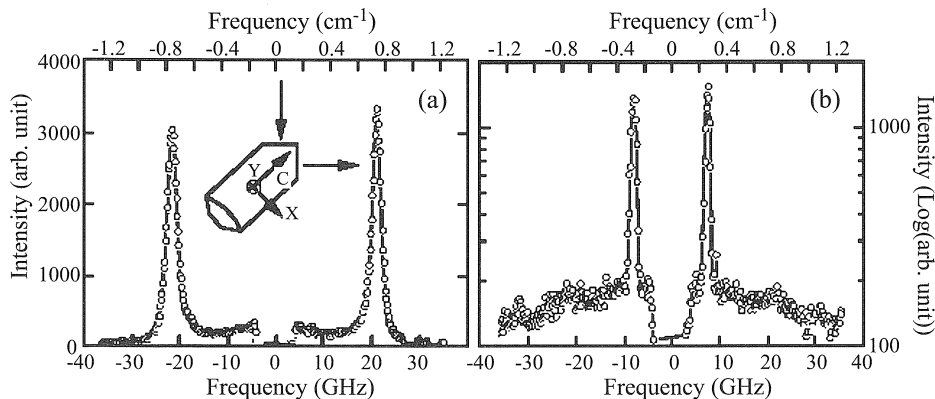


**Fig. 1** Example of Brillouin scattering spectra taken in right-angle geometry in an hexagonal crystal showing the effect of beams polarization. The hexagonal axis is  $C$ . The orthogonal directions in the basal plane are  $X$  and  $Y$ . (a)  $C-X(Y,Y) C+X$  scattering geometry showing a broad longitudinal doublet sitting on a quasielastic component. (b)  $C-X(Y,C-X) C+X$  scattering geometry revealing the only narrow transverse doublet expected. Notice through the logarithmic intensity scale the practical absence of the longitudinal component in that spectrum. (From Ref. [30].)

processes, or structural disorder. Due to the high frequency of the investigated phonons, inherent to the technique, the influence of linear defects like dislocations is usually negligible. In solids, typical line widths are within tens to hundreds of MHz, and because it is the same order of magnitude as the experimental broadening due to the apparatus function and the finite aperture contribution, a deconvolution is needed in order to obtain a better estimation of the true line width.

The phonon frequency  $\nu_{\text{phonon}} = Vq/2\pi$  is determined by the Christoffel equation,<sup>[11]</sup> which relates the phase velocity of acoustic waves to the elastic constants of the material. The number of elastic constants of a material depends on its symmetry, varying from one for liquids to three for cubic crystals and up to 21 in triclinic crystals. By measuring a number of independent sound velocities at least equal to the number of elastic constants in non-equivalent directions, it is theoretically possible to determine all the elastic constants of the material. Often, structural phase transitions generate acoustic anomalies, which can then be studied by Brillouin scattering by following the evolution versus temperature or pressure of the Brillouin shift and the line width of selected phonons.<sup>[9]</sup> High-frequency noncritical relaxations, in the ps range, also create some anomalies that are more gradual.

## EXPERIMENTAL

Due to the small value of the Brillouin shifts and their line widths, experimental techniques involve interferometric devices. However, resolution is not all, perhaps the more important quality is the contrast, i.e., the ability to

distinguish a small Brillouin line in the wing of a huge elastic Rayleigh line. In the case of a low contrast like in non-scanning interferometers,<sup>[12]</sup> studies are limited to high optical quality materials in right-angle scattering geometry, where the stray light is minimum. Obviously, usual samples are most of the time not of high optical quality, and they do not always present right-angle faces oriented along the more interesting directions. Nowadays, the best trade-off for Brillouin spectrometers is the tandem of plane Fabry-Perot (FP) interferometers (Sandercock mounting) that may offer a resolution about 0.1 GHz and a contrast larger than  $10^{11}$  with an acceptable transmission.<sup>[6]</sup> An FP interferometer consists in two partially reflecting parallel mirrors between which light undergoes multiple reflections, ensuring a higher contrast than with a two-wave interferometer like a Michelson device. A drawback of FP interferometers is the periodicity of their transmission characterized by the free spectral range  $\Delta = c/2ne$  obtained by scanning the distance  $e$  (or the refractive index  $n$ ) between the mirrors by more than a half-wavelength. An interesting feature of the tandem is the “vernier” ratio between the periodicities of the FPs defined by the ratio between their distances  $e_1$  and  $e_2$  chosen to be close to an incommensurate value. In such a case, the free spectral range of the tandem may be 20 times the one of an individual FP. The apparatus function of an FP interferometer characterized by its maximum transmission  $T_M$  is an Airy function:

$$T_i(\nu) = T_M / [1 + (2F_E/\pi)^2 \cos^2(\pi\nu/\Delta_i)]$$

where  $F_E$  is the effective finesse defined as the ratio of the free spectral range  $\Delta$  over the width at half height of the

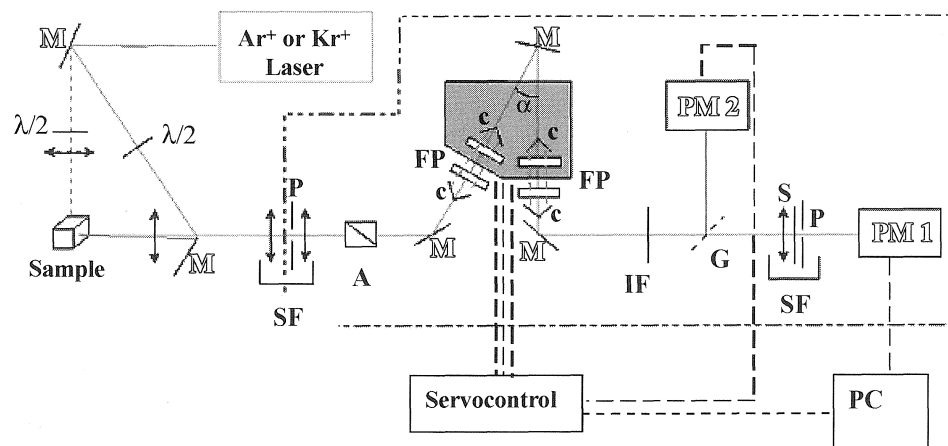


**Fig. 2** Typical Brillouin scattering setup using a tandem of triple-passed Fabry-Perot interferometers. M: mirrors, SF: spatial filters, FP: Fabry Perot interferometers, c: corner cubes, IF: interferential filter,  $\lambda/2$ : half-wave plate, PM: photomultipliers, P: pinholes, A: Glan analyzer, S: fast shutter, G: glass plate, and PC: personal computer for data acquisition. (From Ref. [13].) (View this art in color at [www.dekker.com](http://www.dekker.com).)

maximum of the Airy function. The apparatus function of the tandem being the product of the individual Airy functions, the interest of the loss of periodicity in the total apparatus function is that it allows for easier measurement of the Brillouin shifts, and more specifically, it allows in the same experiment the observation of sharp Brillouin lines and broad quasielastic components with a good rejection of the contribution of higher-order interferences.

The high contrast of the spectrometer is achieved either by triple passing each FP or the whole tandem setup. It results theoretically in an elevation of the apparatus function of each interferometer to the cube, which strongly enhances the contrast defined as the ratio of the maximum transmission over its minimum value. In order to achieve this high contrast, the tandem sits in a highly collimated beam between spatial filters, which also allows the stray light at the entrance to be diminished and the bandwidth at the exit pinhole in front of a photomultiplier or an avalanche diode to be selected (Fig. 2).

Spectra are acquired by a linear scan of the piezoelectrically driven tandem, and data acquisition lasts between a few seconds and several hours, according to experimental conditions and sample characteristics. The long-term stability usually required to collect spectra is realized via a maximum transmission servo-control keeping the best alignment of the tandem checked by an auxiliary photodetector (PM2).

## RESULTS

Results obtained by Brillouin scattering range from the determination of the elastic and photoelastic constants of materials to the analysis of material transformations: phase transitions, polymerization, glass transitions, photoinduced transformations, etc. (It is out of the scope of this presentation to present all.) We will limit our discussion to some examples selected in the field of supramolecular products defined as complexes consisting of two or more chemical entities associated through van der Waals interactions, hydrogen bonds, or charge-transfer mechanisms.<sup>[14]</sup>

### Weak Charge-Transfer (CT) Complex Crystals

Tetracyanobenzene (TCNB) is an electron acceptor that forms charge-transfer complexes with aromatic donor molecules: anthracene (A), naphthalene (N), phenanthrene (Ph), etc. These weak CT complexes crystallize in alternated stacks, leading to insulating properties with CT bands of rather high energy, yielding to colored but transparent crystals. Like many organic crystals, they crystallize in a monoclinic group and are known to present

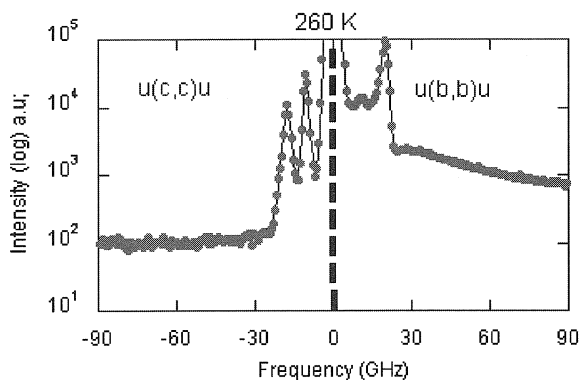


**Fig. 3** Brillouin spectra of naphthalene-tetracyanobenzene taken in a backscattering geometry showing (on the right) the interference scattering between acoustic modes and a quasi-elastic component generated by an overdamped reorientational optic mode. (View this art in color at [www.dekker.com](http://www.dekker.com).)

an orientational disorder, because the cyanide arms of the acceptor define a volume larger than that of donors.<sup>[15]</sup>

In N-TCNB, the disorder is well characterized by molecular jumps of the donor molecule between orientations separated by  $36^\circ$ .<sup>[16]</sup> At room temperature, the relaxation time of these jumps in the few ps range lead to a coupling with acoustic phonons. Then the quasielastic component generated by this relaxational behavior with a width in the 10 GHz range is distorted by coupling with the acoustic modes, which also undergo a severe asymmetry of their profile with a dip on the high-frequency wing (Fig. 3). These profiles can be described by a coupled susceptibilities equation<sup>[17]</sup> relating the oscillator susceptibility of the acoustic phonon with a relaxational susceptibility (Debye type). Another common result from coupling the acoustic modes to other modes is the increase of their line-width. Shown in Fig. 3, on a semi-log scale, are two spectra demonstrating this coupling. On the left side, one observes a usual uncoupled Brillouin spectrum with two peaks: a QL mode around 20 GHz and a QT mode around 10 GHz. In this experiment, the incident and scattered electric fields are perpendicular to the molecular plane (c,c) and, consequently, are not influenced by the electric polarization generated by the rotation of an asymmetric molecule. On the contrary, the right side was recorded along the same direction but with incident and scattered electric fields in the molecular plane (b,b). One also sees two Brillouin lines at about the same frequencies as with the other polarization (except for the birefringence shift), but they are accompanied by a quasielastic component of about 22 GHz half-height half-line-width interfering severely with the QL mode. A signature of this interference scattering is the difference of intensity between the low- and high-frequency wings of a Brillouin line. The dots on the spectra are the

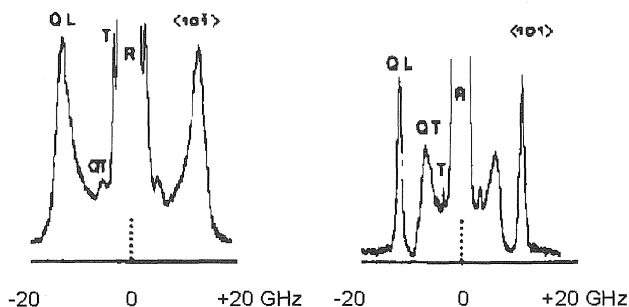


**Fig. 4** Brillouin spectra recorded at atmospheric pressure at  $T_c = 5$  K in right-angle geometry along the direction  $(10\bar{1})$ , nearly parallel to the anthracene long axis (left), and the  $(101)$  direction almost perpendicular to this long axis (right). The  $R$ ,  $T$ ,  $QT$ , and  $QL$  indicate, respectively, the Rayleigh elastic line, the transverse mode polarized along the  $b$  monoclinic axis, and the quasitransverse and quasilongitudinal modes polarized in the  $(a,c)$  plane. The free spectral range is 39.15 GHz. (From Ref. [18].)

experimental data, whereas the continuous line is the fit by the coupled susceptibilities.

By cooling the sample, one observes a narrowing of the quasielastic component and the apparition in the Raman spectrum of a low-frequency mode ( $40\text{ cm}^{-1}$ ) at about 200 K. This mode shifts toward higher frequencies due to the decrease of its damping and presents only a small frequency anomaly at the phase transition ( $T_c = 73$  K).

The disorder is so fast in A-TCNB at atmospheric pressure, that no physical method is able to distinguish well-defined orientations of the donor, which librates in an anharmonic double well, but above the internal energy barrier. It then results in a displacive structural transition characterized by an optical soft mode coupled to acoustic phonons and leading to large elastic anomalies of the relaxational type.<sup>[18]</sup> However, under pressure, this disorder slows, probably under the effect of an increase of the internal barrier, and the structural transition becomes an order-disorder one with an overdamped optic mode that no longer softens.<sup>[19]</sup> This structural phase transition was extensively studied by different techniques, including Brillouin scattering. In particular, it was shown that all elastic anomalies occurring in that compound derive from the coupling between the  $(A)$  librations and the longitudinal acoustic mode propagating along the molecular long axis. The relaxation time of the order parameter presents a critical slowing  $\tau(T) = \tau_0/(T_c - T)$ , with  $T_c = 212$  K and  $\tau_0 = 50$  ps. Shown in Fig. 4, at  $T_c = 5$  K, is the effect of the coupling with the soft optic mode on the Brillouin spectra related to acoustic phonons propagating nearly along the  $(A)$  long molecular axis  $(10\bar{1})$ , where the quasilongitudinal acoustic mode ( $QL$ ) is strongly coupled to the soft mode and is,

consequently, broadened. In a perpendicular direction  $(101)$ , this occurs for the quasitransverse mode ( $QT$ ), also polarized along the  $(A)$  long axis. The true transverse mode polarized along the monoclinic axis is always narrow, because it is not good symmetry to be coupled to the soft mode. Further studies of the fluctuation dynamics also revealed the contribution of disorder to this typical displacive transition.

## Clathrates

Clathrates are typical supramolecular objects with molecules playing the role of host, whereas others are guests. A large variety of structures were imagined and realized (for a recent review see Ref. [20]), but they can be sorted by the dimensionality of the guest assembly. At the lowest level, we get cages inside with zero, one, or two molecules included. With a dimension one, we have tubular or cylindrical pores inside which guests molecules will have a longitudinal interaction. At two dimensions, we will have intercalated molecules between host planes.

A general problem of clathrates is the interaction of guests and host molecules and eventually between guests. In the simplest approach, these interactions are neglected, and it is expected that the elastic properties of the clathrate are only sensitive to the degree of filling of the cages and to the mass of the guest molecules.<sup>[21]</sup> Brillouin scattering is a well-suited technique for such investigations, which should look into the sound velocities of the empty clathrand and differently filled clathrates. First Brillouin scattering experiments on such materials were performed in the early 1990s on methane and xenon clathrate hydrates.<sup>[22]</sup> In these compounds, water molecules build a cubic lattice through hydrogen bonds and define two types of cages inside the lattice—large and small ones—inside which atoms or small molecules are present. Further studies on a larger variety of guests show a decrease in proportion to the square root of the guest mass but not as large as expected in the absence of guest-host interactions, which are found to be repulsive.<sup>[23]</sup>

For these clathrate hydrates, a problem is the comparison to the empty clathrand properties, because the stability of the empty clathrate is often a problem. Dianin's compound and its clathrates are an opposite case, because the stability of the pure compound is good. Consequently, they were more extensively investigated. The structure of this compound is based on a hexamer linked by a network of hydrogen bonds involving the phenolic hydroxyl groups of 4-(*p*-hydroxyphenyl)-2,2,4-trimethylchroman, which is represented in Fig. 5b. A projection of the cell perpendicular to the threefold axis of the space group  $(R\bar{3}i)$  is represented in Fig. 5a,<sup>[24]</sup> showing the six arms of the hexamer, which are



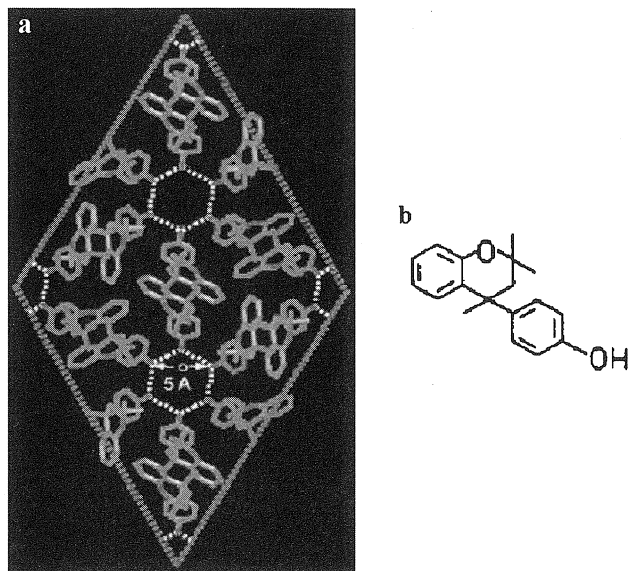


**Fig. 5** (a) Projection of the structure of the Dianin clathrand in the basal plane.<sup>[24]</sup> Carbon atoms are represented in green; oxygen in red; and H bonding by yellow dashed lines. (b) Its building molecule. (From Ref. [24].) (View this art in color at [www.dekker.com](http://www.dekker.com).)

alternately up and down, building around each H-bonded ring an hourglass-like architecture. In the next above layer, three downward arms with the three upwards arms of the represented layer build a cage that is locked by van der Waals interactions. It was shown that the dimensions of the unit cell increase when the cages are occupied, but the more affected distance is the  $c$  axis, which is mainly dependent from the van der Waals interactions between hexamers.

Recently, by comparing sound velocities and elastic constants between Dianin clathrand and the ethanol and heptanol clathrates, quantitative data related to the interactions were reported.<sup>[25]</sup> The main difference between both clathrates lies in the number of molecules per cage: two for ethanol with a noticeable disorder, but only one for heptanol which adopts a folded “gauche” conformation for a better fit inside the cage. Brillouin scattering results show that for the clathrand and the ethanol clathrate, similar sound velocities are observed for the longitudinal modes in the basal plane, whereas the longitudinal mode along the threefold axis presents a 15% decrease of its velocity for the ethanol clathrate. This fact could be explained by the 0.5% elongation strain along the  $c$  axis produced by the two guest molecules. If one compares the heptanol clathrate to the clathrand, more isotropic longitudinal sound velocity decreases are observed in the basal plane (12%) and along the  $c$  axis (18%). This seems in agreement with

the more isotropic elongations of the  $a$  and  $c$  parameters of these compounds, 0.67% and 0.73%, respectively. These strain values lead to the concept of internal pressure that guest molecules would apply to the host ones. It reaches 1 kbar for the heptanol clathrate and two to three times less for the ethanol one. This pressure is produced by an energetically less-favorable state of the guest molecules, estimated at 18 kJ/mol for heptanol. Such studies exemplify the interest of what can be learned from Brillouin scattering experiments coupled with other data sources.

### Urea Inclusion Compounds

Channel-like compounds can also be considered clathrates, because guest molecules are confined inside these channels. Here also, the nature and magnitude of the interactions between the different kinds of molecules are major problems. In addition to the cage situation, the channel geometry may allow longitudinal end-to-end interactions between the guests. Depending on the thickness of the channel walls, a weaker lateral guest–guest interaction is also possible. Elastic properties are again a good probe for all of these interactions. Such compounds are commonly obtained with molecules such as urea or thiourea, but in the case of thiourea, the channel diameter is strongly modulated and firmly localizes guest molecules in pockets along the channels, in a similar fashion as in cages rejoining the previous cage-like compounds. Consequently, we will be more interested in smoother channels like those of urea. Depending on the nature of interactions developed between the host and the guest molecules, it will be possible to obtain a regular crystal by periodic packing of the guests along the channels or to obtain an aperiodic structure.<sup>[26]</sup> The first case is, for example, obtained when firm hydrogen bonds are developed with the host, like in 2–10 undecanedione,<sup>[27]</sup> whereas the second case is typical of alkane molecules that only interact by van der Waals forces. All of these structures are derived from infinite honeycomb-like channels made up of three urea helices interwoven by hydrogen bonds, inside which guest molecules are densely packed to ensure the stability of the composite. The symmetry is often hexagonal, but distortions resulting from the shape of the guest molecules usually lead to orthorhombic symmetries at low temperatures. When such a ferroelastic transition occurs, Brillouin scattering gives valuable data on the order and the regime of transition by recording sound velocity anomalies.<sup>[13,28]</sup>

In aperiodic composites, another degree of freedom occurs due to the infinite degeneracy of the ground state, i.e., all relative positions of the host and guest molecules exist in the structure due to its incommensurability, so that the whole composite has the same energy for any relative

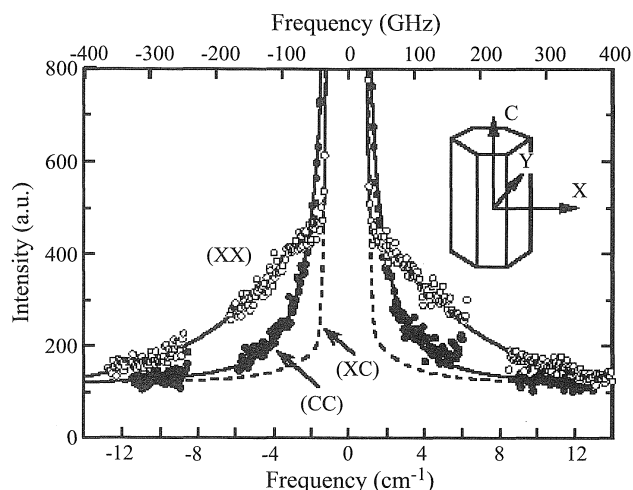


**Fig. 6** Quasielastic components observed in nonadecane/urea at room temperature in tandem with Fabry-Perot interferometers. The central intensity is due to the longitudinal Brillouin doublets. The (XX) component is assigned to the reorientation of alkane molecules, whereas the (ZZ) component is compatible with an overdamped “sliding” motion. (From Ref. [30].)

position of a given host–guest pair. Such a degeneracy leads to a possible sliding motion of the whole urea sublattice with respect to the guest sublattice without any energy cost. This feature is also the one of acoustic phonons, which have zero energy for infinite wavelengths. The main difference is located in the energy dissipation of these vibration modes: sound waves are hydrodynamic modes, and their damping goes to zero like  $q^2$ , because the atomic relative motion also goes to zero for infinite wavelengths. On the contrary, the relative sliding motion is, by essence, optic-like with large relative motions of the hosts and guests so that this motion will dissipate energy or can also be quenched by Nabarro barriers that in crystals, impede the dislocation motion, giving birth to a gap in its dispersion branch at low wave-vectors. The search of an experimental observation of sliding modes is still active and relies on inelastic techniques like neutron and light scattering. Many experiments were performed in alkane/urea compounds without any direct observation of an inelastic peak unambiguously assignable to this sliding mode. The apparition of an extraneous fourth Brillouin peak in the spectrum of heptadecane/urea<sup>[29]</sup> was not confirmed by the following experiments,<sup>[30]</sup> which evidenced the existence of quasielastic components (Fig. 6): one related to the reorientational–librational motion of alkane molecules around their long axis and another one polarized along the channel, which could be compatible with an overdamped sliding mode. Elastic properties of several urea inclusion compounds were investigated, and they showed the weak influence of the

nature of the guest molecules on the sound velocities inside the composites. This is striking, because, along the channel axis, one can expect that the addition of the sublattice stiffness and the one of the guest sublattice should vary with the length and the end-to-end interactions between these molecules. Recently, by applying a hydrostatic pressure to the guest molecules by He atoms directly inside the channels, it was possible to determine the force constant between alkane ( $C_{19}D_{40}$ ) molecules.<sup>[31]</sup> Its weak value 1 N/m compared to the average 10–15 N/m for H-bonded molecules allows us to understand the very small influence of the alkane length on the composite sound velocity. Another characteristic of the dynamics of such a system is the broadening of the longitudinal Brillouin line along the channels, as shown in Fig. 1a, which was taken on nonadecane/urea. High-pressure experiments showed that about 25% of this anomalous broadening (1.7 GHz) is due to the conformational defects of alkane chain ends,<sup>[13]</sup> but the major part is still nonidentified and could be due to a coupling between the overdamped sliding motion and the longitudinal phonon. It should be noticed that the transverse acoustic mode seen in Fig. 1b has a very small damping that is barely measurable on this spectrum. Recent experiments on periodic and aperiodic ketones included in urea also showed relaxations coupled differently to the acoustic phonons than those in alkane/urea inclusion compounds, and this will be reported elsewhere.

## CONCLUSION

All of these results and many others not reported here due to a lack of space prove the interest of Brillouin scattering as a technique of investigation of the elastic and dynamical properties of materials, in particular, for supramolecular compounds. The conclusions derived give better insight to the materials when they are carefully crossed with structural or other dynamical results provided for by complementary techniques. In photoexcitable materials, Brillouin scattering offers the unique opportunity of measuring the elastic properties of the excited volume, because at the same time, the light beams modify the sample and measure its properties. Despite the high technical level reached now, there is still room for further experimental improvements allowing faster and more precise measurements to be made.

## ARTICLES OF FURTHER INTEREST

*Channel Inclusion Compounds*, p. 223  
*Clathrate Inclusion Compounds, Phase Transitions in*,  
 p. 289

*Disorder and Diffuse Scattering*, p. 457  
*Energy- and Electron-Transfer in Supramolecular Systems*, p. 535  
*Inclusion Compounds: Selectivity, Thermal Stability, and Kinetics*, p. 696  
*Incommensurate and Commensurate Structures*, p. 712  
*Inelastic Neutron Scattering*, p. 727  
*Modulated Structures*, p. 873  
*Polymorphism*, p. 1129  
*Soft and Smart Materials*, p. 1302  
*Solid-State Reactivity and Topochemistry*, p. 1316

## REFERENCES

- Mandel'shtam, L.I. (*in Russian*) Zh. Russ. Fiz. Khim. Obshchestva **1926**, 58, 381.
- Brillouin, L. (*in French*) Ann. Phys. (Paris) **1922**, 17, 88.
- Dil, J.G.; Brody, E.M. Brillouin scattering from isotropic metals. Phys. Rev. B **1976**, 14, 5218.
- Sandercock, J.R. Light scattering from surface acoustic phonons in metals and semiconductors. Solid State Comm. **1978**, 26, 547.
- Jiang, F.M.; Kojima, S. Microheterogeneity and relaxation in 0.65Pb(Mn<sub>1/3</sub>Nb<sub>2/3</sub>)O<sub>3</sub>-0.35PbTiO<sub>3</sub> relaxor single crystals. Appl. Phys. Lett. **2000**, 77, 1271.
- Sandercock, J.R. U.S. Patent 4,014,614, 1977.
- Ecolivet, C.; Sougotti, M.; Delugeard, D.; Beaufils, S. High resolution Raman study of the soft mode in the incommensurate bis(4-chlorophenyl sulfone) J. Phys. I (France) **1994**, 4, 1451.
- Vacher, R.; Boyer, L. Brillouin scattering: A tool for the measurement of elastic and photoelastic constants. Phys. Rev. B **1972**, 6, 639.
- Cummins, H.Z. *Light Scattering Near Phase Transitions*; Cummins, H.Z., Levanyuk, A.P., Eds.; North-Holland: Amsterdam, 1983; 359.
- Sandercock, J.R. *Topics in Applied Physics: Light Scattering in Solids III*; Springer Verlag: Berlin, 1982; 173.
- Musgrave, M.J.P. *Crystal Acoustics*; Holden Day: San Francisco, 1970.
- Ko, J.-Y.; Kojima, S. Non scanning Brillouin spectroscopy applied to solid materials. Rev. Sci. Instr. **2002**, 73, 4390.
- Bourgeois, L. Ph.D. Thesis; 2002. Rennes (unpublished).
- Lehn, J.M. Cryptates: Inclusion complexes of macropolycyclic receptor molecules. Pure Appl. Chem. **1978**, 50, 871.
- Lefebvre, J.; Odou, G.; Muller, M.; Mierzejewski, A.; Luty, T. Characterisation of an orientational disorder in two charge-transfer complexes: anthracene-tetracyanobenzene (A-TCNB) and naphthalene-tetracyanobenzene (N-TCNB). Acta Cryst. B **1989**, 45, 323.
- Kumakura, S.; Iwasaki, F.; Saito, Y. Bull. Chem. Soc. Jpn. **1967**, 40, 1826.
- Katiyar, R.S.; Ryan, J.F.; Scott, J.F. Proton-phonon coupling in CsH<sub>2</sub>AsO<sub>4</sub> and KH<sub>2</sub>AsO<sub>4</sub>. Phys. Rev. B **1971**, 4, 2635.
- Ecolivet, C.; Mierzejewski, A. Brillouin scattering study of the elastic anomalies at the structural phase transition in anthracene-tetracyanobenzene. Phys. Rev. B **1990**, 42 (13), 8471.
- Bourges, P.; Ecolivet, C.; Mierzejewski, A.; Delugeard, Y.; Girard, A. *Phonons* 89; Hunklinger, S., Ludwig, W., Weiss, G., Eds.; World Scientific: Singapore, 1990; 1147.
- Langley, P.J.; Hulliger, J. Nanoporous and mesoporous organic structures: New openings for materials research. Chem. Soc. Rev. **1999**, 28, 279.
- Whalley, E. J. Geophys. Res. **1980**, 85, 2539.
- Whiffen, B.L.; Kieft, H.; Clouter, M.J. Determination of acoustic velocities in xenon and methane hydrates by Brillouin spectroscopy. Geophys. Res. Lett. **1982**, 9, 645.
- Kieft, H.; Clouter, M.J.; Gagnon, R.E. Determination of acoustic velocities of clathrate hydrates by Brillouin spectroscopy. J. Phys. Chem. **1985**, 89, 3103.
- Kiang, Y.-H.; Lee, S.; Xu, Z.; Choe, W.; Gardner, G.B. Persistent honeycomb structures in porous and other two-component solids. Adv. Mat. **2000**, 12 (10), 767.
- Sandstedt, C.A.; Michalski, D.; Eckhardt, C.J. Quantitative measurement of guest-host interactions in supramolecular systems: A comparative Brillouin scattering study of the Dianin's compound clathrand and two of its isostructural clathrates. J. Chem. Phys. **2000**, 112 (7), 7606.
- Hollingsworth, M.D.; Harris, K.D.M. *Comprehensive Supramolecular Chemistry*; Pergamon: New York, 1996; Vol. 6, 177.
- Brown, M.E.; Hollingsworth, M.D. Strees-induced domain reorientation in urea inclusion compounds. Nature **1995**, 376, 323.
- Ollivier, J. Ph.D. Thesis; 1997. Rennes (unpublished).
- Smicker, D.; Van Smaalen, S.V.; de Boers, J.L.; Haas, C.; Harris, K.D.M. Observation of the sliding mode in incommensurate intergrowth compounds: Brillouin scattering from the inclusion compound of urea and heptadecane. Phys. Rev. Lett. **1995**, 74, 734.
- Ollivier, J.; Ecolivet, C.; Beaufils, S.; Guillaume, F.; Breczewski, T. Light scattering by low-frequency excitations in quasi-periodic n-alkane/urea adducts. Europhys. Lett. **1998**, 43, 546.
- Bourgeois, L.; Ecolivet, C.; Toudic, B.; Bourges, P.; Breczewski, T. First one-dimensional stress-strain experiments inside an aperiodic inclusion compound: Evidence of depinning effects. Phys. Rev. Lett. **2003**, 91 (2), 25504.

# Calixarenes and Their Analogues: Cation Complexation

Anthony W. Coleman

Adina N. Lazar

Eric Da Silva

*Institut de Biologie et Chimie des Protéines, Lyon, France*

## INTRODUCTION

The calixarenes, calixresorcinarenes, and analogues are macrocyclic molecules containing phenolic rings bridged by methylene functions and are among the most ubiquitous of organic molecular host molecules in supramolecular chemistry.<sup>[1]</sup> The basic molecular scaffolds are, in general, simple to prepare in high yields from inexpensive starting compounds. In the case of the calixarenes, the size of the macrocycle synthesized is dependent on the nature of the cation used in the base-catalyzed cyclization, demonstrating that from the start, these molecules are excellent choices for cation complexation.

They possess sterically divergent reactive centers, either phenolic or aromatic in chemical nature, that may be modified fully or selectively to introduce functionalities capable of complexing a wide variety of cations. The chemical and physical robustness of the macrocycles allows their use for the complexation of a wide range of metal cations, including radioactive isotopes.

The introduction of ligand groups, such as ethers or crown ethers, amides, esters, or carboxylic acids, or sulfonates and phosphonates allows for the fine tuning of capacity for complexation with regard to mono-, di-, tri-, and tetravalent metal cations; cationic metal complexes; and organic cations, including mono-, di-, and trivalent ammonium systems, amino acids, peptides, and even certain proteins.

Further fine-tuning of the physicochemical and chemical properties of the derivatives allows for their use for extraction of cations, sensing at surfaces and interfaces, conducting of polymers, and specific-site targeting in biological macromolecules.

## CATION COMPLEXATION: GENERALITIES

The structures of the calixarenes and analogues are given in Figs. 1A,B. While calix[4]arene possesses four conformers—cone, partial cone, 1,2-alternate cone, and 1,3-alternate cone—that are sufficiently stable to be separated or to be blocked in place under certain conditions, the higher analogues have a much higher degree of confor-

mational mobility. These conformational properties were used to prepare preformed receptors for cation binding or to allow the ligands to wrap around the cation to form the binding site.

The basic molecular skeletons do not possess useful ligand sites for the binding of cations and a large body of research was devoted to the selective introduction of ligand groups for cations Fig. 1c. In general, these groups are of two types: soft or hard electron donor groups for coordination (sulfur, nitrogen, and oxygen donor atoms), or negatively charged groups for electrostatic (ion-pairing) interactions with cations (phosphonates, phosphates, sulfonates, and carboxylates).

## INORGANIC CATION COMPLEXATION

### Direct Complexation

Direct complexation of cations to unmodified calixarenes or their analogues occurs generally by formation of ion pairs arising from deprotonation of one or more phenolic groups under basic conditions. A comprehensive study of alkali metal–calixarene ion-pair complexes in solution and the solid state was undertaken by Gutsche.<sup>[1]</sup> Extraction of alkali metals from basic aqueous solutions shows strong selectivity for Cs<sup>+</sup> by calix[4]arene and calix[6]arene and selectivity for both Rb<sup>+</sup> and Cs<sup>+</sup> for calix[8]arene.<sup>[2]</sup>

Interfacial complexation of various alkali cations by the amphiphilic acyl-calix[4]arenes is achieved without deprotonation and shows strong selective binding for Rb<sup>+</sup>. The binding of cations by these molecules is also strongly dependent on the counteranion.<sup>[3]</sup>

### Ester, Amide, and Ketone Derivatives

The main classes of calixarene derivatives for the complexation and extraction of alkali and alkali earth cations are based on the total substitution at the lower rim by alkoxyester, alkoxyamide, or alkoxyketone functions, Fig. 2. In this way, suitable donor ligand functions for cation complexation are introduced. Such derivatives were used for the complexation and solvent-to-solvent

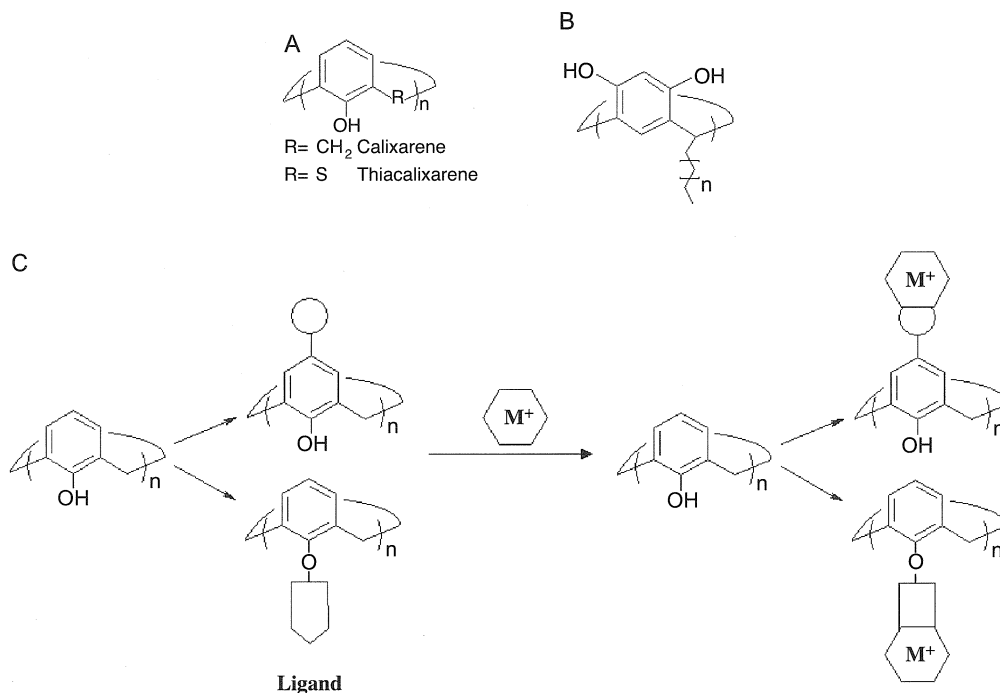


**Fig. 1** Molecular structures of the calixarenes, where, commonly,  $n = 4, 6$ , and  $8$  and the calixresorcinarene (A). The strategy for cation complexation by the introduction of ligand groups at either the lower or upper rims of calixarene derivatives (B). Metal complex with upper and lower rim functionalized calix-[ $n$ ]-arenes (C).

extraction of a wide range of metal ions, including alkali metals  $\text{Li}^+$ ,  $\text{Na}^+$ ,  $\text{K}^+$ ,  $\text{Rb}^+$ ,  $\text{Cs}^+$ ,  $\text{Ag}^+$ ; alkali earth metals  $\text{Mn}^{2+}$ ,  $\text{Mg}^{2+}$ ,  $\text{Ca}^{2+}$ ,  $\text{Cu}^{2+}$ ,  $\text{Sr}^{2+}$ ,  $\text{Ba}^{2+}$  and lanthanides  $\text{La}^{3+}$ .

The size of the calixarene macrocycle can govern the selectivity with regard to the different cations. For example, the ester derivative of calix[4]arene presents a high selectivity for the smaller cations  $\text{Na}^+$  and  $\text{Li}^+$ .<sup>[4]</sup> However, the analogous ester derivative of calix[5]arene and calix[6]arene interact strongly with  $\text{Cs}^+ = \text{Rb}^+ > \text{K}^+$ . No selectivity with regard to cations is observed for the calix[7]arene and calix[8]arene ester derivatives.

The conformation of the calixarene derivative also plays a role, and thus, the 1,3-alternate conformation of calix[4]arene can interact with other metals such as silver.<sup>[5]</sup>

The selectivity of the complexation and extraction is also determined by the chemical nature of the ligand

group, where inversion of the selectivity between  $\text{Na}^+$  and  $\text{Cs}^+$  is achieved by changing the ligand function from ester to ketone or amide for the calix[4]arene derivatives. Amide substituents play a role in the extraction of alkali metals or alkali earth metals.<sup>[6]</sup> The calixarene amide derivatives interact with  $\text{Na}^+ > \text{K}^+ = \text{Li}^+ > \text{Rb}^+ = \text{Cs}^+$ . With regard to the divalent cations,  $\text{Ca}^{2+}$  and  $\text{Sr}^{2+}$ , high selectivity in complexation is seen for derivatives carrying amide functions, and similar selectivity is seen for the mixed diacid, diamide derivative.<sup>[7,8]</sup>

### Ether and Crown Ether Derivatives

Given the structural analogy with the crown ethers, the calixarenes were alkylated to produce ether ligands at the phenolic face. These molecules complex various cations including alkali metal ions. Complexation may take place

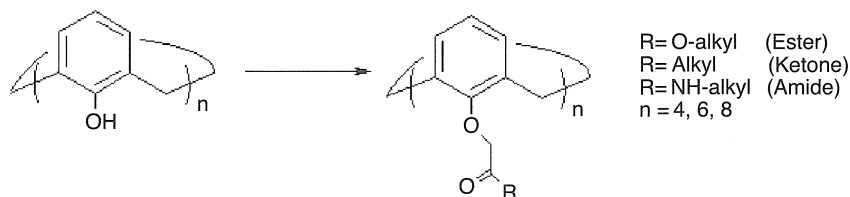


**Fig. 2** Molecular structure of calixarene derivatives substituted at the lower rim.

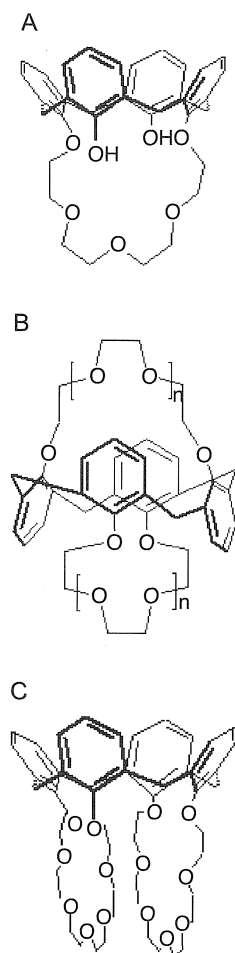


**Fig. 3** Molecular structure of 1,2-*bis*-calix crown ether (A); 1-3 alternate calix crown ether (B); and 1,3-*bis*-calix crown ether (C).

at the phenolic groups for  $\text{Na}^+$  and by cation–aromatic interaction in the case of  $\text{Ag}^+$  and  $\text{K}^+$ .<sup>[9,10]</sup>

The construction of calix-crown molecules is achieved by grafting ethylene glycol chains in a loop at two of the phenolic functions (Fig. 3A).

The 1,3-*bis* crown-ether calix[4]arene (Fig. 3B) was shown to be highly effective in the extraction of the radioactive isotope cation  $\text{Cs}^+$ .<sup>[11]</sup> As compared to other possible extractants, the stability of the calix[*n*]arene skeleton is an important factor in their potential use. The 1,2-*bis*-crown ether calix[4]arene (Fig. 3C) interacts more strongly with the  $\text{Rb}^+$  cation than with the  $\text{K}^+$  and  $\text{Na}^+$  cations. In this case, the binding of the  $\text{Cs}^+$  is relatively weak.<sup>[12]</sup>

### Amino Derivatives

In order to complex transition metal cations, including chromium (VI), molybdenum (VI), rhenium (VII) and

selenium (VI), suitable hard ligands based on nitrogen donor groups were introduced onto the basic calix[*n*]arene skeleton, for example, alkyl amino chains.<sup>[13]</sup> Recently, Regnoui de Vains synthesized calixarene derivatives having heterocyclic pendant ligands, including bipyridyl, and observed strong bonding of transition metal cations, including  $\text{Co}^{2+}$ ,  $\text{Cu}^+$ , and  $\text{Cu}^{2+}$ .<sup>[14,15]</sup>

### Sulfonate Derivatives

The sulfonate derivatives (Fig. 4A), in which introduction of suitable ligand functions takes place at the *para*-position of the aromatic ring, are the most widely studied of the water-soluble calixarenes. Their solid-state binding to a wide range of metallic cations and complexes was reviewed by Raston and Atwood.<sup>[16]</sup> The ability of these molecules to intercalate cations in expandable layers between bilayers of *para*-sulfonato-calix[4]arene led Atwood and Coleman in 1988 to name these systems “Organic Clays.” (Fig. 4C).<sup>[17]</sup> Since then, Atwood extended the structural types observed to include liposomal analogues, tubes, and various Archimedean and Platonic solids.<sup>[18]</sup>

### Phosphonate Derivatives

The calix[4]arene molecule was modified at both the upper (*para*) and lower (phenolic) rims by the introduction of phosphate and phosphonate groups, mainly by the group of Kalchenko (Fig. 4B).<sup>[19]</sup> Such derivatives complex and allow the extraction of lanthanide and actinide tri- and tetravalent cations. Detoxification of radioactive waters may be possible in this way, as the chemical and physical robustness of the calix[*n*]arenes makes them particularly suitable for this task.

Double complexation of the  $\text{Zn}^{2+}$  and Histidine amino acid cations to 1,3-diphosphate cation occurs selectively with regard to the cation and the amino acid,<sup>[20]</sup> as demonstrated by electrospray mass spectrometry.

### Miscellaneous

Cations bind to nanoscopic colloidal assemblies, supramolecular solid lipid nanoparticles of amphiphilic calix[4]arene derivatives, leading, in certain cases, to the clustering of such assemblies in the presence of divalent cations  $\text{Mg}^{2+}$  and  $\text{Ca}^{2+}$ . Such clustering was imaged by atomic force microscopy.<sup>[21]</sup> Such effects have particular relevance to the use of such transport systems in physiological media.

### Others

The interaction of thiacalixarene ester derivatives (Fig. 1A) alkali metal cations, is strongly conformation of calixarene.

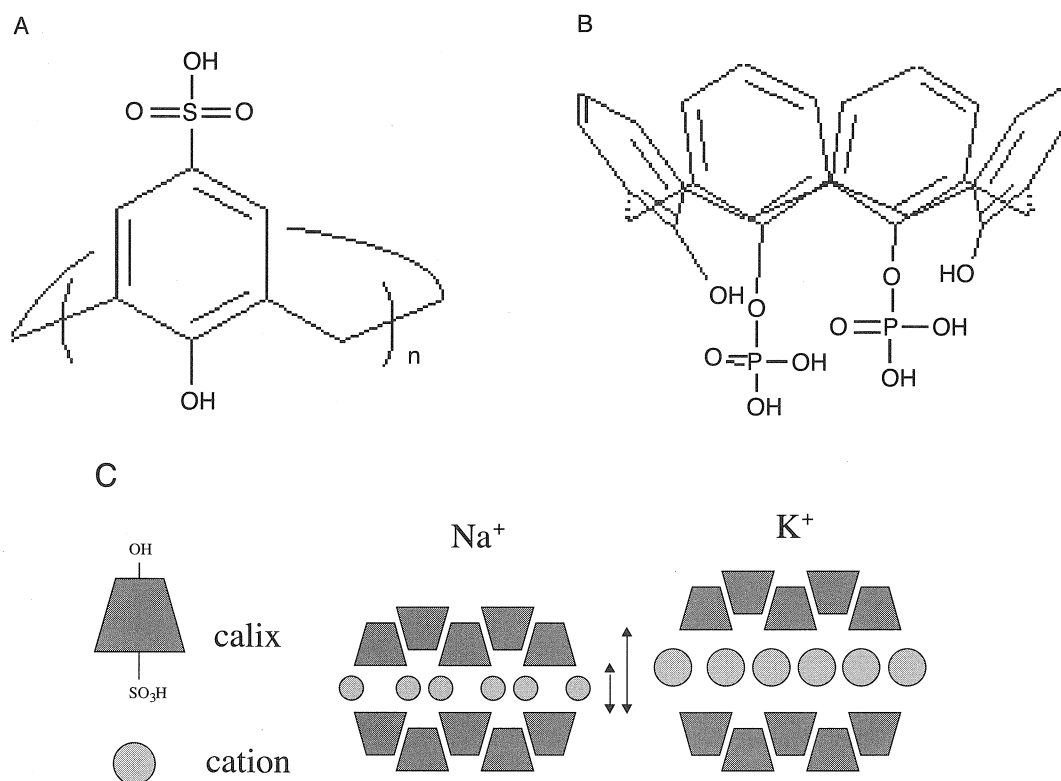


**Fig. 4** Molecular structure of water-soluble calixarene: (A) *p*-sulfonato-calix[*n*]arene, where *n* = 4, 6, 8; (B) crystal packing of *p*-sulfonato-calix[4]arene in the presence of salts *b* calix[4]arene diphosphonic acid; and (C) schematic of the bilayer packing of para-sulfonato-calix[4]arene showing how, as with clays, an increase in the cation size leads to an increase in the height of the hydrophilic interbilayer space. (View this art in color at [www.dekker.com](http://www.dekker.com).)

The cone conformation presents a high selectivity for the sodium cation, while the partial cone and 1,3-alternate conformations show selectivity for potassium and cesium cations.<sup>[22]</sup>

In the presence of cations, such as bipyridinium, included as guests, *c*-methylcalix[4]resorcinarene is induced to adopt a boat conformation.<sup>[23]</sup>

## ORGANIC CATION COMPLEXATION

In 2002, Abraham published an extensive review of organic cation complexation by calixarenes.<sup>[24]</sup>

### Direct Complexation

The receptor cavity of calix[*n*]arenes favors the formation of complexes with amines by proton transfer. NMR spectrometry and calorimetry techniques allowed for the evaluation of the role of the cavity and the phenolic oxygens in the case of calix[4]arene complexes with aliphatic amines. Hydrophobicity and base strength are important, and thus, the order of binding is *tert*-butyl-

amine > iso-propylamine (>*n*-hexylamine > piperazine > diethylamine > piperidine) > triethylamine.<sup>[25]</sup>

For *p*-*tert*-butylcalix[6]arene, the tetramethylammonium cation is one of the cations included in the cavity, the other one forms an exterior ion pair.<sup>[26]</sup>

The use of electrospray mass spectrometry allowed for observation of complexes of calix[4]arenes with alkylammonium ions, either directly from solution<sup>[27]</sup> or by gas-phase ion-molecule reactions.<sup>[28]</sup>

### Ether and Crown Ether Derivatives

The crown ether derivatives of calixarenes, having a more rigid structure, prove to be more selective in their complexation of organic ammonium cations and are only large enough to accommodate the mono-methylammonium ion and not the larger di-, tri-, and tetramethylammonium ions.<sup>[29]</sup>

A significant improvement in the ammonium-ion-binding properties can be achieved by covalent bridging of two cone conformation crown-ether derivatives. By adjusting the ethylene bridge length and rigidity, the

association constants can be increased by several orders of magnitude.<sup>[30]</sup>

### Esters, Amides, and Carboxylic Acid Derivatives

Selective recognition of butylamines by *p*-*tert*-butylcalix[6]arene ester derivatives shows the influence of steric effects on the binding strength, with *n*-butyl > iso-butyl > *sec*-butyl > *tert*-butyl.<sup>[31]</sup>

NMR studies proved that the calix[4]arene tetracarboxylate is able to form complexes with tetramethylammonium and trimethylanilinium cations, but with a lower stability than in the case where the calixarene is sulfonated at the upper rim.<sup>[32]</sup>

### Sulfonate Derivatives

The presence of a hydrophobic cavity and multiple anionic ligand groups in the *para*-sulfonato-calix[*n*]arenes coupled with their high aqueous solubility, made these molecules the derivatives of choice for the study of binding of organic cations, usually containing ammonium functions.

The stoichiometries of binding organic ammonium cations, such as trimethylanilinium and adamantrimethylammonium, to the *para*-sulfonato-calix[*n*]arenes is controlled by the macrocycle size formed. Thus, for the calix[4]arene and calix[6]arene derivatives, complexes of stoichiometry 1:1 are observed, while for the larger calix[8]arene derivatives a 1:2 stoichiometry occurs.<sup>[33]</sup>

As with the inorganic cations, solid-state organic clay bilayer structures are favored by *p*-sulfonatocalix[4]arene

and were observed with organic cations such as,  $[H_4TMTAA^{2+}]_2$  [*trans*-{Na<sup>+</sup>⊂(18-crown-6)(H<sub>2</sub>O)<sub>2</sub>} and  $[H_4TMTAA^{2+}]_2$  [(C<sub>7</sub>N<sub>2</sub>OH<sub>7</sub><sup>+</sup>)<sub>2</sub>].<sup>[34]</sup>

### Phosphonate Derivatives

1,3-Diphosphatecalix[4]arene is present in the solid state as a self-included dimer with two sets of anionic ligands capable of complexing a wide range of organic ammonium cations, with the propane diammonium cation a complex structure containing a selective water channel (Fig. 5a).<sup>[35]</sup>

The calix[4]arene α-aminophosphonates are highly selective receptors for amino acids. They exhibit excellent selectivity as carriers of the zwitterionic form of aromatic amino acids through supported liquid membranes.

### BIOMOLECULAR COMPLEXATION

The study of the interaction between calix[*n*]arene derivatives and biomolecular cationic functions is mainly limited to two groups of anionic water-soluble calix[*n*]arene derivatives, the *para*-sulfonato- and 1,3-diphosphate systems. These anionic molecules complex strongly to the cationic lateral chains of the amino acids, lysine (Lys, K), arginine (Arg, R), and histidine (His, H). Association constants, as determined by NMR and microcalorimetry, for these three amino acids vary as follows: His < Lys < Arg for the three *para*-sulfonato-calix[*n*]arenes, where *n* = 4, 6, or 8; the stoichiometries of the observed complexes are 1:1 with *para*-sulfonato-calix[4]arene, and are

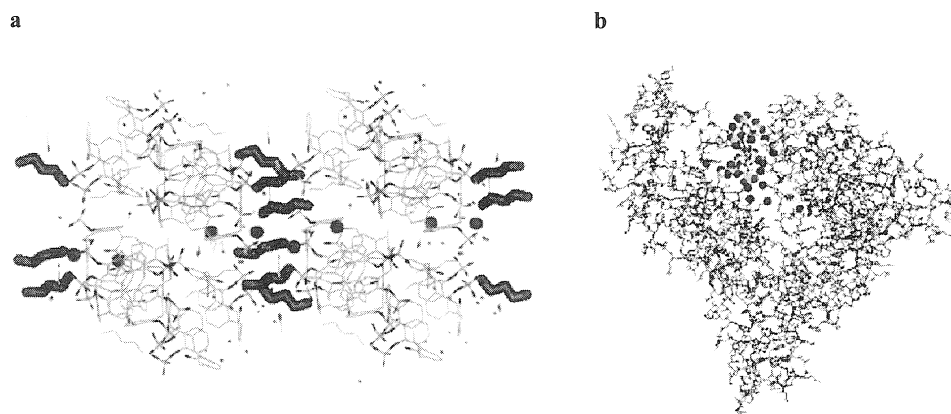


**Fig. 5** View of the large self-assembled structure generated by the complexation of the propane diammonium cation by calix[4]arene diphosphonic acid showing a selective water channel in the crystal packing. The propane diammonium groups act as linkers along the channel (a). Molecular model of bovine serum albumin showing one of the binding sites for *para*-sulphonato-calixarenes. The cationic residues lysine and arginine within the binding pocket are shown in blue; the calixarene molecule is shown as colored spheres (b). (View this art in color at [www.dekker.com](http://www.dekker.com).)



1:2 for *para*-sulfonato-calix[6]arene and *para*-sulfonato-calix[8]arene. Di- and tri-peptides based on Lys and Arg binding increase with the number of basic amino acids present.<sup>[36,37]</sup>

Recognition of this binding to cationic amino acids present at the surface of many proteins and often clustered either by the amino acid sequence or by the tertiary protein structure explains the biological activity of the *para*-sulfonato-calix[*n*]arenes, for example, their enzyme inhibition properties with regard to lysyl oxidase.<sup>[38]</sup>

The binding of the *para*-sulfonato-calix[*n*]arenes to bovine serum albumin (BSA), as demonstrated by electrospray mass spectrometry, involves complexation to lysine and arginine present in anion-binding pockets on the protein surface (Fig. 5b).<sup>[39]</sup>

## APPLICATIONS

The capacity of the calixarenes to exhibit cation selection or to recognize the chirality of amines and amino acids, as well as their ability to form complexes with quaternary ammonium, led to a number of potential and actual applications.

The use of the ethoxycarbonylmethyl derivative of *p*-tert-butylcalix[6]arene as a selective carrier for the separation of amino acids through a chloroform liquid membrane was demonstrated by Chang et al.<sup>[40]</sup> Ionophoric calixarene esters and ethers were applied to ion transport through phospholipid bilayer membranes.

The most widely studied and developed application of the calixarenes is in sensing devices for cation recognition. Devices based on Langmuir Blodgett films, thermally deposited thin films, or where the calixarene derivatives are immobilized into polymer films have been used in such applications. Sensing may occur through potentiometric, fluorometric, or photometric measurements.<sup>[41]</sup>

Their application in the biomedical field is clearly demonstrated by the preponderance of patents as compared to publications in the field. Calixarenes functionalized at the wide rim with sulfonic acid and sulfonamide groups showed anticoagulant and antithrombotic properties, approaching the activity of heparin and coumarin, currently used as anticoagulants in antithrombotic therapy. Calixarene derivatives are also active as antiviral, antimicrobial, and antifungal agents.

## CONCLUSION

Since the recognition of the cyclic nature of the calixarenes by Zinke in 1942, their use in supramolecular

chemistry and for the complexation of cations has seen almost exponential growth. Given the diversity of the nature of the chemical modification is seemingly only limited by the imagination of the chemist, we can expect this growth to continue. The design and construction of calixarenes carrying highly specific ligand functions are leading to their application in the areas of environmental control for detoxification of poisonous metal ions. The field of biological application of calixarenes by their complexation to cationic groups present in biomacromolecules is just starting, but it can be expected that this field will prove to be of great impact in the future.

## ARTICLES OF FURTHER INTEREST

- Amino Acids: Applications*, p. 42
- Biological Ligands*, p. 88
- Calixarenes and Their Analogues: Molecular Complexation*, p. 145
- Calixarenes: Synthesis and Historical Perspectives*, p. 153
- Cation- $\pi$  Interactions*, p. 214
- Crown Ethers*, p. 326
- Fluorescent Sensors*, p. 572
- Ionophores*, p. 760
- Organic Zeolites*, p. 996
- Platonic and Archimedean Solids*, p. 1100
- Protein Supramolecular Chemistry*, p. 1161
- Simultaneous Binding of Cations and Neutral Molecules*, p. 1295
- Stability Constants: Definition and Determination*, p. 1360
- Supermicroscopy: AFM, SNOM, and SXM*, p. 1394
- Supramolecular Chemistry: Definition*, p. 1401
- X-Ray Crystallography*, p. 1586
- Zwitterion Receptors*, p. 1639

## REFERENCES

1. Gutsche, C.D. *Monographs in Supramolecular Chemistry, Calixarenes Revisited*; Stoddart, J.F., Ed.; The Royal Society of Chemistry: Cambridge, U.K., 1998.
2. Roundhill, M.D. Metal Complexes of Calixarenes. In *Progress in Inorganic Chemistry*; Kenneth, D.K., Ed.; John Wiley & Sons, Inc., 1995; 533 pp.
3. Shahgaldian, P.; Coleman, A.W. Anion and cation interactions with *p*-dodecanoylcalix[4]arene monolayers at the air-water interface. *Langmuir* **2001**, *17*, 6851–6854.
4. Arnaud-Neu, F.; Collins, E.M.; Deasy, M.; Ferguson, G.; Harris, S.J.; Kaitner, B.; Lough, A.J.; McKerver, M.A.; Marques, E.; Ruhl, B.L.; Schwing-Weill, M.J.; Seward, E.M. Synthesis, x-ray crystal structures, and cation-binding properties of alkyl calixaryl esters and ketones, a new

- family of macrocyclic molecular receptors. *J. Am. Chem. Soc.* **1989**, *111*, 8681–8691.
5. Akdas, H.; Graf, E.; Hosseini, M.W.; De Cian, A.; Harrowfield, J.McB. Design, synthesis and structural investigation of a 2-D-coordination network based on the self-assembly of the tetracarboxylate derivative of tetra-thiacalix[4]arene and silver cation. *Chem. Commun.* **2000**, *22*, 2219–2220.
  6. Arnaud-Neu, F.; Barrett, G.; Fanni, S.; Marrs, D.; McGregor, W.; McKervy, M.A.; Schwing-Weill, M.-J.; Vetrogon, V.; Wechsler, S. Extraction and solution thermodynamics of complexation of alkali and alkaline-earth cations by calix[4]arene amides. *J. Chem. Soc., Perkin Trans., 2 Phys. Org. Chem.* **1995**, *3*, 453–461.
  7. Ogata, M.; Fujimoto, K.; Shinkai, S. Molecular design of calix[4]arene-based extractants which show high  $\text{Ca}^{2+}$  selectivity. *J. Am. Chem. Soc.* **1994**, *116*, 4505–4506.
  8. Aime, S.; Barge, A.; Botta, M.; Casnati, A.; Fragai, M.; Luchinat, C.; Ungaro, R. A calix[4]arene GdIII complex endowed with high stability, relaxivity, and binding affinity to serum albumin. *Angew. Chem., Int. Ed.* **2001**, *40*, 4737–4739.
  9. Bott, S.G.; Coleman, A.W.; Atwood, J.L. Inclusion of both cation and neutral molecule by a calixarene—Structure of the [para-tert-butylmethoxycalix[4]arene sodium toluene]<sup>+</sup> cation. *J. Am. Chem. Soc.* **1986**, *108*, 1709.
  10. Ikeda, A.; Shinkai, S. On the origin of high ionophoricity of 1,3-alternate calix[4]arenes: *p*-donor participation in complexation of cations and evidence for metal-tunneling through the calix[4]arene cavity. *J. Am. Chem. Soc.* **1994**, *116*, 3102–3110.
  11. Thuery, P.; Nierlich, M.; Arnaud-Neu, F.; Souley, B.; Asfari, Z.; Vicens, J. Silver ion complexation by a calix[4]arene bis(crown ether). Ambivalence towards ether and polyhapto coordinations. *Supramol. Chem.* **1999**, *11*, 143–150.
  12. Arduini, A.; Casnati, A.; Dodi, L.; Pochini, A.; Ungaro, R. Selective 1,2-functionalization of calix[4]arenes at the lower rim. Synthesis of a new type of bis-calixcrown ether. *Chem. Commun.* **1990**, *22*, 1597–1598.
  13. Georgiev, E.M.; Wolf, N.; Roundhill, D.N. Lower rim alkylammonium-substituted calix[4]arenes as “proton-switchable” extractants for chromate and dichromate anions. *Polyhedron* **1997**, *16*, 1581–1584.
  14. Molard, Y.; Bureau, C.; Parrot-Lopez, H.; Lamartine, R.; Regnouf-de-Vains, J.-B. Synthesis of calix[4]arene podands bearing two and four histidine or glycine groups at the lower rim. Complexation properties towards cobalt (II) chloride. *Tetrahedron Lett.* **1999**, *40*, 6383–6387.
  15. Pellet-Rostaing, S.; Lamartine, R.; Regnouf-de-Vains, J.-B.; Fennet, B. A bithiazole-containing calix[4]arene podand as versatile ligand for copper(I) and copper(II). *Inorg. Chem. Commun.* **1999**, *2*, 44–47.
  16. Atwood, J.L.; Barbour, L.J.; Hardie, M.J.; Raston, C.L. Metal sulfonatocalix[4,5]arene complexes: Bi-layers, capsules, spheres, tubular arrays and beyond. *Coord. Chem. Rev.* **2001**, *222*, 3–32.
  17. Coleman, A.W.; Bott, S.G.; Morley, S.D.; Means, C.M.; Robinson, K.D.; Zhang, H.; Atwood, J.L. Sodium calix[4]arenesulfonate with a layered structure. An organic clay? *Angew. Chem., Int. Ed.* **1988**, *100*, 1412–1413.
  18. Atwood, J.L.; Barbour, L.J. Molecular graphics: From science to art. *Cryst. Growth Des.* **2003**, *3*, 3–8.
  19. Lipkowsky, J.; Simonov, Y.; Kalchenko, V.I.; Vysotsky, M.A.; Markovsky, L.N. Molecular and crystal structure of water-soluble 25,57-bis(dihydroxyphosphoryloxy)calix[4]arene. *An. Quim. Int. Ed.* **1998**, *94*, 328–331.
  20. Perret, F.; Morel-Desrosiers, N.; Coleman, A.W. An ESI/MS study of the formation of ternary 25,27-bis(dihydroxyphosphoryloxy) calix[4]arene-metal ion-aminoacid complexes. *J. Supramol. Chem.* **2003**, *in press*.
  21. Dubes, A.; Parrot-Lopez, H.; Shahgaldian, P.; Coleman, A.W. Interfacial interactions between amphiphilic cyclodextrins and physiologically relevant cations. *J. Colloid Int. Sci.* **2003**, *259*, 103–111.
  22. Stoikov, I.I.; Omran, O.A.; Solovieva, S.E.; Latypov, S.K.; Enikeev, K.M.; Gubaidullin, A.T.; Antipin, I.S.; Konovalev, A.I. The synthesis of tetracarbonyl derivatives of thiacalix4arene in different conformations and their complexation properties towards alkali metal ions. *Tetrahedron* **2003**, *59*, 1469–1476.
  23. Brown, P.O.; Enright, G.D.; Ripmeester, J.A. Cationic guests in extended anionic c-methylcalix[4]resorcinarene-inorganic frameworks: Exercising conformational control over c-methylcalix[4]resorcinarene. *J. Supramol. Chem.* **2002**, *2* (4–5), 497–500.
  24. Abraham, W. Inclusion of organic cations by calix[n]arenes. *J. Incl. Phenom. Macrocycl. Chem.* **2002**, *43*, 159–174.
  25. Nachtigall, F.F.; Lazzarotto, M.; Nome, F. Interaction of Calix[4]arene and amines: A combined NMR, spectrometric and conductimetric investigation. *J. Braz. Chem. Soc.* **2002**, *13*, 295–299.
  26. Harrowfield, J.M.; Richmond, W.R.; Sobolev, A. Inclusion of quaternary ammonium compounds by calixarenes. *J. Incl. Phenom. Mol. Recognit. Chem.* **1994**, *19*, 257.
  27. Lippmann, T.; Wilde, H.; Pink, M.; Schaefer, A.; Hesse, M.; Mann, G. Host-guest complexes between resorcinol-derived calix[4]arenes and alkylammonium ions. *Angew. Chem.* **1993**, *105*, 1258–1260.
  28. Wong, P.S.H.; Yu, X.; Dearden, D.V. Complexes of p-tert-butylcalix[4]arene with mono- and dipositive cations in the gas phase. *Inorg. Chim. Acta* **1996**, *246*, 259–265.
  29. Arduini, A.; McGregor, W.; Paganuzzi, D.; Pochini, A.; Secchi, A.; Ugozzoli, F.; Ungaro, R. Rigid cone calix[4]arenes as  $\pi$ -donor systems: Complexation of organic molecules and ammonium ions in organic media. *J. Chem. Soc., Perkin Trans., 2 Phys. Org.* **1996**, *5*, 839–846.
  30. Arduini, A.; Pochini, A.; Secchi, A. Rigid calix[4]arene as a building block for the synthesis of new quaternary ammonium cation receptors. *Eur. J. Org. Chem.* **2000**, 2325.
  31. Chang, S.K.; Jang, M.J.; Han, S.Y.; Lee, J.K.; Hang, Y.S.; No, K.T. Molecular recognition of butylamines by calixarene-based ester ligands. *Chem. Lett.* **1992**, 1937.
  32. Arena, G.; Casnati, A.; Contino, A.; Lombardo, G.G.; Sciotto, D.; Ungaro, R. Water-soluble calixarene hosts that specifically recognize the trimethylammonium group or the benzene ring of aromatic ammonium cations: A combined <sup>1</sup>H NMR, calorimetric, and molecular mechanics

- investigation. *J. Chem. Soc., Perkin Trans.* **2000**, 2, 419–423.
33. Shinkai, S.; Araki, K.; Matsuda, T.; Manabe, O. NMR determination of association constants for aqueous calixarene complexes and guest template effects on the conformational freedom. *Bull. Chem. Soc. Jpn.* **1989**, 62, 3856.
34. Ness, T.; Nichols, P.J.; Raston, C.L. Bi-Layer complexes incorporating large organic cations and anionic tetra-p-sulfonated calix[4]arene capsules. *Eur. J. Inorg. Chem.* **2001**, 8, 1993–1997.
35. Coleman, A.W.; Da Silva, E.; Nouar, F.; Nierlich, M.; Navaza, A. The structure of self-assembled calixarene aqua-channel system. *Chem. Commun.* **2003**, 7, 826–827.
36. Kalchenko, O.I.; Da Silva, E.; Coleman, A.W. Determination of the stability constants of inclusion complexes of p-H-37-(2-carboxy-methyloxy)-calix-[6]-arene and p-sulphonato-37-(2-carboxy-methyloxy)-calix-[6]-arene with 15 amino acids by RP-HPLC. *J. Incl. Phenom. Macrocycl. Chem.* **2002**, 43, 305–310.
37. Guevel-Douteau, N.; Perret, F.; Morel-Desrosiers, N.; Morel, J.-P.; Coleman, A.W. Molecular organisation of positively charged di- and tri-peptides by anionic calix-[n]-arene-sulfonates. *J. Chem. Soc., Perkin Trans.* **2002**, 2, 524–532.
38. Hulmes, D.; Coleman, A.W.; Aubert-Foucher, E. Use of calix(n)arenes for treating fibrotic diseases. *PCT Int. Appl.* **2000**.
39. Memmi, L.; Lazar, A.; Brioude, A.; Ball, V.; Coleman, A.W. Protein–calixarene interactions: Complexation of bovine serum albumin by sulfonatocalix[n]arenes. *Chem. Commun.* **2001**, 23, 2474–2475.
40. Chang, S.K.; Hwang, H.S.; Son, H.; Youk, J.; Kang, Y.S. Selective transport of amino acid esters through a chloroform liquid membrane by a calix[6]arene-based ester carrier. *J. Chem. Soc., Chem. Commun.* **1991**, 217.
41. Diamond, D.; Nolan, K. Calixarenes: Designer ligands for chemical sensors. *Anal. Chem.* **2001**, 73 (1), 22A–29A.

# Calixarenes and Their Analogues: Molecular Complexation

Ivan Stibor  
Pavel Lhoták

*Institute of Chemical Technology, Prague, Czech Republic*

## INTRODUCTION

The ability of calixarenes to act as baskets is said to be one of their most intriguing properties, accounting for much of the interest they received.<sup>[1]</sup> Generally speaking, molecules having convergent concave surfaces are frequently potent receptors, and their cavity can form a binding site where recognition events take place. It is well known that calix[4]arenes and calix[5]arenes, particularly when in their cone conformations, possess an intramolecular cavity that can host neutral molecules or their neutral parts of complementary size. Other conformations of calix[*n*]arenes (*n*=4,5) as well as larger calix[*n*]arenes are also known to form numerous molecular complexes, but factors controlling their complexation selectivity are not well understood, mainly due to their greater conformational flexibilities.<sup>[2–4]</sup>

This entry deals with various facets of molecular complexation by calixarenes. Most studies published on this subject are connected with cone conformation of calixarene skeleton.

The subject is traditionally divided into two parts, considering solid-state systems, first and then proceeding to solution-state systems, having in mind aqueous and nonaqueous solvents. Finally, gas-phase recognition will be mentioned briefly.

## SOLID-STATE COMPLEXES

Many calixarenes form complexes in the solid state, this property having been observed even before the structure of compounds was established. Among the simple calix[*n*]arenes, for example, *p*-*tert*-butylcalix[4]arene forms complexes with chloroform, benzene, toluene, xylene, nitrobenzene, nitromethane, acetonitrile, and many others, while *p*-*tert*-butylcalix[5]arene complexes were studied with lower alcohols, ethyl acetate, toluene, and tetraline. More flexible *p*-*tert*-butylcalix[6]arene was found to form complexes with acetonitrile and *p*-*tert*-butylcalix[8]arene with chloroform. The tenacity with which the guest molecule is held by the calixarene hosts varies widely with the size of macrocycle. Whereas tetramers to hex-

amers usually hold their guests tightly, retaining a residual amount of the crystallization solvent even after prolonged heating at high temperature under vacuum (which makes traditional elemental analysis completely useless at times), *p*-*tert*-butylcalix[8]arene crystallizes from chloroform in beautiful glistening needles that change to white powder within a few minutes at atmospheric pressure.

The structures of complexes of calixarenes are most effectively revealed by x-ray crystallography. The first solid-state complex published was that of *p*-*tert*-butylcalix[4]arene with toluene<sup>[5]</sup> (Fig. 1).

It was quickly found that there are many difficulties connected with the structural studies of even the simplest calixarene complexes.<sup>[6]</sup> In general, the compounds are disordered, often with involvement of guest and host sublattices, and there is evidence for dynamic coupling between them. That is why the use of a synoptic approach has been advanced, where the use of complementary techniques resulted in improved structural models. Without doubt, the combination of crystallography and solid-state nuclear magnetic resonance (NMR) spectroscopy has proven to be remarkably effective in solving a number of complex problems. We can illustrate the complexity of these studies by looking at an almost 10-year-long structural study of the first crystalline calixarene complex mentioned above. The parent *p*-*tert*-butylcalix[4]arene has a flexible upper rim defined by *tert*-butyl groups. In contrast, the lower rim is fixed by in-plane hydrogen bonding. It was found that at room temperature, the toluene guest rapidly reorients between equivalent guest sites, but that below 248 K, the transition to a lower symmetry host lattice takes place. There are two crystallographically distinct molecules, each with a toluene guest that is disordered over two equivalent sites. More detailed study using <sup>2</sup>H, <sup>13</sup>C, variable temperature NMR, calorimetry, and 150 K crystallography show that toluene is static at 129 K, and that it undergoes rapid 180° flip about the molecular C<sub>2</sub> symmetry axis at 180 K and above (*E*<sub>a</sub>=34±3 kJ mol<sup>-1</sup>). These results are consistent with the final structural analysis in which each of two crystallographically different complexes has only a twofold axis of symmetry. Apparently, the structure of solid-state

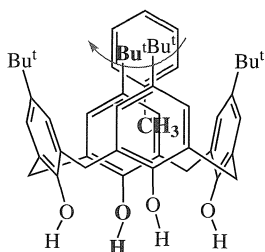


**Fig. 1** The structure of *p*-*tert*-butylcalix[4]arene with toluene. (View this art in color at [www.dekker.com](http://www.dekker.com).)

calixarene molecular complexes is far from being trivial because of the dynamic structural complexity. Similarly, the dynamic structures of other calixarene complexes were recently examined,<sup>[6]</sup> namely, complexes of *p*-*tert*-butylcalix[4]arene with benzene, pyridine, 4-nitrobenzene, cyclohexane, hexane, dodecane, heptane-1-ol, octane-1-ol, and, 1,4-dichlorobenzene. The following extremely important conclusions can be drawn from this pioneering work:

“Most, if not all, molecules of appropriate size form reasonably stable inclusion compounds with *p*-*tert*-butylcalix[4]arene, and this observation suggest that considerable caution should be exercised in interpreting compound stability in terms of specific interactions. By examining series of structurally-related guest compounds it can be seen that the deep cavity is chlorophobic, but the space filling seems to be more important than the avoidance of unfavorable interactions in determining whether compound formation will take place. A similar conclusion can be drawn from the fact that a long molecule will curl up in order to fill space effectively in an inclusion compound rather than exist in a favored all-*trans* conformation without inclusion compound formation.”<sup>[6]</sup>

In an alternative approach, all data available in the Cambridge Structural Database (CDS) for inclusion complexes formed by calix[4]arenes, calix[4]resorcinols, and thiacalix[4]arenes in the cone conformation with neutral organic molecules having acidic CH groups were retrieved. The data for 39 guests and two types of organic molecules with CH acidic groups, namely,  $\text{CH}_3\text{X}$  and  $\text{CH}_2\text{XY}$  ( $\text{X}, \text{Y} = \text{EWG groups}$ ) were critically evaluated.<sup>[7]</sup> First, suitable geometrical descriptors were introduced for precise definition of host geometry as well as position and orientation of the guest inside the cavity. Nitromethane and acetonitrile were chosen as typical guests of  $\text{CH}_3\text{X}$  type. No obvious correlation between simple geometrical characteristics of the host or guest and the strength of inclusion was found. Nonetheless, what is important is the specific position of the guest methyl group inside the cavity, a position that must facilitate the strongest possible

intermolecular interaction with all aromatic walls of the host. Accordingly, dichloromethane, chloroacetonitrile, and malononitrile were chosen as typical guests of the  $\text{CH}_2\text{XY}$  type. The data obtained showed that the intermolecular interactions between the aromatic cavity of the calix[4]arene hosts and the molecule having acidic CH groups are different for  $\text{CH}_3\text{X}$  and  $\text{CH}_2\text{XY}$  guests. There is no evidence for hydrogen-bond-like characteristics of  $\text{CH}_3\text{X}$  interactions. These results are in agreement with more sophisticated studies (e.g., inelastic neutron scattering) that show that the guest methyl group behaves as an almost free quantum rotor. Conversely, rotation of  $\text{CH}_2\text{XY}$  guests is somewhat inhibited by complex formation. This entropic cost is partially compensated for by a higher value of the enthalpic contribution to the bonding, as reflected by the correlation of CH-aromatic distance and acidity of the guest.

There have been several attempts to apply quantum chemistry to the evaluation of structure and properties of solid-state complexes of calix[4]arene receptors. Usually, only molecular mechanics and dynamics can be used to do this job, and information obtained has usually been regarded as supporting evidence of the structure of the complex formed. Recently, an advanced approach was applied to structure elucidation of solid-state inclusion complexes formed by *p*-*tert*-butylcalix[4]arene with different solvents. The method reported<sup>[8]</sup> is based on the following procedure. Various possible geometries of host-guest complexes are modeled using fast force-field optimization. Based on minima structures obtained by this approach, quantum chemical (GIAO)-DFT NMR calculations were performed. Then comparison of theoretical and experimental chemical shifts for free ligand and complex with solvent furnish the spatial arrangements of host and guest. Thus, it is possible for calix[4]arene complexes, using a combination of force-field geometry optimization and GIAO-GFT NMR shift calculations, to screen various starting geometries against experimental data, yielding good structural models for these complexes in the solid state.

## COMPLEX FORMATION IN LIQUID PHASE

### Apolar Media

Calixarenes in general are known to form weak complexes with neutral organic guests in apolar media. This behavior is different from that of cavitands based on calix[4]resorcinols. Molecules of solvent compete with the guest with respect to interaction with the host molecule. That is why the crucial problem to be solved is the proper choice of solvent that is able to dissolve both components and that is not able to interact with the host molecule. For

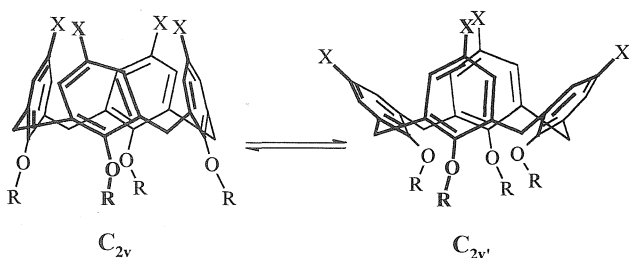


Fig. 2 Dynamic stereochemistry of tetraalkoxycalix[4]arenes in the cone conformation.

calix[4]arenes in the cone conformation, tetrachloromethane is a good example, as it is too big to fit within the cavity and at the same time it has acceptable properties as a solvent. This is perfectly true for calixarenes with rigid cavities, as for example, parent *p*-*tert*-butylcalix[4]-arene, with a circular array of four hydrogen bonds. It is, however, not true for tetraalkylated *p*-*tert*-butylcalix[4]-arenes, where large alkyl substituents are believed to lock the cone conformation. The reason is that most of these compounds retain a limited degree of conformational flexibility, as their cone conformation in which apparent  $C_{4v}$  symmetry is in fact the result of fast interchange between two  $C_{2v}$  flattened cone structures. These are sometimes referred to as pinched cone conformations. This behavior was directly established by variable temperature NMR measurement of tetrakis-*n*-octyloxy-*p*-*tert*-butylcalix[4]arene (Fig. 2).<sup>[9]</sup>

The role of the lower-rim substitution pattern of *p*-*tert*-butylcalix[4]arene was studied for a series of complexes formed by 12 *p*-*tert*-butylcalix[4]arene hosts with 13 guests (eight nitriles and five nitroalkanes).<sup>[10]</sup> It was proven that the complexation ability of these hosts follows the order: monosubstituted > disubstituted > unsubstituted > tetrasubstituted. The suggested explanation of this order is based on the shape of the host cavity and the time-averaged proportion of the host molecule adopting transition shapes during flipping through the annulus. The structure of complex acetonitrile **1** was proven by <sup>1</sup>H-NMR spectroscopy, in which NOEs were found between metaprotons of all the phenolic units of hosts, with the methyl protons of acetonitrile as guests (Fig. 3).

Doing the same study with propionitrile, it was found that methyl and methylene groups are found inside the cavity of the host, with the methylene group positioned somewhat deeper.

These findings are in perfect agreement with other approaches to binding enhancement by “covalent shaping” of the *p*-*tert*-butylcalix[4]arene cavity. The first involves selective 1,2 (proximal) lower-rim functionalization of parent *p*-*tert*-butylcalix[4]arene, yielding the series of *p*-*tert*-butylcalix[4]arene *biscrowns* 2–6 (Fig. 4), where

the conformational flexibility can be tuned by varying the length of the bridging unit.<sup>[11]</sup>

In fact, *p*-*tert*-butylcalix[4]arene *biscrown*-5 **6** is flexible and adopts a flattened-cone conformation in solid state, while *p*-*tert*-butylcalix[4]arene *biscrown*-3 derivatives 2–4 possess a rigid cone structure. The recognition properties of **3** in solution were evaluated in organic solvents (CDCl<sub>3</sub> and CCl<sub>4</sub>) using nitromethane as guest.<sup>[12]</sup> By adding variable amounts of guest to a solution of **3**, a significant upfield shift of the CH protons of the guest and fast exchange conditions were observed. These shifts clearly show an interaction of the acidic protons of the guest with the  $\pi$ -electrons of the calixarene cavity, while excluding a possible interaction of these protons with the crown-ether region, which should result in a downfield shift. The analysis of the data showed the formation of 1:1 complexes and provided quantitative information on host–guest interactions (Table 1).

To gain further insight into the role of rigidity on the molecular recognition properties of hosts, comparison was made with the more mobile hosts **6** and **7**. Interestingly, in **6** and **7**, with nitromethane and malononitrile, no variation of the chemical shift of the guest was observed, while with **5**, complexation occurred but only in CCl<sub>4</sub> and with a lower association constant than with the more rigid **3**. These results demonstrate the importance of rigidity in determining the complexation properties of the  $\pi$ -donor cavity of calix[4]arenes. The group present at the upper rim strongly affects the stability of complexes formed as witnessed by data for compounds 2–4. In fact, increasing the extension of the cavity increases the complexation efficiency toward nitromethane (Table 1). In contrast, malonodinitrile is bound with comparable efficiency by all three hosts, probably for steric reasons. Another interesting observation, which confirms the importance of rigidity and, consequently, the preorganization of the calix[4]arene in the cone conformation, was observed by comparison between hosts **8** and **9**. Here, the well-known

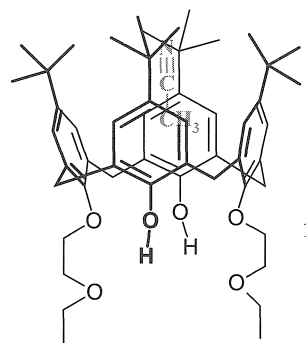


Fig. 3 Complex **1**  $\subset$  acetonitrile in CCl<sub>4</sub> proven by <sup>1</sup>H-NMR. (View this art in color at [www.dekker.com](http://www.dekker.com).)

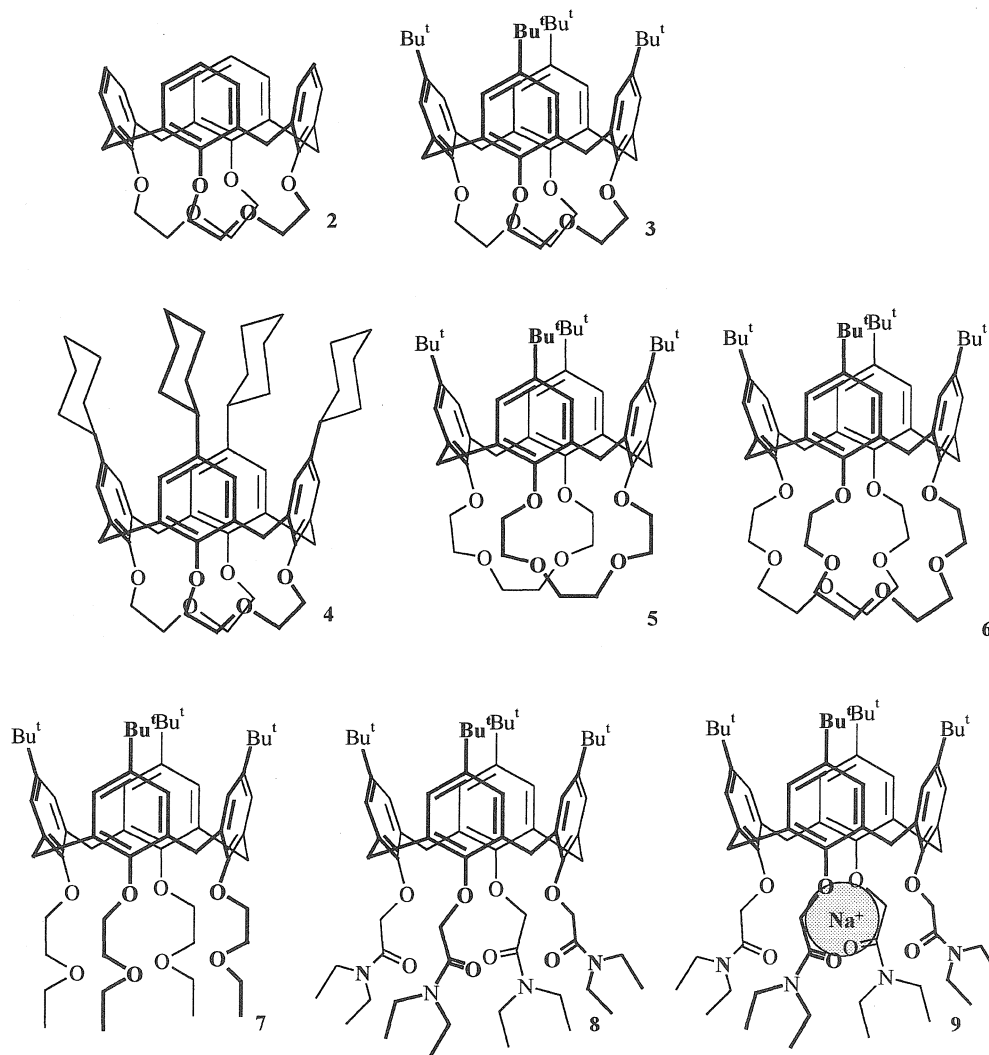


Fig. 4 *p*-*tert*-Butylcalix[4]arenes with different flexibilities of cone conformation.

free ligand and its sodium picrate complex were compared in the complexation of nitromethane in  $\text{CDCl}_3$ . While the conformationally mobile **8** does not show significant complexation, its rigid sodium complex **9**, through a

**Table 1** Association constants ( $K_{\text{ass}}$ ,  $\text{M}^{-1}$ ) of 1:1 complexes of nitromethane and malononitrile with rigidified calix[4]arenes **2–9** at 300 K

Calix[4]arene	$\text{CH}_3\text{NO}_2$		$\text{CH}_2(\text{CN})_2$
	$\text{CDCl}_3$	$\text{CCl}_4$	$\text{CDCl}_3$
<b>2</b>	$5 \pm 2$	$28 \pm 7$	$17 \pm 2$
<b>3</b>	$27 \pm 4$	$230 \pm 60$	$6 \pm 2$
<b>4</b>	$36 \pm 8$	$123 \pm 25$	$23 \pm 5$
<b>5</b>	<sup>a</sup>	$50 \pm 10$	<sup>a</sup>
<b>9</b>	$34 \pm 7$	<sup>a</sup>	<sup>a</sup>

<sup>a</sup>Not determined.

positive allosteric effect, binds nitromethane (Table 1). Similar results were obtained with a corresponding tetraester–acetonitrile system.<sup>[10]</sup> There is also a recent report involving the correlation between the guest acidity and the association constants in the recognition of neutral  $\text{CH}_3\text{X}$  and  $\text{CH}_2\text{XZ}$  species by rigidified calix[4]arene.<sup>[13]</sup> Comparison of  $K_{\text{ass}}$  of acetonitrile ( $\text{p}K_{\text{a}} - \text{DMSO} = 31.3$ ) and nitromethane ( $\text{p}K_{\text{a}} - \text{DMSO} = 17.2$ ), measured in  $\text{CCl}_4$ , shows that these two guests are bound with similar efficiency. This indicates, in agreement with the results obtained in solid state,<sup>[7]</sup> that the complexation of the  $\text{CH}_3\text{X}$  guests is not determined by their acidity. Conversely, as verified in the solid state, the similar data on guests  $\text{CH}_2\text{XZ}$  strongly suggest their dependence on the acidity of the  $\text{CH}_2$  group. This finding is also in agreement with the solid-state study.<sup>[7]</sup> The energetics of the inclusion of guests by rigidified cone conformer of calix[4]arenes in  $\text{CCl}_4$  was also recently reported.<sup>[14]</sup>

The influence of upper-rim substitution was also studied in the series of calix[4]arenes with identical substitution patterns on the lower rim but differing in their upper-rim substitution pattern. Namely, hydrogen, *tert*-butyl, and adamantyl were used as upper-rim substituents.<sup>[15]</sup> The association constants obtained for *p*-adamantylcalix[4]arene complexes are close in their values to those of the corresponding *p*-*tert*-butylcalix[4]arene complexes. The <sup>1</sup>H-NMR spectra of these compounds undergo similar changes caused by complexation as the spectra of their *p*-*tert*-butyl analogues. Thus, complexation-induced shifts of OH and aryl protons of the ligands of both types have similar values, and a significant upfield shift of the protons of the substrate (up to 6 ppm) is observed. It seems apparent that both hosts behave in a similar way, at least in tetrachloromethane solution. In contrast, upper-rim unsubstituted calix[4]arene derivatives form weak complexes with all guests studied. This result can be explained by the fact that the calixarene apolar cavities are not shielded by any substituent and are easily accessible for solvent molecules of any shapes and sizes. The results from all the above studies can be rationalized in the following way. First, the ability of calix[4]arene hosts to form complexes with neutral molecules is controlled by the solvation of its cavity. Second, C–H··· $\pi$  interactions play an important role in the complexation process—the strength of complexes formed by the guests with similar geometries and nature strongly depends on their C–H acidity. Third, the association constants of observed complexes do not exceed 300 M<sup>−1</sup> in CCl<sub>4</sub> and 30 M<sup>−1</sup> in CDCl<sub>3</sub>.<sup>[15]</sup>

In order to improve the recognition efficiency of neutral organic species, suitable binding sites were attached at one or two rims of calix[4]arene or calix[5]arene platform, usually with the ability to act as hydrogen bond donor or acceptor groups. Using this approach, selective binding of several primary amines by a carefully designed dicarboxy- calix[5]arene receptor was studied. As usual

with calix[5]arenes, the synthesis of the receptor is complicated and results from a low-yielding synthetic sequence.<sup>[16]</sup> Also, a molecule of water was found to be complexed selectively by adamantylated calix[4]arene diamide.<sup>[17]</sup> Clear evidence that the hydrogen-bonding groups linked at the upper rim and the cavity are able to cooperate in binding was obtained when rigidified calix[4]arene **10** bearing a methylenephénylureido additional binding site at the upper rim was exploited to recognize low-molecular-weight amides.<sup>[18]</sup> The structure of host and the cooperative binding is shown in (Fig. 5).

The complexation properties of host **10** were evaluated in CDCl<sub>3</sub>, and it was found that it is able to efficiently recognize amides with NH<sub>2</sub> or NHR groups, whereas the substantial decrease of this ability was observed with the guests bearing *N,N*-dialkylamino groups.

### Aqueous Media

One of the main reasons for studying the interactions of calixarenes in water is to exploit hydrophobic effects in order to enhance complexation of apolar guests in their cavities. In order to study this phenomenon, the water-soluble calixarenes are needed in analogy of cyclodextrins and water-soluble cyclophanes. To engender water solubility generally, calixarenes need to be functionalized with groups containing positive or negative charges or with neutral but highly hydrophilic moieties. A predominant part of the work concerning the complexation of neutral molecules by water-soluble calixarenes was carried out in the 1980s and was critically reviewed.<sup>[4]</sup> Classical work was devoted to the inclusion of small neutral organic guests (alcohols, ketones, and nitriles) by water-soluble calix[4]arene hosts (solubility was introduced by sulfonyl groups at the upper rim or carboxy groups at the lower rim, sometimes in combination, and with an ethoxyethoxy group at the lower rim). The guests are included in the host hydrophobic cavity by their apolar aliphatic residues.

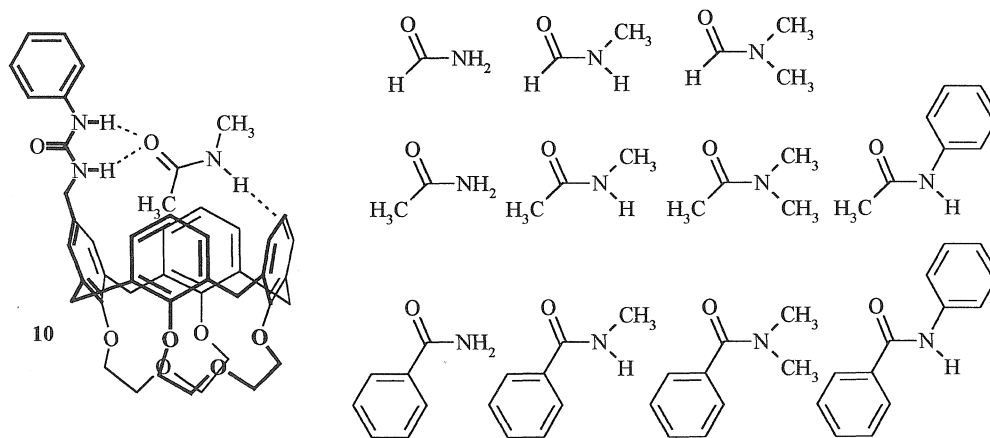


Fig. 5 Structure of complex formed by **10** and several amides.



The binding constants at neutral pH confirm the importance of charge assistance in the apolar binding of guests inside calixarene cavities, and they highlight the role played by the conformational properties of host in the recognition process.<sup>[19]</sup> Recently, the renaissance of interest in all aspects of molecular recognition in water were easily observed in chemical literature. A number of papers appeared on the application of water-soluble calix[*n*]arenes as catalysts or cocatalysts. Thus, Wacker oxidation of alkenes,<sup>[20]</sup> aldol-type condensation and Michael addition,<sup>[21]</sup> and Suzuki coupling,<sup>[22]</sup> were recently reported to be catalyzed by water-soluble calix[*n*]arenes. These results are apparently connected with "green chemistry" procedures with the potential for industrial application, a fact that should boost the research in this area profoundly. The second subject of recent interest is centered around medicinal chemistry application in a broad sense. Water-soluble *p*-sulfonatocalixarenes were recently reported to bind dipeptides and tripeptides containing lysine and arginine. This process, taken as a model for interaction of glycosylaminoglycans with polypeptides, was thoroughly studied by NMR and microcalorimetry.<sup>[23]</sup> There are, however, many examples of water-soluble neutral calixarenes, and most of them belong to the neoglycoconjugates family.<sup>[24]</sup> Such compounds can be used as models of important biological processes like interactions taking place on the surface of the cell. Among them, embryogenesis, cancer metastasis, inflammation, and bacterial and viral infections are examples of biological events that involve the selective recognition of carbohydrates by proteins. However, isolated carbohydrate-protein interactions are typically weak. Nature compensates for the weakness of these isolated interactions by tending to cluster together multiple copies of carbohydrate receptors in order to allow for stronger cooperative binding to take place—the so-called multivalent effect. The role of calixarenes as cyclic oligomers of phenolic nuclei is immediately apparent. No wonder that many water-soluble carbohydrate-appended calixarenes were reported and their properties studied. A recent report on this subject illustrates the state-of-art in this direction.<sup>[25]</sup>

### Gas-Phase and Gas-Solid Interface

The study of host-guest interactions recently expanded from solution chemistry to the gas phase, where solvent effects are not present, allowing better understanding of the intrinsic phenomena responsible for molecular recognition. Many calixarenes were used as hosts in this respect<sup>[26,27]</sup> using CI MS. The less-demanding approach (at least as far as the instrument costs are concerned) involves the application of GC headspace analysis applied

for gas-phase complexation of parent calixarene<sup>[28,29]</sup> and thiacalixarene.<sup>[29]</sup>

### CONCLUSION

No conclusion can adequately summarize the developments in the topic of this article. Host-guest chemistry is still in its infancy as a typical multidisciplinary subject. The progress in all basic disciplines will immediately provoke progress in the level of our knowledge on molecular complex formation by calixarenes. The synthesis of many new ligands and their thorough study will definitely be required to better understand the multifaceted problem of molecular recognition and complex formation.

### NOTE ADDED IN PROOF

Parent *p*-*tert*-butylcalix[4]arene has been found to undergo unprecedented single-crystal-to-single crystal phase transition upon guest uptake and release. Despite the lack of porosity of the material, guest transport through the solid occurs readily until a thermodynamically stable structure is achieved. In order to actively facilitate this dynamic process, the host molecule undergo significant positional and/or orientational rearrangement. This transformation is triggered by weak van der Waals interaction between host (*p*-*tert*-butylcalix[4]arene) and guest (vinyl bromide) molecules.

Atwood, J.L.; Barbour, L.J.; Merta, A.; Schottel, A. Guest transport in nonporous solid via dynamic van der Waals cooperativity. *Science* **2002**, 298, 1000–1002.

### ARTICLES OF FURTHER INTEREST

*The Allosteric Effect*, p. 20

*Biological Ligands*, p. 88

*Calixarenes and Their Analogues: Cation Complexation*, p. 137

*Calixarenes: Synthesis and Historical Perspectives*, p. 153

*Carbohydrates, Recognition of*, p. 169

*Cavitands*, p. 219

*Chiral Guest Recognition*, p. 236

*Classical Description of Inclusion Compounds*, p. 253

*Complexation of Fullerenes*, p. 302

*Concave Reagents*, p. 311

*Concepts in Crystal Engineering*, p. 319

*Dendrimers*, p. 432

*Disorder and Diffuse Scattering*, p. 457

*Drug Delivery*, p. 484

*Guanidinium-Based Anion Receptors*, p. 615